2018

Platelet Factor 4 And Von Willebrand Factor Form An Immunogenic, Prothrombotic Complex In Heparin-Induced Thrombocytopenia

Ian Johnston
University of Pennsylvania, IanJohnston32@gmail.com

Platelet Factor 4 And Von Willebrand Factor Form An Immunogenic, Prothrombotic Complex In Heparin-Induced Thrombocytopenia

Abstract
Heparin-induced thrombocytopenia (HIT) is a prothrombotic, thrombocytopenic disorder that occurs in patients exposed to heparin due to the development of antibodies directed against complexes of platelet factor 4 (PF4) with heparin with other polyanions . We have recently shown that the perithrombus endothelium is targeted in HIT. Using a photochemical injury model and an endothelialized microfluidic system, we now show that PF4 binds to elongated strands of von Willebrand factor (VWF) released from injured endothelium. This binding appears to be periodic along the VWF strand and to favor larger VWF strands, suggesting formation of oligomers that may cross-link individual VWF subunits. KKO, a monoclonal HIT-like antibody, and HIT patient plasma form PF4-VWF-HIT antibody complexes that may stabilize the complexes which, in turn, avidly bind platelets, exacerbating thrombus growth in a human whole blood microfluidic system. This increase in platelet binding is attenuated by blocking either the platelet FcγRIIA or the glycoprotein Ib/IX receptor. Charge-based as well as VWF-binding drugs can disrupt the PF4-VWF-HIT complexes. Dynamic light scattering studies provide additional support for the concept that PF4 and VWF form complexes in vitro. In vivo studies in a passive immunization model of HIT indicate a potential role for VWF in the prothrombotic nature of HIT. Thus, these studies newly identify VWF as a potentially important polymer involved in the formation of HIT antigenic complexes that contribute to the prothrombotic nature of HIT and offer a potential new therapeutic target to mitigate the thrombotic complications of affected patients.

Degree Type
Dissertation

Degree Name
Doctor of Philosophy (PhD)

Graduate Group
Pharmacology

First Advisor
Mortimer Poncz

Second Advisor
Lawrence F. Brass

Subject Categories
Pharmacology

PLATELET FACTOR 4 AND VON WILLEBRAND FACTOR FORM AN IMMUNOGENIC, PROTHROMBOTIC COMPLEX IN HEPARIN-INDUCED THROMBOCYTOPENIA

Ian Johnston

A DISSERTATION

in

Pharmacology

Presented to the Faculties of the University of Pennsylvania

in

Partial Fulfillment of the Requirements for the

Degree of Doctor of Philosophy

2018

Supervisor of Dissertation

_____

Mortimer Poncz

M.D., Professor of Pharmacology and Pediatrics

Graduate Group Chairperson

_____

Julie A. Blendy, Ph.D., Professor of Pharmacology

Dissertation Committee

Lawrence F. Brass, M.D., PhD., Professor of Pharmacology and Medicine (Chair)

John W. Weisel, PhD., Professor of Cell and Developmental Biology

Doug B. Cines, M.D., Professor of Pathology and Laboratory Medicine

Robert J. Levy, M.D., Professor of Pediatric Cardiology

Dedication page

I dedicate this work to my wife, Courtney, whose love and support made all of this possible.

ACKNOWLEDGMENT

I'd like to thank Dr. Mortimer Poncz for his guidance and support. He allowed me to integrate my engineering background with the biology of the lab and venture into very interesting scientific realms. This translated into various conference presentations and collaborations that weren't always available to other graduate students. So I thank him for these opportunities as I know they will be valuable to my future career. I'd also like to thank my thesis committee members, Dr. Skip Brass, Dr. Doug Cines, Dr. John Weisel, and Dr. Robert Levy. Their input provided the extra push which helped me overcome the challenges of graduate school and helped me hone the skills I'll use for years to come.

I'd also like to thank Dr. Carlos Villa, Dr. Colin Greineder, and Dr. Jacob Myerson from the Muzykantov Lab. Their collaborations helped broaden my view of science and research and were essential to the development of the microfluidic model.

Lastly, I'd like to thank a few members of the Poncz lab. I'd like to thank Dr. Randy Lyde and Vincent Hayes for their friendship and support during graduate school.

ABSTRACT

PLATELET FACTOR 4 AND VON WILLEBRAND FACTOR FORM AN IMMUNOGENIC, PROTHROMBOTIC COMPLEX IN HEPARIN-INDUCED THROMBOCYTOPENIA

Ian H. Johnston

Mortimer Poncz, M.D.

Heparin-induced thrombocytopenia (HIT) is a prothrombotic, thrombocytopenic disorder that occurs in patients exposed to heparin due to the development of antibodies directed against complexes of platelet factor 4 (PF4) with heparin with other polyanions . We have recently shown that the perithrombus endothelium is targeted in HIT. Using a photochemical injury model and an endothelialized microfluidic system, we now show that PF4 binds to elongated strands of von Willebrand factor (VWF) released from injured endothelium. This binding appears to be periodic along the VWF strand and to favor larger VWF strands, suggesting formation of oligomers that may cross-link individual VWF subunits. KKO, a monoclonal HIT-like antibody, and HIT patient plasma form PF4-VWF-HIT antibody complexes that may stabilize the complexes which, in turn, avidly bind platelets, exacerbating thrombus growth in a human whole blood microfluidic system. This increase in platelet binding is attenuated by blocking either the platelet FcγRIIA or the glycoprotein Ib/IX receptor. Charge-based as well as VWF-binding drugs can disrupt the PF4-VWF-HIT complexes. Dynamic light scattering studies provide additional support for the concept that PF4 and VWF form complexes in vitro. In vivo studies in a passive immunization model of HIT indicate a potential role for VWF in the prothrombotic nature of HIT. Thus, these studies newly identify VWF as a potentially important polymer involved in the formation of HIT antigenic complexes that contribute to the prothrombotic nature of HIT and offer a potential new therapeutic target to mitigate the thrombotic complications of affected patients.

TABLE OF CONTENTS

LIST OF TABLES

Chapter 3. Endothelial antigen assembly leads to thrombotic complications in heparin-induced thrombocytopenia

LIST OF ILLUSTRATIONS

Chapter 1 -- Introduction

Chapter 2 -- Microfluidic system modeling

Chapter 3 -- Endothelial antigen assembly leads to thrombotic complications in heparin-induced thrombocytopenia

Chapter 5 -- Neutrophil accumulation and NET release contribute to thrombosis in HIT

Chapter 6 -- ICAM-1 – targeted thrombomodulin mitigates tissue factor – driven inflammatory thrombosis in a human endothelialized microfluidic model

CHAPTER 1 - Introduction

Hemostasis: Pro-coagulative Factors

Hemostasis can be seen as the crucial balance between pro-coagulative and anti-coagulative processes present on and within the vasculature. On the pro-coagulative side, hemostasis assures that minor vascular injuries are sealed by platelets (platelets) preventing unnecessary blood loss. On the anti-coagulative side, hemostasis assures that excessive platelet accumulation or clot formation is mitigated to a level that sustains blood flow through an injured vessel[1,2]. Pro-coagulative processes are driven in large part by the serine protease thrombin (activated Factor (F) II, IIa or FIIa), a pivotal component of the coagulation cascade. This cascade consists of a series of zymogens that when activated, cleave and activate subsequent zymogens culminating in FIIa. The “intrinsic” pathway of this cascade leading to IIa initiates with the activation of the plasma zymogen FXII bound to a negatively-charged surface, e.g. a catheter, within the vascular lumen. Alternately, the “extrinsic” pathway is activated via FVII binding the transmembrane receptor, tissue factor (TF), which normally sequestered from the cell surface[3–5]. In either case, FIIa leads to a positive feedback loop by activating FV, FVII and FXI, which generates additional FIIa (**Figure 1.1**). FIIa ultimately promotes coagulation via direct and indirect pathways. Directly, FIIa cleaves the plasma protein fibrinogen, which generates fibrin monomers that polymerize and constitute most of the protein mass within fibrin clots. Indirectly, FIIa activate platelets by cleaving protease-activated receptors (PAR) PAR-1 and PAR-4, and activates endothelial cells (ECs) via PAR-1, generating inflammatory cytokines in addition to promoting coagulation[2,6,7].

Hemostasis: Anti-coagulative Factors

ECs lining the vasculature have a major role in preventing undesirable clot formation (**Figure 1.2**). ECs release prostacyclin (PGI2), nitric oxide (NO), and cluster of differentiation (CD) 39 which down-regulate platelet activation within a healthy vascular lumen[8–11]. Additionally, ECs are covered with a layer termed the glycocalyx, a negatively charged meshwork composed of glycoproteins and glycolipids that provide a protective coating to the vascular wall, by repelling inadvertent interactions of blood cells with the vascular surface[12–17]. EC's also express thrombomodulin (TM), a multidomain transmembrane glycoprotein that binds FIIa, inhibiting its capacity to cleave fibrinogen and activate platelets. Binding of FIIa of TM catalyzes (>1000-fold) the formation of activation Protein C (APC) from Protein C (PC). When bound to its cofactor, Protein S, APC reduces FIIa production indirectly by inactivating the upstream enzymes, FVa and FVIIIa. PC also interacts with the PC binding receptor (EPCR) expressed on the EC surface that causes a 20-fold increase in APC production. APC is capable of detaching from this complex and imposing the previously mentioned anti-coagulative effects; alternatively, while still bound, APC is capable of inducing cytoprotective effects including dampening inflammation and improving endothelial barrier function via PAR-1. This improved EC barrier contributes to APC's anti-coagulative effects by reducing the production of pro-coagulative EC surfaces and access to the pro-coagulative extracellular matrix (ECM)[2,8,18–22]. EC's also produce tissue plasminogen activator (tPA) and plasminogen activator inhibitor-1 (PAI-1); tPA cleaves plasminogen into plasmin which is responsible for lysis of fibrin clots. On the other hand, inhibition of tPA by PAI-1 prevents premature clot lysis. APC also inhibits PAI-1 allowing for greater tPA activation of plasmin[23–25].

Under physiological conditions, in which minor injuries or damage occurs, hemostasis is maintained within the vasculature by a balance between these pro- and anti-coagulative processes, allowing clot formation where and only as long as it is needed.

Thrombosis

Thrombosis is an imbalance of these pro- and anti-coagulative factors on a local or systemic level favoring clot formation. An imbalance leading to thrombosis can be caused by a variety of ailments which include, but are not limited to, significant vascular damage, an excessive immune (antibody) or inflammatory response[26–28]. In any of these scenarios, significant changes occur in the microenvironment of the blood vessel promoting pro-coagulant processes (**Figure 1.3**).

When ECs are activated they shed or endocytose TM and suppress EPCR expression[19,22,29–33]. This decreases APC production leading to an increase in FIIa with the effects on coagulation mentioned above. Excess FIIa also enhances PAR 1 cleavage leading to increased endothelial inflammatory responses and a decrease in EC barrier function[21]. Moreover, the lack of APC minimizes the inhibition of PAI-1, while increased FIIa increases PAI-1 production. Increased PAI-1 significantly inhibits tPA activity, leading to greater fibrin clot stability. Additionally, activated ECs express intracellular adhesion molecule 1 (ICAM-1) and vascular cell adhesion molecule (VCAM-1) adhesion proteins that promote white blood cell binding which further enhance EC activation[16,26,34]. Furthermore, ECs begin to develop additional pro-coagulative properties such as expression of TF and release of VWF. TF contributes through its previously mentioned function of binding FVIIa and increasing FIIa production. VWF, a multimeric glycoprotein, is released from the Weibel-Palade bodies within ECs and helps to stabilize FVIII and promote platelet adhesion under high shear stresses[35–38]. Lastly, the glycocalyx, which

normally provides a thick, negatively charged mesh can become damaged or partially shed from the EC surface. This allows greater access to the EC surface and greater interaction of plasma proteins and circulating cells with the glycosaminoglycan (GAG) that make up the glycocalyx; both of these can contribute to pro-coagulative processes by co-localizing blood cells and cytokines to the EC wall leading to cell activation[12,16,17].

Platelets play a significant role in hemostasis and, consequently, thrombosis. As mentioned previously, platelets transiently bind VWF released from injured ECs via their membrane receptor, GPIb-IX-V, which slows down platelet rolling along the vascular surface. These transiently bound platelets then can undergo activation by interaction with the receptor GPVI, commonly associated with collagen. Platelets also can link other platelets via their integrin $\alpha_{IIb}\beta_3$, which can bind fibrin or collagen leading to platelet activation. As mentioned previously, platelets are also activated by thrombin[1,8]. In any setting, platelets an also be fully activated via their autocrine and paracrine signaling. Activated platelets release agonists such as thrombin, TxA_2, and ADP which amplify the process by promoting the activation of surrounding platelets[1,36,39,40]. This creates a positive feedback in which platelet activation leads to further platelet activation that contributes to thrombus structure and stability. This amplification affect can be seen in the structure of growing thombi in which platelets toward the center of a thrombi (core) are highly activated and densely packed while the outer layers are less activated and loosely packed (**Figure 1.4**).

Heparin-Induced Thrombocytopenia (HIT): An Iatrogenic Prothrombotic Disease

HIT is an iatrogenic immune disorder that develops after treatment with heparin. HIT is characterized by a fall in platelet count often accompanied by various thrombotic complications, which include pulmonary emboli, myocardial infarction, and deep vein

thrombosis[41–45]. Recently, rare cases of HIT have been described where no prior heparin exposure was identified[46]. HIT can be thought of as developing in three steps: initiation, activation and propagation (**Figure 1.5**). Step 1, initiation of HIT is caused by the introduction of heparin, a commonly used anticoagulant. Due to its highly negative charge, heparin is able to bind the platelet-specific chemokine, platelet factor 4 (PF4, CXCL4) and form soluble heparin/PF4 complexes. In some individuals this leads to the formation of pathogenic HIT antibodies. This leads to the Step 2: activation, in which these HIT antibodies bind to PF4/heparin complexes and cell surface PF4/GAGs complexes, leading to cell activation via their surface FcγIIA receptors (FcRγIIA) and perhaps by complement activation. Dermatan sulfate and heparin sulfate are among the GAGs with the highest affinity for PF4 that can form complexes that are recognized by HIT antibodies[47–49]. Among the cells expressing FcγRIIA that are activated are platelets, likely accounting for the observed thrombocytopenia, and monocytes that likely contribute to thrombosis by expressing TF[43,50,51]. ECs are also activated though the lack FcγRIIA, perhaps by adherent activated platelets and leukocytes and via activation of complement[42,43,52]. In studies described in Chapter 3, we demonstrate that the endothelium is an additional key target in HIT. Thus, in Step 2, the activation of the vasculature and several intravascular lineages can contribute to the prothrombotic nature of HIT. In Step 3, propagation of thrombosis after discontinuation of heparin, we propose that PF4 interacts with other polymeric molecules that allow thrombi to extend downstream of the initial thrombus. Among these are polyphosphates released by injured/activated platelets and perhaps endothelial cells[53]. Polyphosphates bind PF4 and become antigenic for the HIT-like monoclonal antibody KKO. That they form large complexes in vitro demonstrated using dynamic light scatter (DLS) technology.

We have now observed while simulating HIT in a microfluidic system that PF4 bound to injured endothelium not only occurs in a diffuse fashion (likely to the glycocalyx), but also along specific strand-like structures, which we identify in Chapter 4 as VWF. The details of this in vitro and in vivo analysis are described as well as examining the effect of targeted therapeutic intervention based on this approach. Another polymeric structure identified by us to which PF4 binds are neutrophil extracellular traps (NETs) released by activated neutrophils as described in Chapter 5. This effect appears to be more prominent in the venous system in in vivo murine studies of HIT. Thus, the release of three polymeric molecules will have been described that we propose as central to the propagation and the prothrombotic nature of HIT.

The established treatments for HIT are the immediate cessation of any heparin product and the use of direct thrombin inhibitors (DTIs), specifically lepirudin and argatroban that bind and inhibit the prothrombotic actions of FIIa or inhibitors of FXa such as fondaparinux, rivaraxoaban, or apixaban. These interventions are only partially effective in decreasing morbidity and mortality from the thrombotic complications in HIT. Such treatments also have limitations in that some require frequent monitoring, have increased risk of bleeding, may accumulate with hepatic or renal insufficiency, and some are associated with high cost and require hospitalization[41,44,54]. In Chapters 2-4 we propose and test various novel therapeutics based on our observations on the novel new mechanisms we describe in HIT.

HIT Modeling

The recognition that there was a clinical prothrombotic disorder in patients treated with heparin took several decades to appreciate[55]. Progress was and is still limited by the severity of illness and the complex clinical settings in which it often develops. Furthermore,

clinical diagnosis is challenging and the laboratory confirmation relies on functional assays that are often limited to tertiary care centers[41,44]. To help gain better insight into the pathogenesis of HIT, a passive immunization model was developed using double transgenic mice that express human platelet IgG Fc receptor IIA FcγRIIA (present on human but not on mouse platelets) and human PF4 (hPF4), often on a mouse PF4 knockout background[43,47,56]. HIT is induced by infusing KKO, a monoclonal antibody that recognizes heparin/hPF4 and heparin-like/hPF4 complexes or HIT immunoglobulins isolated from patients with a high likelihood of having HIT. When infused with KKO, mice experience thrombocytopenia followed by fibrin-rich thrombi in multiple organs, including the pulmonary vasculature. This model is used and elaborated on in the following sections to investigate how thrombi develop in the setting of HIT. We recognize that these in vivo studies suffer from being mostly based in the murine vasculature and coagulation system and concerns arise over translatability to the clinic[57,58]. We therefore have focused on developing an in vitro system that can be either human or murine based and that also allows isolation and targeted manipulation of specific cellular components and combining these components to obtain specific details of the mechanism of thrombosis in HIT. This system, especially the use of the endothelial-lined Bioflux system where a targeted hematoporphyrin-photochemical injury is induced in the lining, was key to many of the observations on the role of the endothelium in HIT (Chapter 3), the prothrombotic nature of PF4-VWF-HIT antibody complexes (Chapter 4), and the formation of PF4-NETs-HIT antibody complexes (Chapter 5) in HIT.

Sepsis: An Immune-Based Systemic Disorder

Sepsis is a life-threatening condition characterized by impaired microclearance combined with sustained excessive inflammation and activation of coagulation. The

dysregulated host response to infection leads activation of the complement system and systemic thrombosis, among other adverse outcomes to the host. Through exposure to the invading pathogen or the resulting inflammatory cytokine release, sepsis can interfere with many of the previously mentioned EC-based anti-coagulant mechanisms that normally prevent thrombosis. These include, but are not limited to, increasing TF-mediated FIIa generation and impairing endogenous anticoagulant mechanisms and fibrin removal[33,59–62] (**Figure 1.6.**). During our studies into the progression of HIT, we became interested in lessons that may be applicable to sepsis and other inflammatory thrombosis models in which patients experienced thrombocytopenia and some develop disseminated thrombosis. Patients often develop HIT in the setting of major surgery or widespread inflammation as seen in the initial steps of sepsis. Moreover, sepsis and HIT each initiate similar elaborate multicellular pathways leading to thrombosis that include activating ECs with release of VWF, activation of neutrophils with the release of NETs, activation of platelets and sustained progressive pathology that may worsen over the course of hours to days[33,59–62]. Consequently, with collaborators, we developed a microfluidic model of inflammatory thrombosis (Chapter 2) and investigated a novel ICAM-1 targeted TM therapeutic to combat the formation of fibrin clots (Chapter 6). This allowed us to better understand how ECs change in the setting of inflammation and determine if said changes could be used to develop new approaches to therapy, especially those that could be used in combination with currently employed approaches to treatment with maximally tolerated anti-thrombotic drugs.

Summary

Our incomplete understanding of how thrombosis in HIT is propagated and sustained even when heparin is withdrawn and even when maximally tolerated

antithrombotic therapy is employed creates a need to see if potential avenues for treatment have been overlooked. Furthermore, with only murine models available, there are intricacies of the pathogenesis that are difficult to investigate without incorporating human ECs. Consequently, this thesis aims to address these shortcomings in several ways. First, we used an in vivo laser injury model of HIT in mice to inform the development of a “humanized” in vitro microfluidic model (Chapter 2). Chapter 3 summarizes an in vivo murine model of HIT that provided the framework for the questions then addressed in the “humanized” setting. Chapter 3 describes the proclivity of PF4 and HIT antibody to interact with the perithrombus ECs both upstream and downstream of an initial injury site. This understanding of ECs involvement led to developing an in vitro microfluidic model using human blood that demonstrated similar patterns of PF4 binding to the surface of ECs. With this new understanding concerning the importance of ECs to the formation of PF4-HIT antibody complexes, Chapter 4 and Chapter 5 summarize our understandings of how vascular and intravasular cells and proteins contribute to the pathogenesis of HIT. Chapter 4 summarizes our finding that VWF released from injured ECs may contribute to HIT by forming PF4-VWF-HIT antibody complexes. In vitro work displays how these complexes induce greater platelet accumulation that is both FcγRIIA and GPIb dependent. We also showed that VWF targeted therapeutics disrupted these complexes and, in an in vivo setting, attenuated thrombosis enhanced by HIT antibodies. Chapter 5 summarizes how activated neutrophils release NETs that present an additional site on which PF4-HIT antibody complexes form. In vitro microfluidic work in this chapter displays how the presence of PF4 impacts NET conformation and causes resistance to deoxyribonuclease I (DNase I). The work is translated in vivo showing a significant contribution of neutrophils to venous thrombi in a model of HIT through increased neutrophil-EC adhesion and neutrophil infiltrations of thrombi leading to even greater cell activation. Considering the

impact of inflammation on HIT, Chapter 6 summarizes the use of the inflammatory thrombosis model described in Chapter 2 to investigate EC activation as well as a novel therapeutic. Chapter 6 presents data from a humanized microfluidic setting that help to evaluate the changes in EC protein expression, fibrin deposition, and thrombi formation that can occur in the inflammation that accompanies HIT or the similar pathology seen in some cases of sepsis. Moreover, this chapter provides insight into the use of a novel ICAM-1 targeted TM therapeutic. This thesis culminates with Chapter 7 presenting the conclusions, clinical impacts, and future directions for the described studies.

Figures

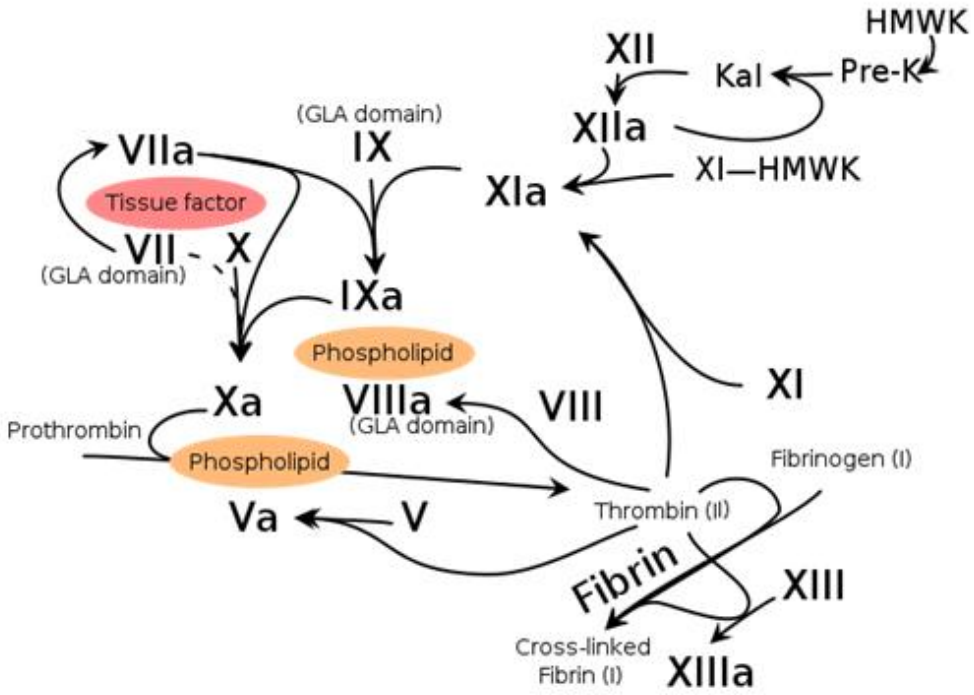

Figure 1.1. The coagulation cascade produces fibrin clots via production of FIIa and various positive feedback loops.

Binding FXII to a negatively charged surface accelerates its autoactivation which generates XIIa which cleaves FXI to FXIa, which initiates the intrinsic pathway. High-molecular-weight kininogen (HMWK) and prekallikrein (Pre-K) accelerate these initial activation steps. Kal =kallikrein. Binding of FVII/FVIIa to TF localizes FVIIa, initiating the extrinsic pathway. Each of these contributes to the activation of subsequent zymogens, including FXa, which is directly responsible for the activating FII. FIIa cleaves fibrinogen into fibrin, while also activating FXIII which further assists in clot stability. FIIa indirectly contributes by feeding back into the activation of FVIIIa and FVa. Image adapted from drawing presented by Professor Dzung Le at UCSD Clinical Chemistry Conference, October 2014.

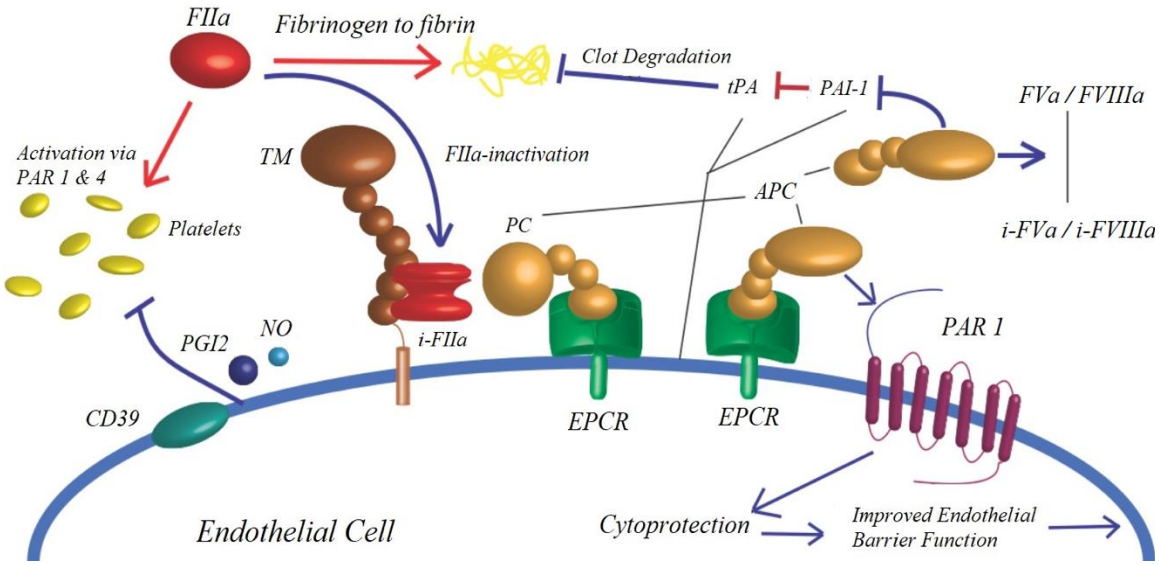

Figure 1.2. Quiescent ECs provide anti-thrombotic activity.

The antithrombotic effects of the TM/APC pathways and quiescent ECs. Quiescent ECs release PGI2, NO, and CD39 to limit platelet activation. TM binds and lessens FIIa mediated conversion of fibrinogen to fibrin by forming a complex which increases APC production. APC can stay bound to EPCR and cleave PAR-1 on ECs leading to improved cytoprotection and enhanced barrier function. APC can also inactivate FVa and FVIIIa and also inhibit PAI-1 allowing for tPA to more effectively cleave fibrin clots. i-IIa/ i-Va/ i-VIIIa = inactivated enzymes.

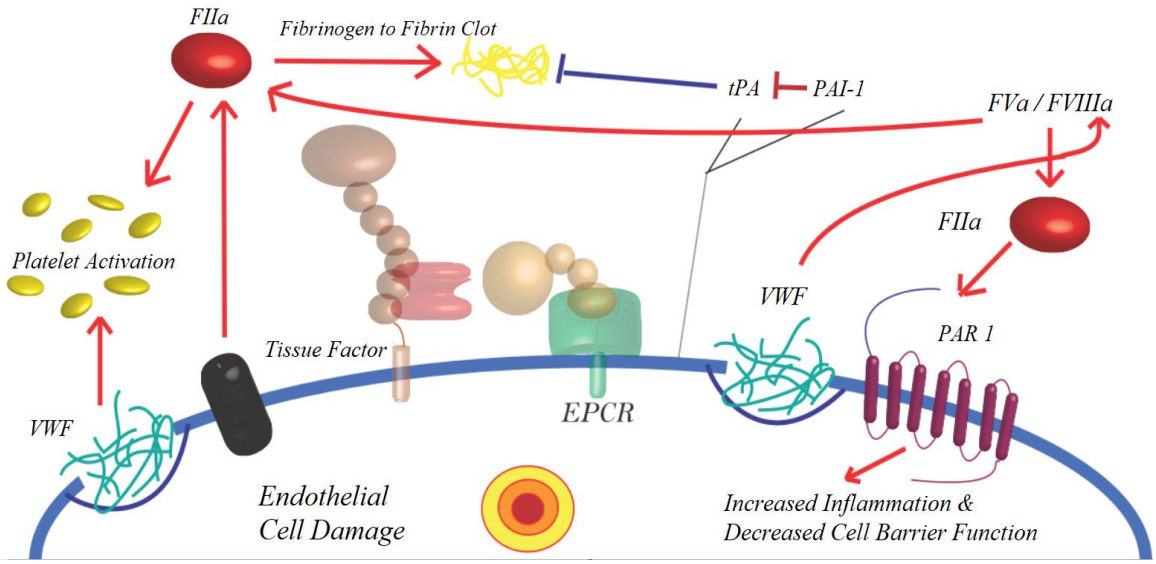

Figure 1.3. EC activation promotes pro-thrombotic activity.

When ECs experience significant damage, they promote pro-coagulative effects that contribute to thrombosis. ECs release VWF which bind platelets under high-shear stresses and express TF, which promote additional FIIa production. FIIa can also cleave PAR-1 leading to increased inflammation and reduced cell-barrier function. Additionally, ECs shed or endocytose their TM and suppress their EPCR in the setting of inflammation. This allows for greater increases in FIIa and greatly relinquishes the anti-coagulative impact of APC.

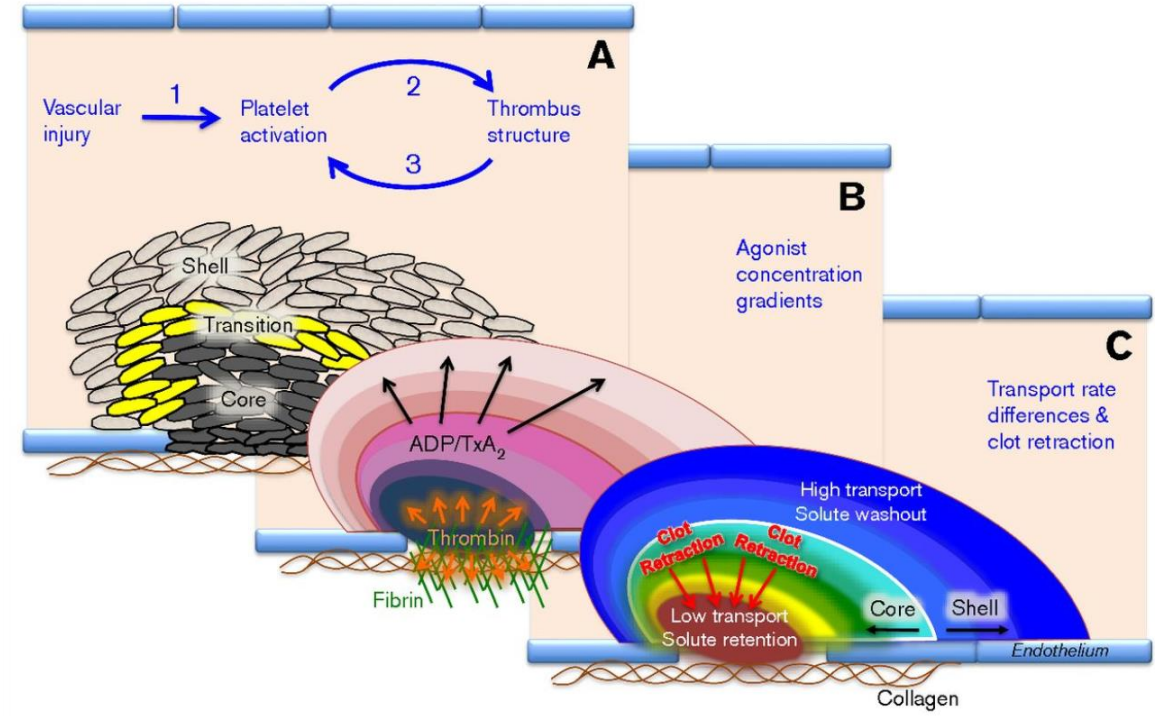

Figure 1.4. The gradient of platelet activation that occurs within a clot.

(**A**) Displays the presence of a highly activated, densely packed platelet core that is overlaid with a loosely packed shell of less activated platelets with an intermediate transition zone. (**B**) As with the gradient of platelet activation, there is a gradient of agonists with thrombin being focused at the sight of injury while ADP and TxA_2 persist in the transition zone and outward to the thrombi shell. (**C**) Displays how the high density of platelets in the thrombus core provide low transport and high solute retention while the outer shells provide high transport with low solute retention. Image taken from Brass LF, et al. 2016 Blood Advances.

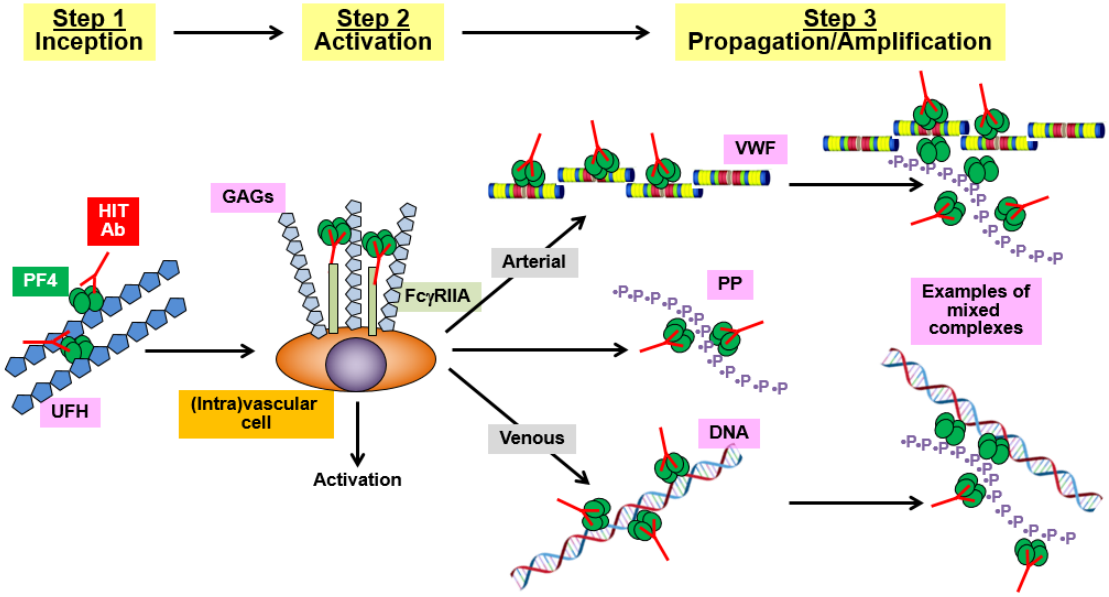

Figure 1.5. Proposed sequential steps in the development of prothrombotic pathways in HIT.

Step 1. HIT is initiated by ultralarge immune complexes composed of heparin/PF4 and HIT antibody (left). Step 2. PF4 also bind to GAGs on the surface of (intra)vascular and cells leading to the activation of platelets, monocytes, ECs, and neutrophils via FcγRIIa and/or complement pathways. Step 3. ECs activated by immune complexes release VWF, neutrophils release DNA in the form of NETs and diverse cell types release PPs, each of which combines with PF4 to form antigenic complexes that amplify and propagate the thrombus downstream. Studies of novel Step 3 pathways, focused on NETs, but especially VWF, form the core of this thesis.

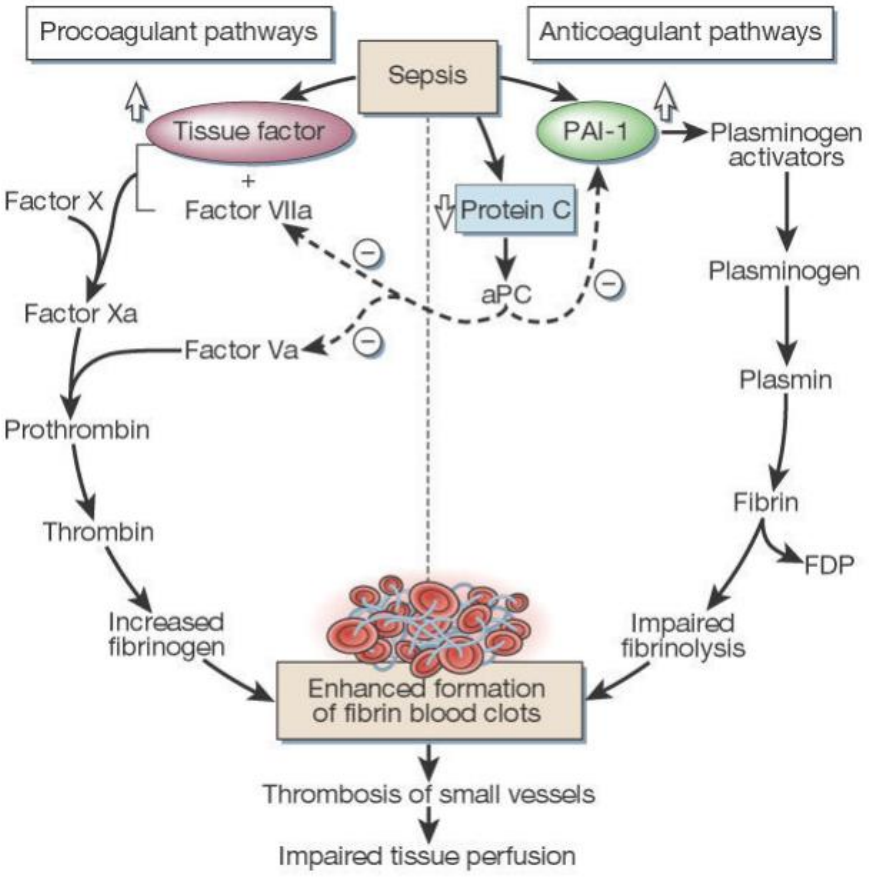

Figure 1.6. Sepsis promotes thrombosis by disturbing the normal balance between pro and anti-coagulant mechanisms.

Sepsis promotes thrombosis by activating various cells including ECs via inflammatory cytokines such as TNF-α and IL-1β which results in the increase of TF expression. Sepsis causes a decrease in PC and subsequently APC further bolstering TF production. The activation of ECs under septic conditions causes a reduction in TM which furthers the lack of APC production. Sepsis both directly and indirectly, through APC reduction, causes an increase in PAI-1 which further promotes thrombosis. Image taken from Cohen J, 2002, Nature.

CHAPTER 2 – Microfluidic system modeling

This chapter presents work featured in the articles:

Hayes, et al., (2017) *Journal of Clinical Investigation 127(3):1090-1098*

Greineder, C., Johnston, I., et al. (2017) *Blood Advances* 1(18): 1452-1465

Motivation for Developing an Endothelialized Microfluidic System

In the Introduction, I discussed the limitations of the passive immunization murine model for mechanistic studies of HIT, including that it is limited to a mostly murine system and the difficulties with manipulating individual lineages[56–58]. Although platelets and monocytes have been shown to be significant contributors to the pathogenesis in HIT, the contribution of ECs was less developed[43,50,53,63]. Consequently, the motivation for these studies was to investigate avenues through which ECs, particularly following vascular injury, contribute to HIT pathogenesis. Understanding these factors could provide valuable insight into why thrombosis in HIT propagates in the vasculature, forming long, platelet-rich "white clots"[64–67]. We posited that a major contributor is the injured endothelium in HIT and that a model system that allowed either diffuse or local endothelial injuries was deemed necessary. For diffuse injury, we utilized a tumor-necrosis factor alpha (TNFα) injury, which we found leads to increased platelet and neutrophil binding to the endothelium in the presence of PF4 and HIT antibodies[26,51,68]. We utilized a previously described hematoporphyrin-induced photochemical endothelial injury to establish a focused, localized injury[69,70]. Such an injury did not result in endothelial loss from the microfluidic device or loss of apparent cell-cell contact. Pursuing these studies not only provided greater insight into pathogenesis of HIT, but also novel therapeutic avenues based on those mechanisms to limit HIT-associated thrombosis.

Microfluidic Device and Setup

This chapter will focus on the description and characterization of that microfluidic model. The model used the Fluxion Bioflux 1000 microfluidic platform with micro-channels connecting corresponding wells that allows for the infusion of reagents via an air pressure mechanism. The walls of the vessel lumen are composed of the polymer

polydimethylsiloxane while the bottom of the plate is a glass cover slip allowing for visualization of the channel in real time. This additionally allows, in most cases, for coating with an extracellular matrix alone or with subsequent ECs (**Figure 2.1**). Throughout the following chapters, this model was used to provide a human cell-based in vitro system that incorporated shear stress to better recapitulate the physiological conditions seen in the vasculature. In some instances, the channels were only coated with fibronectin (50 µg/ml, Sigma-Aldrich) in phosphate-buffered saline and incubated for 1 hour at 37°C. Once coated, these channels were flowed with isolated cells, primarily neutrophils, re-calcified human whole blood, or platelets for experimentation (Chapter 5). In other instances of using this model, once coated with fibronectin, human umbilical vein ECs (HUVECS, 6-8 x 10^6 cells/ml, Lonza) were infused and allowed to grow to confluency (**Figure 2.2**).

At confluency (3-5 days), we characterized the monolayers to understand the quality of our in vitro "vessel". We stained the channels (**Figure 2.3**) for platelet endothelial cell adhesion molecule (PECAM-1, CD31) (rabbit anti-human CD31, abcam), actin (Alexa Fluor 488 Phalloidin, ThermoFisher Scientific), VWF (rabbit anti-human VWF polyclonal antibody, Dako; alternatively, FITC-sheep anti-human VWF polyclonal antibody, abcam), P-selectin (rabbit anti-human P-selectin polyclonal antibody, abcam). PECAM-1 verified that proper junctions were forming between ECs and that minimal spacing was found between adjacent cells, while actin showed that the cells grew with proper cytoskeletal support[71]. VWF and P-selectin staining on uninjured channels showed that the internal structure of the ECs where Weibel-Palade bodies would be located, were quiescent as they were punctate in nature and not seen on the surface or released from the EC monolayer[34,36,72,73]. Additionally, when uninjured channels were flowed with re-calcified human whole blood, minimal to no platelet accumulation was observed.

Injury Settings: Hematoporphyrin-Induced Endothelial Injury

Hematoporphyrin is a heme-pathway intermediate that in porphyria cutanea tarda is present in excess due to the absence of uroporphyrinogen decarboxylase (UROD), resulting in a light-dependent sclerosing of tissues. Prior studies by others in a microfluidic device induced injury to ECs using changes in pressure[74], γ radiation[75], hypernatremia[76], physical vascular wall puncturing[77], hypoxia[78], lasers (405nm)[79], and localized heat[80]. However, many of these injuries lacked the ability to be localized, are limited in widespread reproducibility, and/or cannot cause EC injury without also denuding them from the microfluidic channel wall. In our microfluidic system, we added hematoporphyrin (50 µg/ml final concentration, Sigma-Aldrich) and illuminated a localized area of the channel to create a demarcated region of endothelial injury. We characterized this injury model by showing localized activation of endothelialized microfluidic channels made as described above and in **Figure 2.4** as represented by localized VWF release detected using a rabbit polyclonal anti-human VWF antibody (DAKO) in combination with a goat anti-rabbit Alexa Fluor secondary antibody (ThermoFisher Scientific). Additionally, we showed that ECs were not denuded by the injury as verified by nuclei stain using Hoescht staining. The continued presence of the endothelial lining following injury is essential for our thrombosis studies to distinguish from binding of platelets to the underlying fibronectin-coated channels. Moreover, when recalcified human whole blood was introduced either during or after the injury, platelet accumulation was localized to the injured ECs, but not to the upstream or downstream uninjured ECs. Additionally, when looking at hPF4 binding, that it was localized to the injury area and was present on the luminal surface of ECs, but not in the subliminal space. By altering the shutter on the microscope, we were able to alter the radius of this injury causing it to injure more or less of the channel.

Injury Settings: TNFα-Induced Endothelial Injury

To study HIT and the patients vascular state prior to HITs initiation, we developed an endothelial injury within our microfluidic system that utilized the inflammatory conditions experienced during and post-surgery. TNFα is an inflammatory cytokine primarily released by activated macrophages that induces changes in ECs that promote thrombosis. These include the upregulation of ICAM-1, VCAM-1, TF and the down-regulation of TM[26,51,68]. In our microfluidic model, we induced an inflammatory injury by incubating our endothelialized microfluidic channels with basal media containing TNFα (0-10 ng/ml for 0-6 hours) at a variety of shear stresses (1-5 dynes/cm^2) We characterized this injury model by verifying increases in the surface expression of ICAM-1 (mouse anti-human monoclonal ICAM-1 antibody, abcam) and VCAM-1 (rabbit anti-human monoclonal VCAM-1 antibody, abcam) when endothelialized microfluidic channels were exposed to TNFα (**Figure 2.5**). We saw increases in ICAM-1 and VCAM-1 as seen under physiological conditions. Changes in TF and TM were only slightly detectable due to low signal to background ratio (not shown). Additionally, we verified that when recalcified human whole blood was flowed through TNFα-activated channels, fibrin clots formed in a time, and TNFα concentration-dependent manner.

Discussion

This chapter describes two endothelialized microfluidic systems important for my studies of Step 3 propagation in HIT. The photochemical injury model especially allowed me to identify VWF strands as an important target binding PF4 and forming HIT antigenic sites that have a high affinity for binding platelets that form the core of this thesis.

Figures

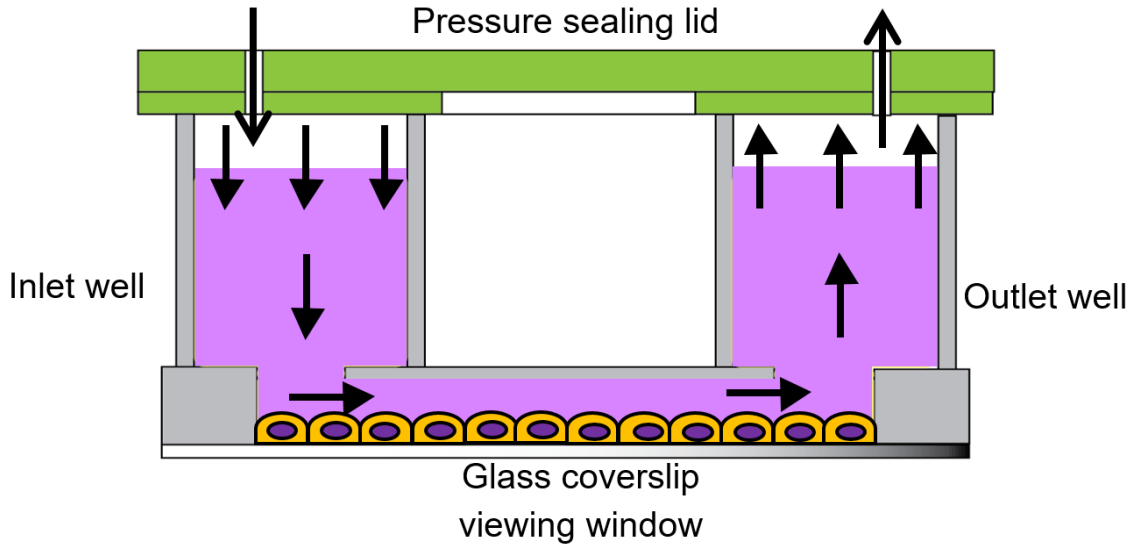

Figure 2.1. Schematic of an endothelialized Fluxion Bioflux 1000 microfluidic plate. This microfluidic platform consists of a microfluidic channel that connects two 1 ml wells. Using filtered air pressure infused through a pressure sealing lid, the Bioflux is able to perfuse reagents from one well, through the endothelialized microfluidic channel, into the "outlet" well. The bottom of the microfluidic channel is formed by a glass coverslip allowing for real time or post-experimental imaging. In most cases, the microfluidic system is coated in extracellular matrix alone or with subsequent ECs. Orange spheres with purple center = ECs with nuclei; Lilac solution = reagent solution representative of various reagents used in experiments.

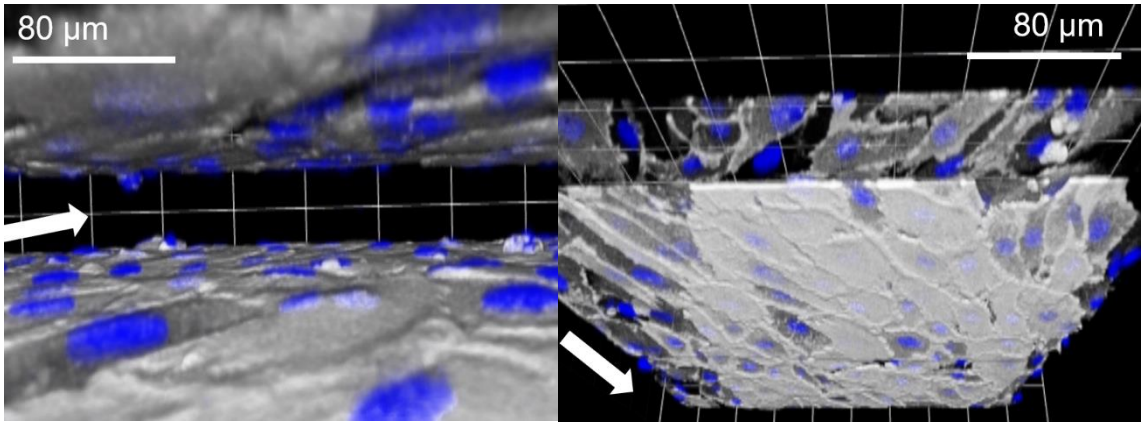

Figure 2.2. EC growth to confluency in three dimensions of the microfluidic model. Three-dimensional (3-D) renderings from confocal images of microfluidic channels coated with ECs showing confluency along the top and bottom of channels. Looking down the channel (left) and looking along the bottom of the channel (right) with EC nuclei (blue, labeled with Hoescht) and cell membranes (white, Vybrant DiD cell labeling from ThermoFisher Scientific) microfluidic channels showing the connectivity of cell membranes covering the underlying fibronectin coating.

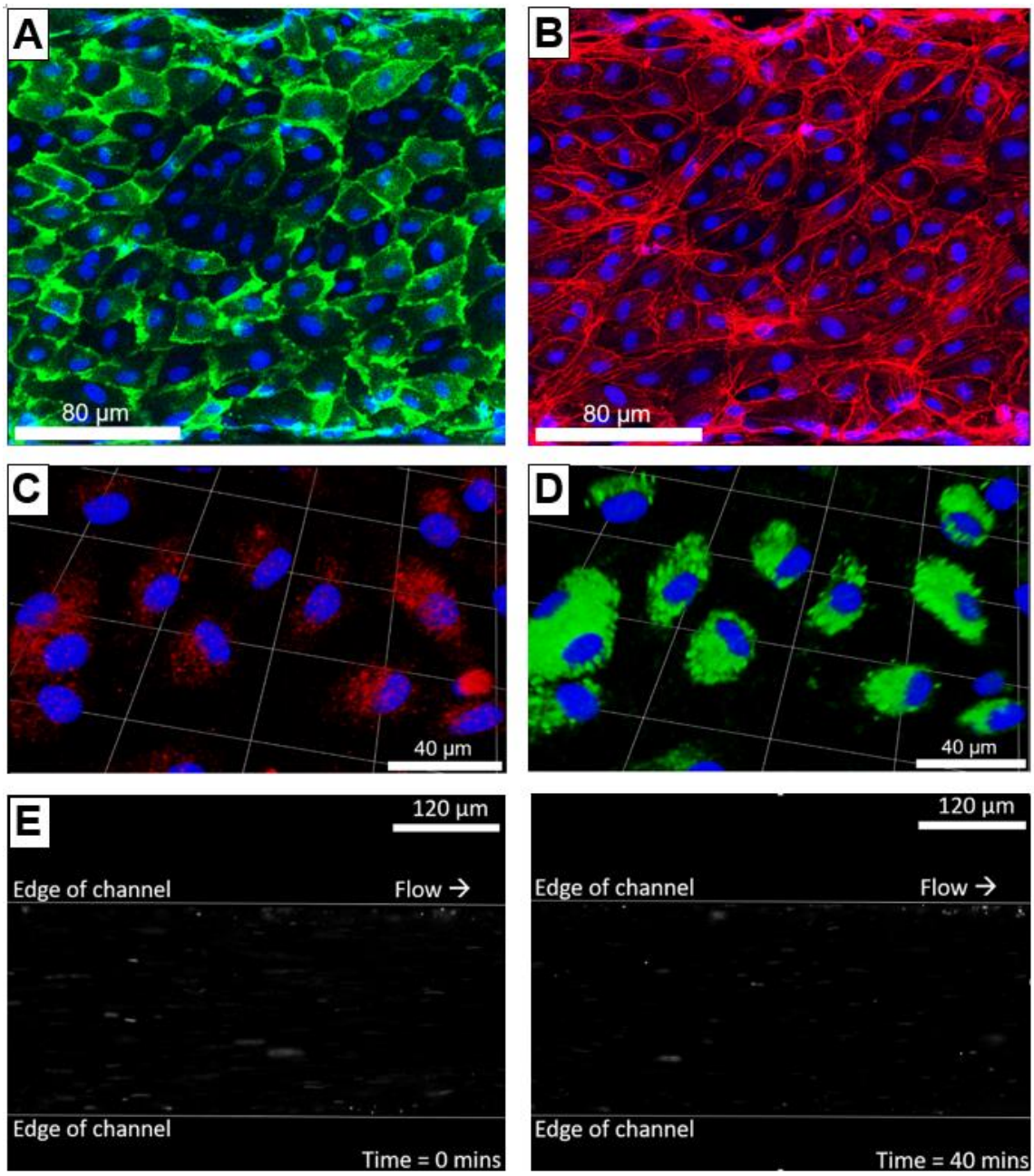

Figure 2.3. Characterization of the endothelialized microfluidic channel by identifying key protein structures and displaying quiescence by introducing human whole blood.

(**A**) Confocal images that show PECAM-1 signal around the periphery of cells indicative of junctions forming between neighboring ECs and (**B**) actin throughout the cell body

showing the forming of internal cytoskeletons as expected of healthy cells based on previous publications. (**C**) P-selectin and (**D**) VWF are localized to the nuclei where they are presumably stored within the Weibel-Palade Bodies of the ECs as oppose to being released or dispersed across the EC monolayer. Nuclei stained with Hoescht (blue) are presented in all images. (**E**) Fluorescently imaged stills from a 40-minute video of whole blood being flowed through an endothelialized microfluidic channel taken at 10x. The whole blood was labeled with calcein AM which labels platelets and white blood cells. The stills show that after 40 minutes of blood flow, there is no significant accumulation of platelets within the channel which is indicative of the ECs being quiescent.

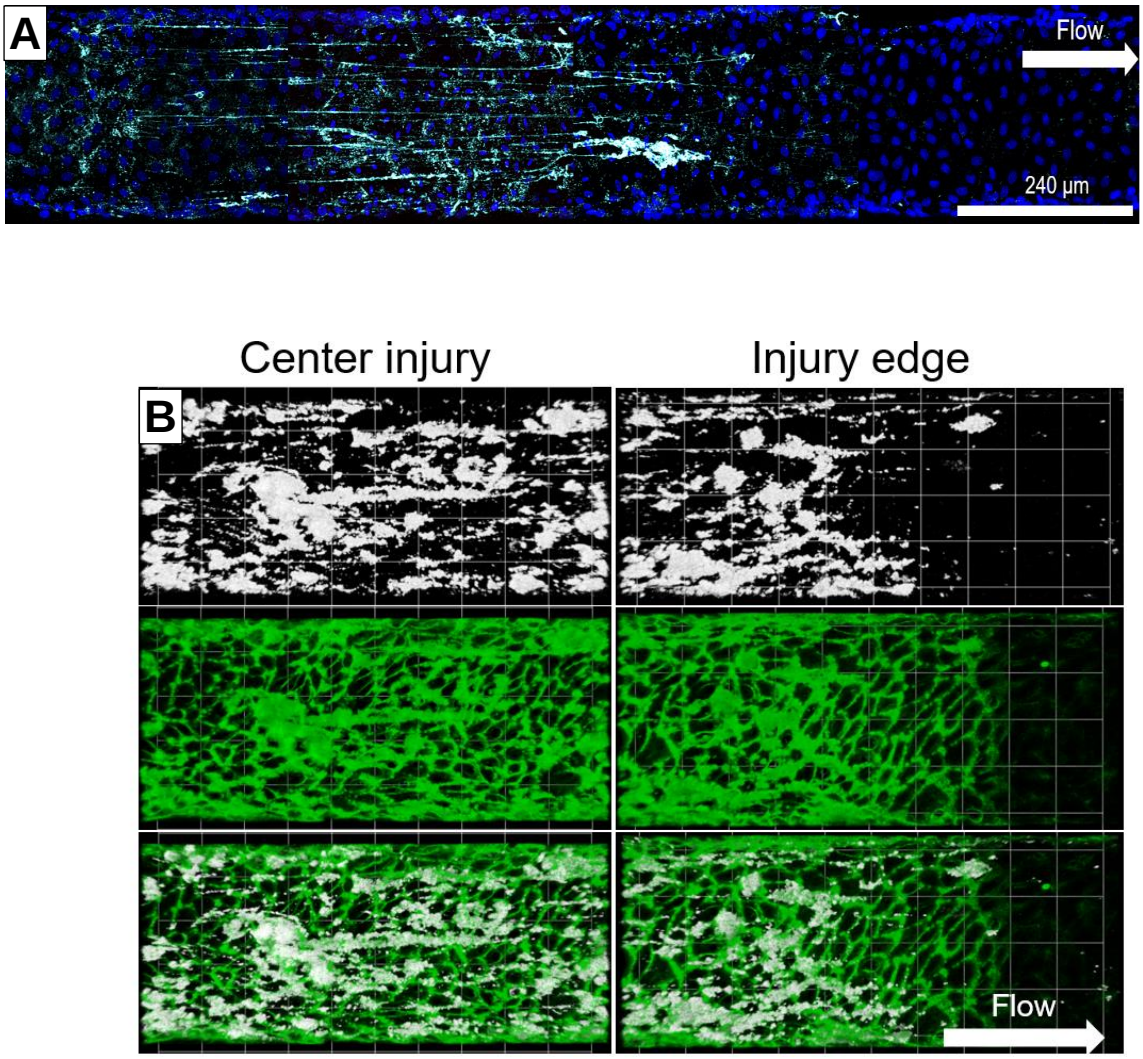

Figure 2.4. Hematoporphyrin injury causes a localized release of VWF leading to localized platelet accumulation and hPF4 deposition.

(**A**) Endothelialized channels after an hematoporphyrin injury showing the localized release of VWF (cyan) in the channels with minimal to no VWF release downstream. Additionally, ECs indicated by their nuclei (blue) are shown to persist throughout the channel after injury showing no denudation. (**B**) Shows that the platelet accumulation (white) and hPF4 (green) deposited during injury of re-calcified human whole blood is localized to the injury area in which VWF is released.

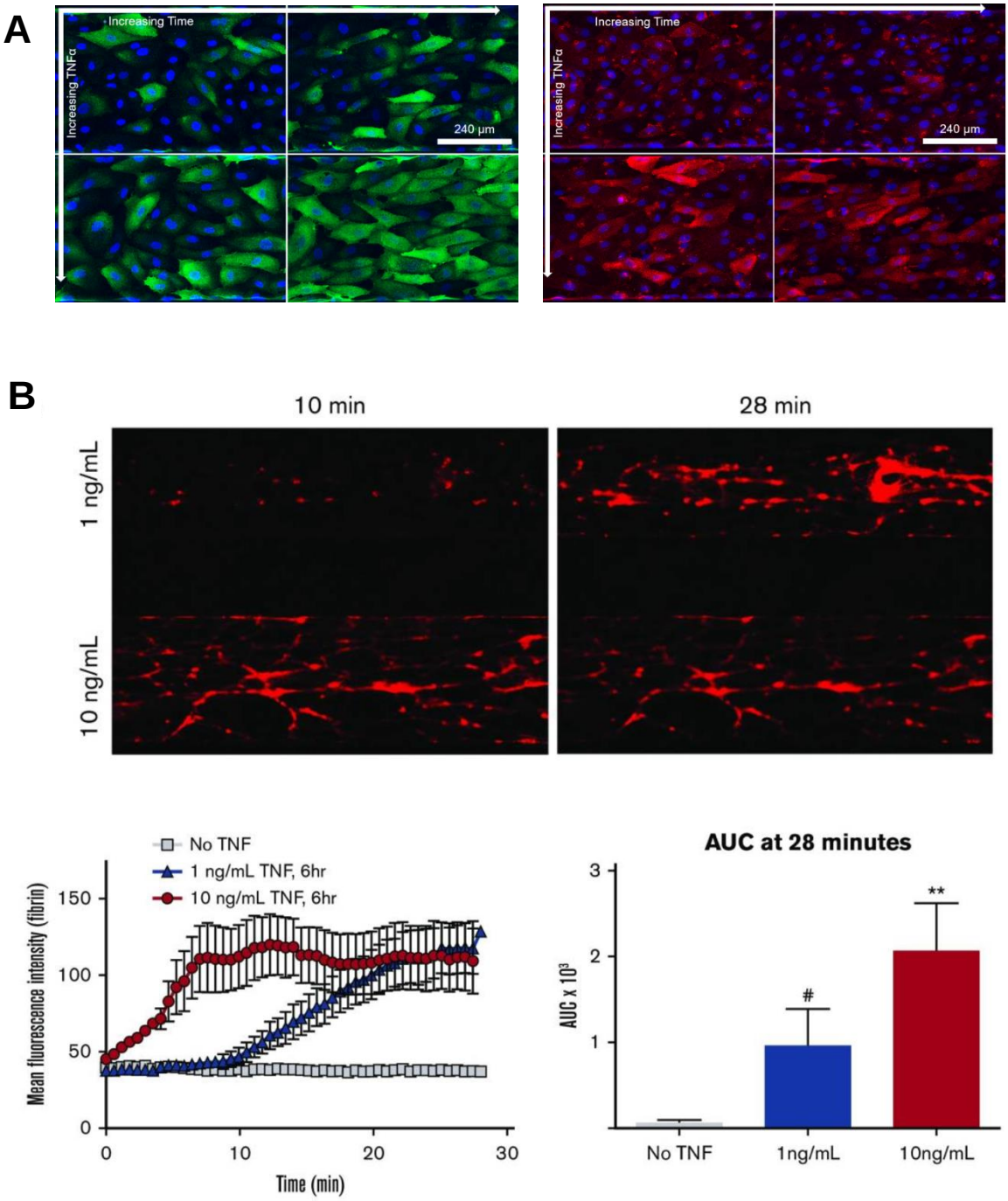
A
Increasing Time
Increasing TNFα
240 µm
Increasing Time
Increasing TNFα
240 µm
B
10 min
28 min
1 ng/mL
10 ng/mL
No TNF
1 ng/mL TNF, 6hr
10 ng/mL TNF, 6hr
Mean fluorescence intensity (fibrin)
150
100
50
0
0
10
20
30
Time (min)
AUC at 28 minutes
AUC x 10³
3
2
1
#
**
No TNF
1ng/mL
10ng/mL

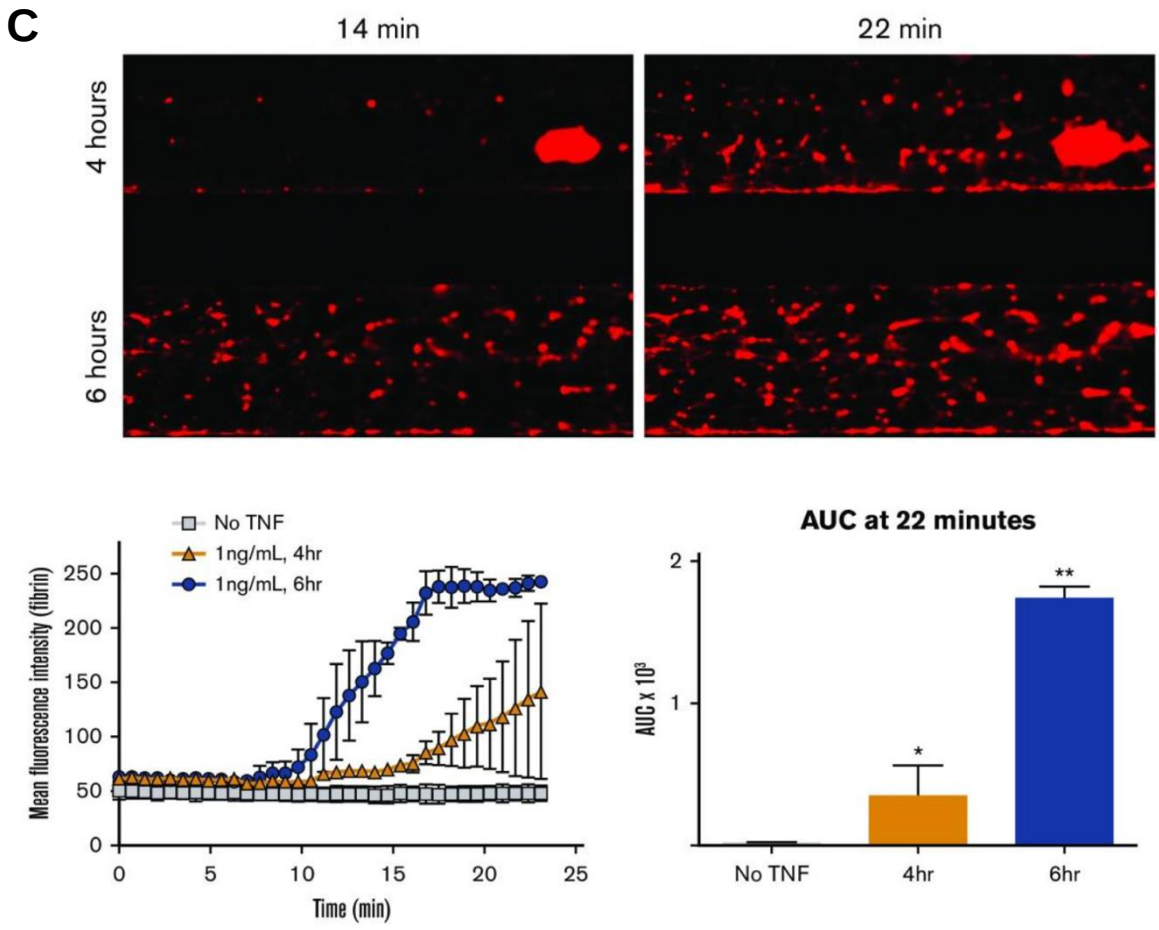

Figure 2.5. Inflammatory thrombosis model displays changes in surface proteins and fibrin deposition dependent on TNFα concentration and time of exposure.

(**A**) Displays fluorescent confocal images showing increases in ICAM-1 (left, green signal) and VCAM-1 (right, red signal) in a TNFα (1-10 ng/ml) and time dependent (2-6 hours) manner. (**B** and **C**) Displays how the accumulation of fibrin varies with (**B**) increasing concentration of TNFα (1 versus 10 ng/ml, each for 6 hours) and (**C**) duration (4 hours versus 6 hours, each 1 ng/ml) of TNFα preactivation; fibrin deposition occurs more quickly with increased TNFα or prolonged channel exposure. Top panels show representative fluorescent images at various time points. Left panels show mean fluorescent intensity

versus time, with mean ± standard error of the mean (SEM) shown for N = 2 channels for control (no TNF) groups and N = 3 channels for each experimental group. Right panels shows AUC analyses. *P < 0.05 versus control; **P < 0.05 versus each other condition; #, not significant (P = 0.14). Fibrin deposition was monitored via red fluorescent anti-fibrin monoclonal antibody during perfusion of whole blood through TNFα-activated endothelialized channels at shear stress of 5 dynes/cm^2. Video stills taken at 10x magnification.

Chapter 3 – Endothelial antigen assembly leads to thrombotic complications in heparin-induced thrombocytopenia

This chapter presents work featured in the article:

Hayes, et al., (2017) *Journal of Clinical Investigation 127(3):1090-1098*

Abstract

HIT is a prothrombotic disorder initiated by antibodies against complexes between hPF4 and heparin. A better understanding of the events in Steps 2 and 3 of HIT that start and propagate the prothrombotic state may improve approaches to antithrombotic management. Here, we visualized thrombus formation in an in vivo murine model and an endothelialized microfluidic system that simulate the pathogenesis of HIT. hPF4 released from platelets predominantly bound to peri-injury endothelium and formed HIT antigenic complexes that were dissociated by heparin. In mice expressing both hPF4 and human FcγRIIA, infusion of KKO increased fibrin and platelet deposition at sites of injury, followed immediately by antigen formation on proximate ECs. After a few minutes, HIT antigen was detected within the thrombus itself at the interface between the platelet core and the surrounding shell. We observed similar results in the humanized, endothelialized microfluidic system. hPF4 and KKO bound preferentially to photochemically-injured endothelium at sites where surface glycocalyx was reduced. These studies support the concept that the perithrombus endothelium is a key site of HIT antigen assembly in Steps 2 and 3. This suggests that disrupting antigen formation along the endothelium or protecting the endothelium may provide a therapeutic opportunity to prevent thrombotic complications of HIT, while sparing systemic hemostatic pathways.

Introduction

HIT is an iatrogenic disorder initiated by antibodies directed against a complex between a positively charged chemokine, hPF4, and heparin[81] that can lead to limb- and life-threatening arterial or venous thrombi[82], which often occur at sites of vascular injury[83]. HIT remains a common and serious disorder, even though the use of unfractionated heparin has been restricted to settings such as cardiopulmonary surgery[84,85], where it remains the anticoagulant of choice[86]. Present-day management with intense anticoagulation has not reduced the incidence of death or amputation, provides substantial, but incomplete, protection against recurrent thromboembolism, and is associated with a risk of bleeding for which antidotes are not available[87]. A better understanding of the pathobiology of HIT might lead to novel disease-specific approaches that prevent immune complex–mediated thrombus formation and propagation, with less reliance on intense systemic anticoagulation.

We have proposed a model to help explain the inordinate risk of thrombosis in patients with HIT compared with the thrombosis risk with other antibody-induced thrombocytopenias[50,88]: PF4 released from activated platelets binds to surface GAGs on intravascular and vascular cells. Infused heparin, which has a higher affinity for PF4 than for other GAGs, removes surface-bound PF4, forming circulating antigenic PF4-heparin complexes that fix complement and bind to CD21 on circulating antigen-presenting B cells[89]. PF4 also forms antigenic complexes with GAGs on the surface of platelets[88], monocytes[50], and neutrophils[90], leading to cell activation via Fc receptors[91], which promotes the generation of thrombin and other prothrombotic pathways[92].

ECs are targeted by HIT antibodies, at least in vitro[93–95], but the mechanism and in vivo relevance are unclear. The endothelium is covered by a complex surface layer termed the glycocalyx, which contains heparan sulfate–rich proteoglycans, glycoproteins,

and associated plasma proteins[17,96] that would be predicted to bind PF4 with greater affinity than the platelet surface. Binding of HIT antibody to cultured ECs induces platelet adhesion and expression of TF[94], but there is little direct evidence that HIT antibodies impair the natural antithrombotic properties of the endothelium in more biologically relevant models.

The spatial and temporal events that initiate thrombus development in HIT are not well delineated, but are potentially of considerable import. Studies of platelet degranulation in the cremaster arteriole laser injury model by our group and others[97–99] showed that the release of PF4 from platelets activated within a growing thrombus is likely to develop within the compacted core after a 2- to 3-minute delay and then expand outward[99]. This would suggest that this high local concentration and sequestration of PF4 would lead to antigen formation on platelets within the core and the surrounding shell in preference to circulating leukocytes or endothelium and that HIT-associated antibodies must penetrate the core to propagate platelet-mediated thrombus extension. However, in HIT, we posit that antigen assembly occurs on multiple cell surfaces including monocytes, neutrophils, and ECs. This difference is important, because one places the emphasis on interrupting platelet-platelet interactions, while the other suggests the value of therapies targeted to ECs, among other cell types.

In this study, we used a previously described passive immunization model of HIT in mice double-transgenic for human PF4 and FcγRIIA (referred to hereafter as hPF4^{+}/FcγRIIA^{+})[50,56] and the cremaster arteriole laser injury model[100] to study in situ thrombus development in HIT. We extended these in vivo findings by using endothelialized microfluidic chambers, which allowed us to introduce localized hematoporphyrin-based photochemical injury to study the contribution of activated endothelium in a humanized system. Our data show that the perithrombus endothelium is a predominant site of HIT

antigen formation, surprisingly at sites where the glycocalyx is depleted, followed by lower levels of antigen expression at the interface between the thrombus core and shell. These studies shift the focus of studies on HIT pathogenesis and intervention to factors that regulate antigen assembly and the thrombotic consequences of antibody binding to the endothelium, which is the core of this thesis and addressed in the subsequent chapter.

Methods

Mice and human samples.

Transgenic mice expressing platelet-specific hPF4[101] (hPF4^{+}) and/or human FcγRIIA expressing its R^{131} isoform[102] (FcγRIIA^{+}) were studied. All transgenic mice were on a *Cxcl4*$^{-/-}$ background[103], as murine PF4 is not targeted by HIT-associated antibodies[47]. This knockout setting, common to all the mice studied, is not specified hereafter. Genetic alterations were confirmed by the appropriate PCR analyses[101,102]. Mice were studied at 6 to 10 weeks of age. Only male mice were studied for the cremaster vessel injuries; however, we have not noted any prior sex difference in thrombosis in the passive immunization HIT murine model using a photochemical injury model[50].

Human blood (10–25 ml) from healthy volunteers for in vitro studies was drawn by gravity through a 19-gauge butterfly into sodium citrate (Sigma-Aldrich; 0.38% final concentration). Blood samples were stored at room temperature and used within 1 hour of being drawn. Deidentified plasma samples were obtained from patients who had a high pre-test probability of HIT on the basis of their clinical history[104], a positive PF4/heparin ELISA, and a positive serotonin release assay[105]. For plasma samples from healthy donors, whole blood was centrifuged (200 *g*, 15 minutes), followed by centrifugation (2,000 *g*, 15 minutes) of the resultant platelet-rich plasma.

Heparins, antibodies, pooled IgGs, and other labeled probes.

Unfractionated porcine heparin (BD Biosciences) and low-molecular-weight heparin (enoxaparin; Novaplus) were used in this study. KKO, a mouse IgG $2b_K$ anti-hPF4/heparin monoclonal antibody, and TRA, a monoclonal IgG isotype control antibody [47], were purified from hybridoma supernatants. $F(ab')_2$ fragments of the monoclonal anti-mouse CD41 antibody MWReg30 (BD Biosciences) were used to detect murine platelets in the cremaster laser injury model. Anti–fibrin 59D8 monoclonal antibody was provided by Hartmut Weiler of the BloodCenter of Wisconsin (Milwaukee, Wisconsin, USA)[106]. Annexin V labeled with Alexa Fluor 647 was purchased from ThermoFisher Scientific. Recombinant FXa labeled with Alexa Fluor 488 was provided by Rodney Camire of the Children's Hospital of Philadelphia (CHOP). Mouse anti-human P-selectin antibody (clone CTB201) was purchased from Santa Cruz Biotechnology. Polyclonal rabbit anti-human VWF antibody was purchased from Dako. hPF4 was visualized using polyclonal rabbit anti-hPF4 antibody (abcam). All antibodies were either labeled using Alexa Fluor antibody–labeling kits according to the manufacturer's instructions or species-appropriate Alexa Fluor–conjugated secondary antibodies (all from ThermoFisher Scientific). IgG was isolated from plasma from HIT patients and healthy donors using protein G agarose (Pierce, ThermoFisher Scientific).

Cremaster laser injury studies.

Intravital microscopy was performed as previously described[107]. Vascular injury was induced with an SRS NL100 pulsed nitrogen dye laser (440 nm) focused on the vessel wall through the microscope objective. Arterioles of 20 to 40 μm diameter were selected, and the laser was pulsed until the vessels were perforated and a small number of red blood cells escaped. Antibodies and unfractionated porcine heparin were infused as 100-

μL boluses via a catheter placed into the jugular vein. Widefield and confocal microscopy were performed as described previously[98]. Data were collected and widefield time-lapsed images of platelet and fibrin accumulation were analyzed using Slidebook 6.0 (Intelligent Imaging Innovations). Confocal *Z*-stacks were analyzed using Volocity 6.3 (PerkinElmer). hPF4$^+$, FcγRIIA$^+$, and hPF4$^+$/ FcγRIIA$^+$ mice were studied. We studied 1–10 injuries per mouse during a maximum experimental time of 1 hour.

Endothelialized microfluidic studies.

Microfluidic studies were performed using a BioFlux 1000 Controller (Fluxion) with an attached heating stage set to 37°C as described previously[108]. The BioFlux controller was used in conjunction with a Zeiss Axio Observer Z1 inverted microscope equipped with a motorized stage and an HXP-120 C metal halide illumination source. The microscope and acquisition were controlled using BioFlux Montage software with a MetaMorph-based platform (Molecular Devices). HUVECs and adult human aortic endothelial cells (both from Lonza), at passage 3–4 (5×10^6 cells), were seeded onto fibronectin-coated (50 μg/ml, Sigma-Aldrich) channels of 48-well BioFlux plates allowed to adhere, then cultured at 37°C under 5% CO_2 in EC growth media (Lonza) until they reached confluency.

A HIT-like state was induced by adding KKO (10 μg/ml) to sodium citrate–anticoagulated whole blood from healthy donors immediately before infusion. Platelets in the whole blood were labeled by incubating the blood with 2 mM calcein AM (Thermo Fisher Scientific) for 20 minutes prior to infusion. To cause photochemical injury without disrupting the EC lining, hematoporphyrin (50 μg/ml final concentration; Sigma-Aldrich) was also added to the whole blood prior to infusion[69]. Channels were exposed to blue light using the HXP-120 C light source with 475-nm excitation and 530-nm emission filters, allowing real-time, concurrent visualization of calcein AM-loaded platelets and reactive

oxygen species (ROS) generation from hematoporphyrin. An exposure time of 50 msec at the highest intensity setting on the light source was used for all experiments. The blood was recalcified immediately before infusion with calcium chloride (11 mM final concentration). Infusion into endothelialized channels was done at a rate of 10 dynes/cm^2. Following injury, channels were washed with PBS and fixed with 2% paraformaldehyde (BD Biosciences) for confocal studies of P-selectin, PF4, and KKO. To measure the glycocalyx thickness, HUVECs lining the channels were stained with 1 μg/ml DyLight 488–labeled *Lycospersicon esculentum* lectin (Vector Laboratories) for 20 minutes prior to fixation[109]. EC nuclei were visualized after staining with 5 μg/ml Hoescht 33342 (ThermoFisher Scientific) for 20 minutes. Stained channels were imaged with a Zeiss LSM 710 laser scanning confocal microscope. Data were analyzed using Slidebook 6.0 for photochemical injuries or Volocity 6.3 (PerkinElmer) for confocal images acquired after fixation.

Statistics and human and animal Institutional permission.

Differences between 2 groups were compared using a 2-sided Student's *t* test or a Mann-Whitney *U* test. Differences between more than 2 groups were determined by 2-way ANOVA with Sidak's correction for multiple comparisons. Occlusion studies were compared using a 2-sided Fisher's exact test. Statistical analyses were performed using Microsoft Excel 2011 and GraphPad Prism 6.0 (GraphPad Software). Differences were considered significant when *P* values were less than or equal to 0.05.

All animal procedures were approved by the IACUC of the CHOP and in accordance with NIH guidelines (*Guide for the Care and Use of Laboratory Animals*. National Academies Press. 2011.) and the Animal Welfare Act. Human blood was collected after signed, informed consent was provided by healthy donors, and approval

for studies using human blood was obtained from the CHOP Institutional Human Review Board in accordance with Declaration of Helsinki principles.

Results

Distribution of HIT antigen after nonimmune vascular injury in hPF4$^+$ mice.

We previously proposed that a key step in the development HIT was the formation of antigen that occurs when positively charged hPF4 binds to negatively charged GAGs found on many cell surfaces[88]. This model predicts that HIT antigen will form at sites of vascular injury, even in the absence of HIT-associated antibodies. We tested this hypothesis in vivo using a cremaster arteriole laser injury model in hPF4$^+$ mice. Following injury, hPF4, detected using a polyclonal anti-hPF4 antibody, and HIT antigen, detected using the HIT-like monoclonal antibody KKO[47], were present almost immediately on widefield microscopy, and the involved area expanded over the ensuing 3 minutes (**Figure 3.1, A** and **B**, respectively). This result demonstrates that hPF4 released from hPF4$^+$ platelets as a result of thrombus formation accumulates locally in the form of PF4-containing complexes that can be recognized by HIT antibody prior to the development of HIT.

We had reported that high doses of heparin attenuated the severity of thrombocytopenia in hPF4$^+$/ FcγRIIA$^+$ mice [88]. We postulated that this occurred because heparin can dissociate antigenic complexes from platelet surfaces at these concentrations[88], given its higher affinity for hPF4 than for surface GAGs[110]. In turn, this generates the circulating hPF4-heparin complexes needed to induce an immune response[110,111]. Therefore, we asked whether infusing unfractionated or low-molecular-weight heparin into hPF4$^+$ mice would mobilize prebound PF4 and decrease retention of the HIT antigen at the site of thrombus formation. Binding of KKO to the site of thrombus

formation decreased proportionally with the dose of either unfractionated heparin (**Figure 3.1C**) or low-molecular-weight heparin (**Figure 3.2**) infused into hPF4^{+} mice. Importantly, however, even when mice were given 1,000 U/kg unfractionated heparin – a dose approximately 10-fold higher than therapeutic doses [112] – about 25% of the HIT antigen remained, suggesting that the vasculature continues to be a potential target for immune injury. Also of note, mice that did not receive heparin had the highest level of local HIT antigenicity, with an approximate 2-fold increase in HIT antigen compared with mice receiving a dose in the range normally given clinically (100 U/kg)[113].

Study of the prothrombotic state in a murine HIT model.

We have previously shown that infusion of KKO or HIT-associated IgG (HIT-IgG) induces thrombocytopenia and a prothrombotic state in hPF4^{+}/ FcγRIIA^{+} mice[50,56,88]. We recapitulated the prothrombotic state in the cremaster arteriole laser injury model. Injection of KKO into hPF4^{+}/FcγRIIA^{+} mice enhanced platelet and fibrin accumulation in hPF4^{+}/FcγRIIA^{+} mice, but not in hPF4^{+} mice or in hPF4^{+}/FcγRIIA^{+} mice exposed to the isotype control monoclonal antibody TRA[47] (**Figure 3.3A**).

Patients with HIT may be predisposed to develop thrombi at sites where vessels have been injured by catheters[83]. To simulate this sequence in the cremaster model, we induced a thrombus in hPF4^{+}/FcγRIIA^{+} mice, followed 5 minutes later by infusion of KKO or HIT-IgG. Preexisting thrombi expanded in mice given KKO or HIT-IgG, but not control antibodies (**Figure 3.3B**). These data may underestimate the severity of the prothrombotic state because virtually all the vessels became occluded, limiting further thrombus expansion (**Table 3.1**). Neither TRA nor normal IgG control infusions led to renewed growth of thrombi or vascular occlusion (**Figure 3.3B** and **Table 3.1**). Of note, thrombus regrowth began immediately after KKO was infused, and accelerated with time,

demonstrating that a preexisting thrombus provides a potent nidus for expansion, leading to vascular occlusion in the setting of HIT antibodies.

Analysis of thrombus development in HIT by confocal microscopy.

To begin to understand why thrombus regrowth was enhanced in HIT, we used confocal microscopy to examine the initial steps in thrombus formation following laser-induced arteriole injury in animals preinfused with KKO. Remarkably, the predominant site of KKO binding was the endothelium underlying and surrounding the thrombus, extending both upstream and downstream from the site of thrombosis (**Figure 3.4A**). The upstream binding appeared to be related to turbulent blood flow in this area. By 5 minutes after injury, KKO began to appear on platelets within the clot, which intensified over time at the boundary between the tightly packed core and surrounding looser shell of the thrombus[99] (enlarged image in **Figure 3.4A** and **Figure 3.4B**). We posit that this hemispheric zone of antigen was formed by the slow spread of α-granule release outward within the core until reaching the core-shell interface[99]. Our studies suggest that more loosely bound platelets on the surface of the thrombus or caught in turbulent flow around the thrombus may make a more immediate and more significant contribution to the detectable PF4 in the thrombus. Moreover, the PF4 released from surface-bound platelets probably adheres better to the peri-injury endothelium, with its glycocalyx, which is rich in high-affinity heparan sulfate and dermatan sulfate[96], rather than to the platelets within the thrombus that express chondroitin sulfate on the surface, which has lower affinity for heparin[114,115]. The platelet-bound PF4 is likely swept downstream. The overlap of injured endothelium and KKO binding for annexin V is shown in **Figure 3.4B** and for FXa in **Figure 3.5**

Infusion of KKO prior to laser injury in hPF4^{+}/ FcγRIIA^{+} mice further increased the size of the platelet-rich clot, and the total amount of HIT antigen in the perithrombus

endothelium increased by approximately 3-fold compared with that detected in controls (**Figure 3.4C**). We observed similar increases in binding of annexin V and FXa to the perithrombus endothelium, suggesting that HIT antibodies exacerbated endothelial injury that could potentially cause a feed-forward cycle involving PF4-antigen formation, antibody binding, new injured endothelium, and spreading thrombosis.

Microfluidic studies of thrombosis in HIT.

The in situ cremaster laser injury model enabled us to study the details of thrombus formation. However, the model is not fully humanized, and it is difficult to deduce the separate contributions from individual cellular components. To examine the role of the endothelium in HIT in a fully humanized context, we utilized the endothelialized microfluidic set up described in Chapter 2. In these studies, we utilized the microfluidic model with the hematoporphyrin injury to induce an upstream localized injury during the perfusion of human blood containing hematoporphyrin (**Figure 3.6A**). As described in Chapter 2 and expanded on here, platelets adhered to the injured part of the channel, but not downstream (**Figure 3.6B**). Released PF4 was found surrounding platelet clumps and along the endothelium within the injured area. A decreasing gradient of PF4 binding to "uninjured" endothelium downstream of the injury was also in evidence (**Figure 3.6, B–D**). PF4 did not escape between injured ECs to the abluminal surface (**Figure 3.6D**), a finding that was consistent with retention of cell-cell contact.

HIT was induced by adding KKO and hematoporphyrin to infused human whole blood prior to photochemical injury. KKO induced a significant increase in platelet adherence to HUVECs in the injured area compared with that observed with TRA (**Figure 3.7A**) and had a similar effect on similarly prepared adult human aortic endothelium (**Figure 3.8**). Downstream of the injury, no difference was noted between KKO and TRA

exposure in the uninjured endothelium (**Figure 3.7B**). KKO also caused an increase of approximately 7-fold in PF4 binding to the injured endothelium compared with binding to the uninjured area, which was accompanied by an increase of approximately 16-fold in KKO binding to the injured endothelium compared with uninjured endothelium (**Figure 3.7C**). The injured endothelium showed an increase of approximately 50-fold in P-selectin surface expression ($P < 0.0001$, **Figure 3.7D**) and a decrease of approximately 55% in glycocalyx staining by lectin compared with uninjured endothelium ($P < 0.01$, **Figure 3.7D**). Thus, the increase in binding of PF4 to the endothelium correlated with the loss of glycocalyx and its associated GAGs, as had been seen following other EC injuries[17,116]. Consistent with the results obtained with infusion of KKO, infusion of HIT-associated IgG (300 μg/ml) along with whole blood led to occlusion of 6 of the 6 channels studied compared with 1 of 6 channels exposed to control IgG (P= 0.02, **Table 3.1**).

Discussion

HIT differs from other antibody-mediated thrombocytopenias by its propensity for significant thromboembolism[82,117]. We have attributed the prothrombotic state to the concurrent activation of multiple cell types by immune complexes. Platelets are dually activated by immune complexes through FcγRIIA[91] and by monocyte-generated thrombin[108]; however, to date, the proposed involvement of the endothelium is based entirely on in vitro findings using cultured cells.

To better understand the prothrombotic nature of HIT in Steps 2 and 3 of the proposed pathogenic pathway, we performed video examination of thrombus formation in HIT both in vivo and in vitro. These in vivo cremaster studies involved laser-induced thrombi rather than spontaneous thrombi, but they allowed a detailed temporal analysis of events. We anticipate that the results of future similar studies of spontaneous thrombi in

HIT mice would be consistent with our findings. Our in vivo studies showed that released PF4 was associated with formation of the HIT antigen, as identified using KKO and by the binding of HIT-IgG to every thrombus. Infused heparin stripped this bound and antigenic PF4 away from the thrombus, decreasing surface antigenic complexes. These findings suggest that the pathogenic contribution of heparin to the development of HIT is solely the presentation of antigenic sites on PF4 to immunogenic cells and not enhancing the targeting of HIT antibodies onto thrombi. Indeed, stopping heparin may pose an increased risk of thrombosis that must be countered by instituting alternative anticoagulants[118].

Our in vivo findings also showed that soon after laser injury and thrombus formation, PF4 was localized predominantly on ECs underlying and in the immediate vicinity of the clot. It is likely that endothelium-bound PF4 originated from transiently adherent platelets within the thrombus "shell"[99] or by platelets that had undergone activation within areas of turbulent blood flow. Only minutes later did PF4 begin to appear at the core-shell interface within the platelet-rich thrombus as a result of spreading degranulation, consistent with the appearance of surface P-selectin described by several groups[98,99,119] and perhaps due to less flow-induced dissociation within the core and transition zone within the shell of the clot[99]. Our studies suggest that most α-granule proteins are released from outer layers or the exterior of the thrombus by transiently adherent platelets. Proteins that do not have a high affinity for surrounding cell surfaces are probably rapidly washed away, while those like PF4 may adhere to cells within or surrounding the thrombus.

The studies in this chapter support a scenario describing the pathogenesis of HIT, in which binding of PF4 leads to the formation of immune complexes on the endothelium, which may enhance platelet adhesion, enhance thrombin generation, and cause the release of additional PF4, which would sensitize the downstream endothelium and lead to

a feed-forward pathway that propagates thrombosis. This role would implicate ECs as a key contributor to both Steps 2 and 3 in the pathogenesis of HIT (**Figure 1.5**), which has not been previously suggested. Such a phenomenon could contribute to the vessel occlusion we observed in the HIT cremaster arteriole model (**Figure 3.3B**) and, as observed by others, to the presence of platelet-rich thrombi, resulting in the alternative name for this disorder of "white clot syndrome"[65]. Whether these extended clots are related to a recruitment of undamaged endothelium in HIT needs to be examined. If this model is correct, it will be important to identify as potential therapeutic targets the biophysical and biochemical changes in the endothelium that promote antigen and antibody binding. Moreover, these studies suggest that EC–targeted anti-inflammatory and antithrombotic drugs[120,121] might provide a rational intervention focused on the primary vortex of prothrombotic reactions that lead to thrombotic vascular occlusion.

The microfluidic photochemical injury studies, while involving a more diffuse vascular injury than did the cremaster injuries, support the conclusion that the endothelium is a predominant initial harbor for PF4 released from activated platelets and a target for HIT antibodies. While PF4 and KKO bind directly to platelets[88], monocytes[50], and neutrophils[122], we found that binding was more intense on injured ECs. This is surprising, given that the glycocalyx is highly enriched for negatively charged side chains on its constituent proteoglycans, syndecans, and glypicans[96]. These are candidate receptors for binding PF4, and one would have expected that with their loss, PF4 binding would have decreased. The loss of the glycocalyx involves multiple glycosidases or sheddases[123]. We posited that the enhanced binding to injured glycocalyx may be due to the unveiling of a novel high-affinity binding site in the glycocalyx or the release of novel binding molecules from the injured endothelium that then reside in the remaining glycocalyx. Surprisingly, when we began these studies for a specific PF4-binding target in the next chapter, we

discovered that it was VWF that was a prime target and this novel finding serves as the central focus of this thesis.

Figures

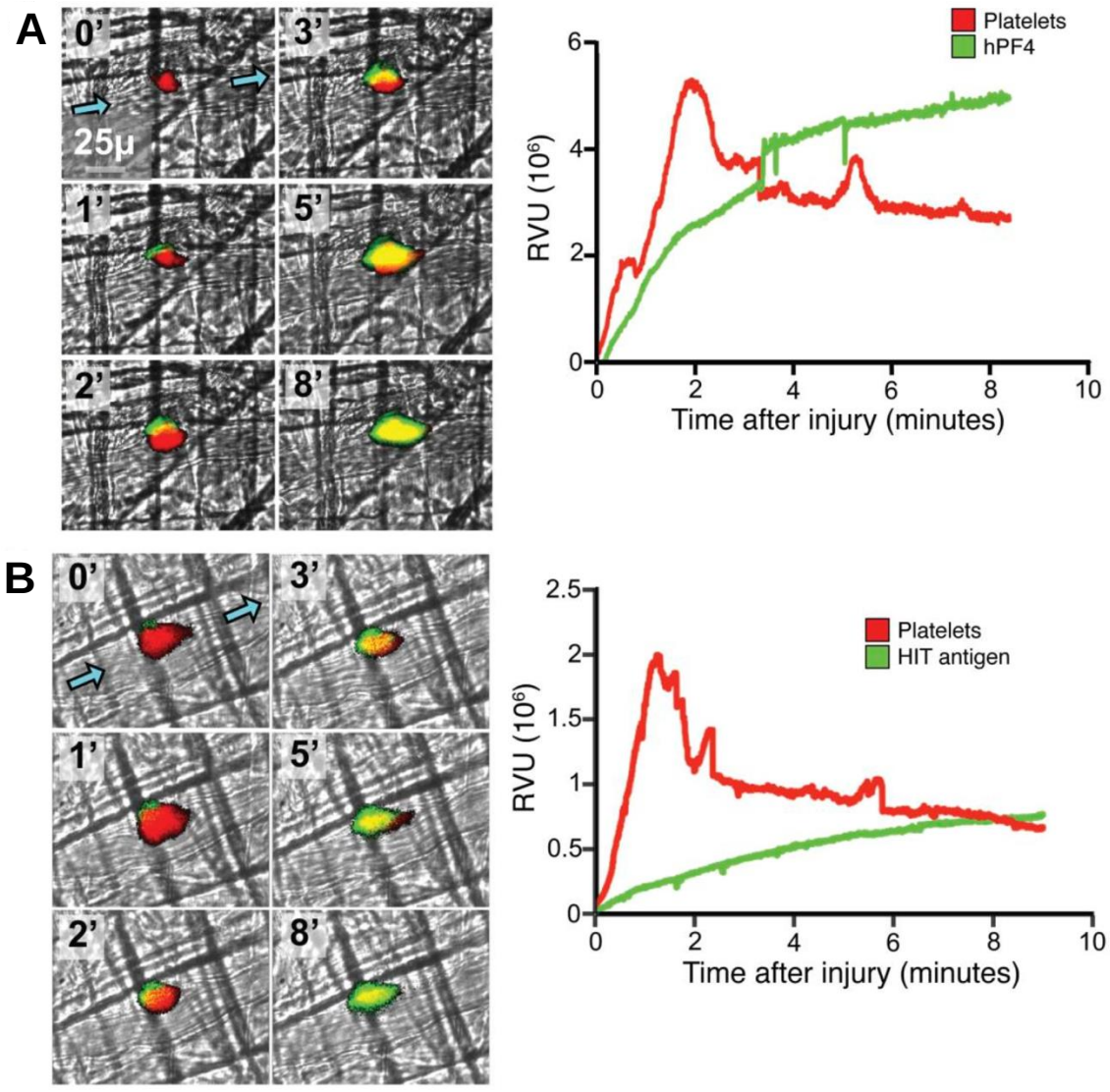
A
0'
3'
25µ
1'
5'
2'
8'
Platelets
hPF4
RVU (10⁶)
Time after injury (minutes)
B
0'
3'
1'
5'
2'
8'
Platelets
HIT antigen
RVU (10⁶)
Time after injury (minutes)

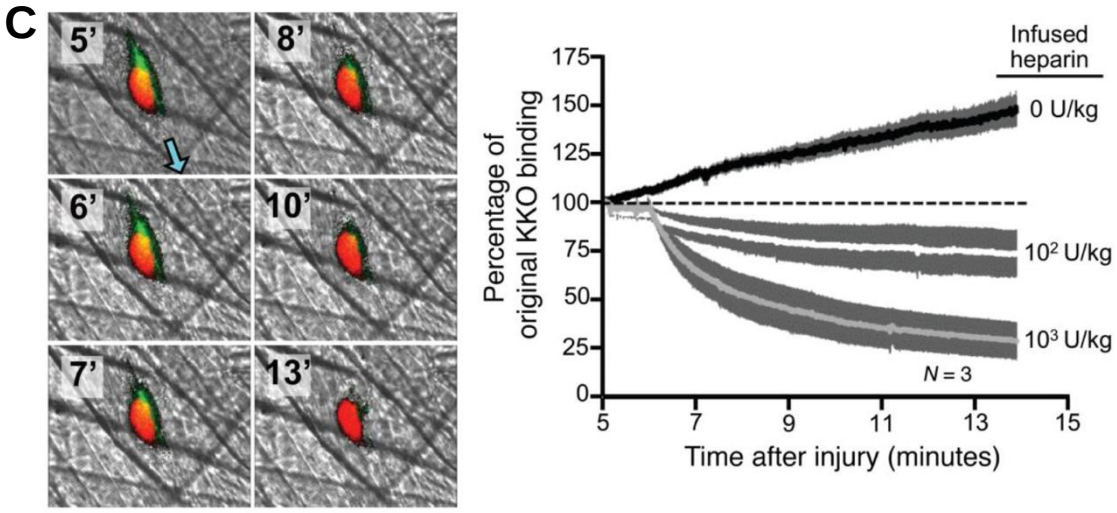

Figure 3.1. Widefield cremaster laser injury in a non-HIT hPF4+ murine model: In situ studies of hPF4 and HIT antigen distribution in thrombi.

(**A**) Representative widefield study of more than 10 cremaster laser injuries in $hPF4^{+}$ mice, with time 0 indicating the onset of injury. Images from a video of a laser injury; platelets are indicated in red, hPF4 is indicated in green, and the direction of blood flow in the vessel is denoted by blue arrows. Graph shows the accumulation of platelets and hPF4 over the study in relative value units (RVU) compared with time 0. (**B**) Same as in (A), but with green showing binding of KKO to indicate the appearance of the HIT antigen. (**C**) Representative images from an experimental video beginning 5 minutes after injury, the point at which 10^3 U/kg heparin was infused intravenously (IV). Platelets are indicated in red and KKO binding in green. The graph indicates that various doses of heparin were infused beginning 5 minutes after the cremaster injury. Percent mean ± 1 SEM for binding of KKO after heparin relative to the 5-minute time point is shown. The

dashed line represents no change in KKO binding after heparin infusion compared with the 5-minute heparin time point. Original magnification, ×60.

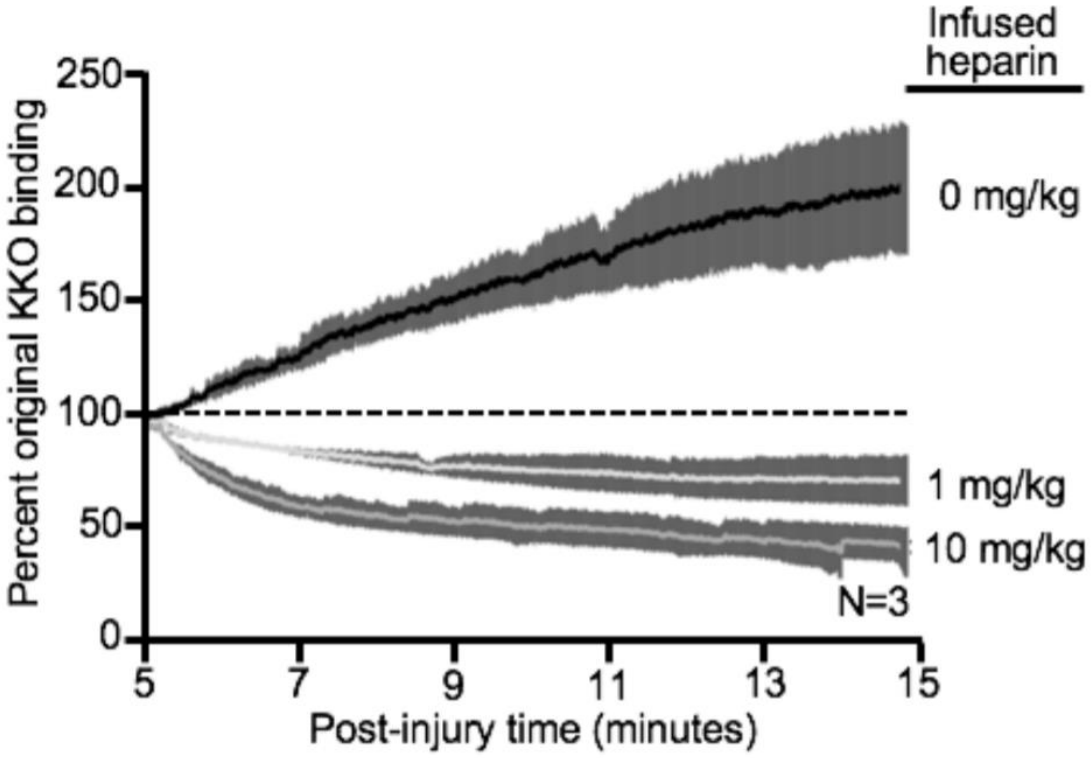

Figure 3.2. Effect of low molecular weight heparin on KKO binding to a thrombus. Effect of various doses of low molecular weight heparin infused beginning 5 minutes after the cremaster injury. Mean ± 1 SEM for binding of KKO after low molecular weight heparin was infused relative to the 5-minute time point is shown. The dashed line indicates the value of KKO binding if there were no change in KKO binding after heparin infusion compared to the 5-minute heparin time point.

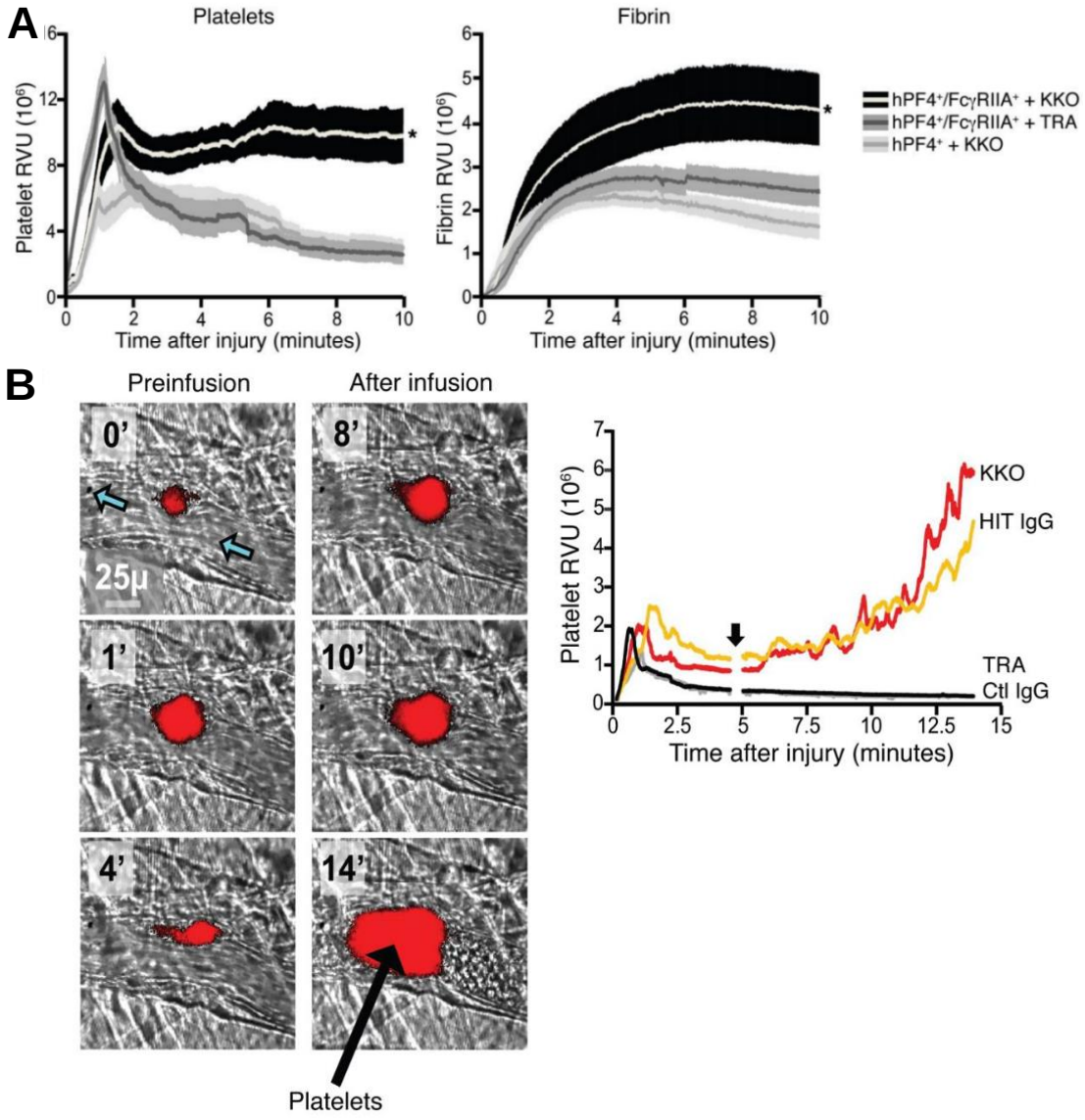

Figure 3.3. Widefield in situ studies of the prothrombotic state in a murine HIT model.

(**A**) Widefield cremaster arteriole laser injuries were performed in hPF4^{+}/FcγRIIA^{+} and hPF4^{+} mice infused with KKO or control TRA prior to injury. Platelet accumulation is shown on the left and fibrin on the right. Six mice from each arm were studied, and each mouse had five to six injuries. The AUC was calculated for each injury, then compared

between groups by a 2-tailed Mann-Whitney U test. Data represent the mean ± 1 SEM. *P < 0.05 comparing hPF4^{+}/FcγRIIA^{+} plus KKO versus either other group. (**B**) An experiment similar to the one depicted in (A), but the injury was performed at time 0, and KKO (1 μg/g, IV) was infused 5 minutes later. Images are from an experimental video, in which platelets (red) were incorporated into a thrombus 0-4 minutes before or 5-15 minutes after the infusion of KKO. Blue arrows indicate the direction of blood flow in the arteriole; black arrow denotes the growing platelet thrombus. Graph shows the mean values for platelet incorporation into thrombi, with a break in the data just before 5 minutes, when antibodies were infused (vertical arrow). Three injuries were studied in each arm. Original magnification, ×60. Ctl, control.

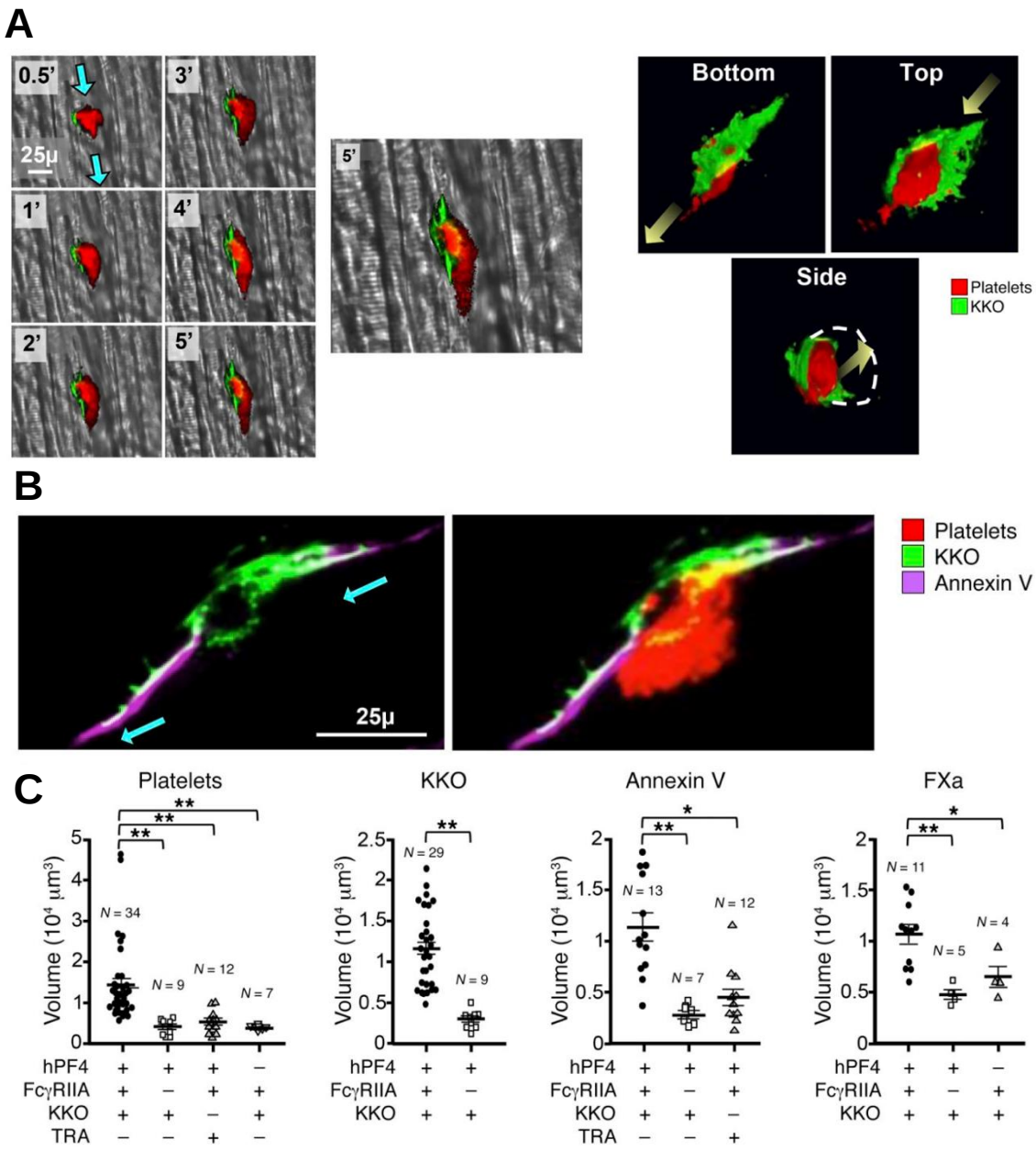

Figure 3.4 Confocal microscopic studies of a growing thrombus in HIT showing perithrombotic events.

(**A**) Confocal microscopic images showing events in a representative cremaster arteriole injury in an hPF4^{+}/FcγRIIA^{+} mouse infused with KKO. Platelets are shown in red. KKO binding is shown in green. Images on the left are from a real time experimental video

and include blue arrows showing the direction of blood flow. The image in the middle is an enlargement of the 5-minute time point, clearly showing a yellow semi-circle at the interface between the core and shell of the growing thrombus just becoming visible at 4 minutes. Images on the right show 3 different views of a 3-D reconstruction of a thrombus, with the yellow arrow indicating the direction of blood flow. The dashed white circle indicates the outline of the vessel. (**B**) Confocal microscopic images, as in (A), of another thrombus showing platelet accumulation (red) and binding of KKO (green) as well as staining with annexin V shown in purple as an indication of endothelial injury (50) and overlap with KKO binding shown in white. (**C**) Mice were preinfused with either KKO or TRA prior to creation of a thrombus. Binding of platelets, KKO, annexin V, and FXa to sites of vascular injury is shown. Data from the individual studies are shown as well as the mean ± 1 SEM (wide and narrow horizontal lines, respectively). The number of injuries studied for each parameter is indicated. *$P < 0.001$ and **$P < 0.0001$, by 2-way ANOVA. Original magnification, ×60.

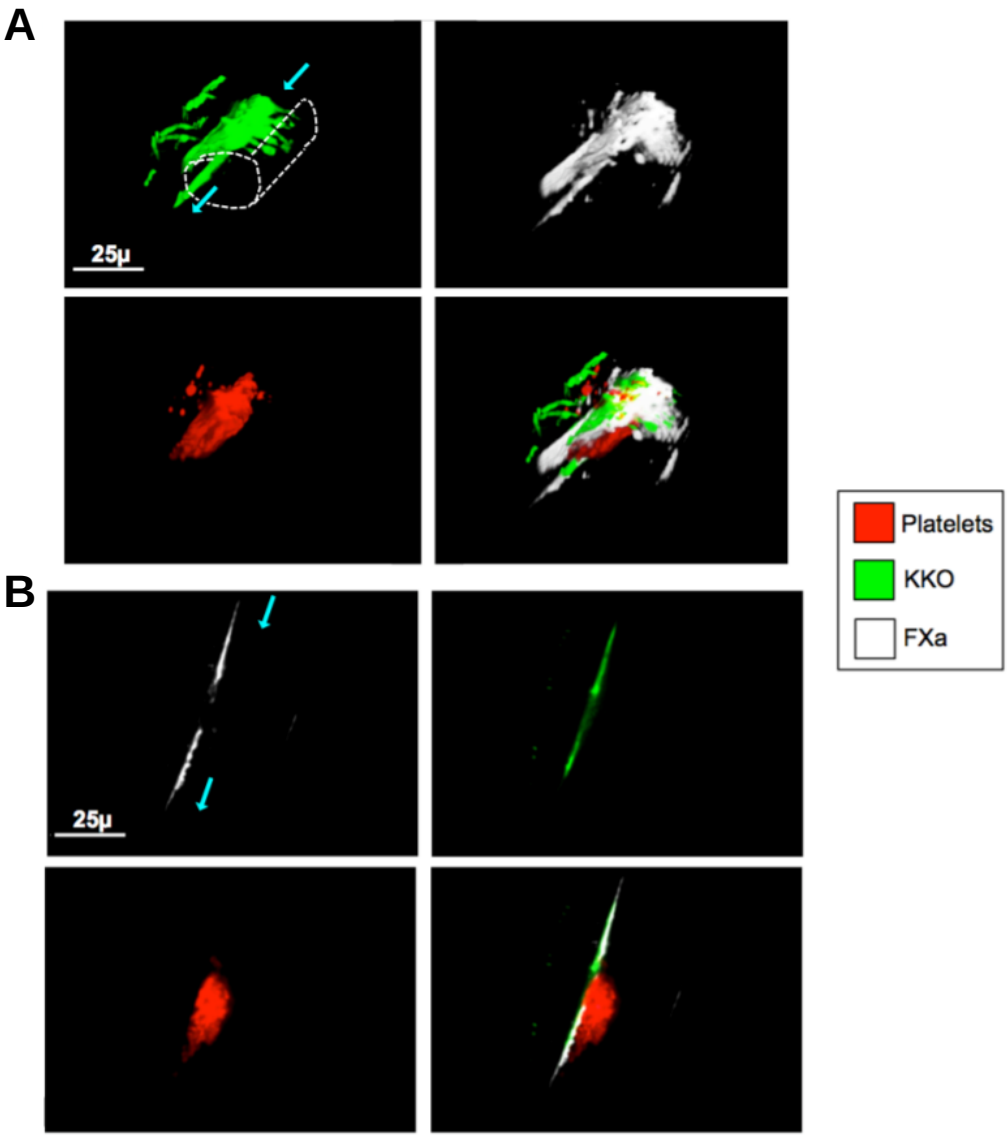

Figure 3.5. Overlap in binding of KKO and FXa as an indicator of activated endothelium at the site of thrombosis.

(**A**) and (**B**) are confocal images of a representative cremaster laser injury thrombus in a HIT mouse done as in Figure 3.4. (A) is the reconstructed image shown from the top/front with KKO binding in green (top left image), FXa binding in white (top right), accumulated platelets in red (bottom left) and a merged image (bottom right). The direction of blood

flow is indicated by the arrows in the KKO alone image as is the magnification. A dotted white outline of the vessel is also included in this image for better visualization. (B) is a more lateral single cut through the same thrombus as in (A), further showing that the KKO binding and FXa binding are at the base of the clot and overlap with directional arrows and magnification in the top left image.

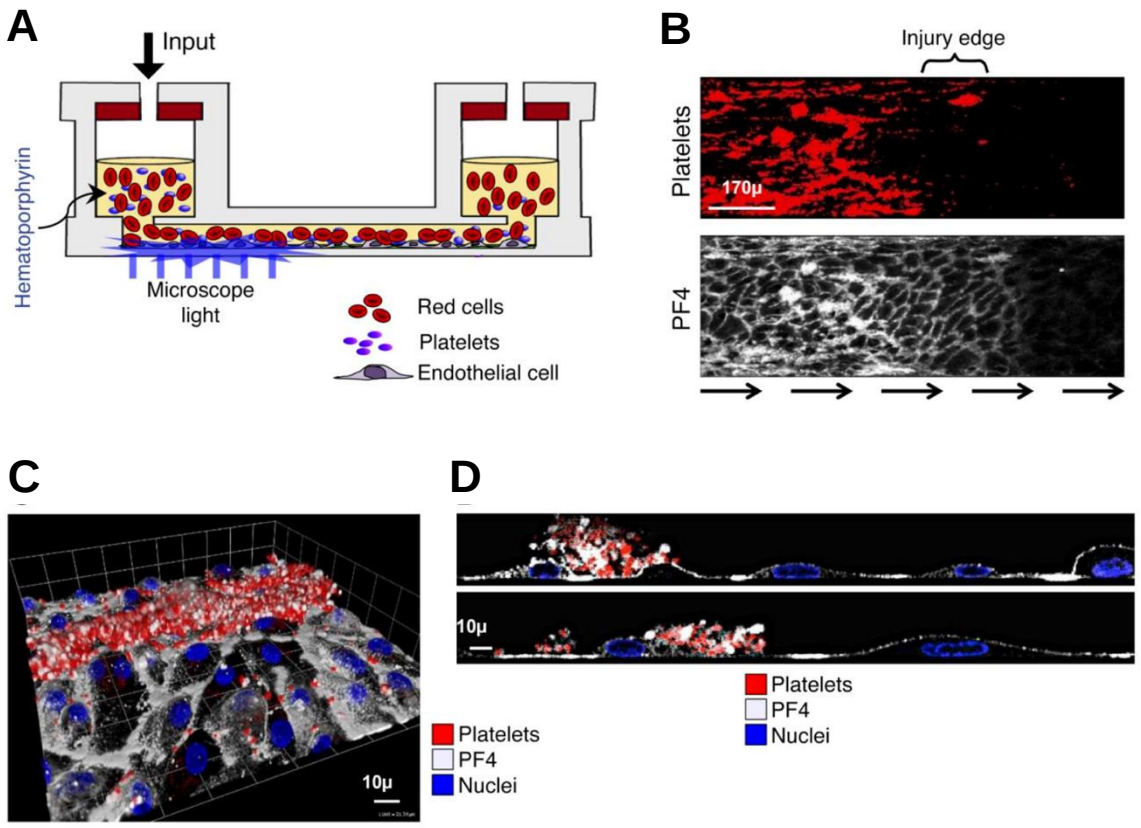

Figure 3.6. Studies of endothelialized microfluidic channel after photochemical injury.

(**A**) Schematic of microfluidic chamber with whole blood containing hematoporphyrin flowing into an EC–lined channel, with a light source to injure the endothelium. (**B**) Adhesion of platelets (red, top) and PF4 (white, bottom) at the junction between the injured and uninjured area from a representative study with infused blood, as in (**A**). (**C**) and (**D**) Confocal images of the injured endothelium. (C) Top-down image of adherent platelets and released PF4 in the photochemically injured area. (D) Same image as in (C), in a sagittal view. Original magnification, ×10 (B) and ×40 (C) and (D).

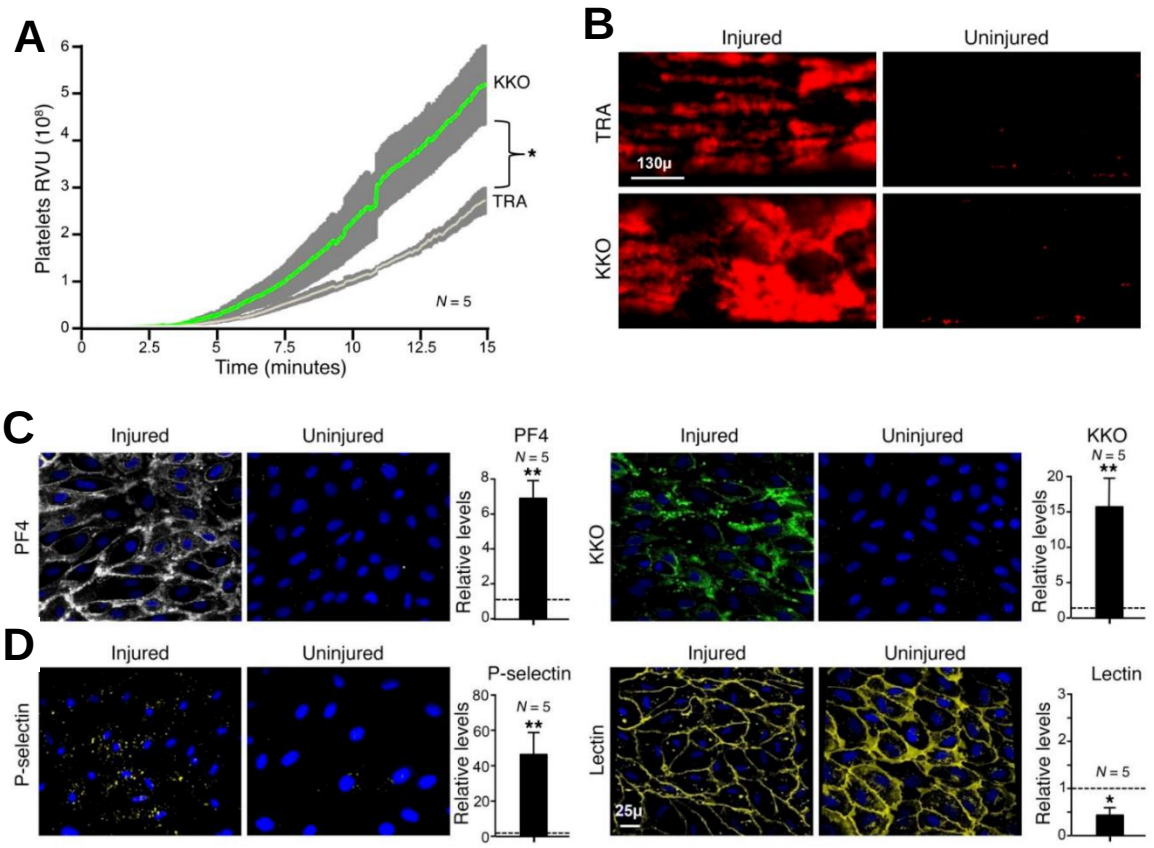

Figure 3.7. Studies of HIT in the endothelialized microfluidic channel photochemical injury system.

(**A**) Platelet accumulation along HUVECs after photochemical injury perfused for 15 minutes with whole human blood containing either KKO or TRA. Data represent the mean ± 1 SEM. *P < 0.0001, for KKO versus TRA exposure by 2-tailed Student t test. (**B**) Images demonstrate platelets bound to representative fields of photochemically injured and uninjured areas of the channels shown in (A) from whole blood containing TRA or KKO. (**C**) Images of representative uninjured and injured areas and graphs of overall comparative measurements showing enhanced binding in injured versus uninjured areas of PF4 (white) and KKO binding (green) after infusion of whole blood, as in (A). The mean relative binding for injured versus uninjured endothelium ± 1 SEM is shown. *P < 0.01 and

P < 0.001, by 2-sided Student's t test for injured versus uninjured areas, with an expectation of 1 and no change in binding (dashed line). (D**) Same as in (**C**), except for P-selectin staining (yellow) and lectin binding (yellow) in injured endothelium versus the downstream uninjured area. Lectin staining of the endothelium was decreased after injury. Original magnification, ×20.

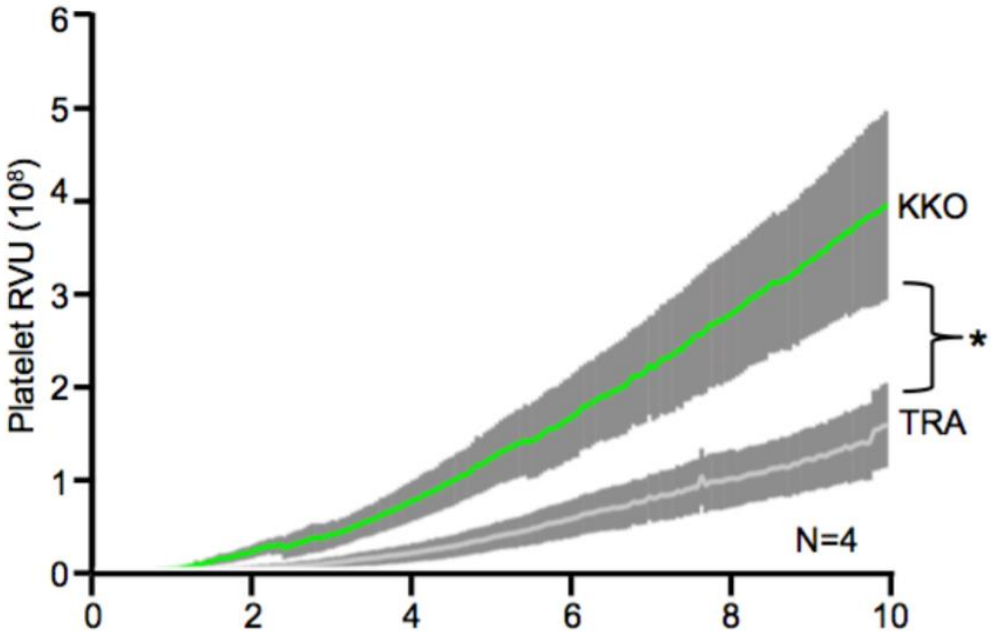

Figure 3.8. Thrombus growth during photochemical injury in the presence of KKO. Similar studies as in Figure 5A, but microfluidic chamber coated with adult human aortic ECs. Platelet accumulation along endothelium after photochemical injury perfused with whole human blood containing either KKO or TRA for 10 minutes. Mean ± 1 SEM are shown.*P<0.01.

Tables

	KKO (1 μg/g)	HIT IgG (50 μg/g)	TRA (1 μg/g)	Control IgG (50 μg/g)
No. of injuries	33	6	22	7
No. of occluded vessels	24	6	0	0
% of occluded vessels	72.7%[A]	100%[B]	0%	0%

Table 3.1. Secondary growth of thrombi in hPF4$^+$/FcγRIIA$^+$ mice leading to an occluded vessel.

Cremaster arterioles were injured by laser, and the accumulation of platelets was assessed. Five minutes later, KKO or TRA or HIT IgG was infused IV at the indicated dose, and the site of injury was observed. The number of injured and occluded vessels with cessation of blood flow is indicated. ^$P < 0.0001$, comparing the outcome after KKO versus TRA by 2-tailed Fisher's exact test. $^B P < 0.001$, comparing the outcome after HIT IgG versus control IgG by 2-tailed Fisher's exact test.

CHAPTER 4 – Platelet factor 4 and von Willebrand factor form an immunogenic, prothrombotic complex in heparin-induced thrombocytopenia

This chapter presents work featured in the article to be submitted:

Johnston, et al., (2018).

Abstract

HIT is a prothrombotic, thrombocytopenic disorder that occurs in patients exposed to heparin due to the development of antibodies directed against complexes of PF4 and heparin and other polymeric molecules. We have recently shown that the perithrombus endothelium is especially targeted in HIT. Using a photochemical injury, endothelialized microfluidic system, we now show that PF4 selectively binds to released VWF strands on injured endothelium. This binding appears to be periodic along the VWF strand and to favor larger VWF strands, *raising the possibility that binding of PF4 crosslinks VWF polymers.* KKO and HIT patient plasma recognize these complexes, forming PF4-VWF-HIT antibody complexes, which, in turn, avidly bind platelets, exacerbating thrombus growth in a human whole blood microfluidic system. This increase in platelet binding can be attenuated by that blocking either the platelet FcγRIIa or the GPIb/IX receptor. HIT antibodies may stabilize PF4-VWF complexes but charge-based approaches as well as drugs that disrupt VWF oligomerization can disrupt PF4-VWF-HIT complexes. In vitro studies using dynamic light scattering further support the formation of PF4-VWF complexes. Strategies directed at blocking formation PF4-VWF complexes reduce the prothrombotic state in a passive immunization murine model of HIT. Thus, these studies identify VWF as a newly described and potentially important polymer on which HIT antigenic complexes form and propagate the risk of thrombosis in HIT even when heparin has been discontinued (Step 3). The PF4-VWF complexes contribute to the prothrombotic nature of HIT and may provide a new therapeutic target.

Introduction

HIT is initiated by antibodies targeted to complexes of PF4 and heparin[48]. HIT antibodies, through activation of various cell types such as platelets[88], monocytes[50], and ECs[43,93–95] promote the limb and life-threatening pro-thrombotic environment experienced by HIT patients. Although initiated with heparin, other polymeric molecules are capable of binding PF4 and then being recognized by HIT antibodies, including cell surface GAGs[88], DNA[124], polyphosphates[53], and bacterial wall components[125]. Notwithstanding the recent identification of these additional potentially antigenic sites, a more complete understanding of their contribution to thrombosis is needed to develop alternative treatments options for patients with or at risk for HIT[41,118].

The endothelium has been recognized to bind PF4 and become activated in the presence of HIT antibodies over thirty years ago[94]. We recently showed that both in vitro in an endothelialized microfluidic chamber and in vivo in HIT cremaster laser injury studies in a murine HIT model that HIT-like antibodies predominantly bound to peri-thrombotic endothelium that had undergone vascular injury[43]. When injured, the endothelium retracts or denudes and exposes collagen within the basal membrane[52,126–128]. The endothelium also exhibits changes to its glycocalyx, including a decrease in its thickness that may enhance access to proteins on the endothelial luminal surface[14–17]. Injured, activated endothelium also may express a diverse range of new or activated receptors and ligands, and procoagulant factors such as TF and P-selectin on their vascular luminal surface[7,34,100,129–131].

In this study, we focus on binding of PF4 to VWF, which are, in part, stored within Weibel-Palade bodies in resting endothelial cells and which are released following EC activation or injury[40,72,132]. Initial studies focused on our previously described endothelialized microfluidic model wherein we induced a localized photochemical injury

using hematoporphyrin[69,70]. Prior studies have shown that these injured endothelial cells release VWF as elongated strands under the influence of shear induced by flow[43]. We now find that these VWF strands bind PF4 and subsequently HIT antibodies. We show that in this model, platelets bind to these PF4-VWF-HIT antibody complexes and that this binding could be reduced by the FcγRIIA-blocking antibody IV.3[88,122,133] as well as the GPIbα-blocking antibody AK2[36,134,135]. In vitro studies using dynamic light scattering confirms the formation of PF4-VWF complexes. In a passive immunization murine model of HIT, photochemical injury to the carotid affirms the development of PF4-VWF-HIT antibody complexes and their contribution to thrombosis. These studies provide new insights into the prothrombotic pathways activated in HIT and extend the number of pathobiological polymeric molecules that can contribute to Step 3 in the propagation of thrombi in HIT. The clinical implications of these findings are discussed.

Methods

Human blood samples.

Deidentified samples of whole blood from healthy human volunteers with no history of a bleeding diathesis or known use of medications with anticoagulant effects was drawn by gravity through 19-gauge butterfly needles into sodium citrate (0.38% final concentration, ThermoFisher Scientific). Blood samples were maintained at room temperature and used within 1 hour of being drawn. Deidentified plasma samples were also obtained from patients determined to have HIT based on a combination of clinical assessment, HIT ELISA positivity, and positive serotonin-release assay (SRA) as described previously[44,104,105]. Similar samples from patients with low probability of HIT based on history and negative ELISA and SRA results were used as negative controls. Deidentified HUVEC (referred to ECs) were purchased (Lonza). Human blood samples

were collected after signed, informed consent from healthy donors. Approval for these studies was obtained from the CHOP Institutional Human Review Board in accord with the Helsinki Principles.

Mice and mouse blood samples.

Wildtype C57Bl6 mice and transgenic mice on a *Cxcr4* gene knockout background[103], were studied. These double-transgenic mice, previously termed "HIT mice", develop thrombocytopenia and a prothrombotic state when injected with the HIT-like antibody murine monoclonal antibody KKO or IgG isolated from patients with HIT in a passive immunization model of HIT[56,88].

Recombinant proteins and antibodies.

Recombinant hPF4 was isolated from S2 cell media using the Drosophila Expression System (Invitrogen), purified, and characterized as described[47,136]. Final protein concentrations were determined using the bicinchoninic acid protein assay (Pierce) using bovine serum albumin (BSA) as the standard. KKO, the mouse anti-hPF4-heparin HIT-like monoclonal antibody, and TRA, a monoclonal IgG isotype control antibody, were purified from hybridoma supernatants[47]. Antibodies used in these studies also included a polyclonal rabbit anti-hPF4 antibody (Abcam), a polyclonal rabbit anti-human VWF (hVWF) antibody (DAKO) or a FITC-prelabeled polyclonal sheep anti-hVWF antibody (Abcam). Bound HIT-patient IgG was detected using a rabbit polyclonal, anti-human IgG antibody (Jackson Immuno Research Laboratories). All antibodies were either labeled using Alexa Fluor antibody-labeling kits (ThermoFisher Scientific) or were detected using species-appropriate Alexa Fluor-conjugated secondary antibodies (all from ThermoFisher Scientific). The FcγRIIA-blocking monoclonal antibody IV.3[88,122,133] was

produced in hybridoma cells and purified on Protein G (Invitrogen). The mouse anti-human CD42b monoclonal antibody AK2 was purchased from Biorad.

Endothelialized microfluidic setting.

Endothelialized microfluidic studies were performed as we described previously[43] and in Chapter 2. Briefly, studies were performed using the Bioflux 1000 Controller system with an attached 37°C heating stage. The microscope was equipped with a motorized stage and an HXP 120 C metal halide illumination source. 48-well Bioflux plates were coated with fibronectin (50 µg/ml, Sigma-Aldrich), seeded with HUVECs (passage 3-4, 6-8 x 10^6 cells) that were allowed to adhere and cultured at 37°C under 5% CO_2 in EC growth media (Lonza; basal culture medium (BCM) bovine brain extract with heparin, human endothelial growth factor, hydrocortisone, ascorbic acid, gentamicin, amphotericin B, fetal bovine serum) until confluent. To induce a photochemical injury, hematoporphyrin (50 µg/ml final concentration, Sigma-Aldrich) was added to samples and exposed to a blue light using the HXP-120 C light source with a 475-nm excitation and 530-nm emission filter for 20-30 seconds during perfusion causing a reactive oxygen species injury[43,70]. PF4 and VWF were detected using Alexa Fluor-labeled antibodies. Endothelial cell nuclei were labeled with Hoescht 33342 (ThermoFisher Scientific) for 15 minutes at room temperature. On the day of experimentation, BCM (described above) was flowed over the channels for 3-4 hours prior to the experiment. All imaging was performed on a Zeiss Axio Observer Z1 inverted microscope or a Zeiss LSM 710 laser scanning confocal microscope as described[43]. Data was analyzed using Imagej or, for confocal images, using Volocity 6.3. Colocalization of fluorescent signals was analyzed using a built-in function of Volocity 6.3 providing Coste's colocalization coefficients.

Analysis of PF4-VWF-HIT antibody complexes.

All experimental solutions were made in BCM. A localized photochemical injury was induced using hematoporphyrin and then the channels were washed with BCM and then infused with hPF4 (0-25 µg/ml) in BCM for 10 minutes. In some experiments, at the 10-minute mark, KKO or TRA (each at 10 µg/ml) or plasma from HIT patients (1:100 dilution) or a polyclonal rabbit anti-hPF4 antibody (at 2 µg/ml final concentration, PeproTech) was added to the PF4 solution and allowed to flow continuously for an additional 10 minutes. After a total flow time of 20 minutes, channels were briefly washed with BCM, and then fixed for 15 minutes at room temperature with Cytofix Fixation Buffer (BD).

Experiments were performed to determine if PF4 bound primarily to VWF released from injured ECs or to plasma VWF. Once VWF-PF4-KKO complexes were formed, a BCM solution containing BSA (equimolar to 10 µg/ml of VWF, Sigma-Aldrich) or purified human VWF (10 µg/ml final concentration, Haematologic Technologies, Inc.), was flowed through the channels. Channels were fixed, labeled for VWF, PF4, and KKO, and binding was quantified via confocal imaging to determine how the protein solutions flowed through the channels affected formation of VWF-PF4-KKO complexes.

To examine the effects of drugs known to cleave strands of VWF or drugs known to strip PF4 from vascular surfaces, channels with formed PF4-VWF-HIT antibody complexes were exposed to various interventions; channels were flowed at 10 dynes/cm^2 for 10 minutes with therapeutics including unfractionated porcine heparin (0-50 units/ml final concentration, Novaplus), ADAMTS13 (0-7 nM, R&D Systems), and N-acetylcysteine (NAC, 0-10 mg/ml final concentration, Auromedics). In some experiments, heparin (0-0.4 units/ml) was added to a PF4 (25 µg/ml) and KKO (10 µg/ml)-containing solution and then introduced to channels containing PF4-VWF-HIT antibody complexes. After the 10-minute

infusion, channels were washed with BCM, fixed with Cytofix Fixation Buffer (BD Biosciences), and imaged to observe the presence of PF4, KKO, and/or large VWF strands.

Platelet accumulation on PF4-VWF-HIT antibody complexes.

To track platelet accumulation by PF4-VWF-HIT antibody complexes, whole blood from healthy volunteers was collected and labeled with calcein AM (2 µg/ml final concentration, ThermoFisher Scientific) at room temperature for 15 minutes. Whole blood was recalcified immediately before infusion using 2M $CaCl_2$ (final concentration of 12 mM, Sigma-Aldrich), and flowed through the channels at 10 dynes/cm^2. Platelet accumulation was quantified via total fluorescent intensity within the localized injury area. To test the impact of blocking specific receptor/ligands on platelet accumulation on PF4-VWF-HIT antibody complexes, IV.3[88,122,133] (20 µg/ml) and/or AK2[36,39,135] (60 µg/ml) were added to whole blood and allowed to incubated for 30 minutes prior to running the experiment.

Biophysical interaction between VWF and PF4.

To further examine the physical interaction between VWF and PF4, we utilize dynamic light scattering (DLS) analysis. Sample solutions are prepared and allowed to mix at room temperature for 15-20 minutes. Samples (500 µL) are then transferred to zeta disposable cuvettes (Fisherbrand) and measured in a Zetasizer Nano ZS (Malvern). In these experiments, solutions containing hPF4 (10 µg/ml) alone, hVWF alone (0-10 µg/ml), and solutions containing hPF4 (10 µg/ml) with various concentrations of hVWF (0-10 µg/ml) were studied. The size distribution of the resultant soluble particles was measured as described previously[53,110].

Role of VWF in thrombosis in HIT in vivo.

Thrombosis was induced using a previously described murine model of HIT[56,88] by infusing KKO following rose bengal photochemical injury to the carotid artery[25,50]. HIT mice were anesthetized using nembutal (80 mg/kg, CHOP animal facilities). Using standard surgical methods, the left jugular vein was exposed and mice were infused with either TRA (2 mg/kg), KKO (2 mg/kg), or KKO (2 mg/kg) + NAC (0.8 mg/g, Auromedic Pharma) in a PBS (220 µL total volume). The injected materials were allowed to circulate for 10-15 minutes during which time the right common carotid artery was surgically exposed. Rose Bengal (50 mg/kg, Sigma-Aldrich) was then infused and a miniature Doppler flow probe (Model 0.5VB; Transonic Systems) was positioned around the artery. After 5 minutes of measuring flow to assure sufficient signal, a green laser (540 nm) was targeted to the carotid artery to induce an occlusive thrombus. Using the data points from Doppler flow probe, we evaluated the time to occlusion (blood flow <10% of original and stable for 10 minutes), and the relative area under the curve (AUC) as measure of clot mass. When clots were formed and stable for greater than 10 minutes, measurements were stopped and mice euthanized; if vessel occlusion did not occur, experiments were ceased at a 2-hour time point. When mice were euthanized prior to the 2-hour time point, the final flow measurements were extrapolated to estimate AUC.

Statistics.

Differences between 2 groups were compared using a 2-sided Student's t-test. Differences between more than 2 groups were determined by 1-way ANOVA. All analyses were performed on GraphPad Prism 6.0 (GraphPad Software). Differences were considered significant when the *P* values were less than or equal to 0.05.

Results

PF4 binds to elongated strands of VWF released from injured endothelial cells in a microfluidic system.

We described how PF4 released from activated platelets bound predominantly to peri-injured endothelium in both the endothelialized microfluidic and in an vivo murine model of HIT[43] in Chapter 3; however, the target(s) to which the PF4 bound and subsequently HIT-like antibodies bound, was not identified. To begin to explore the potential PF4-binding sites on injured endothelium, we utilized the hematoporphyrin injury model in a HUVEC endothelialized microfluidic model. This model enables us to explore a human endothelial surface, to control the composition of the thrombus, and to contrast binding to injured and adjacent uninjured endothelium (**Figure 4.1A**). As previously described, this photochemical injury model does not cause the endothelium to detach or to lose cell-cell contact[43]. VWF was clearly released within the injured zone (**Figure 4.1B**). Post-injury, solutions containing recombinant hPF4 were flowed across channels. The most extensive binding of hPF4 was restricted to the injured area, less so in the immediate downstream region, and was at near-background levels further downstream (**Figures 4.1C** and **4.1D**). Binding of PF4 within these regions typically followed a linear pattern, remarkably similar to the pattern of VWF following release from endothelial cells. Therefore, we asked whether the PF4 was indeed binding to the released VWF. Co-staining for VWF and PF4 showed significant (P=0.02) co-incidental binding as seen in enlarged images (**Figure 4.2A**). PF4 bound preferentially to the most elongated strands of VWF (**Figure 4.2B** and **4.2C**).

A HIT-like monoclonal antibody and HIT patient IgGs bind PF4-VWF complexes in vitro.

PF4 binds to polymeric molecules other than heparin, including various glycoasminoglycans (GAGs)[47], DNA and RNA aptamers[124], and polyphosphates[53]. All of these complexes are also antigenic for HIT-like antibodies, at least in vitro. Binding of PF4 to heparin leads to the formation of high molecular weight oligomers that increase antibody avidity[47,137]. To determine if PF4-VWF complexes are antigenic for HIT-like antibodies, we induced injury in the microfluidic chambers and introduced PF4 and the HIT-like mouse monoclonal antibody KKO, known to replicate key features of patient-derived HIT-like antibodies[47]. Binding of KKO followed the same distribution seen with PF4, with both co-localizing with the strands of VWF strands released by the injured endothelium (**Figure 4.3A**). Binding of KKO was localized primarily to the area of endothelial injury and to the immediately downstream region (**Figure 4.3B**). An enlarged image of this field (**Figure 4.4A**) shows that the binding of the KKO to the VWF strands follows a periodic pattern with little KKO seen in association with smaller VWF deposits. Detailed analysis of co-localization confirmed that KKO showed significantly more binding to elongated strands of VWF (**Figure 4.4B** and **4.4C**).

We then asked whether plasma from patients with positive clinical histories, ELISAs, and SRAs for HIT IgG would also bind to the PF4-VWF complexes. A representative field of IgG binding from one HIT patient compared to a control patient with low probability of having HIT is shown (**Figure 4.3C**). Three of 6 samples from patients with HIT caused significant binding of IgG to the VWF released from injured endothelium in the presence of added PF4 that was not seen with the control patient sample with low probability of HIT (**Figure 4.3D**).

Physical characterization of the PF4-VWF complexes in vitro.

We used DLS as an independent method to study the binding of PF4 to VWF. We first examined the particle size of PF4 and VWF alone. PF4 followed a Gaussian-size distribution (all less than 10 nm), while VWF displayed a more complex size distribution consistent with its polymeric nature and tendency to polymerize[138] (**Figure 4.5A**).

When PF4 was added to VWF (PF4:VWF = 10 µg:5 µg), particles with a single narrow range of masses that followed a Gaussian distribution was seen. The mean mass of PF4 ~6-fold higher than the of mass PF4 alone, clearly establishing binding between the reactants (**Figure 4.5B**). When more PF4 was added (PF4:VWF = 10 µg:1 µg), the mass of the complex increased to ~40-fold higher than PF4 alone. If using masses of PF4 tetramers and VWF monomers, it can be estimated that the molar ratio in this scenario is about 84:1 (PF4:VWF=316 nM:3.84nM). The molar ratio of reactants cannot be more definitively estimated, as we do not know the number of VWF monomers present in the starting VWF, the number of molecules in an “open” (permissive) conformation (see below) or whether PF4 enhances oligomerization of VWF in vitro. However, of possible relevance to this issue, at the highest concentration of PF4 studied (PF4:VWF = 10 µg:10 µg), the apparent mean mass of the PF4-VWF complexes widened with an appearance similar to that of VWF alone. One possible interpretation of these data are that over a limited molar ratio of reactants, binding of PF4 cause reorganization of VWF multimers, consistent with the appearance of extended strands containing PF4-VWF-KKO observed in the microfluidic model. At higher concentrations, PF4 may bind to smaller VWF multimers, albeit with lower affinity, which are not cross-linked in the process. This parabolic outcome recapitulates the growth and disappearance of PF4/heparin complexes in solution and PF4/GAG complexes on cell surfaces as the PF4/polyanion ratio increases[47,53].

The appearance of PF4 is predominantly along elongated strands of VWF released by activated ECs. Shear stress alters the 3-dimensional conformation of VWF exposing its “A” domains[138–140]. However, we next wanted to determine if PF4 also binds to plasma VWF or to other plasma proteins. To test this, we injured the endothelium as describe previously and introduced PF4 and KKO to form PF4-VWF-KKO complexes. Then channels were exposed to flowing solutions that contain BSA or purified human VWF. Purified human VWF was used at plasma concentrations (10 µg/ml) and BSA was used an equimolar concentration. PF4 and KKO binding was assessed by confocal microscopy to determine if soluble VWF or BSA would remove complexes formed on released VWF compared with buffer alone (**Figure 4.5C**). Heparin, which removes PF4-HIT antibody complexes from other vascular surfaces[43,141], was used as the positive control. Heparin, at 10x therapeutic concentrations (4 U/ml), removed PF4-VWF-HIT antibody complexes from the injured endothelium (**Figure 4.8A**). In contrast, infused BSA had minimal effect on PF4 and KKO binding (**Figure 4.5D**). Soluble VWF did not elute PF4 and KKO and, in some experiments, appeared to increase PF4 and KKO binding. This might be due to binding of soluble VWF to unoccupied sites on PF4 and becoming incorporated within pre-existing EC-VWF strands. VWF self-association has been shown to be homotypic as soluble VWF – but not BSA – is known to associate with immobilized VWF under flow[142,143]; moreover, the self-association of VWF has been shown to assemble hemostatically active filamentous networks and induce platelet activation under shear[17,39,144–146]. These findings and recent studies suggest that tethered VWF strands released from ECs are preferentially form PF4-VWF-KKO complexes that are not removed by soluble VWF, which may actually enhance antigen formation.

PF4-VWF-HIT antibody complexes are prothrombotic in vitro.

Do the PF4-VWF-HIT antibody complexes contribute to the prothrombotic state seen in HIT? Using the microfluidic system described in **Figure 4.1**, we show that the endothelium needed to be injured to cause platelet accumulation upon infusion of whole human blood (**Figure 4.6A**). Platelet accumulation was greatest when both PF4 and KKO are included and coat the VWF strands (**Figure 4.6B** and **4.6C**). Neither KKO alone nor PF4 plus the isotype control monoclonal antibody TRA[47] enhanced platelet accumulation. Platelet accumulation in the presence of PF4- and KKO-coated VWF became more pronounced the longer blood was infused into the channels.

We were interested in understanding which components contribute to platelet accumulation on VWF strands. Platelets bind to shear-activated VWF via the GPIb/IX complex, in a pathway that can be blocked by the anti-GPIbα monoclonal antibody AK2. The PF4-VWF-KKO complexes could also enhance platelet activation and adherence via their FcγRIIA, a process that can be blocked by the anti-FcγRIIA monoclonal antibody IV.3. We demonstrate that both antibodies blocked the enhanced adherence of platelets in whole blood to the VWF strands (**Figure 4.7A** and **4.7B**), though by 40 minutes post-infusion, blocking the GPIb/IX-VWF axis appears to be more effective. AK2 plus IV.3 was not more effective than AK2 alone, suggesting the GPIb/IX-VWF axis plays a crucial role in supporting the binding of platelets to the PF4-VWF-HIT antibody complex.

Drug interactions with the PF4-VWF-HIT antibody complexes in vitro.

Patients who develop HIT are often on therapeutic heparin when they develop thrombi[41,43,44]. Heparin binds to PF4 with high affinity. Therapeutic heparin levels range

from 0.1-0.4U/ml[147]. Therefore, we asked whether PF4-VWF-HIT antibody complexes are stable and would persist bound to the endothelium at pharmacologic levels of heparin. Heparin at ≥0.4 U/ml reduced PF4 and subsequent KKO binding to the VWF released from injured endothelium in the microfluidic system within 10 minutes (**Figure 4.8A**). However, during thrombus development, PF4 levels are estimated to exceed 100 µg/ml[122] and are likely to be persistently released from platelets trapped with thrombi as well. To recapitulate this setting, we tested the effect of a flowing a solution containing increasing PF4 concentrations (0-100 µg/ml) at a fixed pharmacologic concentration of heparin (0.4 U/ml) as well as HIT antibody. As PF4 levels increased, both bound PF4 and KKO levels increased in the presence of heparin, consistent with the known risk of continuing this anticoagulant in patients with clinically active HIT (**Figure 4.8B**).

Therapeutic strategies to prevent VWF-related pathobiology have included the use of the metalloproteinase ADAMTS13 to lyse WVF strands[38,148,149] or NAC to prevent their assembly[69,150]. We asked whether PF4 and or HIT antibody would cause resistance to the effect of ADAMTS13 or NAC on reducing the number and length of extruded VWF strands after endothelial injury in the microfluidic system. PF4 alone did not protect VWF strands from digestion by ADAMTS13 (7 nM) when looking at the number of strands present after flow. PF4 plus KKO showed a trend towards protection from ADAMTS13 but the effect did not reach statistical significance in the 10 minute time frame in which experiments were performed (**Figure 4.9A** and **4.9B**). Neither PF4 with nor PF4 plus KKO protected VWF from the effects of NAC (**Figure 4.9A** and **4.9B**). There was no significant differences between the length of VWF strands after exposure ADAMTS13 or NAC in the presence of PF4 or PF4 plus KKO (**Figure 4.9A** and **4.9C**).

The role of VWF in the prothrombotic HIT murine model.

The data shown in **Figure 4.9** suggest that PF4 and HIT antibody binding do not protect released VWF strands and therefore that both VWF-targeted therapeutics have the potential to remove PF4-VWF-KKO targets in vivo. However, we could not test this hypothesis by imaging intra-thrombi VWF, which show diffuse staining and cannot be used to follow the resolution of elongated strands of multimeric VWF[151,152]. Consequently, we used a functional evaluation to assess the effect of NAC on thrombosis in the HIT mouse using the rose bengal photochemical carotid arterial injury model[50]. We confirmed our prior findings in this model and showed that NAC both prolonged the time to full occlusion induced by KKO and the relative AUC (**Figure 4.10A** and **4.10B**). Thus, it appears that VWF contributes to arterial thrombosis in this model of HIT and suggests the utility of VWF targeted therapeutics.

Discussion

HIT is an unusually prothrombotic disorder that can have devastating consequences even with the withdrawal of heparin and the institution of present-day anticoagulants[41,43,44,67]. While the disease clearly involves the induction of antibodies that oligomerize PF4 with heparin and with surface GAGs on the surface of platelets, its prothrombotic nature now is clearly recognized to be in part due to the fact that PF4 also forms antigenic complexes with GAGs on other cells including monocytes, endothelial cells and neutrophils, leading to the induction of prothrombotic processes[43,48,50,88,93,95], e.g. the elaboration of tissue factor[94]. More recent finding indicate that additional polyanions induced by HIT antibodies can bind PF4 and serve as antigenic targets that promote thrombus extension[64–67] and propagate the disorder even when heparin has been stopped (Step 3) (Figure 1.5). These include polyphosphates released from platelets and perhaps endothelial cells[53] DNA found in neutrophil extracellular traps (NETs) released by

activated neutrophils[122], which appear to be especially important in the growth of venous thrombi.

We now show that PF4 also forms antigenic complexes with VWF strands released from activated endothelial cells, most likely localized primarily to the arterial side of the circulation. The PF4 appears to bind periodically along the elongated strands of VWF. Binding of HIT antibodies to PF4-VWF complexes along the vasculature likely offer an Fc-rich surface that permit binding intravascular cells that express FcγRIIA, including platelets, neutrophils and monocytes[47,50] and provide a surface for activating complement[89]. Our result appear initially differ from a prior study showing PF4 did not enhance binding of VWF to platelets[153] but did not address whether PF4 can bind to VWF as examined in our system. This negative result is, however, consistent with what we report: PF4 binds selective to large VWF strands that form under flow in preference to VWF in solution. Binding of platelets to PF4-VWF strands was markedly enhanced when a HIT-like antibody was also present. We propose that PF4-VWF-HIT antibody complexes activate platelets through FcRγIIA which stabilizes platelet adhesion to the EC-VWF strands under flow. (**Figure 4.6** and **4.7**).

Of interest, unlike other polymeric molecules like heparin and polyphosphates, VWF is not a polyanion. The mechanism by which VWF becomes a binding site for PF4 will require additional study. We hypothesize that the binding sites within vWF are exposed by shear forces which may also enhance their proximity and thereby enhance their avidity for PF4. This is similar to what has been postulated for the effect of unfractionated heparin compared with low molecular weigh heparins and fondaparinux.

NAC, which prevents VWF oligomerization[150] attenuated carotid arterial occlusion induced by HIT antibody. Unfortunately, attempts to directly visualize the released VWF and its complex with PF4 and HIT antibodies were unsuccessful because of intense

diffuse staining which impeded identification of individual VWF strands. Studies using confocal microscopy are in progress in an attempt to circumvent this problem.

In summary, PF4 binds to VWF strands extruded from injured endothelial cells and forms HIT antigenic complexes. Such targets are periodically distributed along the VWF strands under flow conditions, but binding to soluble VWF was not observed. These complexes bind platelets through a pathway that involves both FcγRIIA- and GPIb/IX-based pathways. We propose that the release of VWF strands expose a high-density epitope that fosters binding of PF4 and HIT antibodies and promotes binding and activation of platelets, monocytes and neurtrophils through by their surface FcγRIIA and/or by activating complement. Depolymerization of VWF strands by NAC attenuates thrombotic arterial occlusion induced by HIT antibodies in a mouse model. These findings suggest that VWF may play a significant role in the propagation of HIT in space and in time (Step 3) (**Figure 1.5.** VWF may thereby play a role on the arterial side of the circulation analogous to the effect of NETs in the propagation of venular injuries, which is addressed in Chapter 5. Drugs targeting VWF biology may be an effective new approach to therapy in HIT, especially for arteriolar thrombi.

Figures

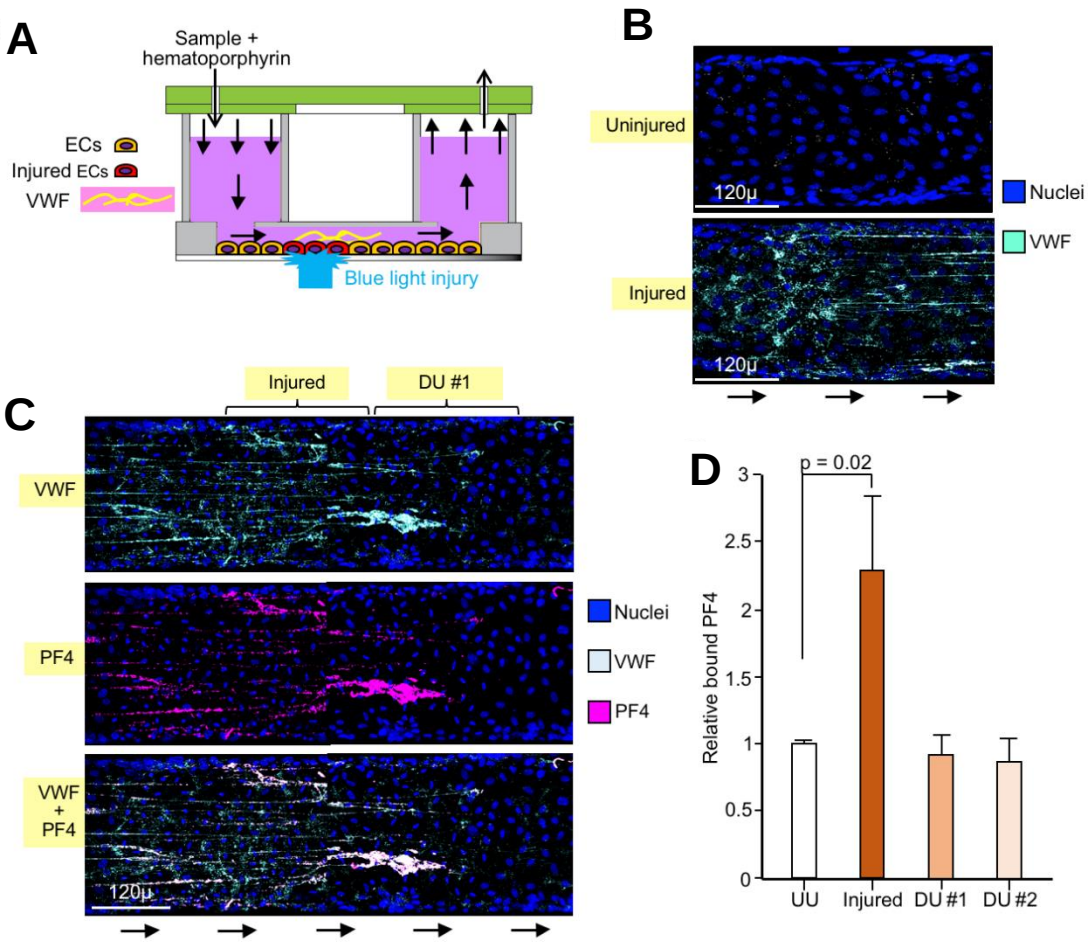

Figure 4.1. PF4 binds to elongated strands of VWF released from injured ECs in a microfluidic system.

(**A**) Schematic of the endothelialized microfluidic system used for photochemical injury studies to targeted regions of the endothelium. (**B**) Comparison of a representative area of uninjured endothelium and hematoporphyrin-injured inured area showing pyknotic nuclei and released VWF strands that are only seen after injury. (**C**) and (**D**) are stained for PF4 using a polyclonal anti-PF4 antibody as well as staining for nuclei and released

VWF. (**C**) shows representative microfluidic channel injured and downstream uninjured (DU) areas designated as DU #1 of the first 150µ downstream. Direction of flow is indicated by arrows. (**D**) shows relative binding of PF4 to either an area of 250µ X 150µ of the upstream uninjured (UU) region, the injured region, or the DU #1 and DU #2 regions. Mean ± 1 SEM are shown with N ≥ 3 with n signifying separate microfluidic channels. P values were determined using a one-way ANOVA analysis to compare relative binding to the uninjured upstream area of the channel.

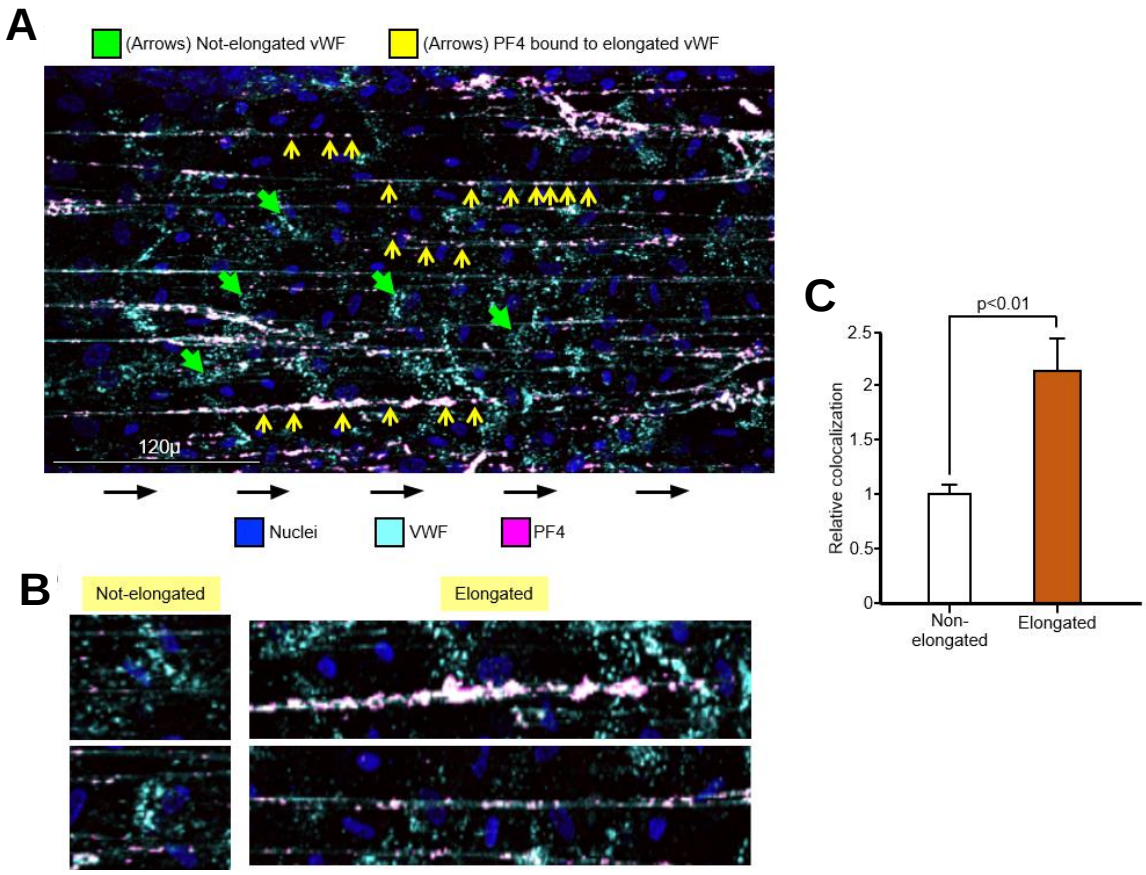

Figure 4.2. PF4 preferentially binds elongated VWF strands over not-elongated.

(**A**) Displays an image of Figure 4.1C showing PF4 (magenta) bound to elongated (yellow arrows) or not-elongated (green arrows) VWF (cyan) with nuclei stained with Hoescht (blue) (**B**) Enlarged examples of PF4 bound to elongated or not-elongated VWF isolated from (A). (**C**) The relative colocalization of VWF signal to PF4 signal using Coste's colocalization coefficients showing PF4 binds preferentially to elongated VWF compared with not-elongated VWF. Mean $\pm$ 1 SEM are shown with N $\geq$ 12 with N signifying independent VWF strands analyzed.

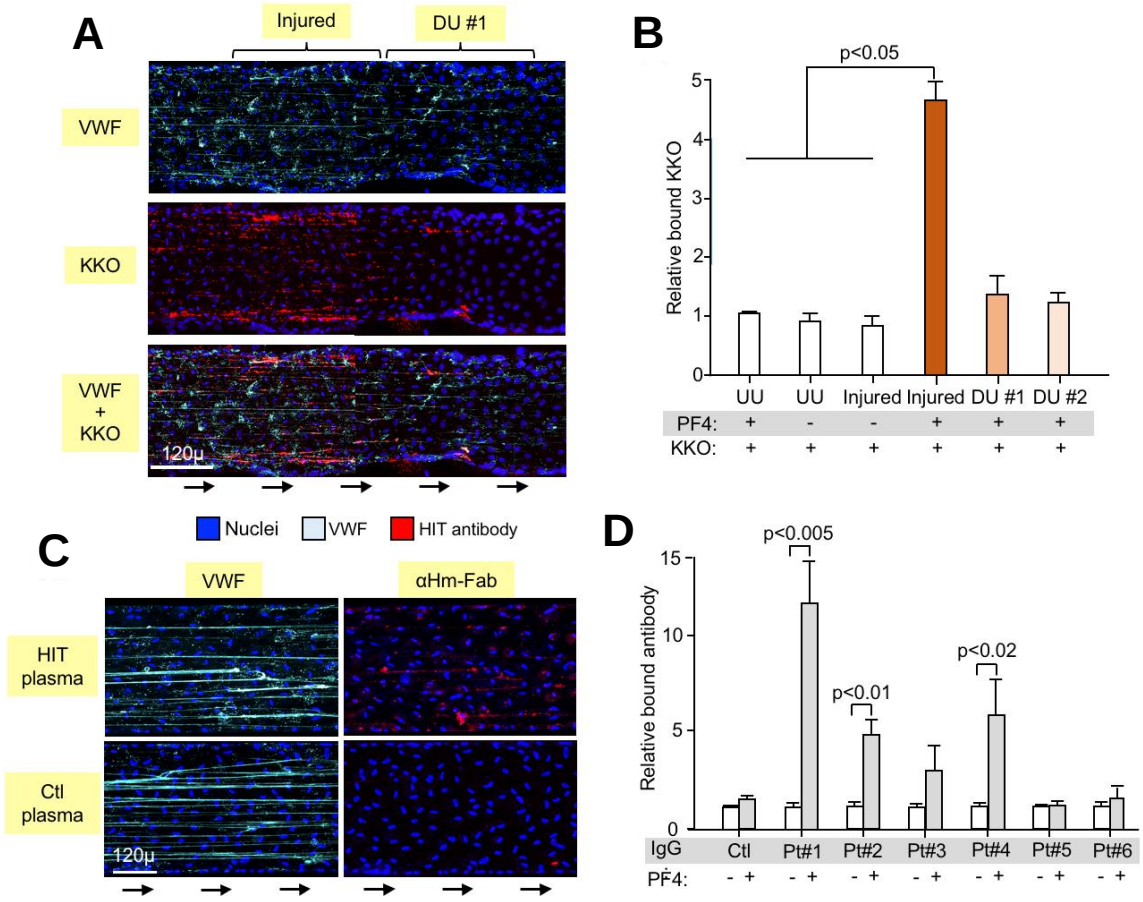

Figure 4.3 A HIT-like monoclonal antibody and HIT patient IgGs bind PF4-VWF complexes in vitro.

(**A**) Representative injured area and downstream areas in the microfluidic channels as in **Figure 1C**, but staining for VWF and KKO. (**B**) Comparison as in **Figure 1D** for total KKO bound. Abbreviations are as **Figure 1D**. Mean ± 1 SEM are shown. N ≥ 3 representing separate microfluidic channels. P values were determined by a one-way ANOVA analysis. (**C**) and (**D**) are similar to (A) and (B) respectively, but showing only the injured areas. In (C), diluted plasma from patients at high risk of having HIT or low-risk controls (Ctl) were used. In (D), diluted plasma from these individuals was quantified. Mean ± 1 SEM are shown. N ≥ 3 separate channels. P values were determined using a one-way ANOVA to

compare relative binding in the absence of PF4 or in the presence of infused PF4 at 25 µg/ml for each IgG sample.

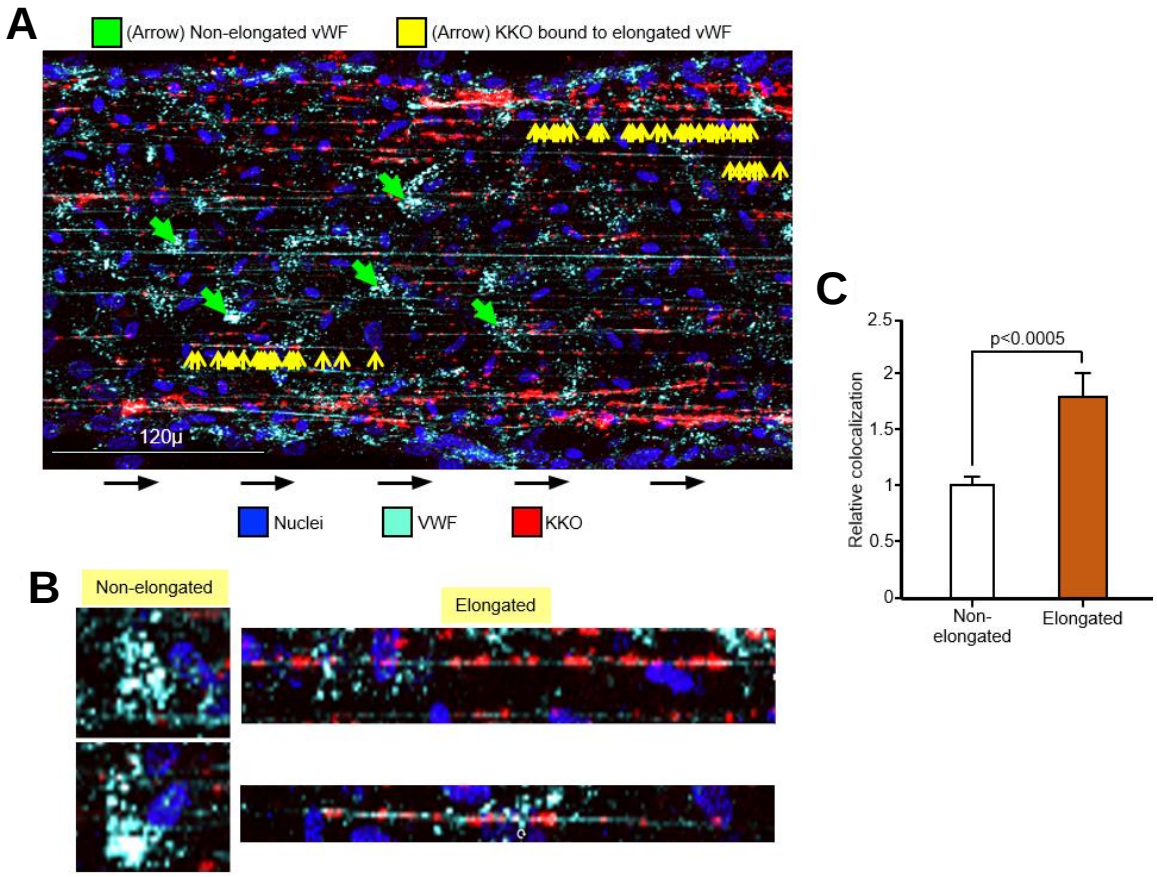

Figure 4.4. KKO preferentially binds elongated VWF strands over not-elongated VWF.

(**A**) Displays an image of **Figure 4.3A** showing KKO (red) bound to elongated (yellow arrows) or not-elongated (green arrows) VWF (cyan) with nuclei stained with Hoescht (blue). (**B**) Enlarged examples of KKO bound to elongated or not-elongated VWF isolated from (A). (**C**) The relative colocalization of VWF signal to KKO signal using Coste's colocalization coefficients showing KKO binds preferentially to elongated VWF compared with not-elongated VWF. Mean ± 1 SEM are shown with N ≥ 12 with N signifying independent VWF strands analyzed.

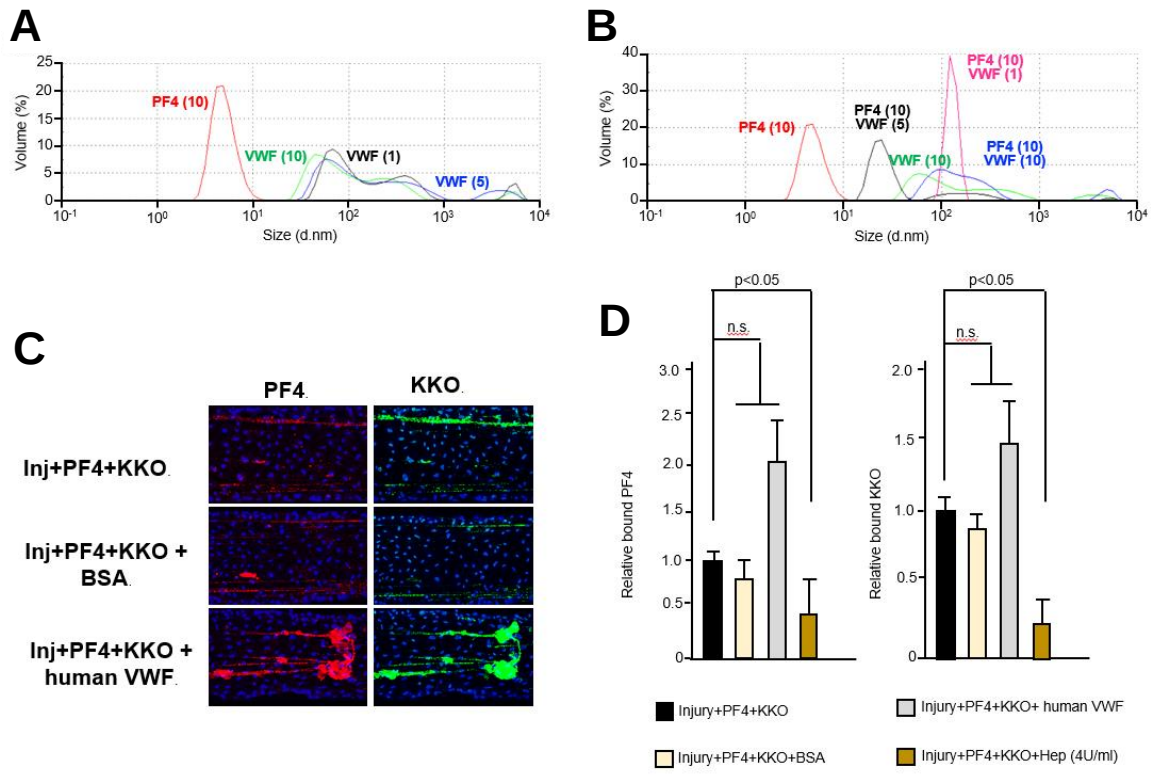

Figure 4.5. Physical characterization of the PF4-VWF complexes in vitro.

(**A**) Volume readouts from dynamic light scatter analysis looking at PF4 alone (red, 10 µg/ml) in comparison to VWF alone at varied concentrations (1 µg/ml = black, 5 µg/ml = blue, 10 µg/ml = green). (**B**) Volume readouts from dynamic light scatter analysis evaluating PF4 (10 µg/ml) mixed with the various concentrations of VWF (0 µg/ml = red, 1 µg/ml = magenta, 5 µg/ml = black, 10 µg/ml = blue). Curves are representative of ≥ 4 separate experiments. (**C**) Confocal images displaying PF4 (red) and KKO binding (green) in channels in which PF4-VWF-HIT antibody complexes were formed and then infused with the indicated solution. Original image magnification is x20. (**D**) Quantification of PF4 and KKO binding showing the flowing a solution containing BSA or VWF does not reduce the binding of PF4-VWF-HIT antibody complexes within the channel. N ≥ 5.

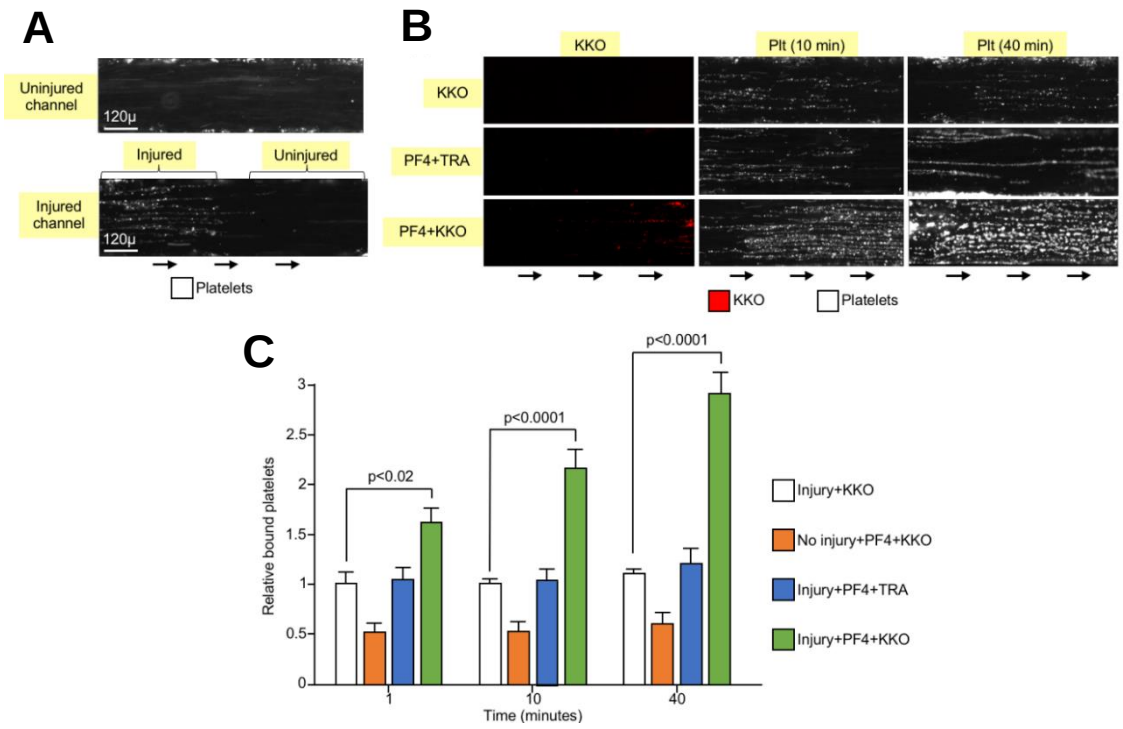

Figure 4.6. PF4-VWF-HIT antibody complexes are prothrombotic in vitro.

(**A**) Representative fields of uninjured (top) and injured (bottom) endothelium after exposure to a flow of recalcified whole human blood for 10 minutes, demonstrating the binding of platelets to the VWF strands. The bottom channel displays the edge of injury showing platelets and an uninjured area that resembles the appearance of the control uninjured channel (top) (**B**) Same as in (A), but with the inclusion of PF4 (25 µg/ml) and the indicated monoclonal antibody (10 µg/ml) and studied at the time points indicated. Binding of KKO and of platelets are shown. (**C**) Mean ± 1 SEM are shown. N ≥ 6 separate studies for the relative level of bound platelets (as quantified by calcein AM) compared to injured endothelium with added KKO in the absence of PF4. P values were determined using a one-way ANOVA analysis.

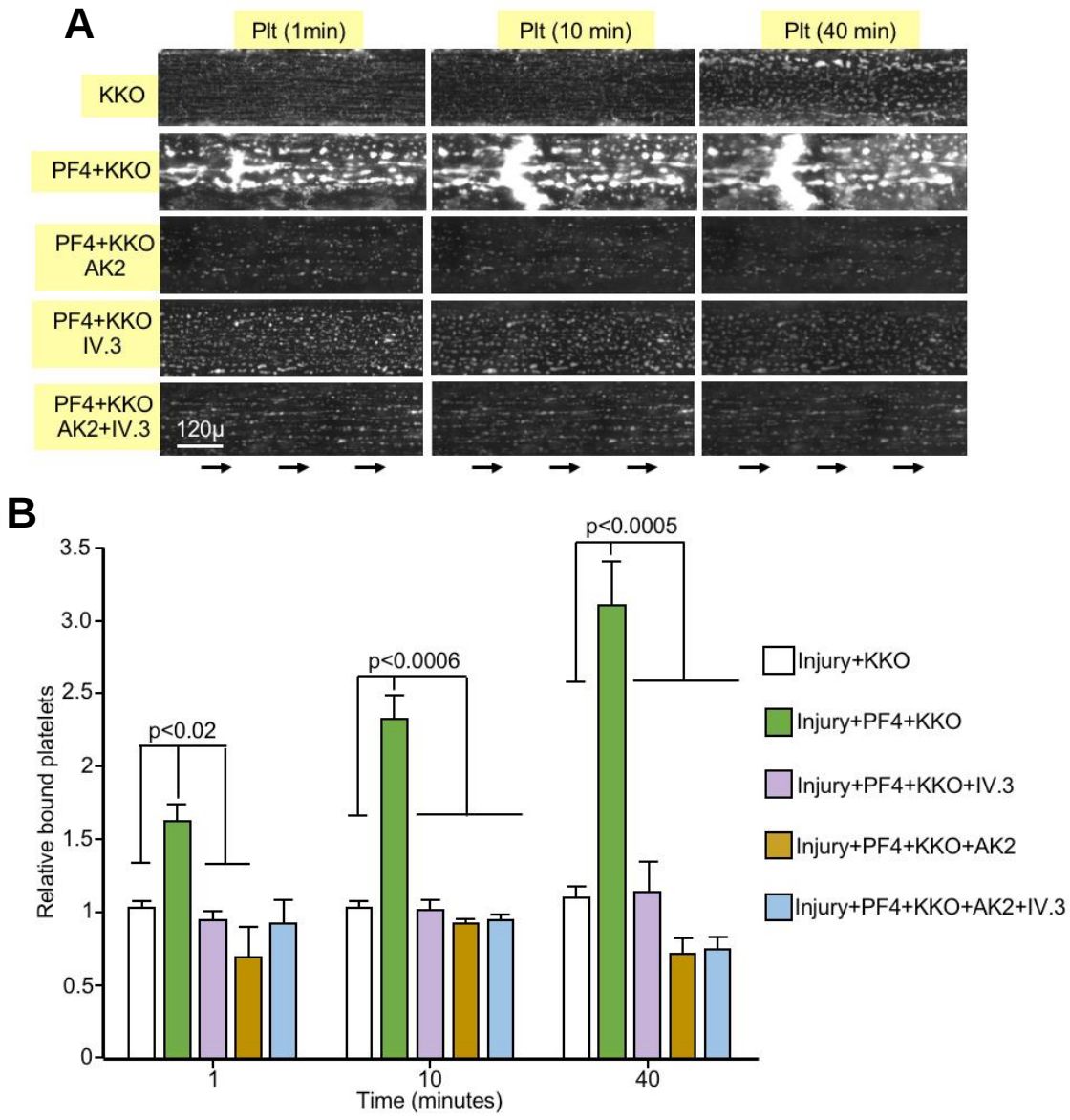

Figure 4.7. Platelet binding to the PF4-VWF-HIT antibody complexes is dependent on both the GPIb/IX receptor and FcγRIIA.

(**A**) As in **Figure 4.6B**, representative fields showing platelet accumulation on injured endothelium after flowing recalcified whole human blood with or without added PF4 and KKO and with or without the GPIb/IX-VWF-blocking antibody AK2 or the FcγRIIA-blocking

antibody IV.3. (**B**) Mean ± 1 SEM for N ≥ 6 separate studies for the relative level of bound platelets compared to injured endothelium with added KKO, but no PF4. Mean ± 1 SEM are shown. N ≥ 3 separate studies with N signifying separate channels. P values were determined using a one-way ANOVA analysis.

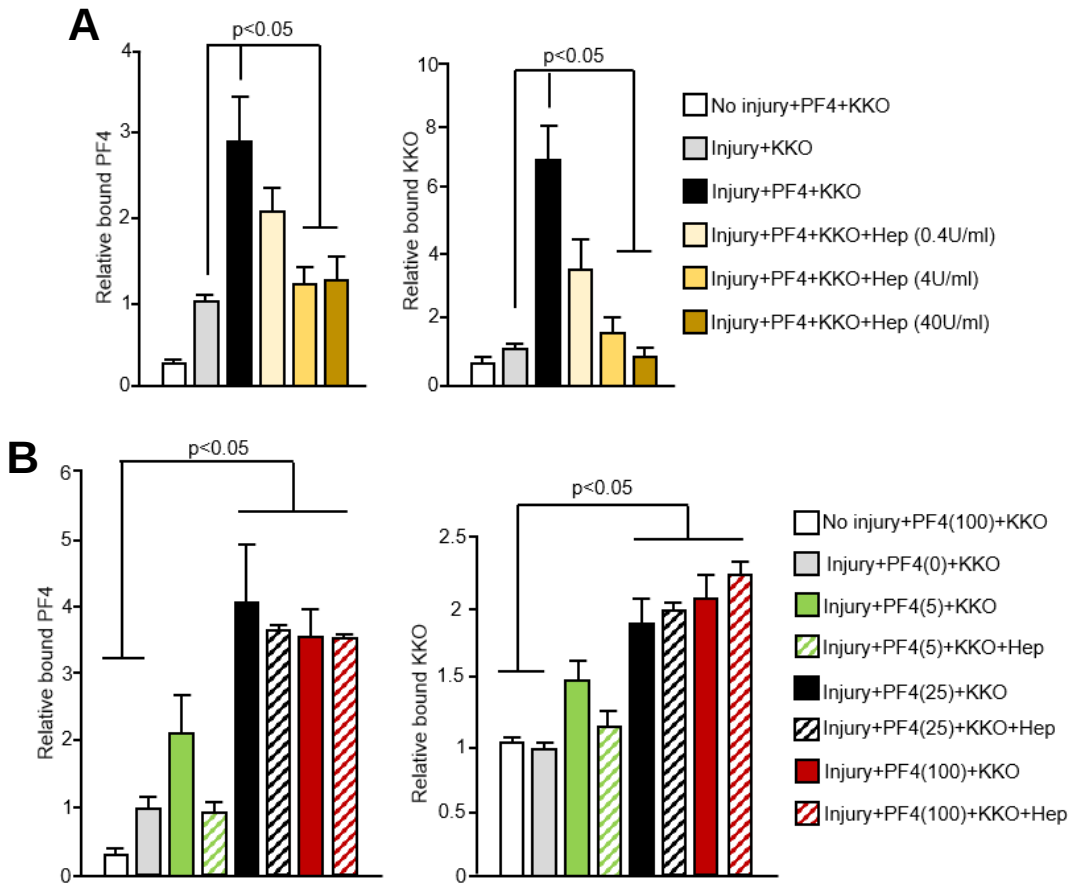

Figure 4.8. Heparin disrupts PF4-VWF-HIT antibody complexes but can be combatted by elevated levels of PF4.

(**A**) Complexes with VWF were formed by flowing PF4 (25 µg/ml) and KKO (10 µg/ml) along the damaged vasculature followed by exposing the channel to a heparin (0-40 U/ml) containing solution for ten minutes. Means ± SEM are shown with N ≥ 4. P values were determined by one-way ANOVA analysis. (**B**) Studies showing how PF4 (25 µg/ml) and KKO (10 µg/ml) binding in PF4-VWf-HIT antibody complexes changed when washed with a solution containing heparin (0-0.4 U/ml), PF4 (5-100 µg/ml), and/or KKO (10 µg/ml) for ten minutes.

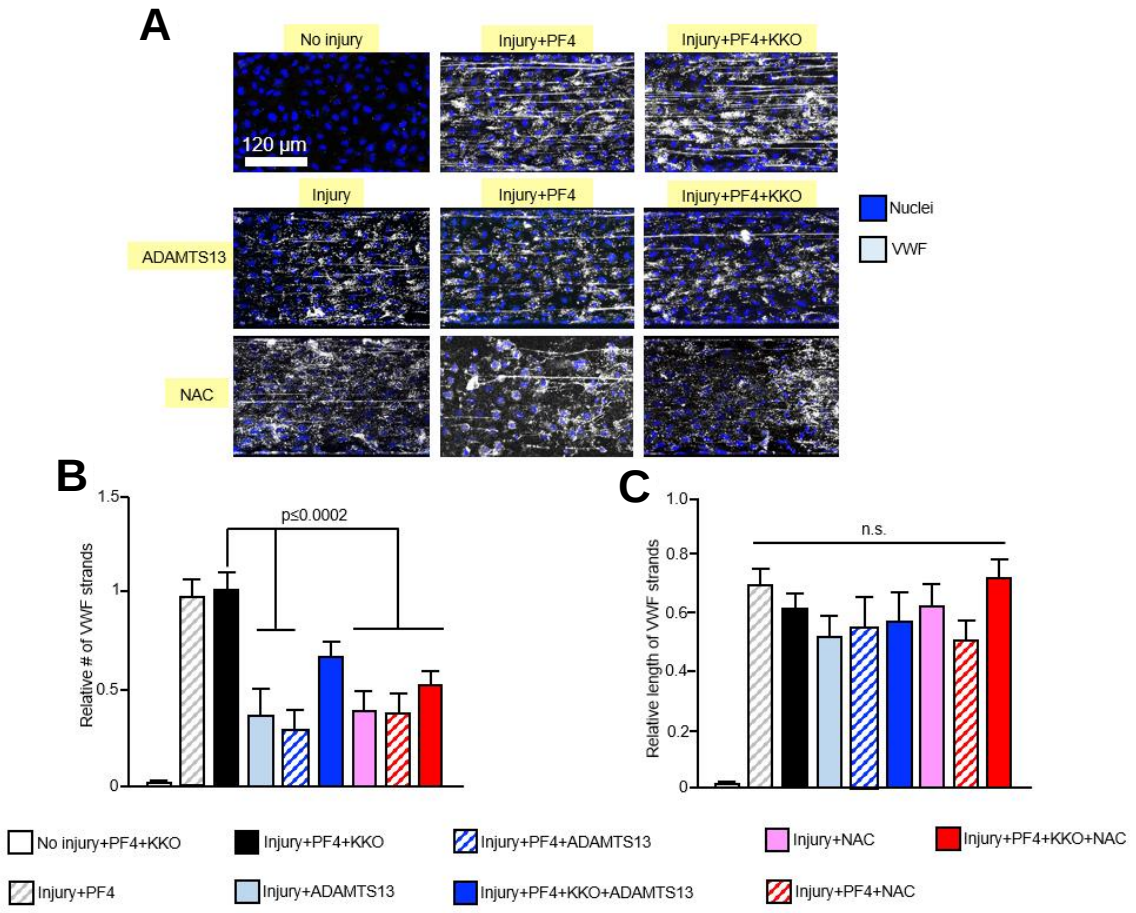

Figure 4.9. Drug interactions with the PF4-VWF-HIT antibody complexes in vitro. (**A-C**) are studies of the effects of ADAMTS13 or NAC on the presence of VWF-PF4 or VWF-PF4-HIT antibody complexes. (A) Shows representative images from studies as in Figure 3A with PF4 25 µg/ml infused into each lane. In some studies, KKO (10 µg/ml), ADAMTS13 (7 nM) and/or NAC (10 mg/ml) was added as indicated. (B) The data shown are the mean ± 1 SEM of the number of VWF strands present in the channel after exposure to the indicated solution relative to those present in channels with injury+PF4+KKO. N ≥ 4 and P values were determined by one-way ANOVA analysis. (C) Shows the mean ± 1 SEM are shown for the length of VWF relative to the length of the viewing window with N ≥ 4 independent channels. P values were determined by one-way ANOVA analysis.

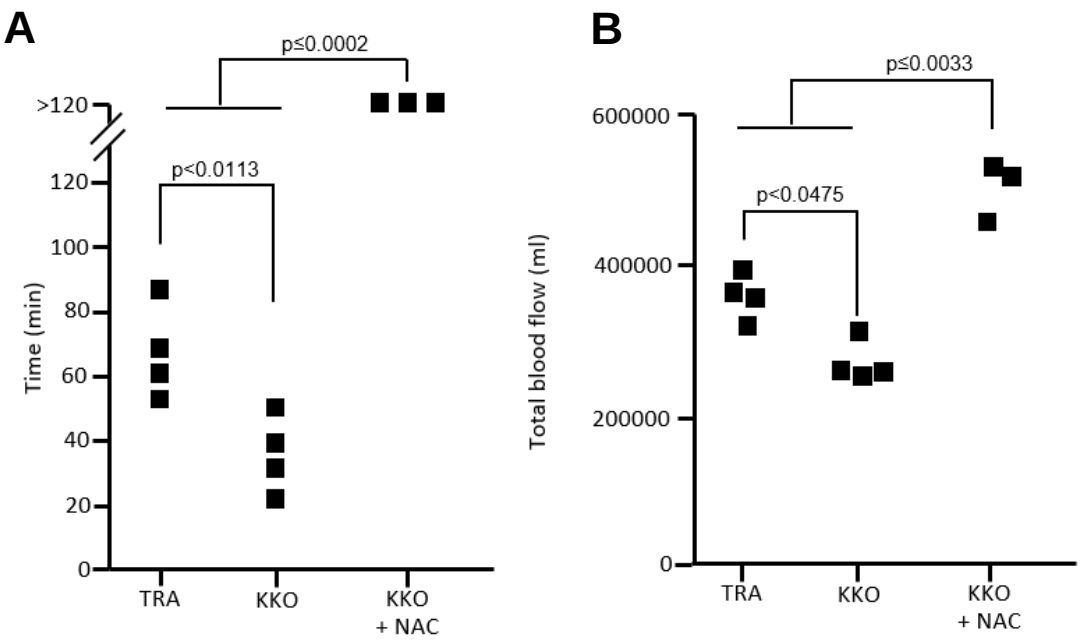

Figure 4.10. NAC impedes HIT-exacerbated thrombosis in a rose bengal carotid arterial injury model.

(**A**) Displays the time (minutes) to occlusion in a rose bengal photochemical carotid arterial injury model comparing mice infused with TRA, KKO, and KKO with n-acetylcysteine. N ≥ 3. (**B**) Displays the estimated AUC measured in total milliliters for the same mice shown in (A).

CHAPTER 5 – Neutrophil accumulation and NET release contribute to thrombosis in HIT

This chapter presents work featured in the article that has been submitted:

Gollomp, K., et al., (2018) *submitted*

Abstract

HIT is an immune-mediated thrombocytopenic disorder associated with a severe prothrombotic state. We investigated whether neutrophils and NETs contribute to the development of thrombosis in HIT. Using an endothelialized microfluidic system and a murine passive immunization model, we show that HIT induction leads to increased neutrophil adherence to venous endothelium. In HIT mice, endothelial adherence is enhanced immediately downstream of nascent venous thrombi, after which neutrophils migrate retrograde via a CXCR2-dependent mechanism to accumulate into the thrombi. Using a microfluidic system, we found that PF4 binds to NETs, leading them to become compact and DNase resistant. PF4-NET complexes selectively bind HIT antibodies, which further protect them from nuclease digestion. In HIT mice, inhibition of NET formation through *Padi4* gene disruption or DNase treatment limited venous thrombus size. *Padi4*$^{-/-}$ did not effect arterial thrombi or severity of thrombocytopenia in HIT. Thus, neutrophil activation contributes to the development of venous thrombosis in HIT by enhancing neutrophil-endothelial adhesion and neutrophil clot infiltration, where incorporated PF4-NET-HIT antibody complexes lead to thrombosis propagation. Inhibition of neutrophil endothelial adhesion, prevention of their chemokine-dependent thrombus recruitment, or suppression of NET release should be explored as strategies to prevent venous thrombosis in HIT.

Introduction

HIT is an immune-mediated thrombocytopenic disorder, characterized by venous and arterial thrombi[154]. Even with early recognition and initiation of appropriate therapy, thromboembolic complications still occur[155]. The current standard of care for patients with suspected HIT involves intense anticoagulation that carries the risk of significant bleeding and only provides partial protection against recurrent thromboembolic events[87]. While avoidance of heparin exposure may prevent the development of HIT[156], there are clinical settings where heparin remains irreplaceable[157]. An improved understanding of the pathobiology of HIT may help identify targeted therapies to prevent thrombosis without subjecting patients to the risk of intense anticoagulation. These insights may also be beneficial in the treatment of other inflammatory, prothrombotic conditions ranging from antiphospholipid syndrome[158] to sepsis[159].

HIT is caused by the development of pathogenic antibodies (HIT antibodies) that recognize complexes of heparin and the platelet-specific human chemokine PF4[88], which is released in high concentrations at sites of platelet activation and then binds to surface GAGs on platelets[160], monocytes[50], ECs[43], and neutrophils[161]. HIT antibodies cross-react with PF4-GAG complexes after which their Fc termini engage FcγRIIA receptors, leading to cell activation[162]. Although the high risk of thrombosis observed in HIT has classically been attributed to the assembly of PF4-GAG complexes on platelets, these complexes also form on the surface of other cells types, including monocytes[50] and neutrophils[122]. Moreover, we recently showed that PF4 and HIT-like antibodies bind predominantly to the endothelial surface after vessel wall injury, leading to an increase in the extent of endothelial damage upstream and downstream of the initial site of injury[43].

There are multiple factors that suggest neutrophils may contribute to the pathogenesis of HIT. Human neutrophils express FcγRIIA[163] and neutrophil activation via

this receptor promotes increased phagocytosis, degranulation, and generation of ROS[164]. PF4 and HIT antibodies have been shown to induce integrin expression on neutrophils[122] and enhance the formation of neutrophil-platelet aggregates[165]. Myeloperoxidase (MPO) levels have also been found to be elevated in plasma obtained from patients with HIT compared to plasma from patients with other causes of thrombocytopenia[165], suggesting that HIT is associated with neutrophil activation. In the setting of infection or inflammation, activated neutrophils can contribute to thrombus formation through NETs released chromatin that can trap platelets, bind clotting factors, and deactivate natural anti-coagulants[166].

These findings led us to hypothesize that neutrophils activated by HIT antibodies may contribute to the prothrombotic nature of HIT. To address this question, we performed studies using an in vitro microfluidic system[43] and a passive murine immunization model of HIT[47]. In both systems, we found that exposure to HIT antibodies lead to enhanced neutrophil adhesion to the venous endothelium. Following cremaster venule laser injury in the murine passive immunization model of HIT, we observed that neutrophils adhered to the downstream endothelium and then followed a chemogradient to migrate retrograde into the growing thrombi. When activated neutrophils undergo NETosis during HIT, their released NETs are bound by PF4, leading to their physical compaction. These PF4-NET complexes bind HIT antibodies and become resistant to circulating DNases. Additional passive murine immunization HIT studies in mice that are resistant to NET formation due to a deficiency in the gene that encodes peptidyl arginine deiminase 4 (PAD4), an enzyme that induces chromatin decondensation through the citrullination of histone lysine residues[167], confirm that NETosis plays a role in the murine model of HIT. The results of a corollary analysis of clinical samples obtained from patients diagnosed with HIT, suggests that NET formation influences the disease in humans. The relevance of these

studies to the development of the prothrombotic state in HIT by Step 3 propagation and potential new targets for therapy based on these studies are discussed.

Methods

Mice and human samples.

HIT mice were transgenic hPF4^{+}/FcγRIIA^{+} [56]. All HIT mice were also on a *Cxcl4*$^{-/-}$ background[168], as murine PF4 is not recognized by HIT antibodies[103]. Genetic alterations were confirmed by appropriate PCR analyses[101]. We used the CRISPR-Cas9 genome editing system[169] to disrupt *Padi4* exon2 in HIT mice (*Padi4*$^{-/-}$/HIT mice, **Figure 5.13**). Guide RNA (gRNA) flanking the targeted exon was designed to minimize off-target interactions[170] (5'-CCTAAGGGCTACACAACCTT-3' and 5'-GCTGGCTGCTTTCACCTG-TAC-3') and injected into harvested embryos at concentrations of 50 ng/μL along with Cas9 mRNA 100 ng/μL by the CHOP Transgenic Mouse Core. Oligonucleotide primers designed to amplify the 0.2 kb region of the gene encasing Exon 2 (5'-CATCTGTTCTGCTGCTGGCTG-3', 5'-CTCCTAAGGGCTACACAACCTTC-3') were used to confirm the presence of the desired gene disruption. Functional abrogation of PAD4 activity was confirmed by stimulating neutrophils isolated from the bone marrow of *Padi4*$^{-/-}$ mice and plated on poly-L-lysine-coated slides (Sigma-Aldrich) with 100 nM of phorbol-12 myristate 13-acetate (PMA, Sigma-Aldrich) overnight at 37°C and then staining the cells with SYTOX green (1 μM) and anti-histone H3 antibody Ab5103 at a dilution of 1:500 to visualize NET release (**Figure 5.13B**). Both *Padi4*$^{+/+}$/HIT and *Padi4*$^{-/-}$/HIT mice were studied at 10-30 weeks of age. Only male mice were used in the cremaster vessel injury experiments; however, in previous studies, we have not appreciated any sex differences in thrombosis in the passive immunization HIT murine model following photochemical carotid artery injury[50].

Deidentified plasma samples were obtained from patients with suspected HIT[104]. All subjects were evaluated with a polyspecific PF4/heparin ELISA (Immucor)[47] and a serotonin-release assay[171,172], and classified as having or not having HIT by a panel of three independent expert adjudicators who based their decision on laboratory results and clinical findings. Control plasma was obtained from healthy individuals and patients diagnosed with immune thrombocytopenia (ITP)[173]. Citrated plasma was stored at -80°C and MPO concentrations were measured by ELISA (Biolegend). IgG was isolated from plasma from some HIT patients and healthy donors using protein G agarose (Pierce)[50].

Antibodies and other labeled probes.

KKO, an anti-PF4/heparin monoclonal antibody, and TRA, a mouse IgG $2b_K$ isotype control monoclonal antibody[47], were purified from hybridoma supernatants. Anti-Fibrin 59D8 monoclonal antibody was provided by Harmut Weiler of the Blood Center of Wisconsin[56] PF4 was visualized using a polyclonal rabbit anti-human PF4 antibody (abcam). A rabbit anti-citrullinated histone 3 (cit-H3, Ab5103, abcam) was used to visualize citrullinated H3 and rabbit anti-MPO antibody (EMD Millipore), was used to label NETs. Both of these antibodies were labeled for visualization with a goat anti-rabbit IgG H&L Alexa Fluor 594 (ab150080, abcam). F $(ab')_2$ fragments of the anti-mouse CD41 monoclonal antibody MWReg30 and of the anti-mouse Ly-6G antibody 1A8 (BD Biosciences) were used to detect murine platelets and neutrophils, respectively, in the cremaster laser injury model. HIT antibodies purified from patient plasma samples were visualized with an anti-human IgG Fc secondary antibody (eBioscience). All antibodies were either labeled using Alexa Fluor antibody-labeling kits according to manufacturer's instructions or species-appropriate Alexa Fluor-conjugated secondary antibodies (all from

ThermoFisher Scientific). Extracellular DNA was visualized using SYTOX green or orange nucleic acid stain (ThermoFisher Scientific).

NET-lined microfluidic channel studies.

Experiments were performed using a BioFlux 1000 Controller (Fluxion) with an attached heating stage at 37°C as described[108]. The BioFlux channels were visualized with an Axio Observer Z1 inverted microscope (Zeiss) equipped with a motorized stage and an HXP-120 C metal halide illumination source. The microscope and image acquisition were controlled by BioFlux Montage software with a MetaMorph-based platform (Molecular Devices). Isolated human neutrophils (2×10^6 cells/ml) were incubated with 1 ng/ml TNFα (Gibco) at room temperature for 10 minutes and then flowed through channels coated with 50 µg/ml of fibronectin (Sigma-Aldrich), to which they adhere, and then incubated with 100 ng/ml PMA overnight at 37°C. Cell-free DNA (cfDNA) release was visualized with 1 µM SYTOX green or orange, and the channels were infused with recombinant PF4 (0-200 µg/ml), expressed and purified as we described[174], with or without unfractionated porcine heparin (0.4 U/ml, BD Biosciences) at 2-5 dynes/cm^2. To confirm that the cfDNA structures adherent to the microfluidic channel walls were NETs, we performed co-immunolocalization in which channels ± PF4 (25 µg/ml) were incubated with either anti-cit-H3 at 4°C overnight or anti-MPO at 37°C for 1 hour, and then incubated with an Alexa Fluor 594 conjugated secondary antibody for 1 hour at 37°C prior to imaging with a Zeiss LSM 710 laser-scanning confocal microscope. Structures with co-localization of cfDNA and MPO or citrullinated histones were deemed to be NETs. PF4-NET complexes were then incubated with 25 µg/ml of KKO or a polyclonal anti-PF4 antibody (abcam) for 1 hour at 37°C. NET digestion studies were carried out by infusing the channels with 100 U/ml DNase I (Sigma-Aldrich) at 2 dynes/cm^2 after which the channels were washed with

phosphate-buffered saline (PBS, Gibco) and fixed with 2% paraformaldehyde (BD Biosciences). To avoid laser-induced changes to the conformation of DNA[175], we minimized laser exposure during our experiments. To account for this effect when studying whether KKO binding to PF4/NET complexes increased resistance to DNase I, we compared NET digestion by analyzing videos in which channels with and without KKO were included in the same visual field and exposed to UV light for the same amount of time. Channels were blocked with PBS with 2% BSA, and PF4-NET complexes were visualized by incubating SYTOX-labeled NETs with a rabbit anti-human PF4 antibody at 37°C for 1 hour, rinsing the channels with PBS flowed at 5 dynes/cm^2 for 5 minutes, and then incubating with an anti-rabbit secondary antibody at 37°C for 1 hour. KKO was labeled with Alexa Fluor 647 (ThermoFisher Scientific) prior to NET channel infusion. NET complexes were imaged with a Zeiss LSM 710 laser-scanning confocal microscope. Similar studies were done using 100 U/ml bacterial-derived micrococcal nuclease (New England Biolabs). Data were analyzed using ImageJ open source image processing software[176].

Endothelialized channel microfluidic studies.

We used the TNFα inflammatory thrombosis microfluidic model described in Chapter 2. Briefly, endothelialized microfluidic channels were incubated with TNFα (1-10 ng/ml) to simulate inflammation. Whole blood samples obtained from healthy human donors were fluorescently labeled with 2 mM calcein AM to visualize leukocytes and platelets and then incubated with KKO or TRA (25 μg/ml) for 15 minutes. The samples were then recalcified with $CaCl_2$ (11 mM final concentration) and immediately flowed through the channels at 5 dynes/cm^2. When using ImageJ to count endothelial-adherent cells, size exclusion thresholds were used to distinguish platelets from leukocytes. To

assess KKO binding to TNFα-stimulated endothelium, the HUVEC-lined channels were infused with PBS containing PF4 (10 μg/ml) and KKO (25 μg/ml) conjugated with Alexa Fluor 488 (Invitrogen) at 5 dynes/cm^2. Following the infusion, the channels were washed with PBS and fixed with 2% paraformaldehyde (BD Biosciences). KKO binding was quantified based on fluorescent measurements obtained from a Zeiss LSM 710 laser scanning confocal microscope. Levels of KKO-endothelial binding were compared to those observed after the whole blood samples containing PF4 and KKO were infused through HUVEC channels that had been subjected to hematoporphyrin (50 μg/ml, Sigma-Aldrich) photochemical injury, as our group has previously described[43].

Femoral vein neutrophil rolling studies.

HIT mice were anesthetized with nembutal and a skin flap extending from the ankle to thigh was removed to expose the femoral vein. SYTOX orange (2 nM) and F(ab′)$_2$ fragments (0.2mg/g mouse) directed against Ly6-G and CD41 were infused as 100 μL boluses via a catheter placed into the jugular vein to detect cfDNA, neutrophils, and platelets respectively. Confocal microscopy was used as described previously[98] to obtain videos of neutrophil rolling and adhesion in the femoral vein at baseline and 10 minutes after 1 μg/g of KKO was infused via the jugular catheter. Data were collected and confocal time-lapsed images were analyzed using Slidebook 6.0 to compare neutrophil behavior before and after KKO exposure.

Isolated human neutrophils.

Human blood was collected after informed consent from healthy aspirin-free volunteers through a 19-gauge butterfly needle into 4 ml vacutainers coated with 7.2 mg of ethylenediaminetetraacetic acid (Becton Dickinson). Blood samples were stored at

room temperature and used within 1 hour. Neutrophils were isolated with negative bead selection using the MACSxpress Neutrophil Isolation Kit (Miltenyi Biotec). The supernatant was collected and centrifuged at 300g for 10 minutes, and the cell pellet was resuspended in 2 ml ammonium-chloride-potassium (ACK) lysing buffer (ThermoFisher Scientific) for 5 minutes to lyse erythrocytes, after which the cells were washed with 10 mLs of Hank's balanced salt solution (HBSS, ThermoFisher Scientific), and then resuspended in HBSS containing calcium chloride (1.3 mM) and then manually counted, with trypan blue dye exclusion (Gibco) for cell viability.

Bioassay for NET digestion.

PF4-induced NET resistance to digestion was quantified using a modified version of a previously described assay[98]. Isolated human neutrophils resuspended in HBSS, were stimulated with TNFα (1ng/ml) for 5 minutes and transferred to a fibronectin-coated (50 µg/ml) 96 well plate with 2 x 10^5 cells placed in each well. The samples were incubated with 100 nM of PMA ≥ 4 hours at 37°C to stimulate NET release. NETs were incubated with PF4 (0-50 µg/ml) ± KKO (25 µg/ml). Released cfDNA was labeled with SYTOX green (1µM), and a baseline reading was obtained with fluorescence spectrometry, excitation 485 nm and emission 537nm (SpectraMax M2, Molecular Devices). The samples were then incubated with 1U/ml DNase I (Sigma-Aldrich) for 30 minutes at 37°C and a repeat fluorescence reading was obtained. The percent original fluorescent intensity was measured for each well with higher values reflecting increased DNase I resistance.

Glass slide NET compaction and digestion studies.

To assess NET behavior without exposure to fibronectin, isolated human neutrophils resuspended in HBSS at a concentration of 2 x 10^6 cells/ml were allowed to

settle on uncoated microscope cover glass slides (Fisherbrand) placed in a 24 well tissue-culture plate (Falcon) for 30 minutes at 37°C. The supernatant was aspirated and 500 µL of HBSS containing PF4 (0-50 µg/ml) was added to the wells and incubated at 37°C for 1 hour. The supernatant was again aspirated and 500 µL of DNase I (100U/ml) was added to the wells and incubated on a standard analog rocker (VWR) at 37°C for 1 hour. Images of the NETs before and after compaction and digestion were obtained with Axio Observer Z1 inverted wide field microscope (Zeiss) and data were analyzed using ImageJ opensouce image processing software[176].

Cremaster laser injury studies.

Intravital microscopy was performed as described[154] using *Padi4*$^{+/+}$ and *Padi4*$^{-/-}$ HIT mice. Arterioles and venules of 20-40µ diameter were studied, and injury was induced with an SRS NL100 pulsed nitrogen dye laser (440nm) focused on the vessel wall and pulsed until the vessels were perforated as indicated by the release of a small number of erythrocytes. Prior to injury induction, SYTOX green or orange (1µM) and $F(ab')_2$ fragments (0.2 mg/g mouse) were infused as 100 µL boluses via a catheter placed into the jugular vein. After 1-3 injures were made, 1 µg/g of KKO or TRA was infused, and an additional 3-4 injuries were made with maximum experimental time per mouse being 2 hours. In some studies, the mice were treated with the CXCR2 antagonist SCH527123 (10 mg/kg, Apexbio) resuspended in distilled H_20 with 5% dimethyl sulfoxide (Sigma-Aldrich). In other studies, the mice were treated with an IV bolus of bovine pancrease-derived DNase 1 (100U/mouse, Sigma-Aldrich) immediately prior to KKO injection and laser injury. Widefield and confocal microscopy were performed. Data were collected and confocal time-lapsed images of platelet and neutrophil accumulation were analyzed using Slidebook 6.0. Confocal *Z*-stacks were obtained immediately following injury at 5 minutes

and again 60 minutes following KKO or TRA infusion. Data were analyzed with Slidebook 6.0 to measure platelet thrombus volumes.

Statistical analysis.

Differences between 2 groups were compared using a 2-sided Student's *t* test with Welsh's correction or a Mann-Whitney *U* test. Normal distribution was tested using the D'Agostino & Pearson normality test. Differences between >2 groups were determined by one- or two-way ANOVA (as appropriate) and a Kruskall-Wallis test was performed when data was not normally distributed. Multiplicity corrected p values are reported for multiple comparisons. Statistical analyses were performed using Microsoft Excel 2011 and GraphPad Prism 7.0 (GraphPad Software). Differences were considered statistically significant when *P* values were ≤0.05.

Study approval.

Animal procedures were approved by the Institutional animal care and use committee (IACUC) of the CHOP and in accordance with NIH guidelines and the Animal Welfare Act. Anonymized human blood was collected after signed, informed consent was provided by healthy donors, and approval for studies using human blood was obtained from CHOP's Human Review Board in accordance with Declaration of Helsinki principles.

Results

Enhanced neutrophil adhesion to the venular endothelium in HIT.

Neutrophils are activated when exposed to PF4 and HIT antibodies[122]. To determine if this activation might impact neutrophil-EC interactions, we infused calcein-AM labeled whole blood through HUVEC-lined microfluidic channels and quantified cell adhesion over time. We observed scant leukocyte-endothelium adhesion in unstimulated channels that was unchanged by the addition of the HIT-like monoclonal antibody KKO or the isotype control TRA (data not shown). However, when the HUVEC cells were pre-treated with TNFα, there was a two-fold increase in the number of adherent leukocytes in samples incubated with KKO, which induces the release of endogenous PF4 from platelets[47], compared to samples treated with the isotype control TRA (**Figures 5.1A, 5.1B, and 5.1C)**. We did not observe that TNFα treatment led to an increase in KKO binding to the HUVECs (**Figure 5.2**) supporting that the increase in leukocyte adhesion seen in vivo was at least in part a result of leukocyte rather than endothelial activation. We then asked if these findings could be recapitulated in vivo using a murine HIT model following injection of KKO[56]. Within 30 minutes of KKO infusion, we observed increased neutrophil rolling and adhesion to uninjured cremaster muscle venules, but no neutrophil rolling or adhesion occurred in uninjured cremaster arterioles before or after the animals were exposed to KKO (**Figures 5.1D** and **5.1E**). We similarly observed an increase in neutrophil adhesion in the femoral vein 10 minutes following treatment with KKO (**Figures 1F** and **1G**).

Enhanced neutrophil involvement in venular thrombosis in HIT.

We next asked whether exposure to HIT antibodies influences neutrophil incorporation into thrombi in vivo in the murine model of HIT. Cremaster vessels were injured at time 0 and adherent neutrophils and platelets were quantified at 5 minutes. The mice were then infused with KKO or TRA, and the thrombi were reexamined at 60 minutes. While there was an increase in platelet accumulation in arterioles following HIT induction, only a small number of neutrophils were incorporated into arteriolar thrombi, with a small but significant increase following treatment with KKO (**Figure 5.3**). At sites of venular injury prior to HIT-induction, there was platelet and fibrin accumulation (**Figure 5.3B** and **Figure 5.4**, respectively) but only a small number of neutrophils adhered to these thrombi (**Figure 5.3A** and **5.3C**). In contrast, following HIT induction, there was marked increase in neutrophil accumulation within venular thrombi (**Figure 5.3C**) with a minimal change in fibrin accumulation (**Figure 5.4**) and platelet volume (**Figure 5.3B**). The rise in neutrophil accumulation was not observed following TRA infusion (**Figure 5.3A** through **5.3C**).

A CXCR2-dependent retrograde migration of neutrophil into venular thrombi in HIT.

To better understand the process of neutrophil accumulation in venular thrombi in HIT, we induced laser injuries in venules following KKO infusion, and monitored platelet and neutrophil accumulation in these lesions over 5 minutes. While platelets quickly adhered directly to the site of venous injury, most neutrophils initially bound to the endothelium 30-40 microns downstream of the injury (**Figure 5.5**). This finding is likely due to a combination of increased neutrophil adhesiveness induced by KKO exposure, documented in **Figure 5.1**, in addition to activation of the endothelium downstream of cremaster laser injuries in HIT that we have previously described[43]. These neutrophils subsequently migrated in a retrograde direction into the evolving thrombus (**Figure 5.5A**) and 60 minutes following the initial injury, a significantly higher number of neutrophils were

present in venular thrombi in mice exposed to KKO compared to those infused with the isotype control TRA (**Figures 5.5A** and **5.5B**). We hypothesized that retrograde migration of adherent neutrophils into the thrombi was induced by a chemoattractant released by activated platelets in the clots. Activated platelets release several chemokines from their α granules that cause neutrophil migration by engaging neutrophil surface CXCR2[177]. To test whether the retrograde recruitment of neutrophils to venular thrombi in HIT was chemokine-dependent, we treated the mice with the CXCR2 antagonist SCH527123[177] prior to the induction of HIT. We observed that thrombi in mice treated with SCH527123 before KKO infusion contained significantly fewer neutrophils within their thrombi (**Figure 5.5**). Furthermore, these neutrophils were located at the periphery of the platelet-rich thrombi and not embedded within them.

In vitro studies of PF4-NET interactions.

After observing marked HIT-induced neutrophil infiltration in venular thrombi, we hypothesized that adherent neutrophils contribute to venous thrombi in HIT, in part, through the release of NETs, as described in deep venous thrombosis[178]. Moreover, platelet activation, one of the hallmarks of HIT, can initiate NETosis in inflammatory states[179,180]. Activated platelets release high levels of PF4, which forms high-molecular weight aggregates with various polyanions, producing antigens that are recognized by HIT antibodies[141]. We postulated that when PF4 is released in HIT, due to its cationic charge, it will bind to cfDNA present in NETs and impact NET biology. To investigate PF4-NET interactions in real time, we studied neutrophils adherent to fibronectin-coated microfluidic channels stimulated with PMA to release NETs. We confirmed that these cfDNA structures were NETs by using co-immunofluorescent staining to show that they contained citrullinated histones and MPO (**Figure 5.6**). The NET-lined channels were then infused

at venular flow rates with buffer containing PF4 at concentrations readily attained at sites of platelets activation (5-100 µg/ml)[122]. Prior to exposure to PF4, NETs labeled with SYTOX were round and transparent, with a cloud like appearance that we termed “fluffy”. When infused with HBSS or human plasma, the NETs extended, and when flow was stopped they rebounded to their former shape. Following treatment with either buffer or plasma containing PF4, the NETs became opaque and narrow with a sharply tapered tail that did not change shape when flow was stopped. (**Figure 5.7A**, **Figure 5.6**). Maximum compaction, with a 50% reduction in NET area, was achieved when the NETs were flowed with HBSS containing PF4 concentrations of ≥10 µg/ml (**Figure 5.7B**, left, for PF4 ≤25 µg/ml and not shown for >25 µg/ml). Confocal imaging of the compacted NETs, labeled with an anti-PF4 antibody and a fluorophore-conjugated secondary antibody, confirmed that PF4 bound to these structures (**Figure 5.7A**). Total NET DNA content measured by fluorescence intensity was preserved following PF4 infusion, excluding the possibility that the compacted NET appearance was due to the dissolution of DNA (**Figure 5.7B**, right). Co-immunofluorescent studies of NETs following PF4 infusion demonstrated that compaction does not lead to displacement of citrullinated histones or MPO (**Figure 5.6**).

We next asked whether PF4-induced changes in NET morphology could impact NET behavior. While PF4-free NETs were highly susceptible to DNase I at a concentration of 100U/ml, with near complete digestion in <2 minutes, PF4-bound NETs were resistant to DNase I, with near-complete protection at PF4 concentrations of ≥10 µg/ml (**Figure 5.7C** and **5.7D**). The infusion of human plasma containing PF4 was also found to confer resistance to DNase I-mediated digestion (**Figure 5.8**) and similar results were observed with the use of bacterial-derived micrococcal nuclease (**Figure 5.9**). Comparable nuclease resistance was also observed in a static system not coated with fibronectin, showing that

fibronectin, which has a DNA binding domain and is known to interact with NETs[181], is not the cause of the observed changes in NET behavior (**Figure 5.8**).

Previous in vitro studies reported that NETs are degraded by exposure to heparin[182], suggesting that NETs should be reduced in patients with recent heparin exposure. We found that at a therapeutic concentration of 0.4U/ml[147] or at a supratherapeutic concentration of 5000U/ml, heparin did not degrade NETs in our microfluidic system; however, we observed that exposure to heparin, reversed compaction with restoration of fluffy morphology (**Figure 5.10A** and **5.10B**). Confocal imaging of NETs labeled with a polyclonal anti-PF4 antibody confirmed that heparin treatment removed PF4 from the NETs (**Figure 5.10A**), and DNase I infusion studies confirmed that decompaction of NETs restored their susceptibility to endonuclease digestion (**Figure 5.10C** and **5.10D**). However, when NETs were exposed to a 25 µg/ml instead of 10 µg/ml of PF4, a concentration still within the range typically observed at sites of thrombosis[88], NET compaction and DNase resistance were maintained during co-infusion with therapeutic concentrations of heparin (**Figure 5.10C** and **5.10D**).

In vitro effects of HIT antibodies on PF4-NET complexes

PF4 has previously been shown to form complexes with DNA aptamers that are HIT antigenic targets[124]. We, therefore examined whether PF4-NET complexes are also recognized by KKO and IgG isolated from HIT patient plasma using the microfluidic chambers to assess binding and function. We found that KKO and HIT IgG suspended in HBSS did not interact with non-compacted NETs, but both bound to PF4-NET complexes (**Figure 5.11A** and **Figure 5.12A**). KKO dissolved in human plasma also bound specifically to PF4-NET complexes. (**Figure 5.12A**). Antibody binding did not induce greater NET compaction, but it enhanced resistance to DNase I digestion (**Figure 5.11B**).

This effect was found to be specific to HIT antibodies, as incubation with a polyclonal anti-PF4 antibody at 25 µg/ml did not provide similar protection from endonucleases (**Figure 5.11C** and **5.11D**). Similar results were seen using NETs immobilized to fibronectin-coated 96-well plates (**Figure 5.11E**)[183].

Thrombosis in the HIT murine model in the presence or absence of PAD4.

We then asked whether enhanced NET endonuclease resistance and the formation of PF4-NET-HIT antibody complexes, observed in vitro, contribute to in vivo thrombus development in the murine model of HIT. We hypothesized that the release of NETs by thrombus-adherent neutrophils and their subsequent modification by PF4 and HIT antibodies may play a role in the prothrombotic state that develops in these animals. To better understand the way in which NETosis may contribute to thrombosis in HIT, we studied *Padi4*$^{-/-}$/HIT mice that are incapable of releasing NETs (**Figure 5.13**). Previous studies have shown that *Padi4* knockout mice do not release NETs and are protected from venous thrombosis[178]. Following KKO injection, severity of thrombocytopenia in *Padi4*$^{-/-}$ /HIT mice was comparable to that seen in *Padi4*$^{+/+}$/HIT controls. (**Figure 5.14A**) The size of arteriolar thrombi following laser injury was unaffected by PAD4 deficiency (**Figure 5.14B**) and neutrophil incorporation into venule thrombi following TRA injection was similar in *Padi4*$^{-/-}$ and *Padi4*$^{+/+}$ HIT mice. However, after KKO injection, the *Padi4*$^{-/-}$/HIT mice developed smaller venular thrombi following injury (**Figure 5.14C** and **5.14D**) with incorporation of fewer neutrophils (**Figure 5.14E**). This difference became more pronounced with the passage of time (**Figure 5.14C**). Consistent with these studies in *Padi4*$^{-/-}$ HIT mice, *Padi4*$^{+/+}$ HIT mice treated with DNase I prior to KKO infusion, had a significant decrease in platelet thrombus volume 60 minutes following injury (**Figure**

5.14C), suggesting that NETs play a role in thrombus growth and stabilization in this model.

Clinical indication of NETosis in HIT

It has been reported that circulating MPO levels are elevated in HIT[165], potentially implicating neutrophils and NETosis in the pathobiology of HIT. We confirmed this clinical finding comparing cfDNA and MPO levels in samples from patients at high- or at low-likelihood of having HIT[44], healthy controls, and patients with immune-thrombocytopenia (ITP). Both MPO levels (**Figure 5.15A**) and cfDNA (**Figure 5.15B**) were significantly higher in individuals diagnosed with HIT compared to healthy controls and patients with an alternative cause of immune thrombocytopenia. However, we did not observe a significant difference in MPO or cfDNA concentrations between patients diagnosed with HIT compared to ill patients evaluated for HIT, but found to have a low probability of having the disease. These findings demonstrate that neutrophil activation and NETosis occur in multiple proinflammatory/prothrombotic states that commonly occur in hospitalized patients.

Discussion

Over the past several years, it has become increasingly clear that the pathophysiology of HIT extends beyond platelet activation in Step 2. It has previously been shown that HIT antibody interaction with other cells types including the endothelium[43] and monocytes[50], leads to cell activation and a prothrombotic state as described in Step 2. Others have also demonstrated that HIT antibodies activate PF4-exposed neutrophils through their FcγRIIA receptors, leading to increased expression of Mac-1 on the cell surface and enhanced neutrophil aggregate formation[122]. In this paper, we explore specific

pathways by which neutrophils may contribute to thrombosis in Step 2, and propose that they do so through multiple steps including the stimulation of neutrophil adhesion to inflamed endothelium, the promotion of neutrophil migration into venular thrombi, and the formation of antigenic PF4-NET-HIT antibody complexes that contribute to propagation via Step 3.

The basis for enhanced binding of HIT-activated neutrophils to the endothelium in large vessels and the microcirculation requires further exploration. Prior studies have shown that HIT antibody exposure increases neutrophil surface expression of Mac-1[122]. ECs are also activated by PF4 and HIT antibodies, increasing surface expression of P- and E-selectins[93]. Our finding of enhanced in vitro neutrophil binding parallels the increased adhesion seen in vivo in the setting of our murine model of HIT, with or without EC injury. We speculate that neutrophil adhesion immediately downstream of growing venular injury may be due to increased turbulent flow around larger thrombi, that is known to enhance neutrophil adhesion to the endothelial lining[184]. It may also be due to the release of PF4 from activated platelets within the thrombus that results in increased assembly of antigenic complexes on the downstream endothelium, leading to more HIT antibody binding and endothelial activation[43]. The role of each of these mechanisms in the accumulation of neutrophils in injured venules requires additional investigation to identify opportunities for intervention.

After adhering to the endothelium downstream of thrombosis, many neutrophils migrate in a retrograde manner and are incorporated into the venular clots. Retrograde migration may occur in response to a chemotactic gradient emanating from degranulating platelets. A similar process termed “directed intravascular migration” has been described in ischemia-reperfusion injuries, in which degranulating platelets release CXCL7 (neutrophil activating peptide 2 (NAP2)) and CXCL5 (epithelial-derived neutrophil-

activating peptide 78 (ENA-78)), leading to CXCR2-dependent neutrophil recruitment[185]. The retrograde migration we observed in venular HIT thrombi is also similar to "neutrophil-swarming," a process in which large numbers of neutrophils rapidly accumulate at sites of infection or sterile injury where they release NETs[186]. In support of this hypothesis, we show that the retrograde migration of neutrophils into venous thrombi can be abrogated with the blockade of CXCR2. Whether NAP2 and/or ENA-78, both released from platelets and bound by CXCR2[187], contribute to the chemogradient remains to be determined. Further investigation needs to be done to ascertain if this pattern of adhesion occurs in other prothrombotic disorders associated with venous thrombosis.

Many groups have proposed that NET release links neutrophil accumulation to thrombus progression[178,188,189]. We posit that NETs released in HIT are uniquely prothrombotic because the binding of PF4 and HIT antibodies causes them to become immunogenic. Previous studies have shown that nucleic acid binding leads to the exposure of the same antigenic epitopes present on PF4/heparin complexes[124]. Mice injected with PF4/nucleic acid complexes develop antibodies that cross-reacted with PF4/heparin complexes[124]. Our microfluidic channel experiments support that PF4 forms complexes with chromatin DNA in the same way as PF4 binds heparin to form macroaggregates[190]. Our studies showing that HIT IgG isolated from human plasma binds to these PF4-NET complexes, confirms that they contain HIT antigenic epitopes.

In addition to producing HIT antigenic complexes, we have observed that PF4 binding leads to chromatin compaction that causes NETs to become DNase resistant. It has previously been shown that NET binding to the cationic peptide LL-37 leads to enhanced protection from nuclease digestion[191], in a manner similar to what we have observed with PF4. While DNase-resistant NETs may have increased antimicrobial activity, impaired NET degradation has been implicated in the pathogenesis of

autoimmune diseases, including anti-phospholipid antibody syndrome and lupus[192,193]. In these disorders, DNase resistance is thought to occur due to the development of anti-NET immunoglobulins that interfere with DNase binding to cfDNA[183]. In HIT, PF4 forms complexes with NETs that are bound by HIT antibodies that provide additional protection from DNases. These stable, compacted PF4-NET-HIT IgG aggregates then serve as a Fc-rich surface that can recruit and activate circulating hematopoietic cells via their FcγRIIA receptors and activate the complement cascade[163].

To test this hypothesis, we generated *Padi4*$^{-/-}$ HIT mice that do not undergo NETosis[167,178,194]. In these animals, venular thrombi generated after HIT induction are markedly smaller than those observed in animals capable of NET release, with fewer incorporated neutrophils and decreased platelet volumes. This suggests that NETs contribute to the early stages of venule thrombus growth, enhancing both platelet accumulation and neutrophil recruitment. This effect was not observed in laser injury-induced arteriole thrombi, which have little neutrophil infiltration irrespective of PAD4 activity. Moreover, the loss of PAD4 activity – and likely NET formation – did not affect the severity of thrombocytopenia in HIT mice, suggesting that the development of venular thrombi is unrelated to the mechanism underlying the development of thrombocytopenia.

In vivo NET visualization is technically difficult, and most in vivo studies rely on functional analysis. We therefore treated HIT mice with DNase prior to cremaster laser injury and found that this led to a significant decrease in cremaster venule thrombus platelet volumes. This finding further supports our hypothesis that NETs play a role in thrombus growth and stabilization in this model. However unlike in the *Padi4*$^{-/-}$/HIT mice, the number of thrombus-adherent neutrophils did not fall in accordance with the decrease in platelet volumes. This difference may occur because *Padi4*$^{-/-}$ mice never release NETs, whereas PF4-compacted NETs are incompletely degraded by DNase and may still expose

PF4-NET-HIT IgG aggregates that can recruit circulating neutrophils. Nonetheless, the decrease in venular thrombus size raises the possibility that DNase treatment may be effective in preventing the venular prothrombotic state in HIT.

In summary, we demonstrate that neutrophils contribute to the prothrombotic state in Step 2 of HIT (Figure 1.5) through enhanced adhesion to the endothelium downstream of venous thrombi and subsequent retrograde migration into these thrombi. There, activated neutrophils release NETs that form complexes with PF4 that are subsequently bound by HIT antibodies. These PF4-NET-HIT antibody complexes are protected from DNases and may contribute to thrombus propagation in Step 3 by exposing an Fc-rich surface. Thus, our studies extend the range of PF4-bound HIT antigenic polyanionic targets beyond heparin, GAGs, and polyphosphates. This would implicate that neutrophil-derived NETs, are a key figure in the venular thrombus propagation in HIT (Figure 1.5). HIT mice that have neutrophils unable to undergo NETosis have smaller venous thrombi, but still develop enhanced arterial clots and thrombocytopenia. Further work is required to understand whether neutrophils contribute similarly to the development of venous thrombi in other immune/inflammatory prothrombotic states such as the anti-phospholipid antibody syndrome and sepsis. More investigation is needed to determine if blocking these pathways will help prevent venous thromboembolic complications in patients with HIT or other prothrombotic disorders.

Figures

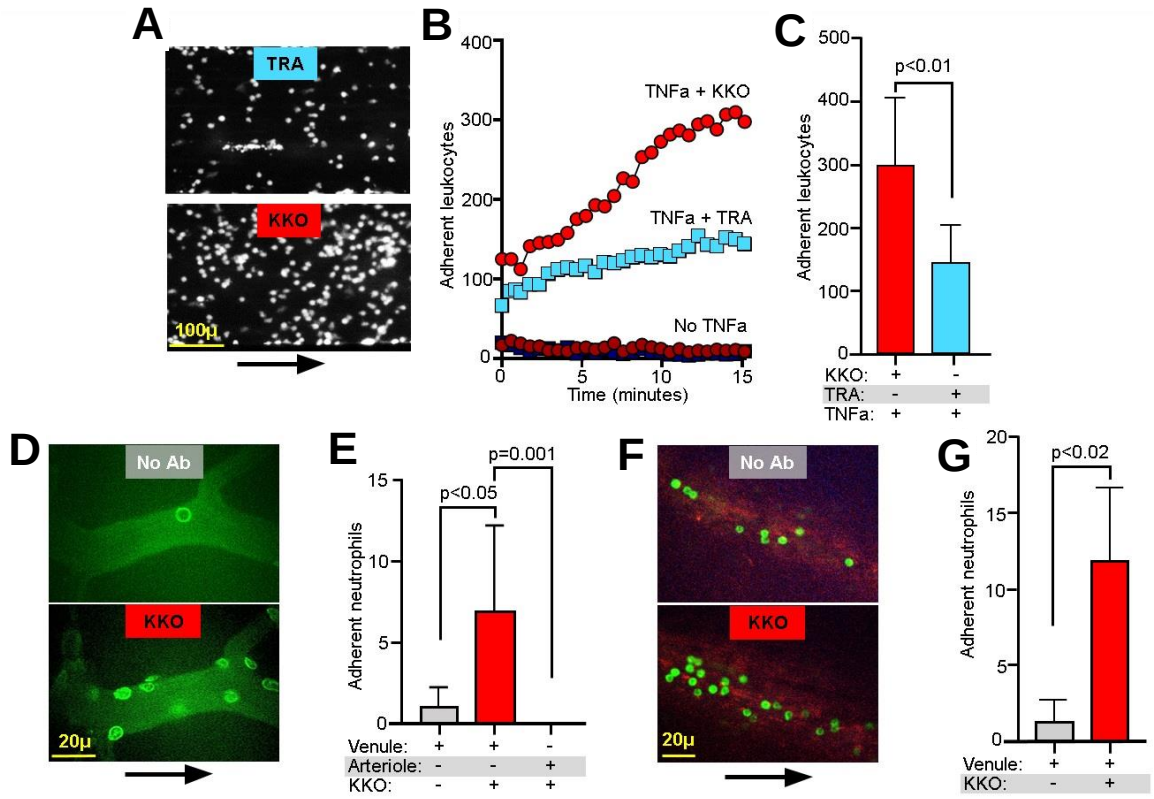

Figure 5.1. Enhanced leukocyte-endothelial adhesion in HIT.

(**A**) Calcein-AM labeled blood incubated with KKO (red) or TRA (blue) was infused through HUVEC-lined channels exposed to TNFα. Representative widefield image of leukocytes (white) adhering to the endothelium is shown. Size bar and arrow indicating direction of flow are included. Image was obtained with an Axio Observer Z1 inverted microscope using x10 magnification. (**B**) Leukocyte-endothelial adhesion was quantified for KKO (red) and TRA (blue). Six channels were studied in each TNFα-exposed arm (lighter colors) and 3-5 channels in the unexposed arms (darker colors). (**C**) The final number of adherent leukocytes at 15 minutes is shown as mean ± 1 standard deviation (SD). Comparative

analysis was performed by Student's t-test. (**D**) Representative confocal image of neutrophils rolling in a venule before and after KKO infusion. Neutrophils were stained using anti-Ly-6G $F(ab')_2$ fragment (green). Size bar and arrow indicating direction of flow are included. Images were obtained with an Olympus BX61WI microscope with a x40/0.8 numeric aperture water-immersion objective lens. (**E**) Neutrophil adhesion to cremaster arterioles and venules was studied in the HIT murine model prior to and 30 minutes after exposure to KKO. Adhesion was defined as neutrophil immobilization for ≥30 seconds. Seven and four animals were studied in the venular and arteriole arm, respectively. Statistical comparison of binding was preformed using a Kruskall-Wallis one-sided ANOVA. (**F**) Representative confocal image of neutrophil rolling and adhering to the femoral vein before and 15 minutes after the infusion of KKO. Images are as in (D). Size bar and arrow indicating direction of flow are included. (**G**) Graph representing neutrophil adhesion to the femoral vein ± KKO infusion as in (F). N = 4 per arm. Statistical comparison was performed by Student's t-test.

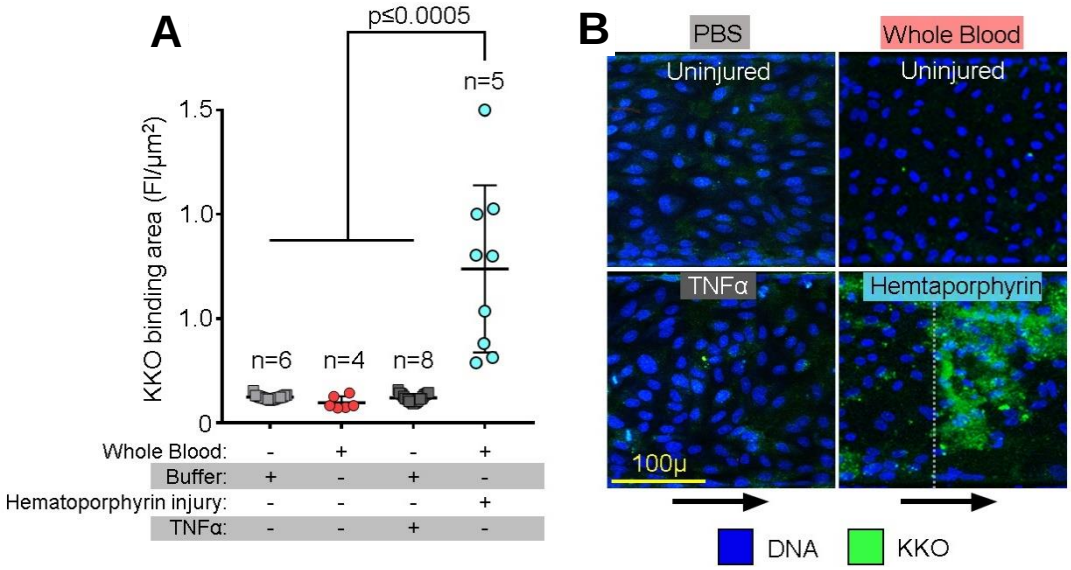

Figure 5.2. TNFα stimulation does not enhance KKO binding to HUVECs.

(**A**) Graph showing the mean ± 1 SD of KKO adhesion to microfluidic channels coated with a confluent layer of HUVECs after infusion of whole blood or PBS containing PF4 (25 μg/ml) and Alexa Fluor 488-conjugated KKO. Two fluorescent measurements were obtained from each channel. The number of channels per arm is indicated on the graph. The channels were either unstimulated, treated with TNFα prior to infusion, or subjected to photochemical hematoporphyrin injury. When whole blood was flowed through TNFα-treated channels, the channels clotted, leading to interference with fluorescence measurements. Therefore, we only infused these channels with PBS. Comparative statistical analysis was done with a Kruskal-Wallis one-way ANOVA. (**B**) Representative confocal images of an unstimulated channel infused with PBS, an uninjured channel infused with whole blood, a TNFα stimulated channel infused with PBS, and a whole blood infused channel subjected to photochemical injury on the right half of the presented field. In this image, KKO only adheres to the injured portion of the channel to the right of the gray dotted line. Scale bar and arrows showing direction of flow are indicated.

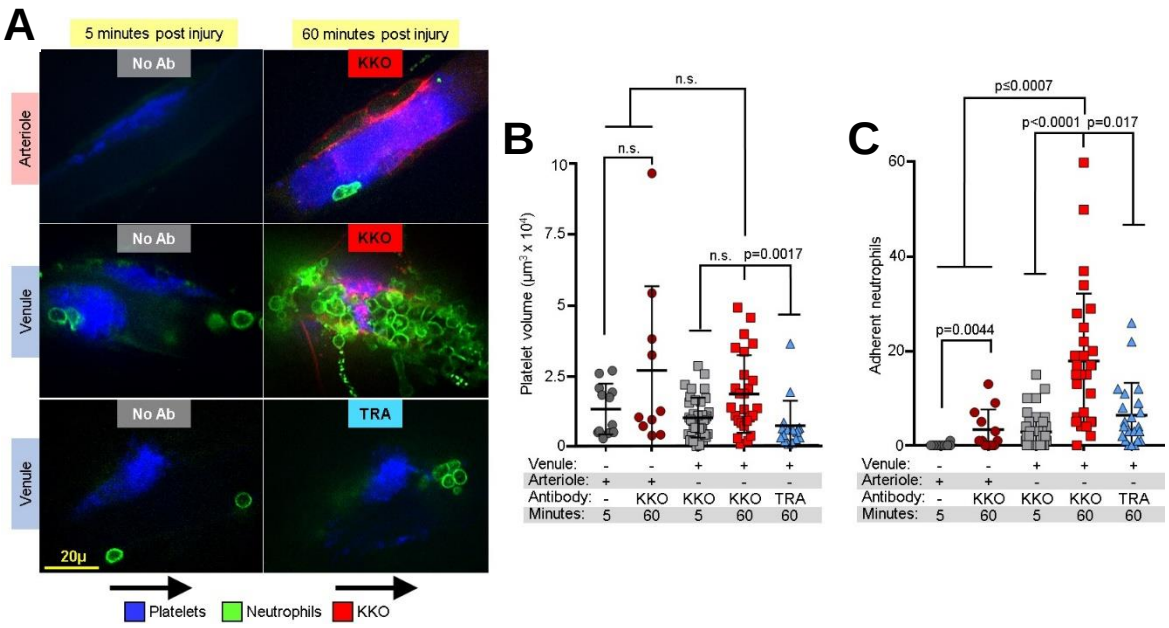

Figure 5.3. Effect of HIT of neutrophil accumulation in cremaster vessels pre- and post-injury.

(**A**) Representative confocal images from cremaster arteriole and venule laser injuries showing platelets labeled with anti-CD41 (dark blue) and neutrophils labeled with anti-Ly-6G (green). Paired images from the same vessel taken at 5 and 60 minutes following laser injury. KKO or TRA were infused intravenously beginning at minute 5 after injury. Size bar and arrow indicating direction of flow are included. Same microscope and acquisition software as in **Figure 5.1D**. (**B**) and (**C**) are graphs quantifying adherent neutrophils and platelets in the same thrombi, respectively. Twenty-eight injuries were made in twelve KKO-treated mice. Sixteen injuries were made in four TRA-treated mice. Twelve arteriole injuries were made in three untreated and three KKO-treated mice. Individual data points and mean ± 1 SD are shown. Comparative statistical analysis between 3 or more groups was performed by Kruskall-Wallis one-way ANOVA and comparisons between two groups was performed with a Student's t-test.

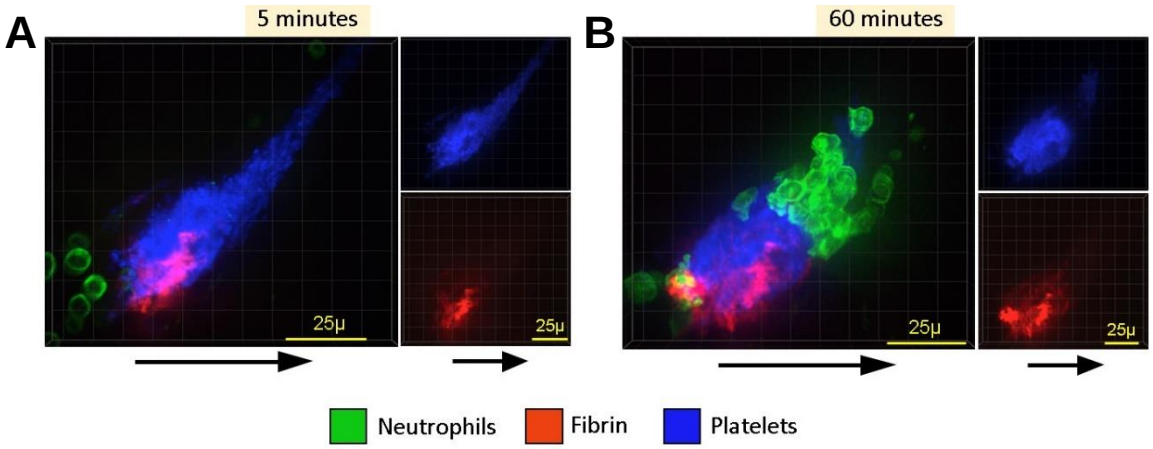

Figure 5.4. Fibrin generation occurs in cremaster laser injuries.

(**A**) Cremaster venule thrombus at 5 minutes after injury but prior to KKO exposure in HIT mice. Scale bar and arrows showing direction of flow are indicated. Fibrin and platelet accumulation are shown alone at the right. A composite image including the neutrophil stain is shown on left. (**B**) The same injury 60 minutes following KKO administration.

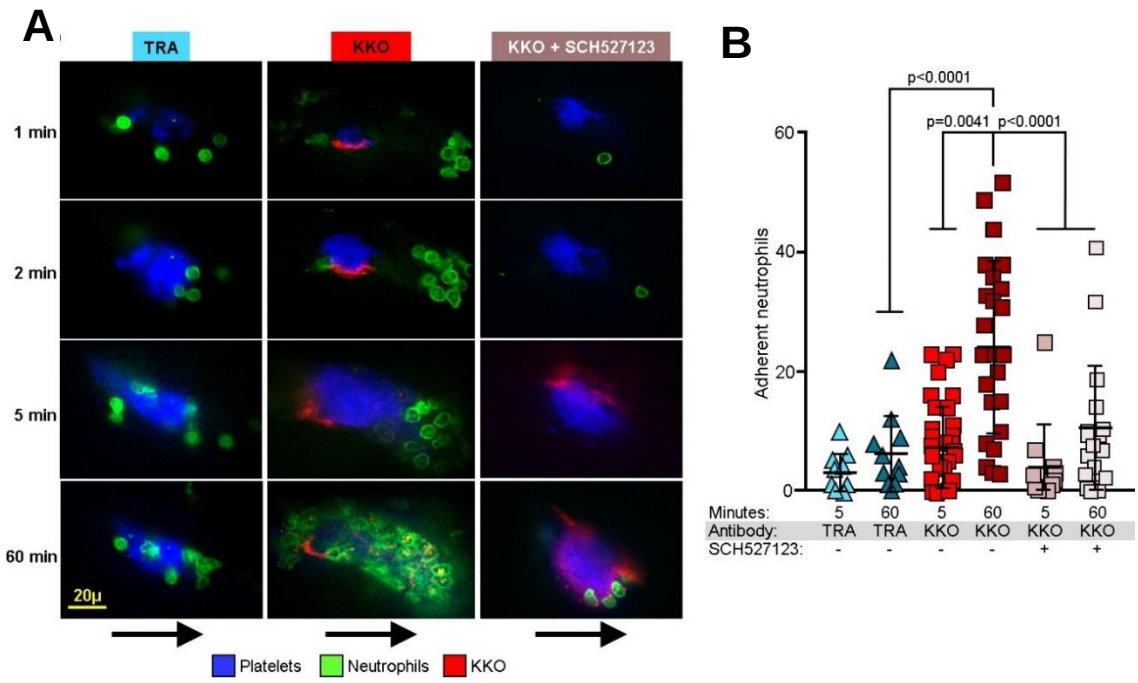

Figure 5.5. Chemokine-dependency of neutrophil accumulation into venous thrombi in HIT.

(**A**) Representative confocal images of cremaster venule injuries showing platelet (blue), neutrophil (green) and KKO staining (red) at 1-60 minutes following laser injury. Typical injuries are shown from mice infused with TRA, KKO, and KKO + SCH527123, a CXCR2 antagonist[195]. Size bar and arrow indicating direction of flow are included. Same microscope and acquisition software as described in **Figure 5.1D**. (**B**) Graphs quantifying adherent neutrophils in venule thrombi 5 and 60 minutes following laser injury. Thirty-two injuries were made in 12 KKO-treated mice. Seventeen injuries were made in 3 TRA-treated mice. Eleven injuries were made in 3 KKO + SCH527123-treated mice. Individual data points and mean ± 1 SD are shown. Comparative statistical analysis was performed by Kruskall-Wallis one-way ANOVA.

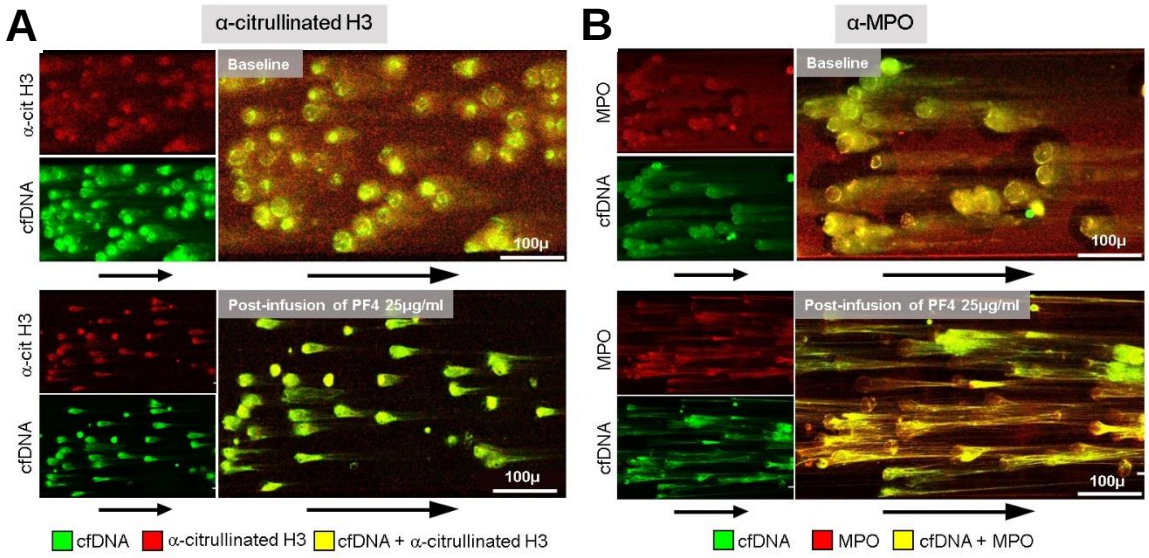

Figure 5.6. PF4-cfDNA complexes contain both MPO and citrullinated H3.

(**A**) Representative confocal image of channel adherent NETs incubated with SYTOX green and an anti-citrullinated H3 antibody before (above) and after (below) a 30-minute infusion with PF4 (25 µg/ml). Scale bar and arrows showing direction of flow are indicated. (**B**) As in (A), but representative confocal image of channel adherent NETs incubated with SYTOX green and an anti-MPO antibody before (above) and after (below) a PF4 infusion.

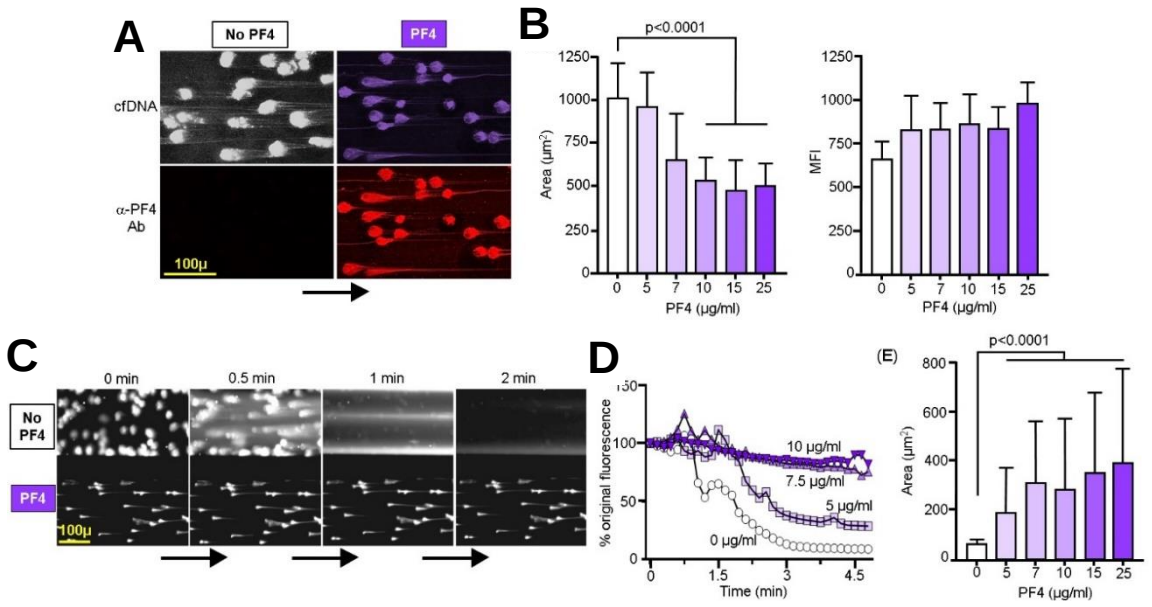

Figure 5.7. Microfluidic studies illustrating PF4-NET interactions.

(**A**) Representative confocal images of NETs exposed to PF4 or buffer, demonstrating change in morphology. PF4 specifically adhered to the NET DNA, visualized by labeling with a polyclonal anti-PF4 antibody (α-PF4 Ab), causing the NETs to become compact. Side bar and arrow indicating direction of flow are included. (**B**) Mean ± 1 SD of area covered by NETs exposed to the indicated PF4 concentration is shown on the left. Simultaneously measured mean fluorescent intensity (MFI) of SYTOX-labeled cfDNA is shown on the right. For both, N = 3-6 channels per PF4 concentration, with visualization of 30-60 NETs per channel. Comparative statistical analysis was performed by Kruskall-Wallis one-way ANOVA. (**C**) Representative widefield images of NETs ± PF4 (10 µg/ml), simultaneously infused with DNase I (100U/ml). Near complete digestion of NETs not exposed to PF4 occurred within two minutes, whereas NETs compacted with PF4 remained intact. Size bar and arrows indicating direction of flow are included. (**D**) Graph showing representative changes in NET fluorescent intensity observed over a 5-minute infusion of DNase I (100U/ml) in the presence of 0-10 µg/ml PF4. These studies were

based on analysis of 3-4 channels for each condition with 30-60 NETs observed in each channel. (**E**) Confocal images were taken of 3 channels per condition following digestion and the residual mean volume ± 1 SD of 30-100 NETs per channel was measured. Comparative statistical analysis was done by Kruskall-Wallis one-way ANOVA.

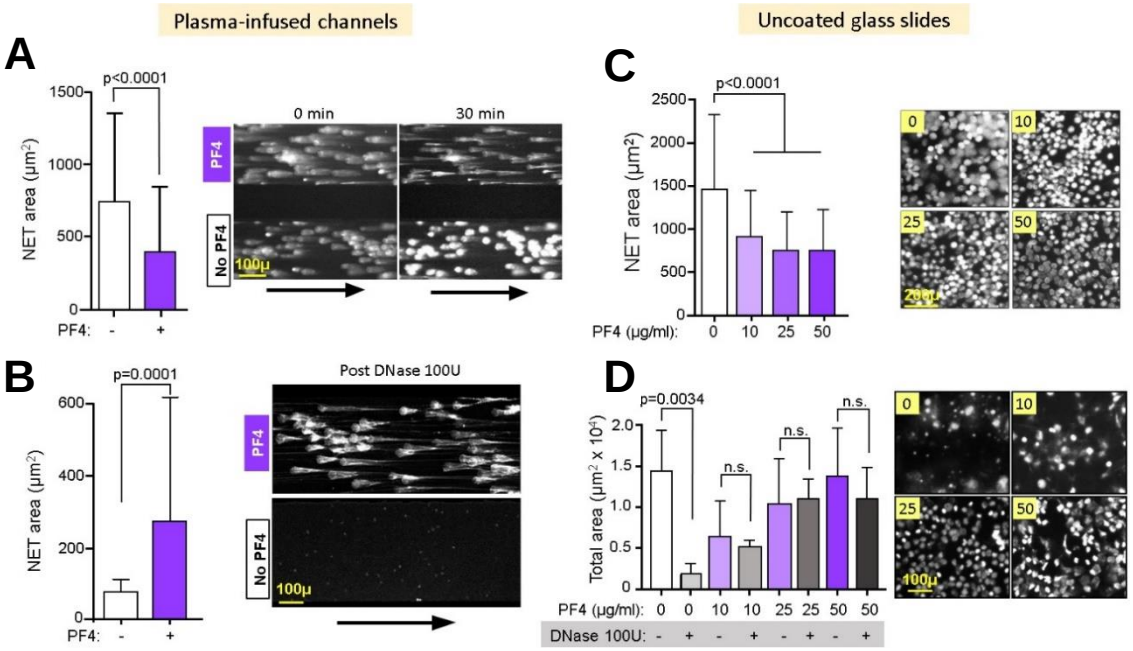

Figure 5.8. PF4 induces NET compaction and DNase I resistance without fibronectin and in the presence of human plasma.

(**A**) and (**B**) are microfluidic channels lined with NETs infused with human plasma ± PF4. In (**A**) on the left is a graph showing the mean NET area ± 1 SD after plasma infusion. NET area was measured in 3 channels per condition with > 150 NETs measured per condition. Comparative statistical analysis was performed with a Mann-Whitney U-test. On the right are widefield representative images showing PF4-induced changes in NET morphology. Scale bar and arrows showing direction of flow are indicated. (**B**) Same as in (**A**), but after a 30-minute infusion of DNase I. NET area was measured in 2 channels per condition with >150 NETs measured per condition. (**C**) and (**D**) Studies of PF4 binding and effects of PF4 incubation on NETs on uncoated glass slides. In (**C**), the graph represents the mean ± 1 SD of NET area following incubation with the indicated concentrations of PF4. Two slides were incubated with each PF4 concentrations, and 75-150 NETs were measured per slide. Comparative statistical analysis was performed with a Kruskal-Wallis

one-way ANOVA. On the right are representative widefield images of NETs incubated with buffer containing 0 - 50µg/ml PF4. A scale bar is included. In (**D**), after the PF4 treatment, the NETs were incubated with DNase I and total NET area was measured. On the left, is a graph showing the mean ± 1 SD of NET area post-DNase I exposure. Three slides were incubated with each concentration of PF4 and comparative statistical analysis was performed with a Student's t-test. On the right, are representative widefield images of NETs as in (**C**), but after DNase digestion. A scale bar is indicated.

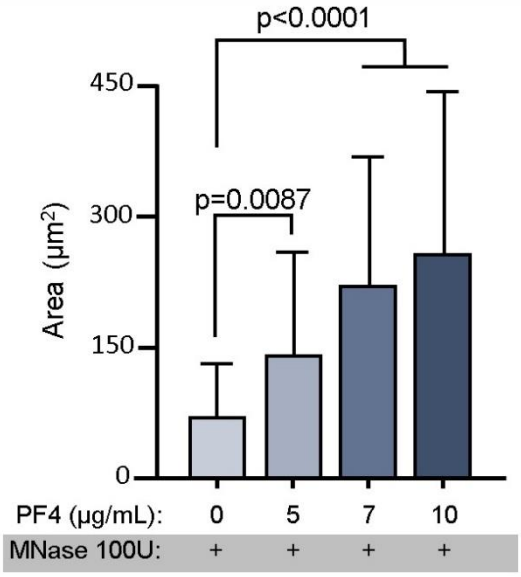

Figure 5.9 Studies showing NET susceptibility to digestion with micrococcal nuclease.

Microfluidic channel adherent NETs were incubated with PF4 (0-25 µg/ml) and then infused with micrococcal nuclease (MNase) at concentrations of 100U/ml for 5 minutes. The graph depicts residual area of the NETs incubated with increasing concentrations of PF4 following MNase digestion ± 1 SD. These studies were based on analysis of 3 channels for each condition with 50-100 NETs observed in each channel. Comparative statistical analysis was done with a Kruskal-Wallis one-way ANOVA.

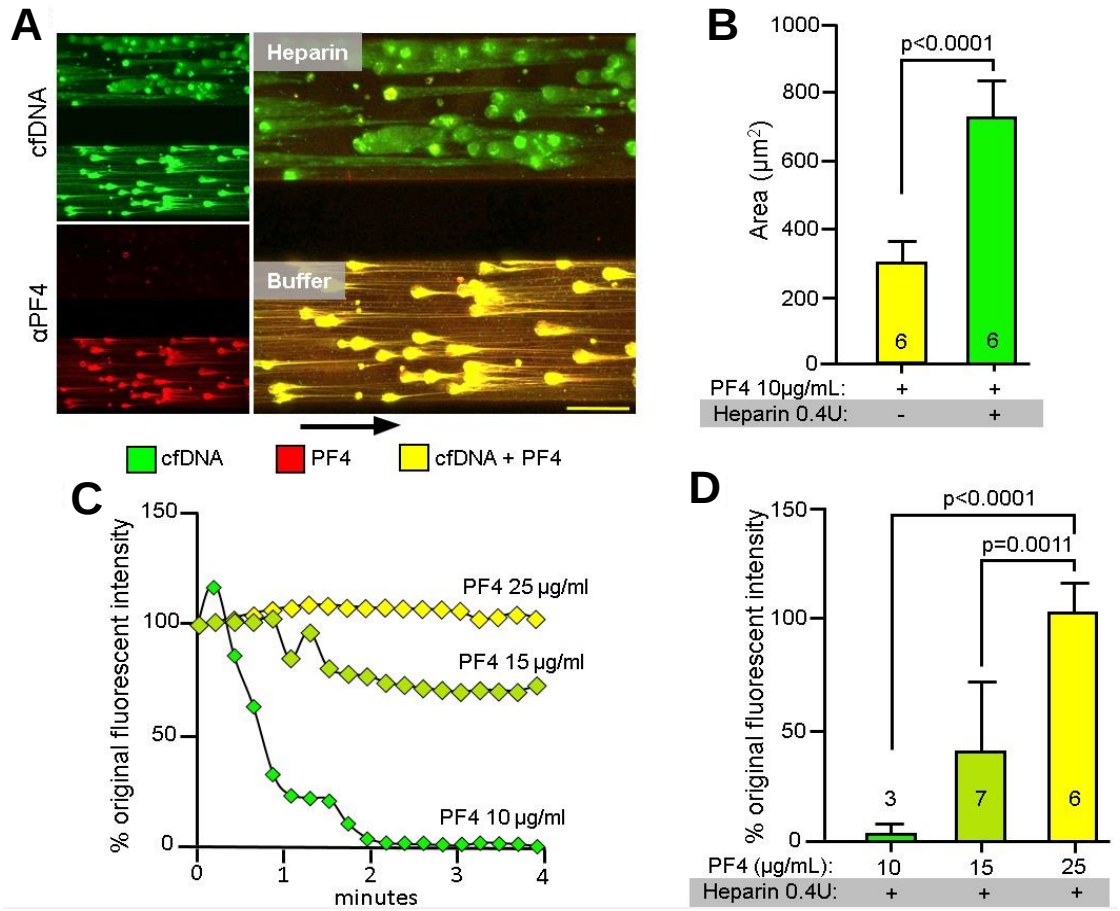

Figure 5.10. Studies of heparin-mediated NET decompaction and restoration of nuclease susceptibility.

(**A**) Representative confocal image showing a comparison of two PF4-compacted NET channels, following a simultaneous 20-minute infusion with a therapeutic concentration of heparin at 0.4U/ml (top) or no added heparin (bottom), after Sytox and anti-PF4 antibody staining. Scale bar and arrow showing the direction of flow in the channel are included. Same microscope and acquisition software as described in **Figure 5.1A**. (**B**) Graph demonstrating the mean ± 1 SD of the area occupied by the cfDNA of PF4/NET complexes with and without heparin infusion. Six channels with 30-60 visualized NETs per channel were studied in each arm and comparative statistical analysis was done with a Student's t-test. (**C**) Graph showing representative changes in NET fluorescent intensity observed

over a 5-minute infusion of DNAse I (100U/ml) in NETs infused with heparin 0.4U/ml and the indicated concentrations of PF4. (**D**) Graph showing the final mean fluorescent intensity ± 1 SD of channels as in (**C**). These studies were based on analysis of 3-7 channels for each condition with 30-60 NETs observed in each channel. Comparative statistical analysis was done by a Kruskal-Wallis one-way ANOVA.

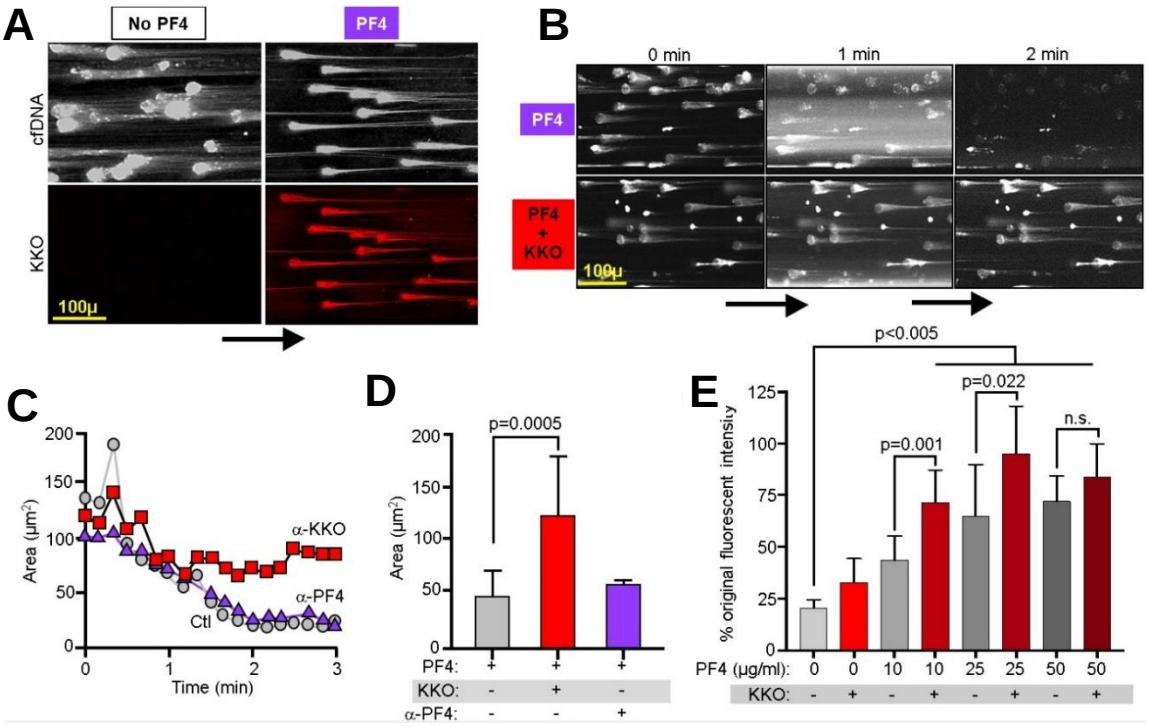

Figure 5.11. Microfluidic studies examining HIT-antibody PF4-NET complex interactions.

(**A**) Representative confocal images of activated neutrophils adherent to fibronectin-coated channels and stained for cfDNA (white) and KKO binding (red) in the absence and presence of 6.5 µg/ml PF4. Size bar and arrow indicating direction of flow are included. Same microscope and acquisition software as described in **Figure 5.1A**. (**B**) Representative widefield images of adherent neutrophils as in (A), but in the presence of 100U/ml DNase1 and 6.5 µg/ml PF4 ± 25 µg/ml KKO over 2 minutes. Size bar and arrow indicating direction of flow are included. (**C**) Representative graph showing the decrease in NET area over a 3-minute DNase I digestion. (**D**) Mean ± 1 SD of the final area of NETs following a 5-minute infusion of DNase I (100 U/ml) in the presence of 6.5 µg/ml PF4 and KKO or an anti-PF4 antibody (αPF4), each at 25 µg/ml. N = 12 in the PF4 and the PF4+KKO treated arms. N = 3 in the αPF4 treated arm. Comparative statistical analysis

was performed by Kruskall-Wallis one-way ANOVA. (**E**) PF4-induced resistance to DNase digestion under static conditions was measured using a previously described NET degradation assay[183]. The graph shows the mean percent original fluorescent intensity ± 1 SD. N = 9-10 per arm. Comparative statistical analysis between 3 or more groups was performed by Kruskall-Wallis one-way ANOVA and comparisons between two groups was performed with the Student's t-test.

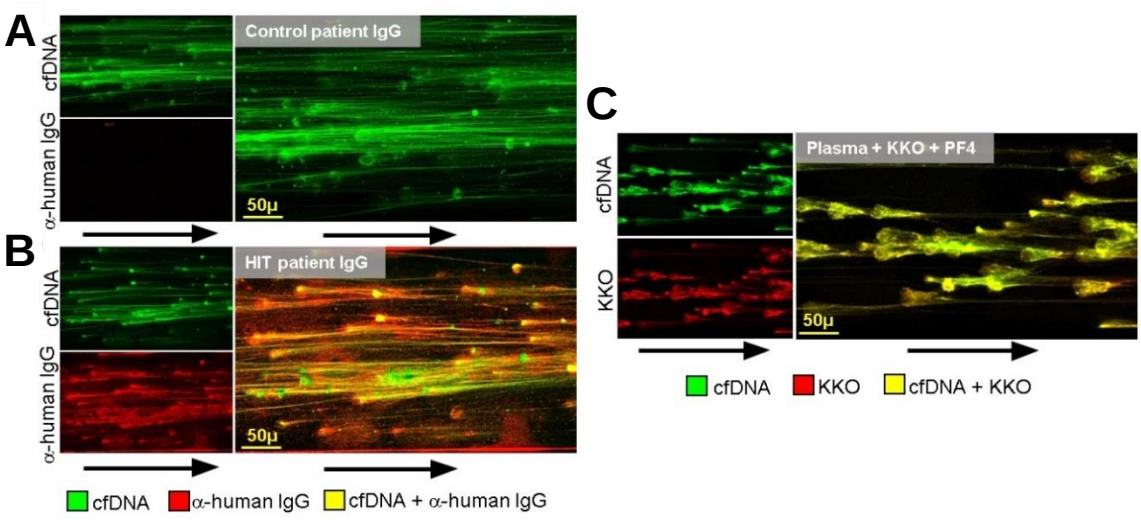

Figure 5.12. IgG isolated from HIT patient plasma binds PF4-NET complexes.

(**A**) Representative confocal image of PF4-NET complexes incubated with IgG (25 µg/ml) isolated from a healthy control patient plasma for 1 hour, stained with SYTOX and anti-human IgG, showing no human IgG adhering to cfDNA present in NETs. Scale bar and arrows showing direction of flow are indicated. (**B**) Representative confocal image of PF4-NET complexes incubated with IgG (25 µg/ml) isolated from the plasma of a patient with a confirmed diagnosis of HIT, stained with SYTOX and anti-human IgG, showing human IgG binding specifically to NET cfDNA. (**C**) Representative confocal image of PF4-NET complexes, stained with SYTOX green, infused with plasma containing KKO, showing that KKO still binds specifically to PF4-NET complexes when added to plasma rather than buffer. Scale bar and arrows showing direction of flow are indicated.

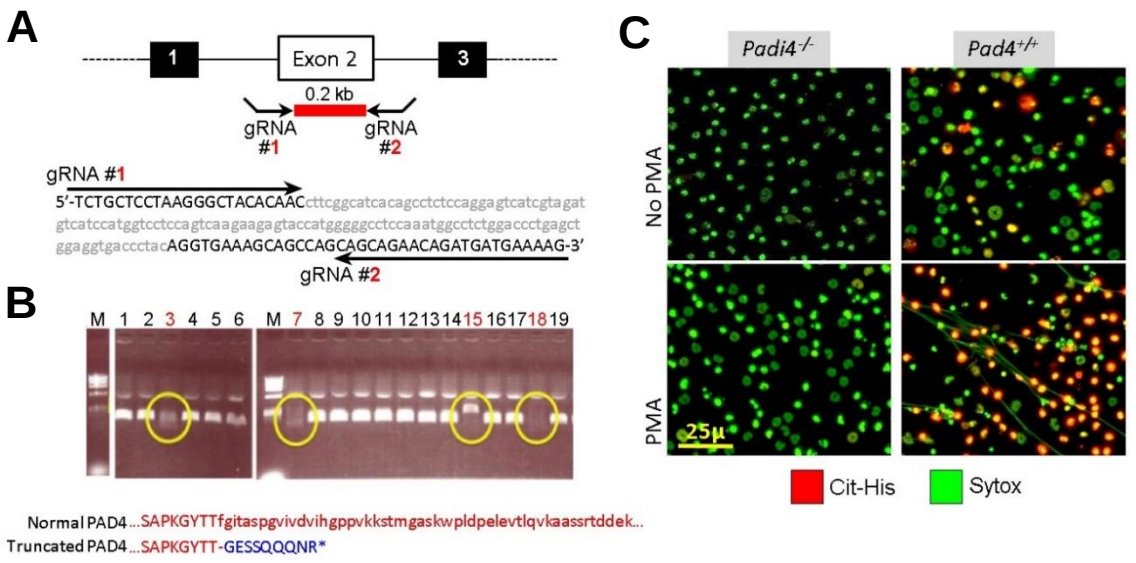

Figure 5.13. CRISPR/Cas9 gene-editing generation of Padi4$^{-/-}$ mice.

(**A**) At the top, is a schematic showing the first three exons of the murine *Padi4* gene and the binding of CRISPR gRNAs designed to disrupt a 0.2 kb region (red) of the *Padi4* gene encompassing Exon 2. Below the schematic are electrophoresis gels demonstrating the disruption of Exon 2 PCR amplification in 4 clones, and below the gels is the DNA sequence analysis from a wildtype mouse with the portion of Exon 2 deleted in clone 18 represented in grey, lower-case letters. At the bottom is the normal murine PAD4 amino acid (aa) sequence in red with caps indicating sequence preserved in Clone 18, and small letters indicating the aa sequence lost in Clone 18. The PAD4 sequence expected in clone 18 is shown below with the preserved first 8 aa in red, followed by a frameshift mutation (-) leading to 9 altered aa in blue with a premature stop codon (*). (**B**) Representative images of bone marrow-isolated neutrophils obtained from clone 18 *Padi4*$^{-/-}$ mice and *Padi4*$^{+/+}$ siblings**,** plated on a poly-L-lysine coated slide, incubated with buffer alone or PMA (100 nM) overnight. Samples were SYTOX green stained to visualize DNA shown in green, and anti-histone H3 (citrulline R2+R8+R17) to visualize citrullinated histones (cit-

His) shown in red. SYTOX and cit-His staining of unstimulated cells shows intact nuclei with cit-His staining only observed in *Padi4*$^{+/+}$ cells. Staining of PMA stimulated cells shows extracellular DNA strands and increased cit-H3 in *Padi4*$^{+/+}$ cells. The microscope and acquisition software were as described in **Figure 5.1A**.

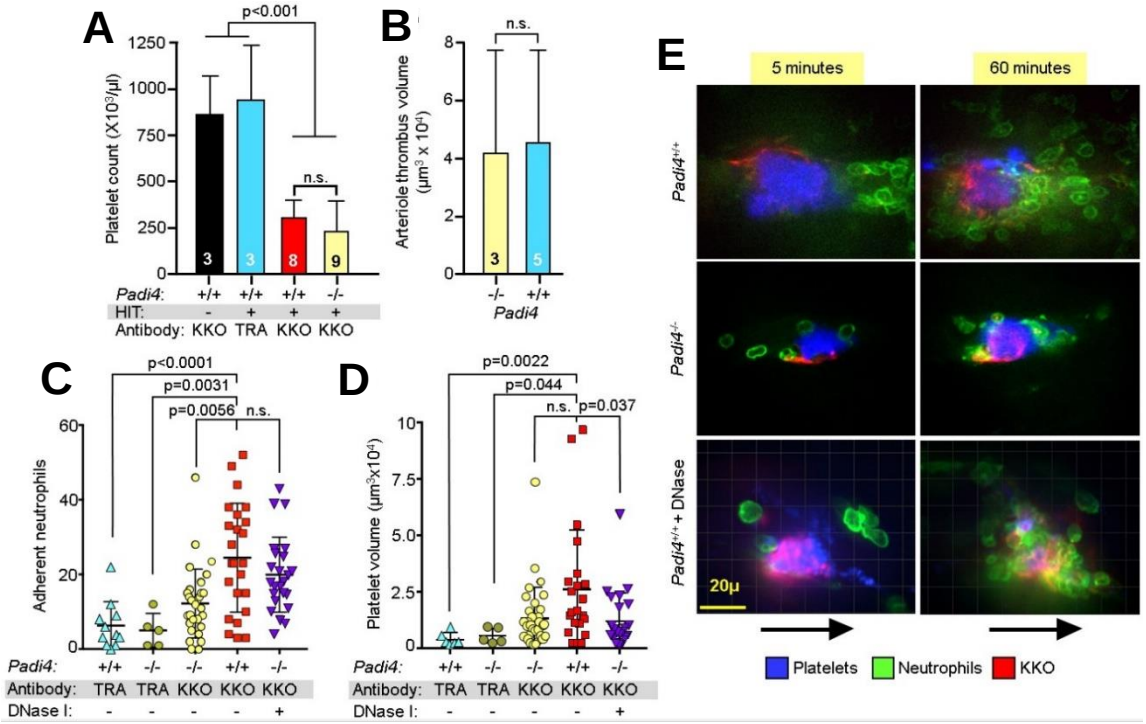

Figure 5.14. NETosis studies in the passive immunization Padi4$^{-/-}$/HIT mouse model. (**A**) Platelet counts 4 hours after intraperitoneal injection of KKO or TRA in HIT or FcγRIIA^{+}, hPF4$^{-/-}$ mice. *Padi4* status is indicated. Mean ± 1 SD is shown. Number of mice studied per arm is indicated in bars. Comparative statistical analysis was performed by Kruskall-Wallis one-way ANOVA. (**B**) Same as in (A), but for arteriole thrombus size as measured on confocal imaging after KKO infusion into HIT mice with *Padi4* status indicated. Statistical analysis performed with a Student's t-test. (**C**) and (**D**) are graphs showing the number of adherent neutrophils and the platelet volumes in cremaster venule thrombi in HIT mice 60 minutes after laser injury. Individual data points and mean ± 1 SD are shown. 6 injuries were made in 3 TRA-treated HIT mice, 33 injuries were made in 8 KKO-treated *Padi4*$^{-/-}$ HIT mice, 5 injuries were made in 1 TRA-treated *Padi4*$^{-/-}$ mouse, 22 injuries were made in 13 KKO-treated HIT mice, and 25 injuries were made in 4 KKO-treated HIT mice

following infusion of DNase. Comparative statistical analysis was performed with a Kruskall-Wallis one-way ANOVA. (**E**) Representative confocal images demonstrating the extent of platelet and neutrophil accumulation at the site of cremaster venule thrombi following HIT-induction, 5 and 60 minutes after the inciting laser injury and infusion of KKO in *Padi4*$^{-/-}$ mice compared to *Padi4*$^{+/+}$ mice ± DNase. Size bar and arrow indicating direction of flow are included. Same microscope and acquisition software as in **Figure 5.1D**.

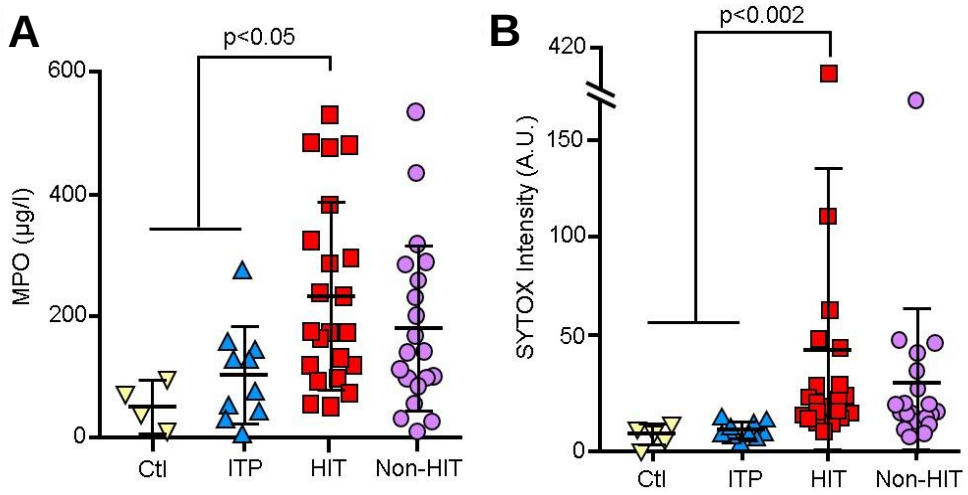

Figure 5.15. MPO and cfDNA levels in clinical samples.

Measurements of (**A**) MPO and (**B**) cfDNA levels in plasma from normal controls (Ctl), patients diagnosed with ITP, and patients evaluated for HIT that either had a confirmed diagnosis ("HIT") or were unlikely to have HIT ("Non-HIT"). Individual measurements and mean ± 1 SD are shown. Comparative statistical analysis was performed by Kruskall-Wallis one-way ANOVA.

Chapter 6 – ICAM-1 – targeted thrombomodulin mitigates tissue factor – driven inflammatory thrombosis in a human endothelialized microfluidic model

This chapter presents work featured in the article:

Greineder, C., Johnston, I., et al. (2017) *Blood Advances* 1(18): 1452-1465

Abstract

Diverse human illnesses are characterized by loss or inactivation of endothelial TM, predisposing to microvascular inflammation, activation of coagulation, and tissue ischemia. Single-chain antibody fragment (scFv/TM) fusion proteins, previously protective against end-organ injury in murine models of inflammation, are attractive candidates to treat inflammatory thrombosis. However, animal models have inherent differences in TM and coagulation biology, are limited in their ability to resolve and control endothelial biology, and do not allow in-depth testing of “humanized” scFv/TM fusion proteins, which are necessary for translation to the clinical domain. To address these challenges, we developed a human whole-blood, microfluidic model of inflammatory, TF-driven coagulation that features a multichannel format for head-to-head comparison of therapeutic approaches. In this model, fibrin deposition, leukocyte adhesion, and platelet adhesion and aggregation showed a dose-dependent response to TNFα activation and could be quantified via real-time microscopy. We used this model to compare hTM/R6.5, a humanized, intracellular adhesion molecule 1 (ICAM-1)–targeted scFv/TM biotherapeutic, to untargeted antithrombotic agents, including soluble human TM (shTM), anti–TF antibodies, and hirudin. The targeted hTM/R6.5 more effectively inhibited TF-driven coagulation in a PC-dependent manner and demonstrated synergy with supplemental PC. These results support the translational prospects of ICAM-targeted scFv/TM and illustrate the utility of the microfluidic system as a platform to study humanized therapeutics at the interface of endothelium and whole blood under flow.

Introduction

More than a century after the first description of purpura fulminans in 1884, the relationship between coagulation and systemic inflammation remains the subject of considerable interest and study[196–198]. The thrombotic process that occurs in the setting of infection or activation of the immune response is recognized as having distinct elements, which distinguish it from normal hemostasis or even other forms of arterial or venous thrombosis[199]. While agents such as antithrombin III and APC initially held promise in treating sepsis, their clinical utility has been limited by a lack of efficacy and bleeding risks[200,201], and the benefit of more standard anticoagulants such as heparin is uncertain[202,203]. Better understanding of the elements of inflammatory thrombosis and identification of targets for safe intervention represent a significant medical priority.

The PC pathway normally functions to limit excessive activation of coagulation, but it is suppressed in the setting of systemic inflammation. Inflamed ECs demonstrate loss of the natural anti-coagulants TM and EPCR from their luminal surface[30,204–207]. Conversely, TF expression on a variety of cell types in systemic inflammation promotes activation of coagulation and is an attractive target for intervention[208,209]. Existing pharmacologic approaches intended to intercept inflammatory activation of coagulation may be limited by their inability to localize to TF-expressing procoagulant surfaces. For example, soluble human TM (shTM), which is currently being evaluated in a phase 3 clinical trial of patients with severe sepsis and coagulopathy (www.clinicaltrials.govidentifier #NCT0158831), lacks any specific affinity for cellular surfaces[210].

My interest in inflammation and the prothrombotic nature of HIT overlapped with that in Dr. Vlad Muzykantov laboratory's interest in pharmacologic approaches to attenuate inflammation by specifically targeting TM to activated cellular surfaces[211]. In their

first report of this strategy, recombinant mouse TM was fused to a single-chain antibody fragment (scFv) specific for mouse ICAM-1 (CD54). In a murine model of acute lung injury, ICAM-1–targeted scFv/TM was found to facilitate interaction with endogenous EPCR, reduce inflammatory markers, and improve transendothelial plasma protein leakage[212]. While these studies demonstrated the potential therapeutic benefit of this approach, the effect on activation of coagulation was not examined.

The challenges in demonstrating the efficacy of ICAM-1–targeted TM in TF-driven inflammatory thrombosis are several fold. First, there is uncertainty over the clinically significant sources of TF in sepsis and related disorders[213,214]. Differences in cellular sources of TF are particularly relevant to scFv/TM, as its distribution is more controlled than untargeted “fluid-phase” agents (i.e., soluble TM) and therefore more likely sensitive to changes in the relative cellular contributions to thrombin generation. It is challenging to discern the contribution of endothelial TF from other sources such as hematopoietic cells, epithelium, fibroblasts, pericytes, and smooth muscle[215–217]. While ECs express TF under inflammatory stimuli in vitro, studies have failed to demonstrate a definitive role of endothelial TF in murine models[218], which may not fully replicate human biology or be sensitive to the contribution of endothelial TF to activation of coagulation[215–217]. TM itself demonstrates species-specific differences in the balance between anti-inflammatory and anti-thrombotic activity[219,220]. Finally, translation to human pathologies has been limited by the absence of species cross-reactivity of the murine therapeutic.

To address these challenges and provide a model that can begin to close this translational gap, my efforts at using a commercially available, multichannel microfluidic system that uses human whole blood perfused through cytokine-activated, human endothelial–lined flow chambers, with real-time microscopy for visualization of underlying pathophysiologic events were combined with the Muzykantov’s group. This joint effort

focused on use of this sytem to study “humanized” scFv/TM therapeutic hTM/R6.5, which incorporates both human TM and a human-specific anti–ICAM-1 scFv. This approach allowed testing of ICAM-1–targeted scFv/TM as an intervention in TF-driven inflammatory thrombosis using an entirely human microfluidic system, employing multiple channels run simultaneously, allowing for a side-by-side comparison of therapeutic interventions within a single experiment.

Methods

Venipuncture and whole blood preparation.

All studies involving human subjects were approved by the University of Pennsylvania institutional review board (protocol 822534). Written informed consent from healthy volunteer donors was obtained for the use of deidentified blood samples. Whole blood samples were collected from the antecubital vein using a 19G butterfly cannula system. The first 5 ml of blood was discarded, followed by collection into vacuum tubes containing citrate and corn trypsin inhibitor (CTI), a FXII inhibitor, with final concentrations of 11 mM and 50 μg/ml, respectively.

In experiments involving inflammatory activation of whole blood, 50 ng/ml lipopolysaccharide (LPS) was added for 90 minutes at 37°C. In experiments involving PC-deficient blood, whole blood samples were centrifuged for 15 minutes at 1500g at room temperature to isolate platelet-poor plasma. 50% of the original plasma was removed and replaced with an equivalent volume of PC-immuno-depleted or normal control plasma. CTI was then added to maintain the final blood concentration at 50 μg/ml.

In all experiments, 5 μg/ml Alexa Fluor 568/anti-fibrin monoclonal antibody was added to whole blood, along with either calcein-AM (2 μg/ml) or fluorescent anti-leukocyte and platelet antibodies (Brilliant Violet anti-CD45 and FITC anti-CD41, each 1.5 μg/ml).

Whole blood samples were recalcified just prior to infusion into the microfluidic channels, adding $CaCl_2$ to a final concentration of 11 mM.

Microfluidic model of inflammatory thrombosis.

Endothelialized microfluidic chambers and a TNFα injury were described in Chapter 2. On the day of experimentation, endothelialized channels were flow adapted for 4 to 6 hours at 5 dynes/cm^2 at 37°C using TNFα. To induce inflammatory activation of ECs, TNFα was added at varying concentrations during the flow adaption period. Fresh media was allowed to flow through the channels for 30 minutes to "wash out" residual TNFα prior to introduction of whole blood. In some experiments, EC-targeted antibodies or recombinant proteins were added during the first 25 minutes of this washout period, followed by 5 minutes of flow to remove nonspecifically bound protein. In other experiments, antithrombotic agents were mixed into the whole blood.

While each Bioflux 48-well plate contains 24 flow chambers, whole blood experiments were run with no more than 8 channels (4 pairs of 2) at once to minimize the time between imaging of each pair of channels. This setup allowed 2 or 3 replicates for each of 3 or 4 experimental conditions (e.g., control, TNFα only, TNFα + therapeutic A, and TNFα + therapeutic B). A computer interface was used to move a motorized microscope stage (Fluxion Biosciences) rapidly between viewing areas, allowing each pair of channels to be imaged approximately every 15 to 30 s. Imaging was performed on a Zeiss Axio Observer microscope under a ×10/0.25 objective. The focal plane was set to be at the interface of the lower wall endothelial layer and the whole blood. Under this objective and aperture, we expect the depth of field to be ~8.5 μm. Fluorescent images were acquired using identical settings for all channels, while bright-field images allowed direct visualization of flow.

Confocal microscopy.

Channels were fixed by flowing 4% paraformaldehyde at 1 dyne/cm^2 into the channel for 15 minutes. The cells were washed with PBS and blocked with 5% donkey serum prior to adding primary and secondary antibody and staining with Hoechst reagent. Imaging was performed using a Zeiss LSM 710 at original magnification ×20.

Data analysis and statistics.

Each figure represents data from a single experiment with means and standard errors derived from replicate channels within that experiment. For analyses, bright-field and fluorescence microscopy images were imported into ImageJ and analyzed frame by frame using identical acquisition parameters for each experiment. Backgrounds were subtracted using an ImageJ rolling-ball algorithm with a radius of 50 pixels. Preset regions of interest, covering the entire channel except the areas immediately adjacent to the side walls, were used to measure MFI in green and red channels or mean signal intensity in the bright-field channel. Frame “time codes” were used to generate time courses, and areas under the curve (AUCs) were calculated for statistical comparisons. First-derivative curves were calculated with GraphPad statistical software and statistical differences were determined using GraphPad Prism 6.0. One-way analysis of variance was performed, followed by appropriate multiple comparison (Tukey) test and calculation of multiplicity adjusted P values. $P < 0.05$ was considered statistically significant.

Cells and cell lines.

HUVECs were purchased and maintained using EGMTM BulletKitTM (Lonza). Drosophila S2 cells were maintained in Schneider’s complete medium and transitioned to

serum free Insect-Xpress (Lonza) supplemented with 0.5 mM $CuSO_4$ for recombinant protein expression. Anti-human ICAM-1 hybridoma (clone R6.5), CHO-hICAM, and CHO-K1 wild type cells were purchased from ATCC.

Antibodies and other reagents.

Human α-thrombin, human PC, CTI, and blood collection tubes containing citrate and CTI were purchased from Haematologic Technologies. Recombinant human TNFα was purchased from Corning. Lipopolysaccharides (LPS) from *E. Coli* 055:B5 and recombinant hirudin were purchased from Sigma-Aldrich. Anti-human VCAM-1 (polyclonal, BBA19) was purchased from R&D systems. Anti-human TF antibodies were purchased from R&D systems and eBioscience (clone HTF-1). FITC conjugated-anti-CD41 (clone HIP8) was also purchased from eBioscience. Anti-human TM (clone Phx-01) and Brilliant Violet anti-CD45 (clone 30-F11) antibodies were purchased from BioLegend. Lyophilized, immunodepleted PC-deficient plasma and normal plasma controls were purchased from Aniara.

Cloning of R6.5 single chain variable fragment (scFv), soluble human TM (shTM), and the hTM/R6.5 fusion protein.

PCR using 5' signal peptide primers was used to isolate full length cDNAs for R6.5 variable heavy chain (VH) and light chain (VL) from hybridoma-derived single stranded cDNA, as previously described[221]. The encoded sequence was compared with the previously published full-length sequence of the R6.5 monoclonal antibody variable domains and found to be identical[222]. VH and VL cDNAs were assembled into an scFv construct in the pMT/Bip expression vector with the triple flag tag appended to the 3' end of the VL domain. Likewise, cDNAs encoding shTM (Glu22-Ser515) and the hTM/R6.5

fusion protein were ligated into the pMT/Bip expression vector (Invitrogen), each with a triple Flag tag appended to the 3' end. For the fusion protein, an Spe I site was added to the 5' end of R6.5 scFv, and the 3' end of shTM, along with a 13-amino acid rigid linker ((SSSSG)2AAA).

Recombinant protein expression and purification.

pMT/shTM, R6.5 scFv, and hTM/R6.5 were each co-transfected with pCoBLAST in S2 cells and selected with blasticidin to generate stable cell lines[216]. Expression and purification was performed as previously described[216]. Briefly, proteins were harvested from S2 cell supernatant using an anti-FLAG (M2) affinity column (Sigma-Aldrich), and assessed for purity via sodium dodecyl sulfate-polyacrylamide gel electrophoresis (SDS-PAGE) and high-performance liquid chromatography (HPLC). The differences in affinity lead to different flow rates and isolation of components from the mixture.

Results

Production and characterization of human-specific anti-ICAM scFv/TM.

To create the humanized anti-ICAM scFv/TM complementary DNA (cDNA) construct (hTM/R6.5), cDNA encoding the extracellular portion of human TM (Glu22-Ser515) was fused with the R6.5 scFv cDNA, containing V_H and V_L domains cloned from the corresponding anti–human ICAM-1 hybridoma[121,223]. The detailed molecular design of each construct is shown in **Figure 6.1A**. Purified R6.5 scFv and hTM/R6.5 migrated as single bands on nonreducing SDS-PAGE (**Figure 6.1B**), with sizes (~35 kDa and ~120 kDa) similar to those seen for previous scFv and scFv/TM fusion proteins (TM runs significantly higher than its predicted size due to glycosylation). Similar purity was seen on size-exclusion high-performance liquid chromatography, although this method

revealed a dimer form of hTM/R6.5, which accounted for ~20% of total absorbance (**Figure 6.1C**). As shown in **Figure 6.1D** and **6.1E**, hTM/R6.5 demonstrated high affinity, specific binding to human ICAM-1 in a flow cytometry based assay with stably-transfected CHO cells (K_d = 24 nM) and a cell-based enzyme-linked immunosorbent assay on TNFα–activated HUVECs (K_d = 9.7 nM), respectively. The fusion protein was functionally active when bound to TNFα–activated HUVECs, demonstrating thrombin-dependent PC activation after binding and washing to remove nonspecifically-bound protein. At concentrations sufficient to saturate available binding sites on these cells (40-50 nM), the fusion protein more than compensated for the loss of APC generation caused by activation of the ECs by cytokine ($P < .01$; **Figure 6.1F**).

Establishing a multichannel system of endothelialized flow channels.

To enable testing of hTM/R6.5 at the interface of human whole blood and endothelium, HUVECs were grown in microfluidic flow chambers until they established 3-dimensional, fully confluent, endothelialized channels (typically 2-3 days) as displayed in Chapter 2. Following 6 hours of flow adaptation at 5 dynes/cm^2, a shear stress typical of postcapillary venules[224], cells displayed the qualities described in Chapter 2.

Characterization of inflammatory thrombosis model.

The inflammatory thrombosis model was characterized as described in Chapter 2. To determine the optimal conditions for testing antithrombotic therapeutics, we defined the extent of coagulation in the microfluidic model as a function of the dose and time of cytokine exposure. Both higher concentration of TNFα (**Figure 2.5B**) and longer duration of stimulation (**Figure 2.5C**) led to greater fibrin deposition upon infusion of whole blood. These experiments also revealed the advantage afforded by the multichannel format,

which allowed comparison of multiple experimental conditions (with replicates) within a single experiment. **Figure 6.2** shows the relatively small variance within a single experiment, compared with the variability across experiments with separate EC preparations and whole blood samples. On the basis of these results, each subsequent experiment was performed with a single blood sample and EC preparation and 8 microfluidic channels.

Apart from fibrin deposition, other physiologically relevant outcomes were found to vary with the extent of cytokine activation of the endothelialized channels. In particular, adhesion of leukocytes and platelets, based on accumulation of green fluorescence, was seen only after TNFα stimulation (**Figure 6.3A**). Higher doses of TNFα also demonstrated earlier disruption and occlusion of blood flow, based on changes in bright-field signal intensity (**Figure 6.3C**). Separately tracking platelets and leukocytes using antibodies to platelet $\alpha_{IIb}\beta_3$ labeled in green and antibodies to leukocyte CD45 labeled in blue, we found that while that the number of adherent platelets varied with TNFα concentration in the range of 1 to 10 ng/ml, the number of adhered leukocytes was similar (**Figures 6.3B**). We confirmed this finding using an automated cell counting algorithm to enumerate adherent leukocytes flowing over TNFα–activated channels and found similar numbers of adhered leukocytes per channel area in channels treated with either 1 or 10 ng/ml TNFα (**Figures 6.4A**). Additional experiments performed across a lower range of TNFα doses (0.1-1.0 ng/ml) revealed a dose response of leukocyte adhesion to TNFα stimulation within this lower range (**Figures 6.4B**). Finally, flowing whole blood over TNFα–activated channels resulted in not only adhesion of leukocytes but also an activation of neutrophils that resulted in deposition of NETs[225], which could be visualized in real time with nucleic acid stains (**Figures 6.5**)[221].

Inflammatory thrombosis model is TF driven.

We next validated the role of TF in initiating coagulation in this model, noting that peripheral blood was collected in the presence of CTI, a FXIIa inhibitor[222]. **Figures 6.6A** shows the experimental design, in which TF inhibitory antibody (or media control) was flowed over TNFα–activated endothelialized channels prior to the infusion of whole blood. As shown in **Figures 6.6B**, TF blockade significantly (P = 0.02) reduced fibrin deposition, confirming the role of endothelial TF as a driver of coagulation in this model. TF antibody decreased the accumulation of green fluorescence (**Figures 6.7A**), reflecting the sum of leukocyte and platelet adhesion. While these cell types were not individually stained in this experiment, the morphology suggested a decrease in platelet rather than leukocyte adhesion.

Endothelial TM regulates inflammatory activation of coagulation.

A similar approach was taken to investigate the role of endogenous endothelial TM in regulating coagulation in the whole blood microfluidic model. Although TNFα stimulation decreases endothelial TM, some APC generation capacity remains (**Figures 6.1F**). To achieve complete inhibition, we used an antibody specific for the fifth epidermal growth factor–like domain of TM, which blocks thrombin binding and eliminates nearly all APC generation capacity (**Figures 6.1F**)[226]. Treatment of TNFα–stimulated channels with this antibody prior to the infusion of whole blood significantly increased fibrin deposition ($P < 0.001$; **Figures 6.6C-D**).

These results established the microfluidic model as a means to test targeted therapeutics in a humanized system, with the hypothesis that the ICAM-1 targeted fusion protein would localize to activated cellular surfaces, reverse the loss of endothelial TM induced by cytokine activation, and abrogate the TF-driven thrombotic response. Indeed,

treatment of TNFα–activated endothelialized channels with 50 nM hTM/R6.5, a concentration chosen based on the prior binding studies (**Figures 6.1E**), produced the opposite effect of the TM-blocking antibody, completely eliminating fibrin deposition (**Figures 6.6B-C**). As seen previously, effects on green fluorescence mirrored those seen for fibrin generation, consistent with a reduction in platelet adhesion (**Figures 6.7B**).

Comparative testing of antithrombotic agents.

Given the effectiveness of hTM/R6.5 in the whole blood microfluidic model, we next took advantage of the multichannel format to compare its antithrombotic efficacy with that of other antithrombotic agents. As a first step, the fusion protein was tested against equimolar concentrations of its individual components, shTM and R6.5 scFv. These proteins had minimal effects on fibrin deposition when infused during the TNFα washout period (**Figure 6.8**). While expected, this confirmed that both domains of the fusion protein are required for its activity and excluded that ICAM-1 blockade alone might be solely responsible for the observed anti-thrombotic effect.

Endothelial-bound hTM/R6.5 was next tested against shTM added directly to whole blood. **Figure 6.9A** shows the experimental design of these experiments. While both agents significantly decreased fibrin deposition (**Figure 6.9B**), the effect of shTM was less sustained (P = .05), even at a dose far greater than its IC50 in TF-induced thrombin generation assays[227]. It should be noted that hTM/R6.5 was limited to the protein bound to the cells, as the targeted protein was not added to whole blood in these experiments. Hirudin (5 U/ml) and hTM/R6.5 (50 nM) were also compared and demonstrated similar results (P = 0.03; **Figure 6.9C**).

hTM/R6.5 was next compared with shTM following a combination of cytokine activation of ECs and inflammatory activation of whole blood (**Figure 6.10A**). The latter

was induced by 90-minute preincubation of the whole blood with 50 ng/ml LPS, conditions previously used to induce neutrophil oxidative burst and monocyte TF expression in human whole blood[228,229]. LPS was chosen to better simulate human disease states, such as sepsis, in which activated leukocytes and other blood components may contribute to inflammatory thrombosis[198,199]. While both agents demonstrated antithrombotic effect in this setting, hTM/R6.5 was significantly more effective in inhibiting fibrin deposition than shTM ($P = 0.05$; **Figure 6.10B**).

hTM/R6.5 is at least partially PC dependent.

We next tested the contribution of PC activation to the antithrombotic activity of hTM/R6.5. A recently reported antibody, HAPC1573, which binds human APC (but not its zymogen) and inhibits its inactivation of FVa and FVIIIa in a dose-dependent manner[230], was mixed into whole blood (**Figure 6.11A**). In naive whole blood, HAPC1573 treatment produced fibrin deposition similar to equimolar isotype control antibody ($P = 0.33$), although shortened time to peak-fibrin generation was observed. APC inhibition markedly increased fibrin deposition in endothelialized channels treated with hTM/R6.5 ($P < 0.05$), although a persistent delay was seen in the time to peak-fibrin generation (**Figure 6.11B-D**). This effect, reported in previous TGA studies, has been attributed to direct inhibition of thrombin by TM[227].

These results prompted investigation of hTM/R6.5 in the setting of PC deficiency, a condition observed in sepsis and other syndromes involving systemic activation of coagulation[231–233]. To achieve the levels of PC deficiency similar to patients with these illnesses, we removed 50% of the plasma from donor whole blood and replaced it with an equal volume of PC-immuno-depleted (or non-depleted control) plasma (**Figure 6.12A**). Like APC inhibition, partial depletion of plasma PC produced fibrin deposition similar to

control whole blood (P = 0.34), with a slight decrease in time to peak-fibrin deposition[234]. PC deficiency dramatically altered the activity of the fusion protein, eliminating its inhibitory effect on overall fibrin deposition (P = 0.34; **Figure 6.12B-D**). In contrast, hTM/R6.5 produced a delay in time to peak-fibrin generation in both PC-deficient and control whole blood, consistent with direct thrombin inhibition by the fusion protein (Supplement Table 10)[227]. Finally, addition of exogenous, plasma-derived human PC to the PC-depleted blood restored the full antithrombotic effect of hTM/R6.5 (P < 0.05; **Figure 6.12B-D**).

Discussion

This is the first report of ICAM-1 targeted fusion proteins as a therapy for TF-driven inflammatory thrombosis. Affinity targeting to cellular surfaces has the potential to dramatically alter local concentrations and interaction with binding partners, particularly in surface-driven phenomena such as coagulation, and the improved efficacy of hTM/ R6.5, compared with other therapeutics, including sTM, hirudin, and anti-TF, demonstrates the translational potential of this approach. hTM/R6.5 bound to the surface of activated human ECs and restored APC generation capacity above that of uninflamed endothelium. hTM/R6.5 shares a number of desirable features with its mouse-specific analog, YN1/mTM[212], and the use of an scFv fragment enables facile genetic fusion to therapeutic cargoes and mitigates the Fc and complement-mediated toxicities seen in clinical trials of the parental antibody, R6.5, or enlimomab[235–238].

To demonstrate the therapeutic efficacy of human-specific hTM/ R6.5, a microfluidic system consisting of entirely human components was developed to model TF-driven inflammatory thrombosis. Sophisticated in vitro systems have been developed that incorporate multiple cell types and reproduce the architecture of microvascular networks[239–243]. Our priority was to establish a comparatively straight- forward model,

suitable for testing and comparing targeted scFv/TM with other antithrombotic drugs[211,244–246]. Although the model lacks subendothelial components of a true vessel, including epithelial tissues, it allows for control over endothelial and leukocyte activation, manipulation and treatment of human WB, and quantification of therapeutic effects with high spatial and temporal resolution. While the present focus was on abrogation of fibrin deposition, additional readouts of inflammatory biology such as leukocyte adhesion and generation of neutrophil extracellular traps were also shown to be possible using this model system. By calculating first-derivative curves of fibrin fluorescence intensity, we provide readouts analogous to common TGA assays. Importantly, the multichannel format of this system allows for parallel testing of multiple therapeutic approaches with a single blood donor and EC preparation, limiting the impact of these variables, which can complicate other complex microfluidic model systems.

Several limitations of the model should be highlighted. First, PDMS flow chambers are rectangular in cross-section and fail to reflect the mechanical compliance of normal vasculature[247]. Use of linear channels with fixed dimensions and no branches limits extrapolation to physiologic vascular beds, where inflammatory, TF-driven thrombosis may occur heterogeneously[248]. The important physiologic sources of TF are a matter of ongoing investigation[249], and as currently constructed, this model is limited to hematopoietic and endothelial sources. In addition, only HUVEC cells were investigated in the current model, although further optimization to enable culture of and comparison with other endothelial sources is ongoing. The current conformation does not permit recirculation, so exposure of endothelialized channels to WB flow was limited in duration by need to avoid cell settling and activation of the contact pathway (CTI provides ;1 hour of inhibition[222]). While our intention was to model TF-driven thrombosis, the use of CTI

may likewise be viewed as a limitation, as it eliminates any contribution of FXII–dependent coagulation, believed to play a role in certain systemic inflammatory syndromes[250].

These limitations notwithstanding, the data presented provide several insights into the role of the endogenous PC pathway and the action of scFv/TM therapeutics. First, the contrasting results with inhibition and augmentation of endothelial TM suggest its importance in regulating coagulation under systemic inflammation. Second, the benefit of ICAM-targeted TM over its soluble counterpart supports the hypothesis that localization of the protein to the cellular membranes enhances its functional activity[212,251,252]. In fact, the difference in potency between these 2 agents may be more significant than their relative concentrations would suggest, as only a fraction of hTM/R6.5 molecules would have bound to the cell membrane. While ICAM-1 targeting of hTM/R6.5 was limited to hematopoietic and ECs in these studies, other cell types, such as epithelium, express ICAM-1, and may be both an important source of TF24 and a valuable target of this approach[253].

There are several reasons why binding of TM to cell membranes may enhance its antithrombotic activity. Cell-surface localization positions TM in proximity to TF and prothrombinase complexes assembled on cell membranes, resulting in immediate inhibition of thrombin and redirection to PC activation as it is produced[254,255]. Experiments involving antibody inhibition of APC and plasma PC deficiency suggest that PC activation is an important mechanism of hTM/R6.5 antithrombotic activity, as the ability of hTM/R6.5 to decrease the peak rate of fibrin generation was PC dependent. EC surface localization may accelerate activation of PC by partnering with endogenous EPCR, promoting PC cleavage by the thrombin/TM complex[256]. Although this was not investigated in the present studies, previous studies with the murine-specific analog of hTM/R6.5 demonstrated APC

generation by cell-bound fusion protein was inhibited when binding of PC to endothelial EPCR was blocked[212].

The contribution of PC activation to the antithrombotic activity of hTM/ R6.5 suggests a benefit with combination therapy, as pharmacologic replacement of TM alone may be insufficient in the setting of PC deficiency (as seen in septic patients[231,232]). While human plasma–derived PC concentrate failed to improve outcomes in sepsis or disseminated intravascular coagulation[22,257], the synergy observed with pairing of PC and hTM/R6.5 suggests that simultaneous PC replacement and targeted delivery of TM may be an effective clinical strategy. Further investigation using patient specimens in our microfluidic model and confirmation in preclinical animal models will be necessary to determine if this combination therapy can surpass numerous previous pharmacologic attempts to prevent TF-driven inflammatory thrombosis and disseminated intravascular coagulation in the clinical setting.

These studies present a novel therapeutic approach in sepsis, but that could be applicable across various Steps 2 and 3 in HIT's pathogenesis (**Figure 1.5**). These studies show that ICAM-1-targeted TM is more effective than its soluble form displaying how thrombi localization can improve therapeutic efficacy. In reference to HIT, this could be utilized to localize therapeutics to HIT relevant targets; these targets could include PF4/GAG (as discussed in Chapter 3), PF4/heparin, PF4-VWF-HIT antibody (as discussed in Chapter 4), or PF4-NET-HIT antibody (as discussed in Chapter 5) complexes. TM could potentially combat HIT thrombosis as it provides both anti-thrombotic and anti-inflammatory components. Alternatively, therapeutics targeting the glycocalyx, VWF, neutrophils, or NETs could also be affective in a localized structure. Moreover, by understanding how each target is significant in particular vessels and injury settings, the therapeutics can be further tailored to patient conditions.

Figures

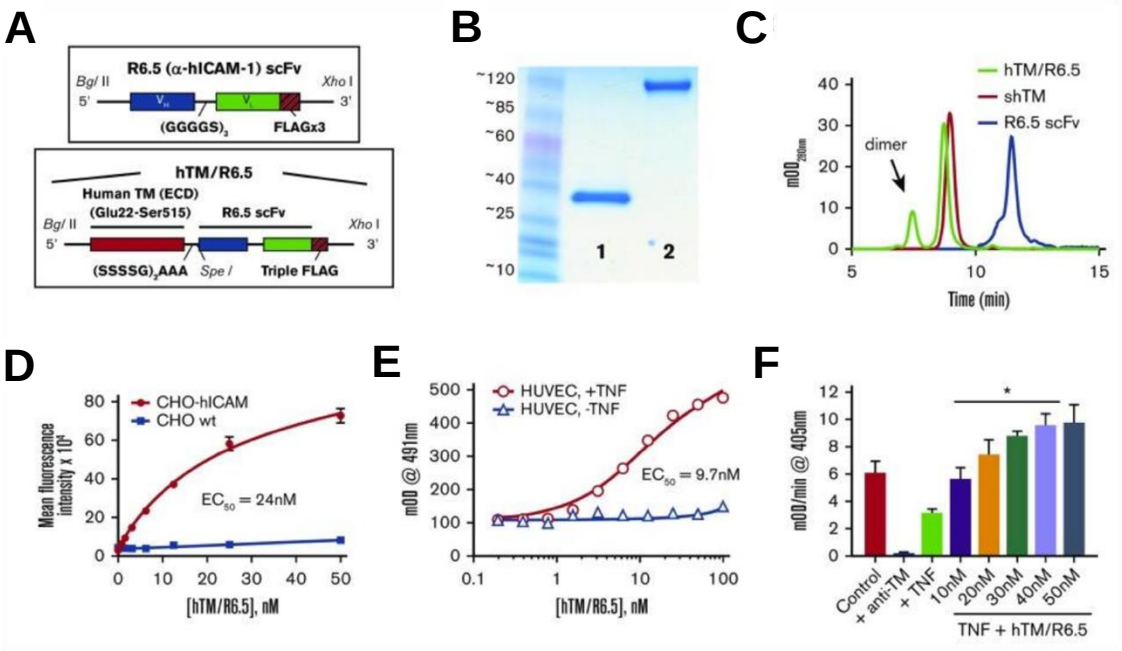

Figure 6.1. Assembly, characterization, and functional activity of hTM/R6.5 biotherapeutic.

(**A**) Molecular design of R6.5 scFv and hTM/R6.5. (**B**) Size and purity of recombinant proteins based on SDS-PAGE (lane 1, R6.5 scFv; lane 2, hTM/R6.5) and (**C**) size exclusion HPLC. hTM/R6.5 has a minor dimer form (indicated by arrow), accounting for ~20% of absorbance at 280 nm. (**D**) hTM/R6.5 binds specifically to human ICAM-1-expressing CHO cells (CHO-hICAM), but not wild type (CHO wt). Flow cytometry was performed on each cell type incubated with different concentrations of fluorescently labeled fusion protein. For each reaction, MFI was calculated for 10 000 events. Each reaction was done twice, with mean ± SD of the MFI shown. (**E**) hTM/R6.5 binds strongly to TNFα-stimulated HUVECs, but only minimally to non-stimulated cells. Cell-based ELISAs were performed on live cells as previously described[19] using anti–FLAG-HRP to probe for cell-bound fusion protein. Graph shows mean ± SD. (**F**) In vitro APC generation

assay by cell-bound fusion protein, as described previously[212]. TNFα-stimulated HUVECs show reduced APC generation capacity due to loss of surface TM, although some residual function is seen in comparison with cells treated with an anti-TM blocking monoclonal antibody. For testing the functional activity of cell-bound hTM/R6.5, bvg-stimulated cells were incubated for 30 minutes at 37°C with various concentrations of fusion protein and then washed to remove nonspecifically bound protein prior to incubation with human thrombin (1 nM) and PC (100 nM). At saturating concentrations of hTM/R6.5 (40-50 nM), the fusion protein more than compensates for the reduction in PC activation induced by TNFα stimulation (*P < .01 versus TNF only). Graph shows mean ± SD, N = 3 for each condition. EC_{50}, 50% effective concentration; mOD, 1/1000th of an optical density unit.

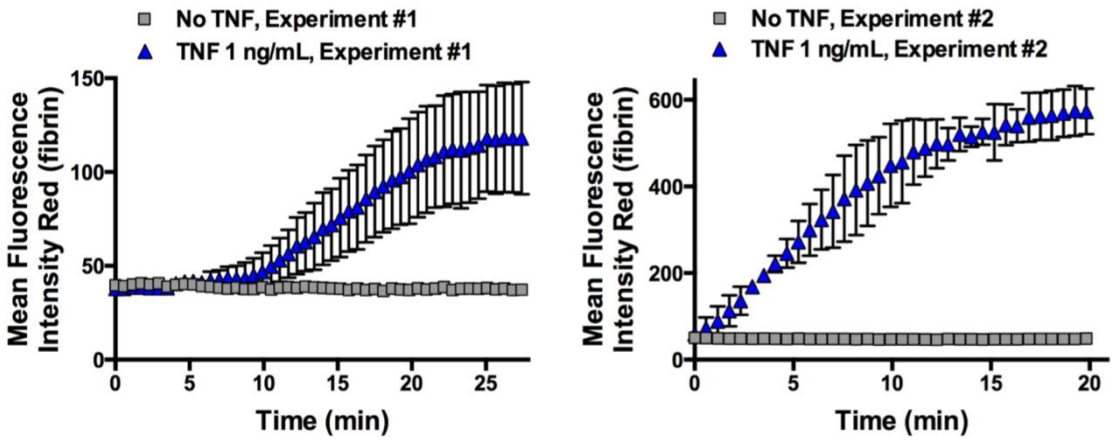

Figure 6.2. Intra- versus inter-experimental variability.

Fibrin deposition data from two independent experiments. While some variation is seen between replicate channels within the same experiment (error bars show mean ± SEM for N = 2-3 channels), the timing and extent of fibrin deposition is fairly consistent, allowing meaningful statistical comparisons between experimental groups. In contrast, the MFI versus. time curve is markedly different between TNFα-stimulated channels run on separate days, preventing pooling of data or comparisons of groups run on separate days.

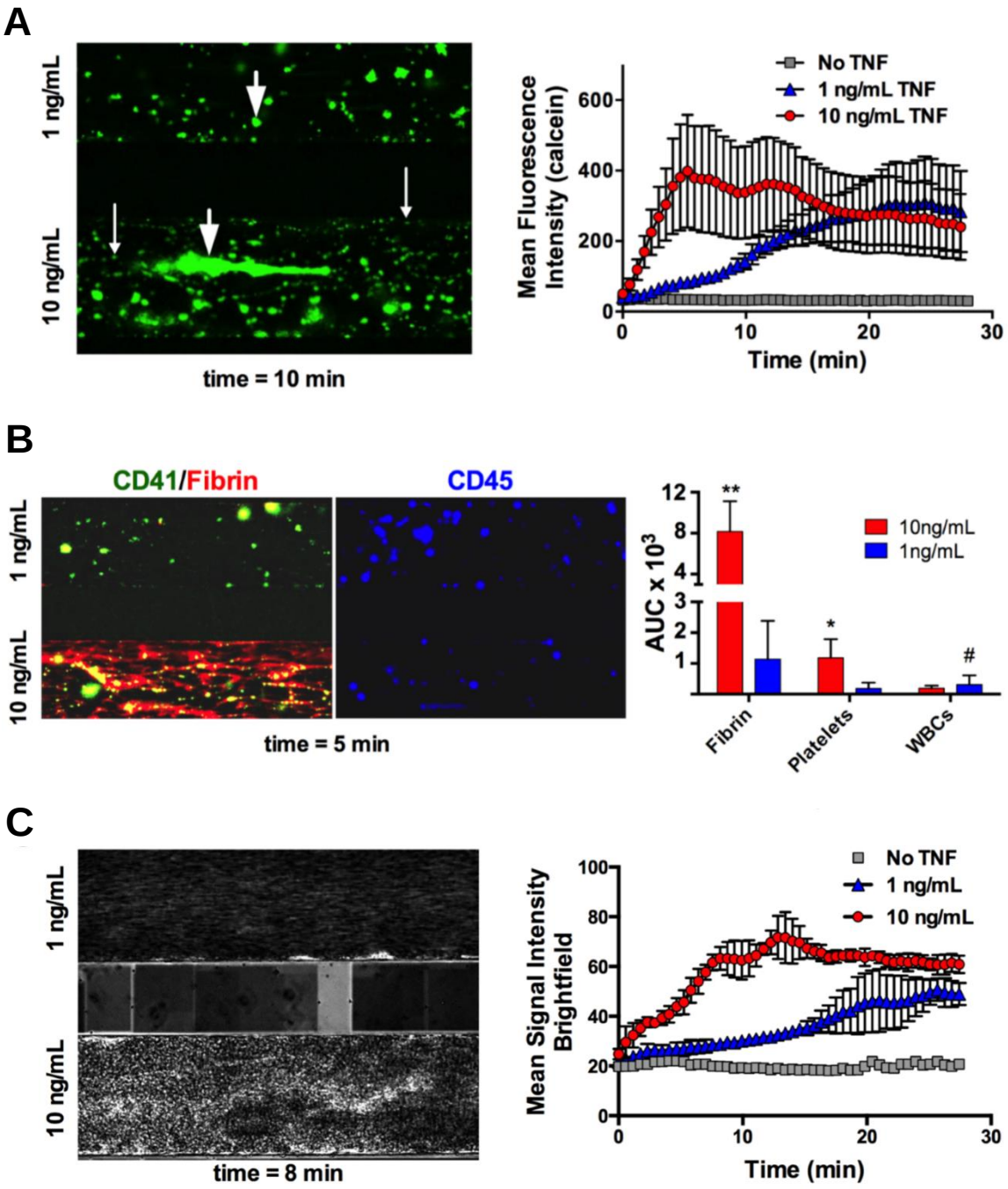

Figure 6.3. Changes in TNFα treatment impact fibrin and platelet accumulation which impact time to occlusion.

(**A**) Green fluorescence, representing adhesion of leukocytes and platelets (both labeled with calcein AM) to the endothelium. Representative image (left panel) shows individual

adherent leukocytes (arrows) as well as variably sized clusters of various cell types (arrowheads). Graph (right panel) shows mean fluorescence intensity versus time for differing TNFα concentrations, mean ± SEM, with N = 2 channels for control and N = 3 channels for each concentration. (**B**) Three color experiment, in which fibrin (red), leukocytes (blue), and platelets (green) were tracked with distinct fluorophores. Left panel shows representative images of endothelialized channels pre-activated with varying doses (1 ng/ml versus. 10 ng/ml) of TNFα. Quantitation (right panel) shows that platelets and fibrin vary with TNFα concentration, but the number of adherent leukocytes is unchanged across doses, ** = $P < 0.01$, * = $P < 0.05$, # = n.s. ($P = 0.54$). (**C**) Use of brightfield signal intensity as a marker of partially disrupted or fully occluded flow, following infusion of whole blood into TNFα-stimulated endothelialized channels. Representative image (left panel) shows characteristic increase in signal in bottom channel, which had occluded at the time point shown. Graph shows mean signal intensity (MSI) versus time for differing TNFα concentrations, mean ± SEM, with N = 2 channels for control and N = 3 channels for each concentration.

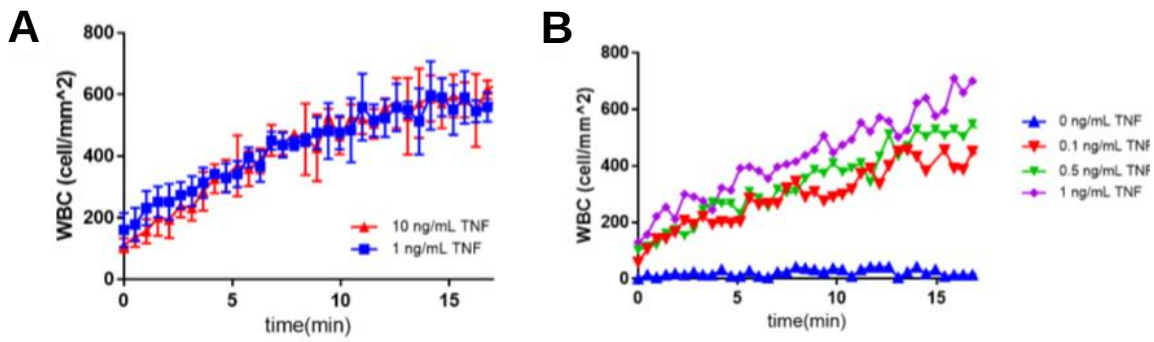

Figure 6.4. Quantification of leukocyte numbers in TNFα-activated channels.

(**A**) Similar density of adhered leukocytes was observed between channels activated with either 1 ng/ml (blue) or 10 ng/ml (red) (N =3/dose) (**B**) A dose-response of adhered leukocytes was seen in a lower range of 0.1-1 ng/ml of TNFα (n=1/dose). Minimal leukocyte adhesion was seen in un-activated channels (blue). The density of adhered leukocytes was calculated using an automated particle counting algorithm (ImageJ). Images from calcein AM-stained blood were converted to binary masks, and particles counted using the included “analyze particles” algorithm with a circularity index of 0.5-1. To minimize interference from large platelet aggregates, blood was not re-calcified prior to infusion over channels in these experiments.

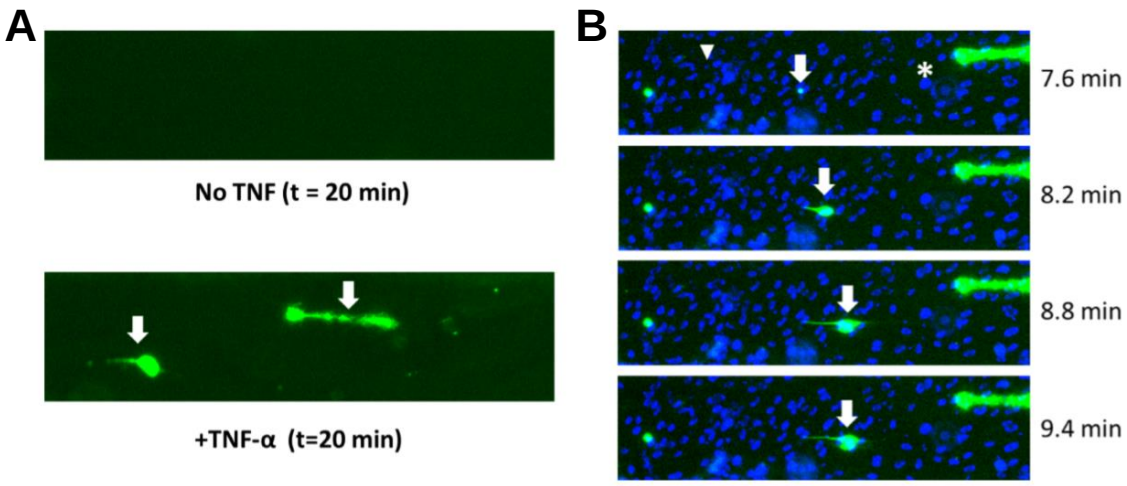

Figure 6.5 Exposure of TNFα-activated channels to whole blood results in deposition of NETs.

(**A**) Staining of extracellular nucleic acid, often in elongated deposits, was seen in TNFα-activated endothelium (bottom), but not in untreated channels (top). (**B**) Formation and growth of NETs could be monitored in whole blood in real time. Whole blood, stained with 1 µM cell-impermeant SYTOX nucleic acid stain (green) and 4 µM Hoeschst cell-permeant nucleic acid stain (blue), was infused over TNFα (0.5 ng/ml)-activated endothelium. Neutrophil nuclei could be seen as small, mobile, poly-lobulated forms (arrowhead), while endothelial nuclei were larger, round, and stationary (asterisk). Extracellular DNA associated with NETs stained brightly with SYTOX, and dimly with Hoeschst (arrows).

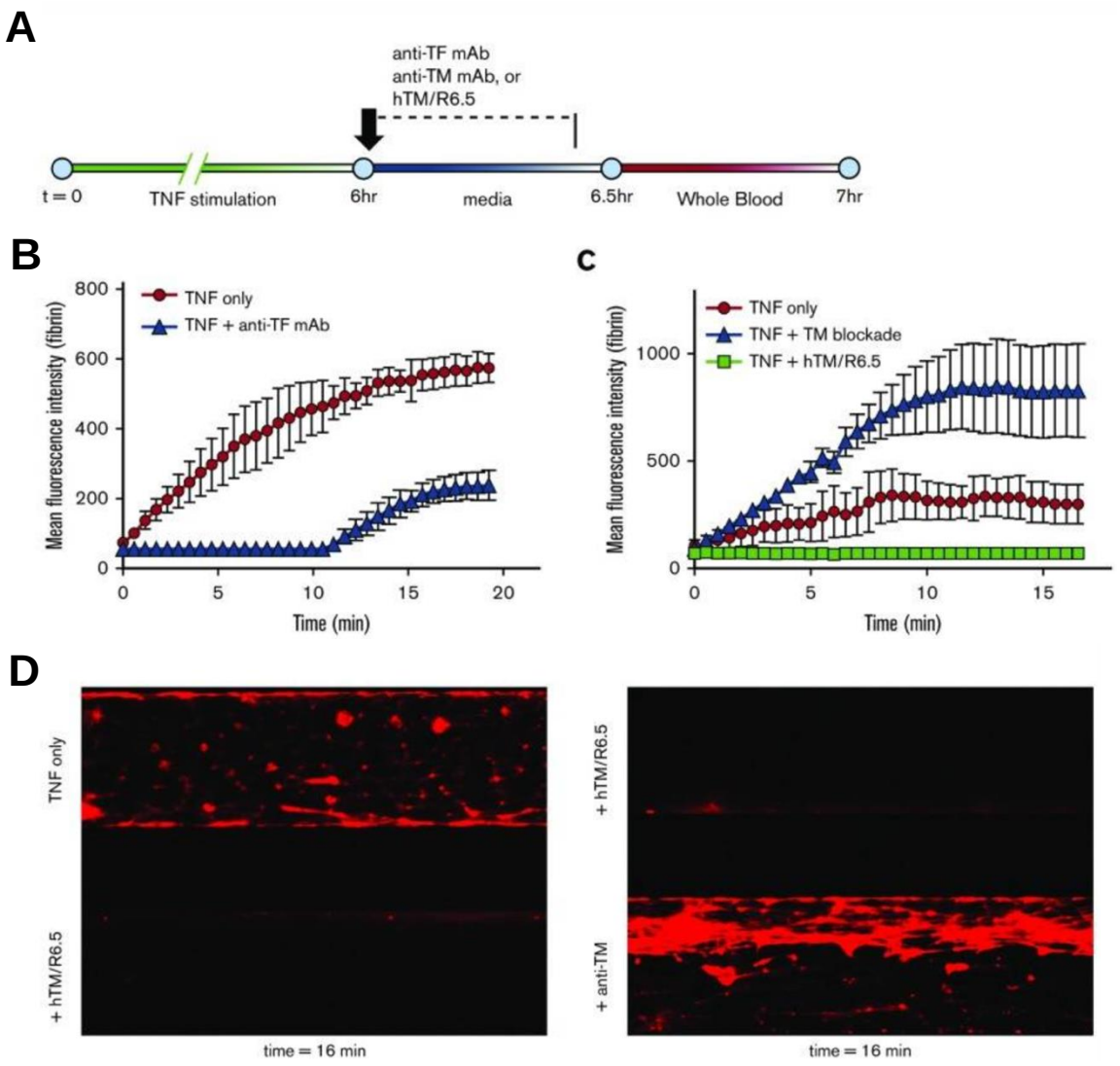

Figure 6.6. Endothelial TM regulates TF-driven coagulation in inflammatory thrombosis model.

(**A**) Schematic showing experimental design. Endothelialized channels were flow adapted at shear stress of 5 dynes/cm^2, stimulated with 1 ng/ml TNFα for 6 hours, and then treated with antibodies or fusion protein during the first 25 minutes of a 30-minute TNFα washout period, followed by a 5-minute wash to remove nonspecifically bound protein and, finally, infusion of whole blood at shear stress of 5 dynes/cm^2. (**B**) Blockade of endothelial TF delays and markedly reduces fibrin deposition (**P** = 0.02 for AUC of TNF versus TNF +

anti-TF antibody). Graph shows mean ± SEM, with N = 2-3 channels per condition. (**C**) Blockade of endothelial TM results in significant increase in fibrin deposition ($P < 0.001$ for AUC of TNF only versus TNF + TM blockade), whereas treatment of TNFα-activated endothelium with hTM/R6.5 scFv fusion protein completely eliminates fibrin deposition (**P** = 0.03 for AUC of TNF only versus TNF + hTM/R6.5). Graph shows mean ± SEM, with N = 2-3 channels per condition. (**D**) Representative fluorescent images for panel C show fibrin deposition within endothelialized channels and demonstrate opposing effects of TM inhibition and augmentation.

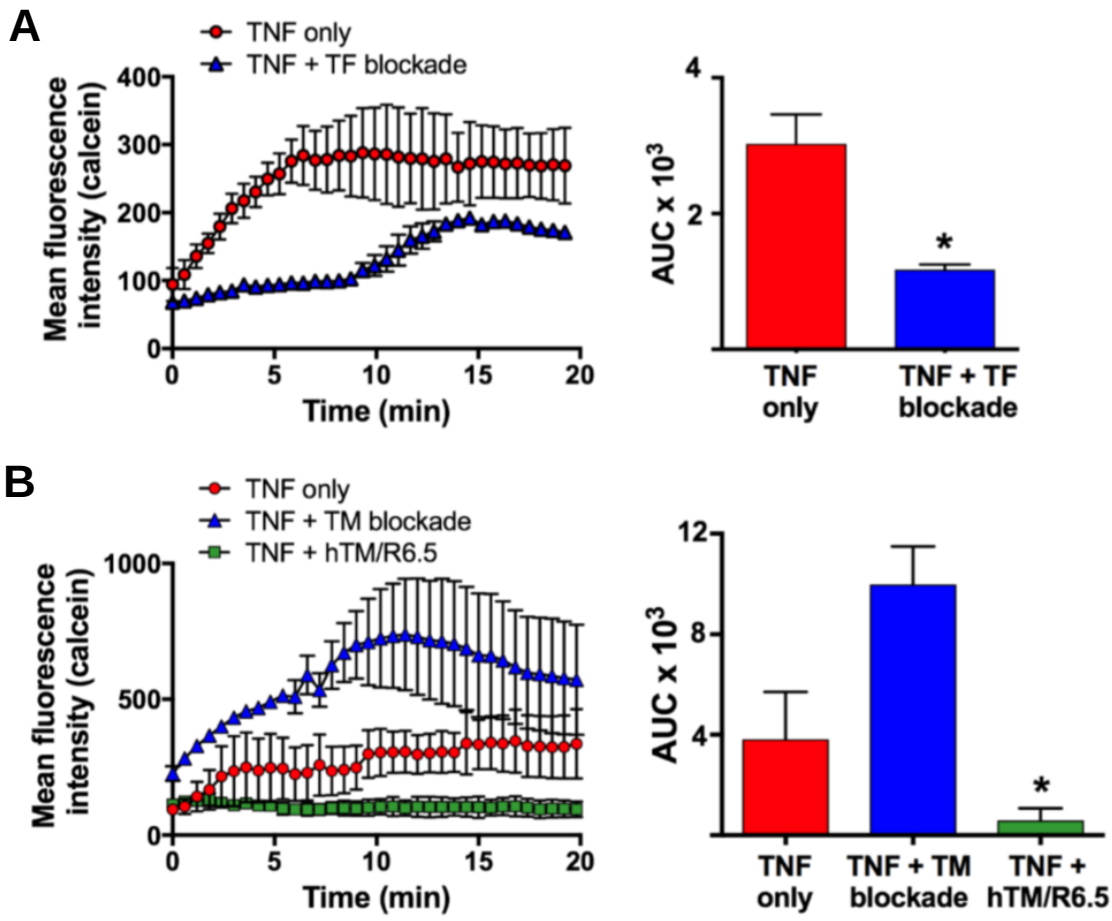
A
TNF only
TNF + TF blockade
Mean fluorescence intensity (calcein)
400
300
200
100
0
0
5
10
15
20
Time (min)
AUC x 10^3
4
2
*
TNF only
TNF + TF blockade
B
TNF only
TNF + TM blockade
TNF + hTM/R6.5
Mean fluorescence intensity (calcein)
1000
500
0
0
5
10
15
20
Time (min)
AUC x 10^3
12
8
4
*
TNF only
TNF + TM blockade
TNF + hTM/R6.5

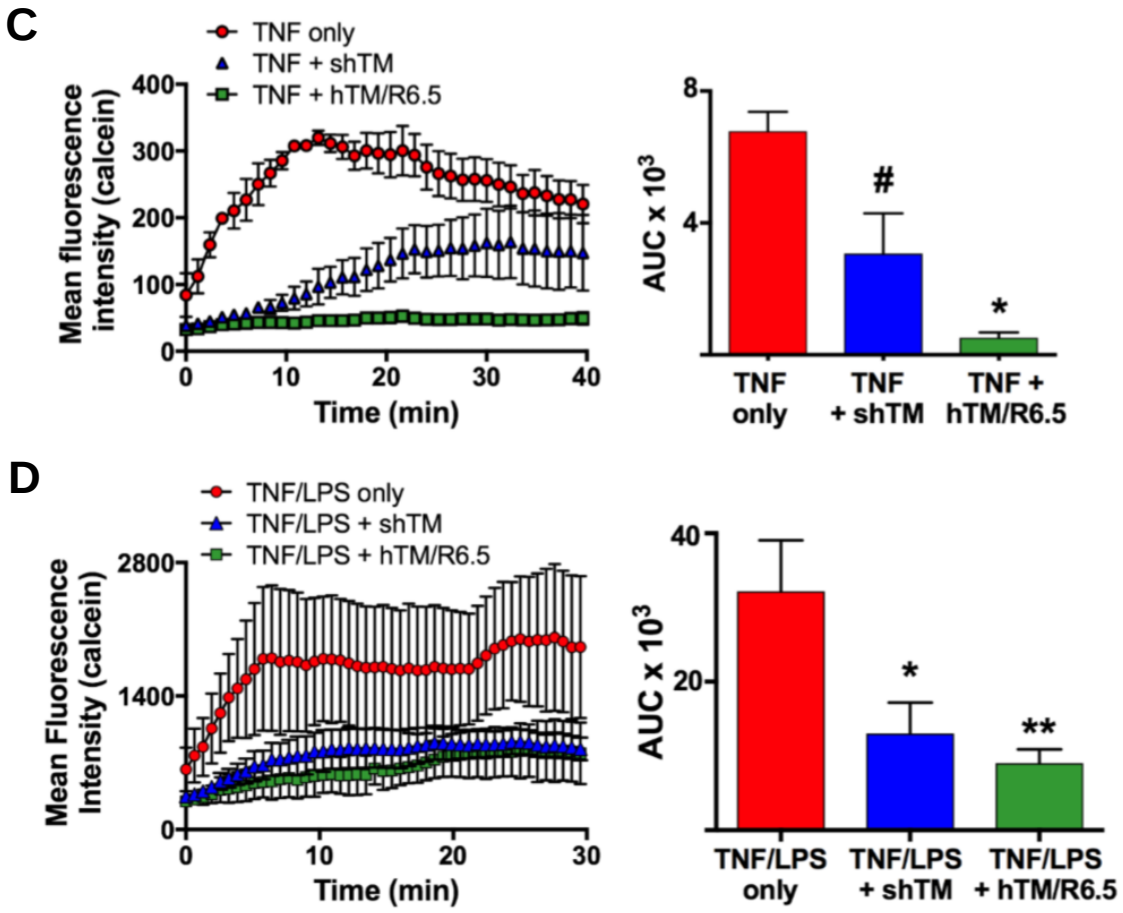

Figure 6.7. Therapeutic comparison of platelet and WBC accumulation during inflammatory thrombosis.

Green fluorescence time curves (left panel) and AUC analysis (right panel), mean ± SEM, from (**A**) TF inhibition experiment (N = 2 channels per condition, *P < 0.05 versus. TNFα only), (**B**) anti-TM versus. hTM/R6.5 experiment (N = 2 channels per condition, *P = 0.03 for hTM/R6.5 versus anti-TM), (**C**) shTM versus hTM/R6.5 experiment (N = 2 channels per condition, *P = 0.03 for hTM/R6.5 versus TNFα only, # P = 0.08 for shTM versus TNFα only), and (**D**) combined TNF/LPS model (N = 2 channels for TNF/LPS only and N = 3 channels for each treatment group, *P = 0.04 for shTM versus. TNFα/LPS only, **P = 0.02 for hTM/R6.5 versus TNFα/LPS only). The effect of each antibody and/or therapeutic on

the accumulation of green fluorescence mirrored its effect on fibrin deposition (**Figures 6.6A**, **6.6B**, **6.10**, and **6.11**, respectively).

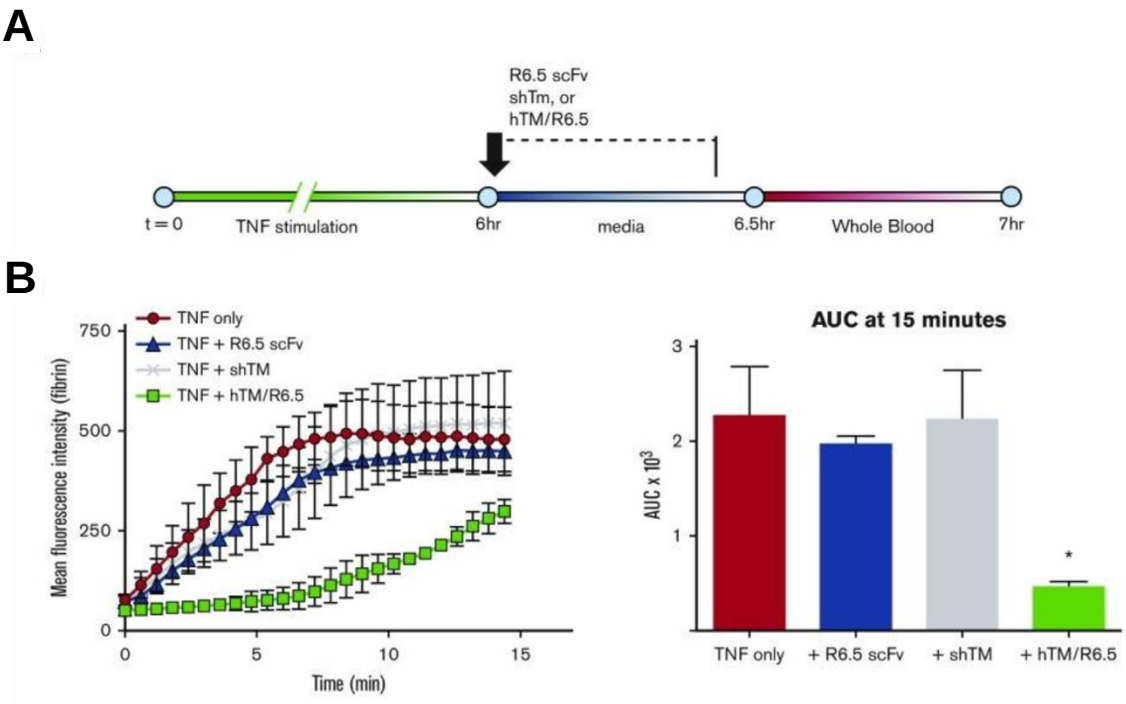

Figure 6.8. Both domains of hTM/R6.5 are required to generate an antithrombotic effect.

(**A**) Experimental design. All proteins were infused in equimolar concentrations (50 nM) during the TNF washout period, followed by a 5-minute wash to remove nonspecifically bound protein. Flow of media and whole blood was at shear stress of 5 dynes/cm^2. (**B**) Only hTM/R6.5 inhibited fibrin deposition, confirming that both the ICAM-1 binding and hTM domains must be present to produce an antithrombotic effect. Left panel shows MFI versus time, mean ± SEM, with N = 2 channels per condition. Right panel shows AUC analysis. * = $P < 0.05$ versus all other conditions.

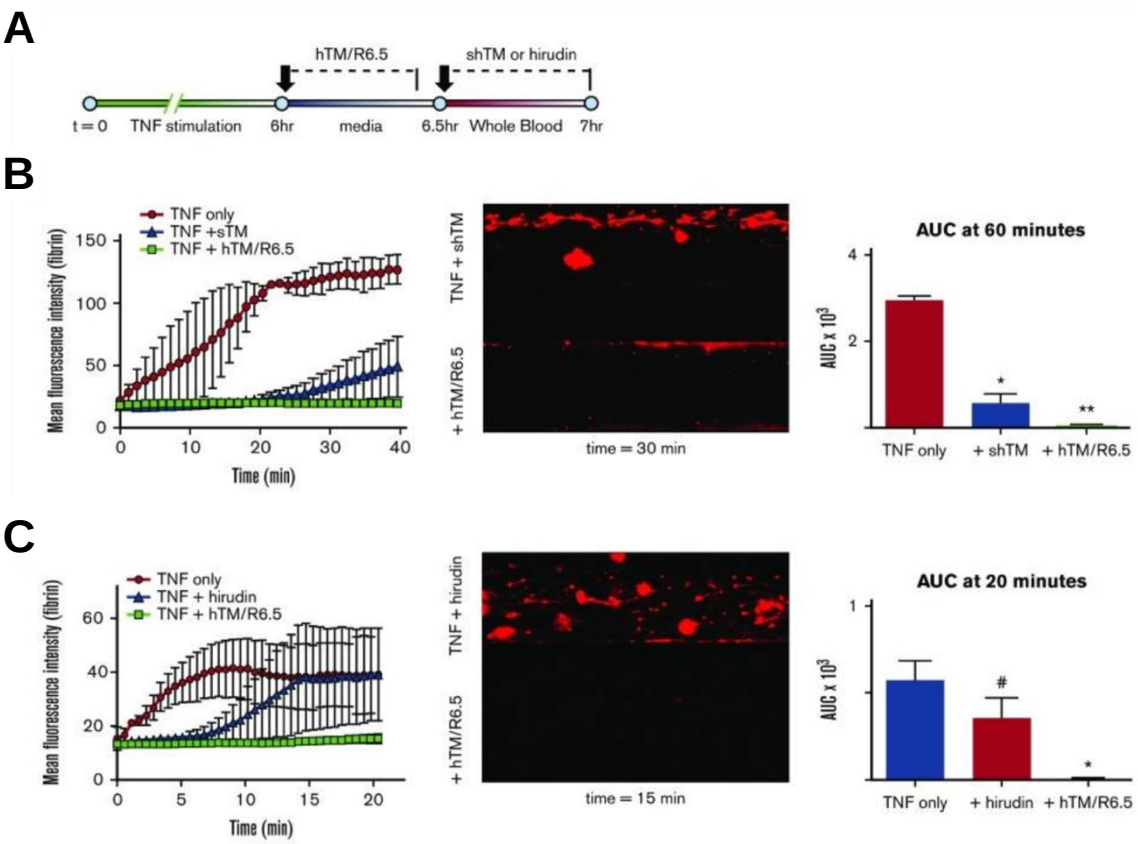

Figure 6.9. Comparative testing of antithrombotic agents.

(**A**) Experimental design, showing distinct timing of treatment with hTM/R6.5 scFv, bound to ECs during the first 25 minutes of the TNFα washout period versus soluble agents, which were mixed into whole blood. (**B**-**C**) Both 100 nM shTM (**B**) and 5 U/ml hirudin (**C**) inhibited coagulation, but were less effective than hTM/R6.5 (50 nM). Left panels show MFI versus time, ± SEM, with N = 2 channels for TNFα only and N = 3 channels for each therapeutic. Middle panels show representative fluorescent images. Right panels show AUC analyses. * = $P < 0.05$ versus TNF only; ** = $P < 0.05$ versus both other conditions; #, not significant ($P = 0.17$).

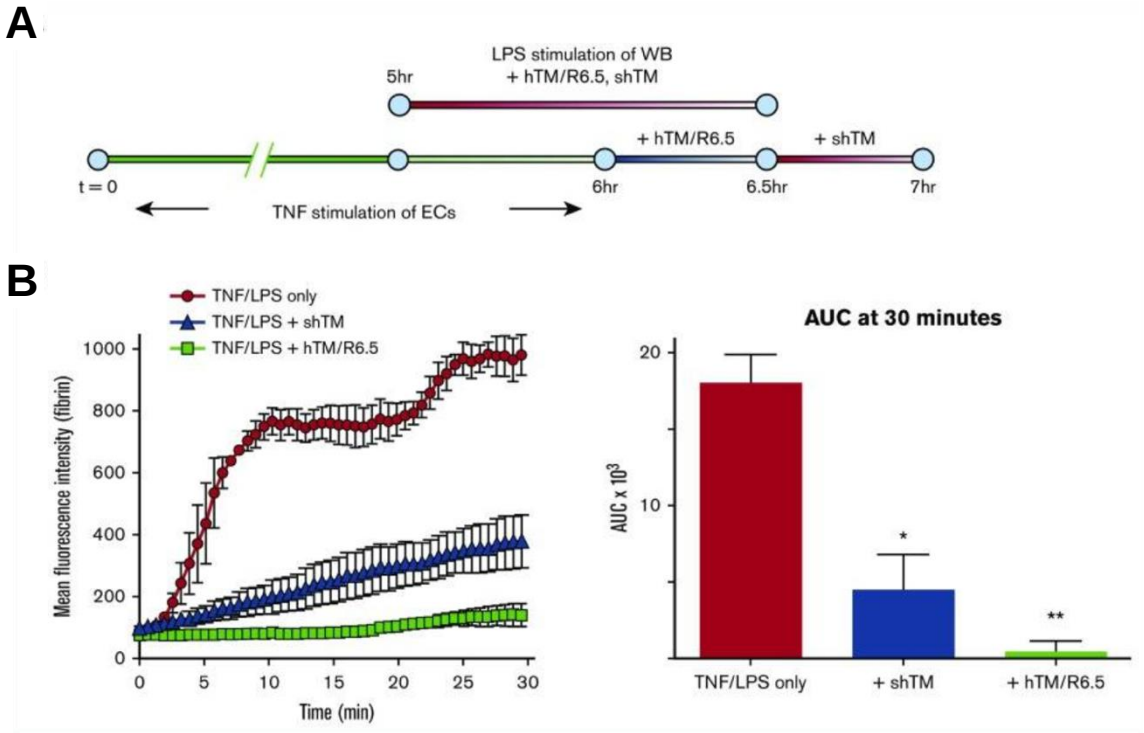

Figure 6.10 hTM/R6.5 has greater antithrombotic activity than shTM in combined model of endothelial cytokine activation and endotoxemia.

(**A**) Experimental design, showing 6-hr stimulation of endothelialized channels with TNFα and 90-minute preactivation of whole blood with LPS (50 ng/ml). In this case, hTM/R6.5 (50 nM) was infused during the TNFα washout period and mixed into the whole blood. (**B**) The fusion protein provided superior antithrombotic effect. Left panels show MFI versus time, mean ± SEM, with N = 2 channels for TNF/LPS only and N = 3 channels for each therapeutic. Right panels show AUC analyses. * = $P < 0.05$ versus TNF/LPS only; ** = $P < 0.05$ versus both other conditions.

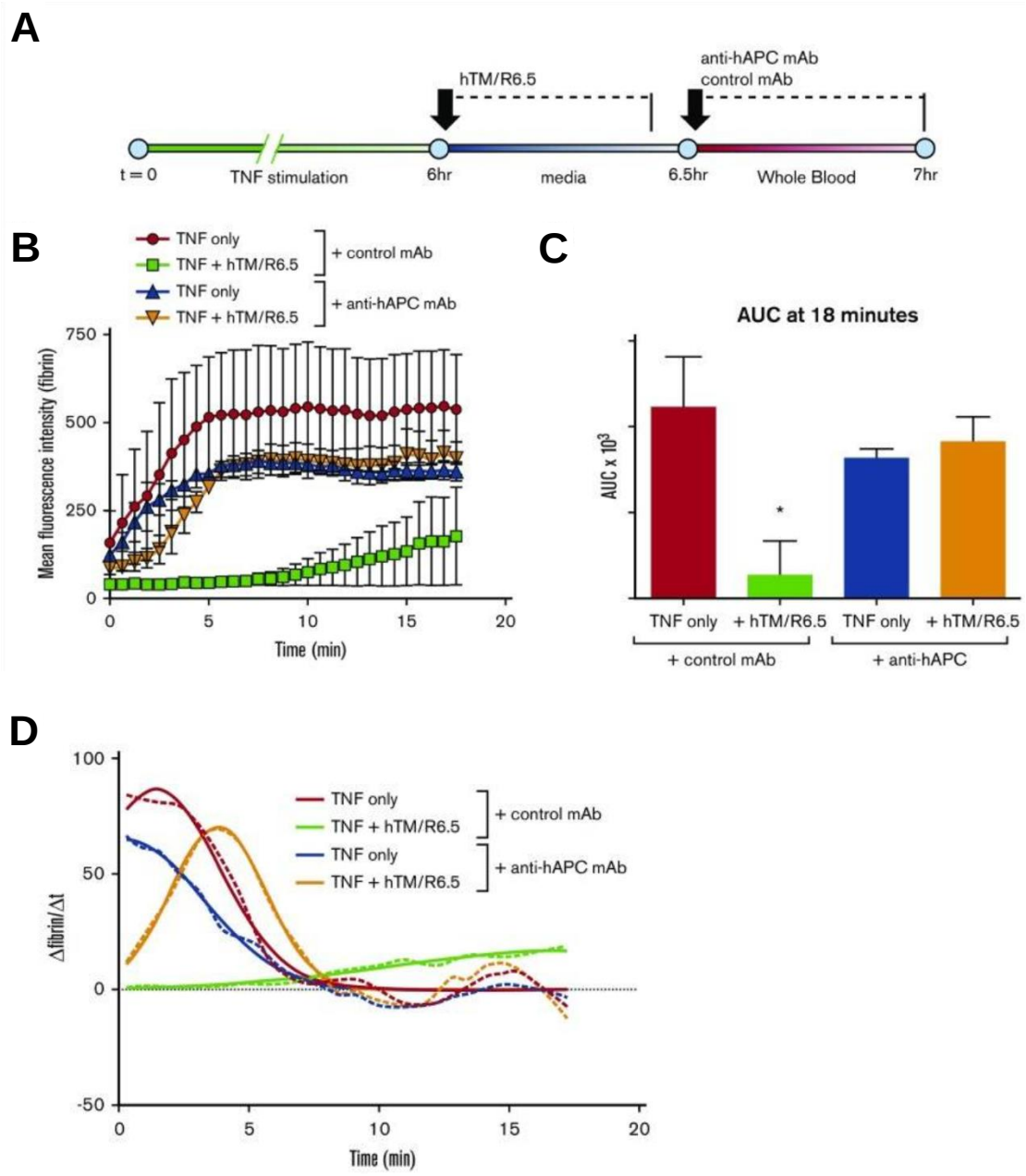

Figure 6.11. Antithrombotic activity of hTM/R6.5 is largely reversed by APC inhibition.

(**A**) Design of APC inhibition experiments. Anti-hAPC antibody (HAPC1573) or equimolar isotype control were mixed into whole blood at 300 nM concentration. (**B**) Inhibition of APC significantly reduced the antithrombotic effect of hTM/R6.5 while not significantly affecting fibrin deposition in endothelialized channels not treated with fusion protein. Graph shows

mean ± SEM, with N = 2 channels for each condition. (**C**) AUC analysis. * = $P < 0.05$ versus all other conditions; #, not significant ($P = 0.47$); ##, not significant ($P = 0.72$). (**D**) Time curves of the first derivative of fibrin fluorescence intensity demonstrate the effects of various combinations of HAPC1573 and hTM/R6.5 on key parameters: peak-fibrin generation rate and time to peak-fibrin generation rate. Dotted lines show actual values, whereas solid lines show Gaussian functions fitted to these data.

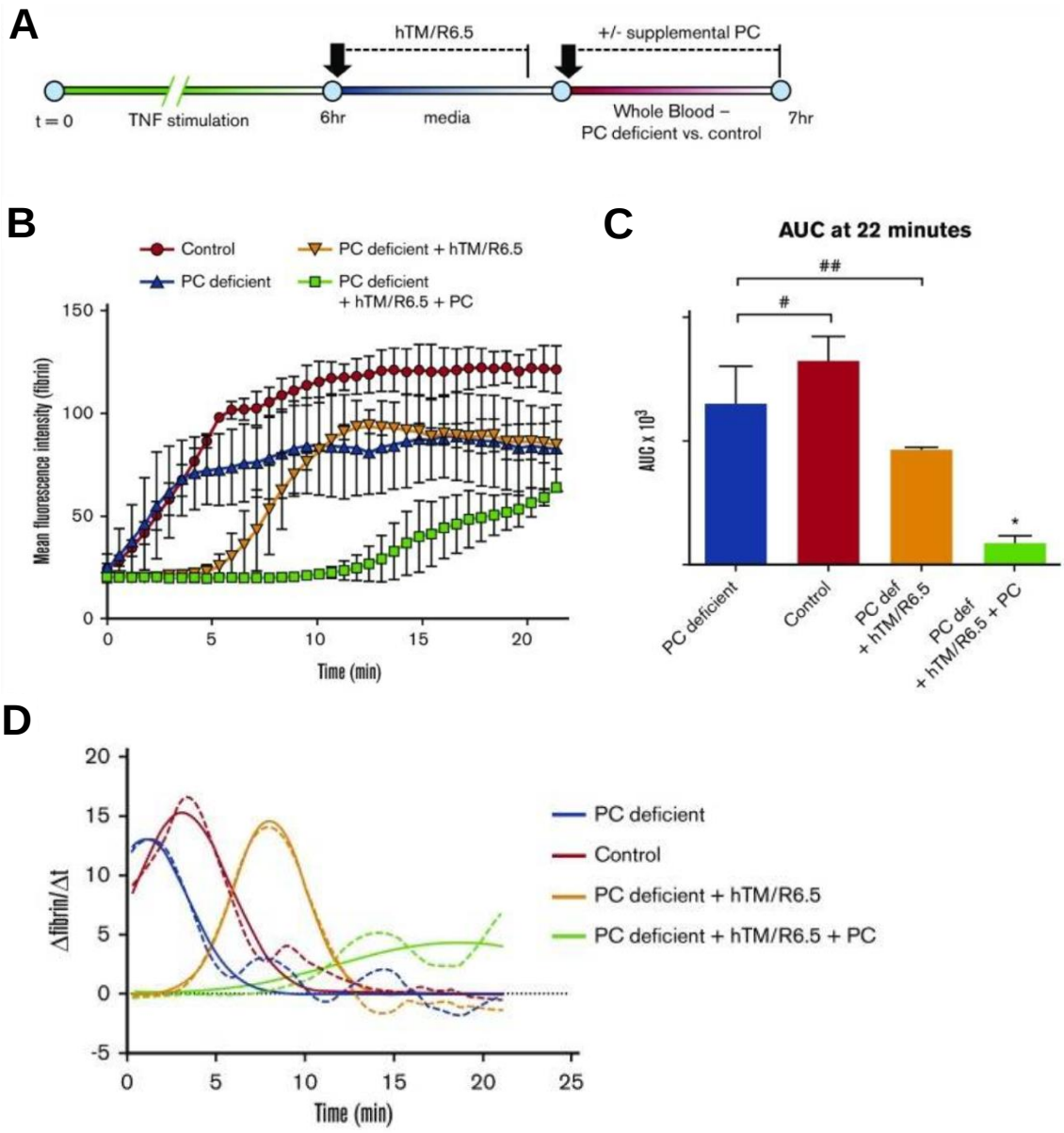

Figure 6.12. Antithrombotic activity of hTM/R6.5 is enhanced by PC supplementation in the setting of plasma PC deficiency.

(**A**) Design of PC deficiency experiments. hTM/R6.5 was infused during the first 25 minutes of the TNFα washout period, followed by infusion of PC-deficient blood versus control blood. (**B**) The anti-thrombotic effect of hTM/R6.5 was reduced in PC-deficient blood and restored with the addition of supplemental PC. Graph shows mean ± SEM, with

N = 2 channels for each condition. (**C**) AUC analysis. * = P < 0.05 versus all other conditions; #, not significant (P = 0.33); ##, not significant (P = 0.28). (**D**) Time curves of the first derivative of fibrin fluorescence intensity demonstrate a delay in peak-fibrin deposition, but not a reduction in peak height by hTM/R6.5 in PC-deficient whole blood. Full efficacy is restored with the addition of supplemental plasma PC.

Chapter 7 – Discussion, Impact, and Future Directions

Discussion

ECs play an important role in the thrombotic complications in HIT.

In Chapter 3, we showed that in a microfluidic photochemical model of endothelial injury and in the cremaster arteriole laser injury model that PF4 and HIT show extensive binding to the EC lining upon which platelets accumulate during the process of thrombus growth. The area targeted by HIT antibodies spreads downstream of the original injury site. These findings are significant because they emphasize the importance of the vasculature as a target in HIT and a focus for novel interventions to complement contemporary antithrombotic therapies. These include therapeutics directed to endothelial PC receptor (EPCR), that block protease-activated receptors[120], modify the glycocalyx coat[258] or inhibit oligomerization of VWF.

APC bound to EPCR activates PAR1 by a noncanonical cleavage[259] leading to improved EC barrier function and resistance to injury by TNFα[260,261]. We have shown that PF4 binds to TM, enhanced APC generation[262]. HIT antibodies block this effect, which we proposed may contribute to thrombus development. To combat or bypass this effect, we envision utilizing the peptide, Parmodulin-2, which blocks the PAR1/Gα_{13}/RhoA pathway and stimulates PAR1/Gα_q/Rak1 signaling[120]. This allows for the cytoprotective signaling of PAR1 on ECs, but blocks the proinflammatory effects. This would allow us to evaluate how maintaining EC health combats being directly bound by PF4 and HIT antibodies. To distinguish between Parmodulin's effects on ECs and its effects on circulating platelets, we intend to study Parmodulin-2 in the photochemical injury model, incubating the drug with whole blood prior to infusion and hematoporphyrin injury as a baseline. Parmodulin-2 would be used in comparison to wildtype APC, and 2 variants that retain cytoprotective effects with little anticoagulant effects. These studies will be made possible by obtaining said parmodulins from Dr. John Griffin at the Scripps Research Institute[263,264]. The variant

5A-APC can be used for studies of murine as well as human endothelium[265], this allows us to study the therapeutics in the HIT passive immunization murine model.

We will modify the glycocalyx using heparinase, chondroitinase, and hyaluronidase to cleave heparin sulfate, chrondroitin sulfate, and hyaluronan, respectively. Treatment with these enzymes reduces the thickness of the glycocalyx layer by 26-43% when used individually and up to 90% when used in combination[12,15,258]. Removal of individual GAGs changes diffusion properties; this would suggest that these three GAGs are not evenly distributed and differ in their contribution to its permeability. Heparinase decreased diffusion, whereas diffusion was enhanced by the other two enzymes[258]. This may imply that heparin sulfate plays a more important structural role and its removal causes the collapse of the glycocalyx which compacts surface GAGs and prevents solute diffusion. How changes in diffusion affects binding of PF4, HIT antigen formation and the impact of immune injury on endothelial coagulant reactions will be studied.

We envision HIT mice will be treated with these enzymes individually or in combination, and then will be subject to injuries to cremasteric vessel as described in Chapter 3. One key preliminary study will be to determine if removal of the glycocalyx affects baseline platelet adhesion and activation by allowing blood cells to interact more freely with the vascular wall. Nevertheless, by tracking PF4 and HIT antigen binding in these settings as presented in Chapter 3, we will shed light on the significance of the glycocalyx to the pathogenesis of HIT.

VWF offers a thrombosis-relevant binding site for HIT antigens and contributes to the propagation of HIT.

In Chapter 4, we showed that elongated strands of VWF released from EC post injury generate extensive binding surfaces for PF4 and HIT antibodies. The PF4-VWF-HIT antibody complexes enhanced platelet accumulation in our in vitro microfluidic model. These findings are significant for various reasons. First, VWF strands are likely to be found in arteries and arterioles and be present under high shear[132,266]. VWF release occurs under inflammatory conditions that often are found in patients with HIT[266,267] and are likely to be release in response to immune injury. Thus, these new observations suggest that control of endothelial activation may reduce the prothrombotic risks of HIT.

These findings suggest that HIT antibodies bind along the surface of ECs to elongated strands of VWF and in doing so enhance platelet accumulation, along with additional mechanisms that may be revealed in the future. The role of VWF in thrombus formation in the cremaster laser injury model has been uncertain, but our group has shown that suppressing ADAMTS13 activity in this model is prothrombotic and results in the generation of elongated thrombi[268]. As visualized in Chapter 4, VWF strands from injured ECs extend downstream along less injured ECs. This quality, in combination with formation of PF4-VWF-HIT antibody complexes, implies that VWF continually sensitizes ECs downstream of an injury site, allowing downstream thrombus extension in a process we called “rolling recruitment” and consistent with thrombus propagation as visualized in Step 3 (**Figure 1.5**). VWF also slows down platelets by allowing them to “roll” along the strands of VWF[132,269], where they may deliver PF4 to the adjacent downstream EC surface extending the area of immune-targeted endothelium. The collective impact of these effects support the role of endothelial cells injury and formation of extended strands of VWF in the propagation of thrombi in space and extension of the procoagulant risk in time.

We also demonstrated that at least one proposed VWF-targeted therapeutic, NAC, attenuated clot extension induced by HIT antibody in an in vivo model of vascular rose

bengal-induced photochemical injury. NAC increased the time to occlusion and indeed was completely prevented over the initial two hours following injury. It would be premature to indicate VWF as a key contributor to all thrombotic events in HIT patients. However, our findings do indicate that VWF-targeted therapeutics may provide a complement or alternative to anticoagulants in some settings, e.g. thrombi in arterioles or large arteries, and thereby increase the efficacy and potentially permit lower doses to be used and thereby decrease the risks of bleeding.

We propose that the PF4-VWF-HIT antibody complexes contribute to arterial thrombi because the necessary antigenic site requires oligomerization of VWF and shear forces that open the individual molecules which exposes the requisite binding site. Therefore, therapies directed at this complex will be mostly efficacious for arterial thrombi. We will test this focusing on the use of recombinant ADAMTS13 as recently described in mice[270]. We propose that such therapeutic intervention will be effective in arteriolar thrombi, but not venule thrombi, and therefore, in the rose bengal carotid artery injury model, but less so in a jugular injury model. This raises the intriguing possibility that VWF-directed therapies may help resolve most limb- or life-threatening thrombi caused by arterial occlusion.

Additionally, we speculate that PF4 bound to VWF is physiologically relevant. Binding of PF4 to VWF strands under shear may protect it from premature cleavage by ADAMTS13 under arterial pressure. This suggests that PF4 might bind near the ADAMTS13 binding site in VWF A2 domain[138]. We therefore propose that future studies should also include a better understanding the 3-D structure of the complex between PF4 and VWF, including identifying the binding site(s). This will include utilizing electron microscopy or cryo-electron microscopy to visualize PF4-VWF strand complexes to compare against the prior crystallographic studies of the HIT complex using PF4 and

fondaparinux[137,271]. Other studies using small drugs or VWF-derived peptides to compete for PF4 binding will be tested as well. Finally, generation of VWF with the site of interest mutated may need to be generated to validate PF4's binding site within the native molecule and to study the effect of shear.

To more definitively evaluate the impact of VWF, we will also be breeding $VWF^{-/-}$ /HIT mice to study vascular injury. This will be achieved by standard breeding to create the double transgenic $hPF4^{+}/Fc\gamma RIIA^{+}$ on the $VWF^{-/-}$ background[272], but we will also perform bone marrow transplant from HIT mice into $VWF^{-/-}$ mice. These mice will still express platelet VWF, but will specifically lack the contribution of EC VWF to thrombi development. These mice will be used in the rose bengal carotid artery and jugular vein injury models, and the cremaster arteriole and venule laser injury models. Formation of the HIT antigen and the time to occlusion will be studied. This will allow us to evaluate how VWF impacts vessel occlusion, contributes to the thrombus growth, and alters HIT antibody binding patterns relative to the site of injury. We believe that both the full VWF knockout and the EC knock will show decreased arterial thrombi, but little or no change in venular thrombi.

Neutrophil accumulation and NET release impact venous thrombosis in HIT.

In Chapter 5, we showed that NETs may play a similar role as VWF in propagating HIT thrombi downstream, but on the venous side. After inducing HIT in the murine HIT model by infusing KKO, we showed that neutrophils adhered to the venous, but not arterial endothelial lining, even without additional injury. Additionally, downstream of a venous laser-injury-induced thrombus, there was a marked increase in adhesion of neutrophils. These migrated retrograde to be incorporated in the growing thrombus. In an in vitro microfluidic model, we displayed that PF4 and HIT antibodies can bind NETs and provide

DNase resistance. These all contribute to venous thrombosis by inducing EC and blood cell activation, physically contributing to thrombus size, and forming PF4/NET/HIT antibody complexes, which further propagate thrombosis. These findings provide insight into how neutrophils selectively contribute to venous thrombosis in HIT.

Moreover, the studies introduce novel avenues for mitigating HIT thrombosis, which include inhibiting neutrophil-endothelial adhesion, preventing the chemotaxis of neutrophils to growing thrombi, and suppressing NET release or NET lysis. Future studies will focus on assessing these therapeutic avenues by using similar models as those described in Chapter 5. To impede neutrophil-endothelial adhesion and neutrophil chemotaxis, we also propose that blocking antibodies to neutrophil-relevant selectins and/or integrins[273,274] might decrease the prothrombotic venous risks of HIT. For example, crizanlizumab, a P-selectin blocking antibody was shown to significantly lower the rate of sickle cell related pain crises in patients with sickle cell disease[274]. Alternatively, CL2 is an antibody that blocks the binding of leukocytes to E-selectin[273] and was shown to reduce the extent of neutrophil transmigration to a site of inflammation during an acute inflammatory response. Each have potential to combat the enhanced adhesion of neutrophils seen to the venous lining seen in our studies and to the downstream accumulation of neutrophils in venous thrombi. Recent studies have also shown a mouse model which utilizes an adenovirus-mediated expression of endomucin to reduce neutrophil adhesion[275]. Endomucin is a membrane-bound glycoprotein that normally prevents leukocyte-EC interaction, but is downregulated with inflammation (TNFα) stimulation. This will allow us to evaluate the most effective and therapeutically relevant means of impeding neutrophil contribution to HIT thrombosis. Additionally, there is an opportunity to target the rates of NET formation or degradation to limit their effects. Our future studies will include investigating such agents, which include N-acetylcysteine,

DNase I, PAD4 inhibitors, and acetylsalicylic acid[150,183,189,194,276,277]. Despite the fact that anti-VWF and NET agents are not considered anticoagulants, they may still result in adverse side effects such as bleeding or immune defects, and therefore, their utility in the murine HIT model in conjunction with DTIs needs to be examined.

Novel ICAM-1 targeted therapeutics reduce inflammatory thrombosis in sepsis model

In Chapter 6, we showed the potential for using ICAM-1-targeted TM to inhibit or delay inflammatory thrombosis in an endothelialized microfluidic sepsis model. We were able to show that this targeted therapeutic was more effective at inhibiting TF-driven thrombosis than untargeted therapeutics such as soluble human TM and hirudin. Moreover, we showed this antithrombotic effect was PC-dependent and was synergistically effective with supplemental PC. This provides significant insight into potential treatments for the inflammatory-driven side of HIT. The current treatments for HIT are DTIs, which have limitations in that they have increased risk of bleeding diathesis, and consequently, require frequent patient monitoring[41,44]. The advantages of targeted TM is that it will primarily bind where inflammation has induced increased ICAM-1 levels; moreover, considering its PC-dependent functionality, the targeted TM will also be selectively antithrombotic in regions in which there is sufficient FIIa to bind TM leading to increased APC production. Furthermore, because the therapeutic is TM, the other TM domains can provide additional anti-inflammatory and anti-activated endothelium effects not seen with DTIs. A site selective antithrombotic that also combats inflammatory components could provide a unique solution to the VWF- and NET-associated EC-related mechanisms of thrombosis seen in HIT. Future studies in this realm will focus on integrating this therapeutic into cremaster murine models of HIT to determine the feasibility for preventing and mitigating HIT thrombosis on both the venous and arterial sides. There

is also interest in utilizing the targeting mechanism used in this therapeutic for other antithrombotics. An intriguing therapeutic could be an scFv-derived from a HIT antibody like KKO that binds to the PF4 antigenic site exposed when it is bound to GAGs, VWF and NETs and that would target a therapeutic to HIT antigen-rich sites.

Impact of the Described Research

Understanding the prothrombotic nature of HIT.

From a broader perspective, this research has the potential to impact our understanding, research approach, and treatment paradigm around HIT. In gaining a better understanding of how the endothelium (Chapter 3), VWF (Chapter 4), and NETs (Chapter 5) can form HIT antigenic complexes, we've provided new insights into the pathophysiology of thrombosis in HIT and the prolonged period of risk for recurrent thromboembolic complications (Step 3). We envision HIT as developing in three distinct all be it, overlapping, steps: Step 1: initiation by PF4/heparin complexes; Step 2: activation of intravascular cells (monocytes, platelets) causing thrombosis; and Step 3: antigen and thrombus propagation during which additional PF4 binding surfaces as generated that create a procoagulant positive feedback loop that is entirely independent of heparin.

With these studies, we have opened doors to additional future research questions: In what situations are these complexes most paramount to the propagation of HIT? How well do the various polymeric targets compete for PF4 in time and space? How do the location and affinity of these complexes impact the clinical course of HIT and what are the implications for response to current therapy? Future research could include in vivo studies using various injury settings with co-visualization of the EC glycocalyx, VWF, and neutrophils/NETs. This research could include using microfluidic studies to identify the binding preference of PF4 under flow in presence of these various polymeric targets in the

absence and/or presence of heparin. Both endothelial cell heterogeneity within the vasculature, genetic and epigenetic risk factors remain wide open to exploration as well.

Ultimately, these studies hold the potential to alter diagnosis and treatment in HIT. Across many healthcare fields, researchers are looking for physiological parameters that can be used for predictive analytics and predictive diagnosis; these predictive measures provide a means of knowing and treating a patient's pathology before it manifests into a tangible phenotype, which helps reduce medical cost, reduce treatment time, and improve patient outcomes. Predictive diagnosis would be very valuable in HIT considering its endpoints and our studies provide additional parameters that could have predictive significance. Prior studies would have placed patients with prior heparin exposure or bacterial infections at risk for HIT. But our studies now implicate the composition of the glycocalyx, levels and glycosylation of VWF, and neutrophil activation as having a higher propensity for HIT associated endpoints. Preemptive measures taken at the first clinical sign of HIT could include the use of non-anticoagulant reagents such as blocking GP1bα (AK2 antibody), blocking FcγRIIA (IV.3 antibody), or removing ultra-large VWF multimers (NAC or ADAMTS13) which may reduce thrombus extension, permit the intensity of anticoagulation to be lowered in the setting of thrombocytopenia, and lessen the risk of recurrent thrombembolism.

New insights into hemostasis and thrombosis in other clinically relevant settings.

These studies may also impact how we should view the relationship between hemostasis and thrombosis. Hemostasis is viewed as a delicate balance between pro- and anti-coagulative forces with thrombosis being the tipping of that scale. Consequently, therapeutics are generally foreign reagents that aim to tip that scale back to balance. This attempt to balance leads to the risk of under or overshooting hemostasis allowing clotting

to continue or causing inadvertent bleeds. Alternatively, our studies show that hemostasis and thrombosis should be viewed as a reestablishment of a standard vascular milieu. As described in Chapter 6, TM was targeted to ICAM-1; this allowed the therapeutic to replenish the TM on the surface of ECs that was shed during injury. Treating thrombosis by replenishing the proteins altered during injury presents a potential avenue to more precise therapeutics with less side effects. In reference to HIT, reestablishing the glycocalyx or correcting concentrations of ADAMTS13 could provide unique treatment strategies with less risk that the currently used DTIs.

These studies have implications for our understanding of other thrombotic disorders. In lupus, antibodies develop to DNA found in NETs. Studies are in progress to assess the impact of such antibodies on NET formation and resistance to DNases and the risk of thrombosis, as are agents that prevent neutrophil accumulation in thrombi and release of NETs. In the catastrophic antiphospholipid syndrome (CAPS), thrombosis may involve diffuse endothelial activation which may also involve the release of VWF, generation of NETs compacted by PF4, similar to the events we describe here in HIT. Whether therapeutics designed to affect thrombus formation of HIT are also pertinent to the management of other thrombotic disorders requires additional experimentation.

Lastly, these studies should impact how to study vascular injury ex vivo. One of the major advances we made was improving the performance of the endothelialized microfluidic system. The ability to observe intravascular cell binding to the endothelium and the development of thrombosis under physiological flows in real time provided insight that would otherwise not be feasible. For example, we observed that the stranded VWF had higher affinity for PF4, and subsequently, KKO. The elongation and conformational changes presented by VWF when tethered to an EC would be difficult to replicate in other ex vivo settings. There are devices that induce shear[138,145,150] and may alter VWF

confirmation, but none provide the environment of an EC monolayer grown to confluency in 3 dimensions displaying large multimeric VWF fibers. Previously, ELISAs or similar technologies were the primary means of measuring PF4 and antibody binding. This has obvious limitations in not allowing for flow, real time imaging, or the overall cellular environment present in the microfluidic setting. Moreover, when considering in vivo models, despite providing great insight, they also present certain limitations. Relevant to studies of HIT, in vivo models make it more difficult to decipher the minute interactions and contributions as we saw with PF4 binding VWF; in vivo imaging of VWF in thrombi have historically displayed diffused staining and have not been able to image the strands of VWF released by ECs. The microfluidic realm gives us the ability to better recapitulate the in vivo environment while still maintaining more control and specificity of unmodified or modified cells studied, flow rates and other physical parameters – such as temperature and oxygen level – and drug exposure. They allow studies of cells from multiple different species and also allow studies of a cell line and primary cells in 3D.

Summary

This thesis focused on studies of the prothrombotic processes underlying HIT. We found that PF4 and HIT antibodies predominantly bound to perithrombus endothelium in the absence of damage and even more so in the setting of HIT. Further investigation led to the discovery that VWF and NETs participate in the prothrombotic propagation of thrombi in HIT. We observed the formation of PF4-VWF-HIT antibody complexes that promoted platelet accumulation that was propagated downstream. These observations offer potential new therapeutic targets in HIT, which will be a focus of future studies. In addition to the studies on NETs, we also define how neutrophils contribute to venous thrombi in HIT. We culminated our studies with an investigation into combatting

inflammatory thrombosis in a sepsis model, which provides insights into the effect of inflammation which may precede or accompany HIT. Using a novel ICAM-1 targeted TM therapeutic, we saw that targeted TM inhibited TF induced thrombosis via a PC-dependent pathway more efficiently than soluble reagents. Collectively, this thesis work provides a more defined understanding of the pathogenesis of thrombosis in HIT and related inflammatory states and provides insights into potential novel therapeutics.

BIBLIOGRAPHY

1. Brass, L. F., Diamond, S. L. & Stalker, T. J. Platelets and hemostasis: a new perspective on an old subject. *Blood Adv.* **1,** 5–9 (2016).
2. Van De Wouwer, M., Collen, D. & Conway, E. M. Thrombomodulin-protein C-EPCR system integrated to regulate coagulation and inflammation. *Arterioscler. Thromb. Vasc. Biol.* **24,** 1374–1383 (2004).
3. Green, D. Coagulation cascade. *Hemodial. Int.* **10,** (2006).
4. Esmon, C. T. The impact of the inflammatory response on coagulation. *Thromb. Res.* **114,** 321–327 (2004).

5. Palta, S., Saroa, R. & Palta, A. Overview of the coagulation system. *Indian J. Anaesth.* **58,** 515–523 (2014).

6. Sagripanti, A. & Carpi, A. Antithrombotic and prothrombotic activities of the vascular endothelium. *Biomed. Pharmacother.* **54,** 107–111 (2000).

7. Yang, Y. & Loscalzo, J. Regulation of tissue factor expression in human microvascular endothelial cells by nitric oxide. *Circulation* **101,** 2144–2148 (2000).

8. Brass, L. Understanding and Evaluating Platelet Function. *Hematology* **2010,** 387–396 (2010).

9. Wang, G. R., Zhu, Y., Halushka, P. V, Lincoln, T. M. & Mendelsohn, M. E. Mechanism of platelet inhibition by nitric oxide: in vivo phosphorylation of thromboxane receptor by cyclic GMP-dependent protein kinase. *Proc. Natl. Acad. Sci. U. S. A.* **95,** 4888–4893 (1998).

10. Radomski, M. W., Palmer, R. M. J. & Moncada, S. Comparative pharmacology of endothelium-derived relaxing factor, nitric oxide and prostacyclin in platelets. *Br. J. Pharmacol.* **92,** 181–187 (1987).

11. Weiss, H. J. & Turitto, V. T. Prostacyclin (prostaglandin I2, PGI2) inhibits platelet adhesion and thrombus formation on subendothelium. *Blood* **53,** 244–250 (1979).

12. Potter, D. R. & Damiano, E. R. The hydrodynamically relevant endothelial cell glycocalyx observed in vivo is absent in vitro. *Circ. Res.* **102,** 770–776 (2008).

13. Koo, A., Dewey, C. F. & Garcia-Cardena, G. Hemodynamic shear stress characteristic of atherosclerosis-resistant regions promotes glycocalyx formation in cultured endothelial cells. *AJP Cell Physiol.* **304,** C137–C146 (2013).

14. Chappell, D. *et al.* The glycocalyx of the human umbilical vein endothelial cell: An impressive structure ex vivo but not in culture. *Circ. Res.* **104,** 1313–1317 (2009).

15. Van Den Berg, B. M., Nieuwdorp, M., Stroes, E. S. G. & Vink, H. Glycocalyx and

endothelial (dys) function: From mice to men. *Pharmacol. Reports* **58,** 75–80 (2006).

16. Mulivor, A. W. & Lipowsky, H. H. Role of glycocalyx in leukocyte-endothelial cell adhesion. *Am. J. Physiol. - Hear. Circ. Physiol.* **283,** H1282–H1291 (2002).
17. Reitsma, S., Slaaf, D. W., Vink, H., Van Zandvoort, M. A. M. J. & Oude Egbrink, M. G. A. The endothelial glycocalyx: Composition, functions, and visualization. *Pflugers Arch. Eur. J. Physiol.* **454,** 345–359 (2007).
18. Esmon, C. T. Thrombomodulin mechanisms function as a model that modulate surface of molecular protease specfficity and at the vessel. **9,** 946–955 (1995).
19. Conway, E. M. Thrombomodulin and its role in inflammation. *Semin. Immunopathol.* **34,** 107–125 (2012).
20. Minami, T. *et al.* Thrombin and Phenotypic Modulation of the Endothelium. *Arterioscler. Thromb. Vasc. Biol.* **24,** 41–53 (2004).
21. Riewald, M., Petrovan, R. J., Donner, A., Mueller, B. M. & Ruf, W. Activation of endothelial cell protease activated receptor 1 by the protein C pathway. *Science (80-.).* **296,** 1880–1882 (2002).
22. Esmon, C. T. Protein C anticoagulant system - Anti-inflammatory effects. *Semin. Immunopathol.* **34,** 127–132 (2012).
23. Brogren, H. *et al.* Platelets synthesize large amounts of active plasminogen activator inhibitor 1. *Blood* **104,** 3943–3948 (2004).
24. Zaitsev, S. *et al.* Targeting of a mutant plasminogen activator to circulating red blood cells for prophylactic fibrinolysis. *J. Pharmacol. Exp. Ther.* **332,** 1022–31 (2010).
25. Eitzman, D. T., Westrick, R. J., Nabel, E. G. & Ginsburg, D. Plasminogen activator inhibitor-1 and vitronectin promote vascular thrombosis in mice. *Blood* **95,** 577–80

(2000).

26. Greineder, C. F. *et al.* ICAM-1–targeted thrombomodulin mitigates tissue factor–driven inflammatory thrombosis in a human endothelialized microfluidic model. *Blood Adv.* **1,** 1452–1465 (2017).

27. Wagner, D. D. & Burger, P. C. Platelets in Inflammation and Thrombosis. *Arterioscler. Thromb. Vasc. Biol.* **23,** 2131–2137 (2003).

28. Kumar, S. & Krishnaswamy, S. Thrombin formation. *Trauma Induc. Coagulopathy* **124,** 55–74 (2016).

29. Malek, A. M., Jackman, R., Rosenberg, R. D. & Izumo, S. Endothelial expression of thrombomodulin is reversibly regulated by fluid shear stress. *Circ. Res.* **74,** 852–860 (1994).

30. Moore, K. L., Esmon, C. T. & Esmon, N. L. Tumour necrosis factor leads to internalisation and degradation of thrombomodulin from the surface of bovine aortic endothelial cells in culture. *Blood* **73,** 159–165 (1989).

31. Montes, R., Puy, C., Molina, E. & Hermida, J. Is EPCR a multi-ligand receptor? Pros and cons. *Thromb. Haemost.* **107,** 815–826 (2012).

32. Danese, S., Vetrano, S., Zhang, L., Poplis, V. A. & Castellino, F. J. The protein C pathway in tissue inflammation and injury: pathogenic role and therapeutic implications. *Blood* **115,** 1121–1130 (2010).

33. McLaughlin, J. *et al.* Regulation of endothelial function by coagulation proteases in sepsis. *Crit. Care* **15,** P251 (2011).

34. Lorenzon, P. *et al.* Endothelial cell E- and P-selectin and vascular cell adhesion molecule- 1 function as signaling receptors. *J. Cell Biol.* **142,** 1381–1391 (1998).

35. Poirault-Chassac, S. *et al.* Terminal Platelet Production is Regulated by Von Willebrand Factor. *PLoS One* **8,** e63810 (2013).

36. Endenburg, S. C. *et al.* On the role of von Willebrand factor in promoting platelet adhesion to fibrin in flowing blood. *Blood* **86,** 4158–65 (1995).

37. Haji-Valizadeh, H., Modery-Pawlowski, C. L. & Sen Gupta, A. A factor VIII-derived peptide enables von Willebrand factor (VWF)-binding of artificial platelet nanoconstructs without interfering with VWF-adhesion of natural platelets. *Nanoscale* **6,** 4765–4773 (2014).

38. Gogia, S., Kelkar, A., Zhang, C., Dayananda, K. M. & Neelamegham, S. Role of calcium in regulating the intra- and extracellular cleavage of von Willebrand factor by the protease ADAMTS13. **1,** (2017).

39. Dayananda, K. M., Singh, I., Mondal, N. & Neelamegham, S. von Willebrand factor self-association on platelet GpIb?? under hydrodynamic shear: Effect on shear-induced platelet activation. *Blood* **116,** 3990–3998 (2010).

40. Hassan, M. I., Saxena, A. & Ahmad, F. Structure and function of von Willebrand factor. *Blood Coagul. Fibrinolysis* **23,** 11–22 (2012).

41. Warkentin, T. E. HIT: Treatment easier, prevention harder. *Blood* **119,** 1099–1100 (2012).

42. Cines, D. B. *et al.* Endothelial cells in physiology and in the pathophysiology of vascular disorders. *Blood* **91,** 3527–3561 (1998).

43. Hayes, V. *et al.* Endothelial antigen assembly leads to thrombotic complications in heparin-induced thrombocytopenia. *J. Clin. Invest.* **127,** 1090–1098 (2017).

44. Cuker, A. & Cines, D. B. How I treat heparin-induced thrombocytopenia. *Blood* **119,** 2209–2218 (2012).

45. Kelton, J. G. & Warkentin, T. E. Heparin-induced thrombocytopenia: A historical perspective. *Blood* **112,** 2607–2616 (2008).

46. Warkentin, T. E., Basciano, P. a, Knopman, J. & Bernstein, R. a. Spontaneous

heparin-induced thrombocytopenia syndrome : 2 new cases and a proposal for de fi ning this disorder. *Blood* **123,** 3651–3654 (2014).

47. Arepally, G. M. *et al.* Characterization of a murine monoclonal antibody that mimics heparin-induced thrombocytopenia antibodies. *Blood* **95,** 1533–40 (2000).

48. Ahmed, I., Majeed, A. & Powell, R. Heparin induced thrombocytopenia: Diagnosis and management update. *Postgrad. Med. J.* **83,** 575–582 (2007).

49. Busch, C., Sawes, J., Pepper, D. S. & Wasteson, A. Binding of platelet factor 4 to cultured human umbilical vein endothelial cells. *Thromb.Res.* **19,** 129–137 (1980).

50. Rauova, L. *et al.* Monocyte-bound PF4 in the pathogenesis of heparin-induced thrombocytopenia. *Blood* **116,** 5021–5031 (2010).

51. Walenga, J. M., Jeske, W. P., Margaret Prechel, M. & Bakhos, M. Newer insights on the mechanism of heparin-induced thrombocytopenia. *Semin. Thromb. Hemost.* **30,** 57–67 (2004).

52. Rabiet, M. J. *et al.* Thrombin-induced increase in endothelial permeability is associated with changes in cell-to-cell junction organization. *Arterioscler. Thromb. Vasc. Biol.* **16,** 488–496 (1996).

53. Cines, D. B. *et al.* Polyphosphate/platelet factor 4 complexes can mediate heparin-independent platelet activation in heparin-induced thrombocytopenia. *Blood Adv.* **1,** 62–74 (2016).

54. Mackman, N. Triggers, targets and treatments for thrombosis. *Nature* **451,** 914–918 (2008).

55. Shuster, T. A., Silliman, W. R., Coats, R. D., Mureebe, L. & Silver, D. Heparin-induced thrombocytopenia: Twenty-nine years later. *J. Vasc. Surg.* **38,** 1316–1322 (2003).

56. Reilly, M. P. *et al.* Heparin-induced thrombocytopenia/thrombosis in a transgenic

mouse model requires human platelet factor 4 and platelet activation through FcgammaRIIA. *Blood* **98,** 2442–2447 (2001).

57. Perlman, R. L. Mouse Models of Human Disease: An Evolutionary Perspective. *Evol. Med. Public Heal.* eow014 (2016). doi:10.1093/emph/eow014

58. Justice, M. J. & Dhillon, P. Using the mouse to model human disease: increasing validity and reproducibility. *Dis. Model. Mech.* **9,** 101–103 (2016).

59. Rello, J., Valenzuela-Sánchez, F., Ruiz-Rodriguez, M. & Moyano, S. Sepsis: A Review of Advances in Management. *Adv. Ther.* **34,** 2393–2411 (2017).

60. Polat, G., Ugan, R. A., Cadirci, E. & Halici, Z. Sepsis and Septic Shock: Current Treatment Strategies and New Approaches. *Eurasian J. Med.* **49,** 53–58 (2017).

61. Van Der Poll, T., Van De Veerdonk, F. L., Scicluna, B. P. & Netea, M. G. The immunopathology of sepsis and potential therapeutic targets. *Nat. Rev. Immunol.* **17,** 407–420 (2017).

62. Xu, J. *et al.* Extracellular histones are major mediators of death in sepsis. *Nat. Med.* **15,** 1318–1321 (2009).

63. Li, Z. Q. *et al.* Defining a second epitope for heparin-induced thrombocytopenia/thrombosis antibodies using KKO, a murine HIT-like monoclonal antibody. *Blood* **99,** 1230–1236 (2002).

64. Melanson, S. W., Silver, B. & Heller, M. B. Deep vein thrombosis, pulmonary embolism, and the white clot syndrome. *Am. J. Emerg. Med.* **14,** 558–560 (1996).

65. Daubert, G. P. The white clot syndrome. *J. Clin. Pharm. Ther.* **30,** 503 (2005).

66. Towne, J. B., Bernhard, V. M., Hussey, C. & Garancis, J. C. White Clot Syndrome: Peripheral Vascular Complications of Heparin Therapy. *Arch. Surg.* **114,** 372–377 (1979).

67. Warkentin, T. E. An overview of the heparin-induced thrombocytopenia syndrome.

Semin. Thromb. Hemost. **30,** 273–283 (2004).

68. Madge, L. A. & Pober, J. S. TNF signaling in vascular endothelial cells. *Exp. Mol. Pathol.* **70,** 317–325 (2001).

69. Nishimura, S. *et al.* In vivo imaging visualizes discoid platelet aggregations without endothelium disruption and implicates contribution of inflammatory cytokine and integrin signaling. *Blood* **119,** e45-56 (2012).

70. Rauova, L. 'Radical' model of thrombosis. *Blood* **119,** 1798–1799 (2012).

71. Cerutti, C. & Ridley, A. J. Endothelial cell-cell adhesion and signaling. *Exp. Cell Res.* **358,** 31–38 (2017).

72. Wagner, D. D. & Bonfanti, R. von Willebrand factor and the endothelium. *Mayo Clin. Proc.* **66,** 621–627 (1991).

73. Kiskin, N. I. *et al.* Protein mobilities and P-selectin storage in Weibel-Palade bodies. *J. Cell Sci.* **123,** 2964–2975 (2010).

74. Estrada, R., Giridharan, G. A., Nguyen, M. D., Prabhu, S. D. & Sethu, P. Microfluidic endothelial cell culture model to replicate disturbed flow conditions seen in atherosclerosis susceptible regions. *Biomicrofluidics* **5,** 1–11 (2011).

75. Jalili-Firoozinezhad, S. *et al.* Modeling radiation injury-induced cell death and countermeasure drug responses in a human Gut-on-a-Chip article. *Cell Death Dis.* **9,** 1–36 (2018).

76. Martin, J. V., Liberati, D. M. & Diebel, L. N. Excess sodium is deleterious on endothelial and glycocalyx barrier function. *J. Trauma Acute Care Surg.* **1,** 1 (2018).

77. Sakurai, Y. *et al.* A microengineered vascularized bleeding model that integrates the principal components of hemostasis. *Nat. Commun.* **9,** 1–9 (2018).

78. Diebel, L. N., Martin, J. V. & Liberati, D. M. Microfluidics. *J. Trauma Acute Care*

Surg. **84,** 1 (2017).

79. Education, M., Bhubaneswar, A. & Sciences, D. Discover the world ' s research. (2015).

80. Sylman, J. L., Artzer, D. T., Rana, K. & Neeves, K. B. A vascular injury model using focal heat-induced activation of endothelial cells. *Integr. Biol.* **7,** 801–814 (2015).

81. Amiral, J. *et al.* Platelet factor 4 complexed to heparin is the target for antibodies generated in heparin-induced thrombocytopenia [4]. *Thromb. Haemost.* **68,** 95–96 (1992).

82. Greinacher, A. *et al.* Clinical features of heparin-induced thrombocytopenia including risk factors for thrombosis. A retrospective of 408 patients. *Thromb. Haemost.* **94,** 132–135 (2005).

83. Hong, A. P., Cook, D. J., Sigouin, C. S. & Warkentin, T. E. Central venous catheters and upper-extremity deep-vein thrombosis complicating immune heparin-induced thrombocytopenia. *Blood* **101,** 3049–3051 (2003).

84. Martel, N., Lee, J. & Wells, P. S. Risk for heparin-induced thrombocytopenia with unfractionated and low-molecular-weight heparin thromboprophylaxis: A meta-analysis. *Blood* **106,** 2710–2715 (2005).

85. Linkins, L. A. End of the road for heparin thromboprophylaxis. *Blood* **127,** 1945–1946 (2016).

86. Riess, F.-C. Anticoagulation management and cardiac surgery in patients with heparin-induced thrombocytopenia. *Semin. Thorac. Cardiovasc. Surg.* **17,** 85–96 (2005).

87. Kelton, J. G., Hursting, M. J., Heddle, N. & Lewis, B. E. Predictors of clinical outcome in patients with heparin-induced thrombocytopenia treated with direct

thrombin inhibition. *Blood Coagul. Fibrinolysis* **19,** 471–475 (2008).

88. Rauova, L. *et al.* Role of platelet surface PF4 antigenic complexes in heparin-induced thrombocytopenia pathogenesis: Diagnostic and therapeutic implications. *Blood* **107,** 2346–2353 (2006).

89. Khandelwal, S. *et al.* The antigenic complex in HIT binds to B cells via complement and complement receptor 2 (CD21). *Blood* **128,** 1789–1799 (2016).

90. Petersen, F., Brandt, E., Lindahl, U. & Spillmann, D. Characterization of a neutrophil cell surface glycosaminoglycan that mediates binding of platelet factor 4. *J. Biol. Chem.* **274,** 12376–12382 (1999).

91. Jg, K. *et al.* Heparin-induced thrombocytopenia : laboratory studies . **72,** (2018).

92. Warkentin, T. E. *et al.* Sera from patients with heparin-induced thrombocytopenia generate platelet-derived microparticles with procoagulant activity: an explanation for the thrombotic complications of heparin-induced thrombocytopenia. *Blood* **84,** 3691–9 (1994).

93. Blank, M. *et al.* Anti-platelet factor 4/heparin antibodies from patients with heparin-induced thrombocytopenia provoke direct activation of microvascular endothelial cells. *Int. Immunol.* **14,** 121–129 (2002).

94. Cines, D. B., Tomaski, A., Tannenbaum, S. & Articles, C. Immune Endothelial-Cell Injury in Heparin-Associated Thrombocytopenia. *N. Engl. J. Med.* **316,** 2018 (2018).

95. Visentin, G. P., Ford, S. E., Scott, J. P. & Aster, R. H. Antibodies From Patients With Heparin-Induced Thrombocytopenia/Thrombosis Are Specific for Platelet Factor-4 Complexed With Heparin or Bound To Endothelial-Cells. *J. Clin. Invest.* **93,** 81–88 (1994).

96. Marki, A., Esko, J. D., Pries, A. R. & Ley, K. Role of the endothelial surface layer

in neutrophil recruitment. *J. Leukoc. Biol.* **98,** 503–515 (2015).

97. Falati, S. *et al.* Accumulation of Tissue Factor into Developing Thrombi In Vivo Is Dependent upon Microparticle P-Selectin Glycoprotein Ligand 1 and Platelet P-Selectin. *J. Exp. Med.* **197,** 1585–1598 (2003).

98. Neyman, M., Gewirtz, J. & Poncz, M. Analysis of the spatial and temporal characteristics of platelet-delivered factor VIII based clots. *Blood* **112,** 1101–1108 (2008).

99. Stalker, T. J. *et al.* Hierarchical organization in the hemostatic response and its relationship to the platelet-signaling network. *Blood* **121,** 1875–1885 (2013).

100. Falati, S., Gross, P., Merrill-skoloff, G., Furie, B. C. B. & Furie, B. C. B. Real time in vivo imaging of platelets, tissue factor and fibrin during arterial thrombus formation in the mouse. *Nat. Med.* **8,** 1175–1180 (2002).

101. Zhang, C. *et al.* Localization of distal regulatory domains in the megakaryocyte-specific platelet basic protein / platelet factor 4 gene locus. **98,** 610–618 (2018).

102. McKenzie, S. E. *et al.* The role of the human Fc receptor Fc gamma RIIA in the immune clearance of platelets: a transgenic mouse model. *J. Immunol.* **162,** 4311–8 (1999).

103. Eslin, D. E. *et al.* Transgenic mice studies demonstrate a role for platelet factor 4 in thrombosis : dissociation between anticoagulant and antithrombotic effect of heparin Transgenic mice studies demonstrate a role for platelet factor 4 in thrombosis : dissociation between . **104,** 3173–3180 (2011).

104. Cuker, A. *et al.* The HIT Expert Probability (HEP) Score: A novel pre-test probability model for heparin-induced thrombocytopenia based on broad expert opinion. *J. Thromb. Haemost.* **8,** 2642–2650 (2010).

105. Sheridan, D., Carter, C. & Kelton, J. G. A diagnostic test for heparin-induced

thrombocytopenia. *Blood* **67,** 27–30 (1986).

106. Hui, K. Y., Haber, E. & Matsueda, G. R. Monoclonal antibodies to a synthetic fibrin-like peptide bind to human fibrin but not fibrinogen. *Science* **222,** 1129–1132 (1983).

107. Celi, A. *et al.* Thrombus formation: Direct real-time observation and digital analysis of thrombus assembly in a living mouse by confocal and widefield intravital microscopy. *J. Thromb. Haemost.* **1,** 60–68 (2003).

108. Tutwiler, V. *et al.* Platelet transactivation by monocytes promotes thrombosis in heparin-induced thrombocytopenia. *Blood* **127,** 464–472 (2016).

109. Barkefors, I., Aidun, C. K. & Ulrika Egertsdotter, E. M. Effect of fluid shear stress on endocytosis of heparan sulfate and low-density lipoproteins. *J. Biomed. Biotechnol.* **2007,** 65136 (2007).

110. Suvarna, S. *et al.* Determinants of PF4/heparin immunogenicity. *Blood* **110,** 4253–4260 (2007).

111. Suvarna, S., Qi, R. & Arepally, G. M. Optimization of a murine immunization model for study of PF4/heparin antibodies. *J. Thromb. Haemost.* **7,** 857–864 (2009).

112. Hirsh, J. & Fuster, V. *Guide to anticoagulant therapy*. *American Heart Association* (1994).

113. Soleimannejad, M. *et al.* Activated Clotting Time Level with Weight Based Heparin Dosing During Percutaneous Coronary Intervention and its Determinant Factors. *J. Cardiovasc. Thorac. Res.* **6,** 97–100 (2014).

114. Nader, H. B. Characterization of a heparan sulfate and a peculiar chondroitin 4-sulfate proteoglycan from platelets. Inhibition of the aggregation process by platelet chondroitin sulfate proteoglycan. *J. Biol. Chem.* **266,** 10518–10523

(1991).

115. Ward, J. V. & Packham, M. A. Characterization of the sulfated glycosaminoglycan on the surface and in the storage granules of rabbit platelets. *BBA - Gen. Subj.* **583,** 196–207 (1979).

116. Ushiyama, A., Kataoka, H. & Iijima, T. Glycocalyx and its involvement in clinical pathophysiologies. *J. Intensive Care* **4,** 4–5 (2016).

117. Warkentin, T. E. *et al.* Heparin-Induced Thrombocytopenia in Medical Surgical Critical Illness. *Chest* **144,** 848–858 (2013).

118. Warkentin, T. E. & Greinacher, A. Heparin-induced thrombocytopenia: Recognition, treatment, and prevention - The Seventh ACCP Conference on Antithrombotic and Thrombolytic Therapy. *Chest* **126,** 4–6 (2004).

119. Gross, P. L. Leukocyte-versus microparticle-mediated tissue factor transfer during arteriolar thrombus development. *J. Leukoc. Biol.* **78,** 1318–1326 (2005).

120. Aisiku, O. *et al.* Parmodulins inhibit thrombus formation without inducing endothelial injury caused by vorapaxar. *Blood* **125,** 1976–1985 (2015).

121. Greineder, C. F. *et al.* Molecular engineering of high affinity single-chain antibody fragment for endothelial targeting of proteins and nanocarriers in rodents and humans. *J. Control. Release* **226,** 229–237 (2016).

122. Xiao, Z., Visentin, G. P., Dayananda, K. M. & Neelamegham, S. Immune complexes formed following the binding of anti platelet factor 4 (CXCL4) antibodies to CXCL4 stimulate human neutrophil activation and cell adhesion. *Blood* **112,** 1091–1100 (2008).

123. Becker, B. F., Jacob, M., Leipert, S., Salmon, A. H. J. & Chappell, D. Degradation of the endothelial glycocalyx in clinical settings: Searching for the sheddases. *Br. J. Clin. Pharmacol.* **80,** 389–402 (2015).

124. Jaax, M. E. *et al.* Complex formation with nucleic acids and aptamers alters the antigenic properties of platelet factor 4. *Blood* **122,** 272–281 (2013).

125. Krauel, K. *et al.* Platelet factor 4 binds to bacteria, [corrected] inducing antibodies cross-reacting with the major antigen in heparin-induced thrombocytopenia. *Blood* **117,** 1370–8 (2011).

126. Donovan, M. J. & Picciano, P. T. Fibrin Peptides That Mediate Endothelial Cell Retraction. 418–428 (1984).

127. Zucker-Franklin, D. & Philipp, C. S. Platelet production in the pulmonary capillary bed: New ultrastructural evidence for an old concept. *Am. J. Pathol.* **157,** 69–74 (2000).

128. Chen, J. & López, J. A. Interactions of platelets with subendothelium and endothelium. *Microcirculation* **12,** 235–246 (2005).

129. Hunt, B. J. & Jurd, K. M. Endothelial cell activation. **316,** 1328–1329 (2014).

130. Chen, M. & Geng, J. G. P-selectin mediates adhesion of leukocytes, platelets, and cancer cells in inflammation, thrombosis, and cancer growth and metastasis. *Arch. Immunol. Ther. Exp. (Warsz).* **54,** 75–84 (2006).

131. Yoshida, M. *et al.* Leukocyte adhesion to vascular endothelium induces E-selectin linkage to the actin cytoskeleton. *J. Cell Biol.* **133,** 445–455 (1996).

132. Ruggeri, Z. M. The role of von Willebrand factor in thrombus formation. *Thromb. Res.* **120,** S5-9 (2007).

133. Carlsson, L. E. *et al.* Heparin-induced thrombocytopenia: new insights into the impact of the FcgammaRIIa-R-H131 polymorphism. *Blood* **92,** 1526–31 (1998).

134. Berndt, M. C., Du, X. & Booth, W. J. Ristocetin-Dependent Reconstitution of Binding of von Willebrand Factor to Purified Human Platelet Membrane Glycoprotein Ib-IX Complex. *Biochemistry* **27,** 633–640 (1988).

135. Beumer, S. *et al.* Platelet adhesion to fibronectin in flow: the importance of von Willebrand factor and glycoprotein Ib. *Blood* **86,** 3452–60 (1995).

136. Park, K. S. *et al.* Biologic and biochemic properties of recombinant platelet factor 4 demonstrate identity with the native protein. *Blood* **75,** 1290–5 (1990).

137. Rauova, L. *et al.* Ultralarge complexes of PF4 and heparin are central to the pathogenesis of heparin-induced thrombocytopenia. *Blood* **105,** 131–138 (2005).

138. Gogia, S. & Neelamegham, S. Role of fluid shear stress in regulating VWF structure, function and related blood disorders. *Biorheology* **52,** 319–335 (2015).

139. Huizinga, E. G., Plas, R. M. van der, Kroon, J., Sixma, J. J. & Gros, P. Crystal structure of the A3 domain of human von Willebrand factor: implications for collagen binding. *Structure* **5,** 1147–1156 (1997).

140. Fu, H. *et al.* Flow-induced elongation of von Willebrand factor precedes tension-dependent activation. *Nat. Commun.* **8,** (2017).

141. Cines, D. B. *et al.* Heparin-induced thrombocytopenia: An autoimmune disorder regulated through dynamic autoantigen assembly/disassembly. *J. Clin. Apher.* **22,** 31–36 (2007).

142. Savage, B., Sixma, J. J. & Ruggeri, Z. M. Functional self-association of von Willebrand factor during platelet adhesion under flow. *Proc. Natl. Acad. Sci.* **99,** 425–430 (2002).

143. Li, Y. *et al.* Covalent regulation of ULVWF string formation and elongation on endothelial cells under flow conditions. *J. Thromb. Haemost.* **6,** 1135–1143 (2008).

144. Barg, A. *et al.* Soluble plasma-derived von Willebrand factor assembles to a haemostatically active filamentous network. *Thromb. Haemost.* **97,** 514–526 (2007).

145. Shankaran, H., Alexandridis, P. & Neelamegham, S. Aspects of hydrodynamic shear regulating shear-induced platelet activation and self-association of von Willebrand factor in suspension. *Blood* **101,** 2637–2645 (2003).

146. López, J. A. & Chung, D. W. VWF self-association: More bands for the buck. *Blood* **116,** 3693–3694 (2010).

147. Brill-Edwards, P., Ginsberg, J. S., Johnston, M. & Hirsh, J. Establishing a therapeutic range for heparin therapy. *Ann. Intern. Med.* **119,** 104–109 (1993).

148. Blanchi, V., Robles, R., Alberio, L., Furlan, M. & Lämmle, B. Von Willebrand factor-cleaving protease (ADAMTS13) in thrombocytopenic disorders: A severely deficient activity is specific for thrombotic thrombocytopenic purpura. *Blood* **100,** 710–713 (2002).

149. Pépin, M. *et al.* ADAMTS-13 and von Willebrand factor predict venous thromboembolism in patients with cancer. *J. Thromb. Haemost.* **14,** 306–315 (2016).

150. Chen, J. *et al.* N-acetylcysteine reduced the size and activity of von Willebrand factor in human plasma and mice. *J. Clin. Invest.* **121,** 593–603 (2011).

151. Brill, A. *et al.* Von Willebrand factor-mediated platelet adhesion is critical for deep vein thrombosis in mouse models. *Blood* **117,** 1400–1407 (2011).

152. Denorme, F. *et al.* ADAMTS13- - - mediated thrombolysis of t- - - PA resistant occlusions in ischemic stroke in mice. **127,** 1–5 (2017).

153. Saku, K., Ahmad, M., Glas-greenwalt, P. & Moti, L. Copyright (c) 1985 Pergamon Press Ltd . All rights reserved . by Editor L . J . Berliner). 201–212 (1985).

154. Nand, S. *et al.* Heparin-induced thrombocytopenia with thrombosis: incidence, analysis of risk factors, and clinical outcomes in 108 consecutive patients treated

at a single institution. *Am. J. Hematol.* **56,** 12–16 (1997).

155. Wallis, D. E. *et al.* Failure of early heparin cessation as treatment for heparin-induced thrombocytopenia. *Am. J. Med.* **106,** 629–635 (1999).

156. Linkins, L.-A. *et al.* Treatment and Prevention of Heparin-Induced Thrombocytopenia. *Chest* **141,** e495S–e530S (2012).

157. Zhou, A. *et al.* Is the incidence of heparin-induced thrombocytopenia affected by the increased use of heparin for VTE prophylaxis? *Chest* **142,** 1175–1178 (2012).

158. Cervera, R. Antiphospholipid syndrome. *Thromb. Res.* **151,** S43–S47 (2017).

159. Donze, J., Ridker, P., Finlayson, S. R. G. & Bates, D. Impact of sepsis on postoperative risk of arterial and venous thrombosis. *J. Am. Coll. Cardiol.* **63,** A2047 (2014).

160. Rauova, L. *et al.* Platelet and monocyte antigenic complexes in the pathogenesis of heparin-induced thrombocytopenia (HIT). *J. Thromb. Haemost.* **7,** 249–252 (2009).

161. Arepally, G. M. Clinical platelet disorders heparin-induced thrombocytopenia. *Blood* **129,** 2864–2872 (2017).

162. Thrombocytopenia, H. & Poncz, M. Mechanistic Basis of. 73–79 (2005). doi:10.1053/j.semtcvs.2004.12.007

163. Qiao, J., Al-Tamimi, M., Baker, R. I., Andrews, R. K. & Gardiner, E. E. The platelet Fc receptor, FcγRIIa. *Immunol. Rev.* **268,** 241–252 (2015).

164. Mayadas, T. N., Tsokos, G. C. & Tsuboi, N. Mechanisms of immune complex-mediated neutrophil recruitment and tissue injury. *Circulation* **120,** 2012–2024 (2009).

165. Khairy, M. *et al.* Polymorphonuclear leukocyte and monocyte activation induced by plasma from patients with heparin-induced thrombocytopenia in whole blood.

Thromb. Haemost. **92,** 1411–1419 (2004).

166. Martinod, K. & Wagner, D. D. Thrombosis: Tangled up in NETs. *Blood* **123,** 2768–2776 (2014).

167. Li, P. *et al.* PAD4 is essential for antibacterial innate immunity mediated by neutrophil extracellular traps. *J. Exp. Med.* **207,** 1853–1862 (2010).

168. Kowalska, M. A., Rauova, L. & Poncz, M. Role of the platelet chemokine platelet factor 4 (PF4) in hemostasis and thrombosis. *Thromb. Res.* **125,** 292–296 (2010).

169. Cong, L. *et al.* Multiplex genome engineering using CRISPR/Cas systems. *Science (80-.).* **339,** 819–823 (2013).

170. Doench, J. G. *et al.* Optimized sgRNA design to maximize activity and minimize off-target effects of CRISPR-Cas9. *Nat. Biotechnol.* **34,** 184–191 (2016).

171. Cuker, A. Clinical and laboratory diagnosis of heparin-induced thrombocytopenia: An integrated approach. *Semin. Thromb. Hemost.* **40,** 106–114 (2014).

172. Arepally, G. *et al.* Comparison of PF4/heparin ELISA assay with the 14C-serotonin release assay in the diagnosis of heparin-induced thrombocytopenia. *Am J Clin Pathol* **104,** 648–654 (1995).

173. Lambert, M. P. & Gernsheimer, T. B. Clinical updates in adult immune thrombocytopenia. *Blood* **129,** 2829–2835 (2017).

174. Sachais, B. S. *et al.* Dynamic antibody-binding properties in the pathogenesis of HIT. *Blood* **120,** 1137–1142 (2012).

175. Drexler, G. A. & Ruiz-Gómez, M. J. Microirradiation techniques in radiobiological research. *J. Biosci.* **40,** 629–643 (2015).

176. Schindelin, J. *et al.* Fiji: An open-source platform for biological-image analysis. *Nat. Methods* **9,** 676–682 (2012).

177. Chapman, R. W. *et al.* A novel, orally active CXCR1/2 receptor antagonist,

Sch527123, inhibits neutrophil recruitment, mucus production, and goblet cell hyperplasia in animal models of pulmonary inflammation. *J. Pharmacol. Exp. Ther.* **322,** 486–93 (2007).

178. Brill, A. *et al.* Neutrophil extracellular traps promote deep vein thrombosis in mice. *J. Thromb. Haemost.* **10,** 136–144 (2012).

179. Jenne, C. N., Urrutia, R. & Kubes, P. Platelets: Bridging hemostasis, inflammation, and immunity. *Int. J. Lab. Hematol.* **35,** 254–261 (2013).

180. McDonald, B., Urrutia, R., Yipp, B. G., Jenne, C. N. & Kubes, P. Intravascular neutrophil extracellular traps capture bacteria from the bloodstream during sepsis. *Cell Host Microbe* **12,** 324–333 (2012).

181. Monti, M. *et al.* Integrin-dependent cell adhesion to neutrophil extracellular traps through engagement of fibronectin in neutrophil-like cells. *PLoS One* **12,** 1–2 (2017).

182. Fuchs, T. A. *et al.* Extracellular DNA traps promote thrombosis. *Proc. Natl. Acad. Sci.* **107,** 15880–15885 (2010).

183. Hakkim, A. *et al.* Impairment of neutrophil extracellular trap degradation is associated with lupus nephritis. *Proc. Natl. Acad. Sci.* **107,** 9813–9818 (2010).

184. Begandt, D., Thome, S., Sperandio, M. & Walzog, B. How neutrophils resist shear stress at blood vessel walls: molecular mechanisms, subcellular structures, and cell–cell interactions. *J. Leukoc. Biol.* **102,** 699–709 (2017).

185. Ghasemzadeh, M. *et al.* The CXCR1/2 ligand NAP-2 promotes directed intravascular leukocyte migration through platelet thrombi. *Blood* **121,** 4555–4566 (2013).

186. Kienle, K. & Lï¿½mmermann, T. Neutrophil swarming: an essential process of the neutrophil tissue response. *Immunol. Rev.* **273,** 76–93 (2016).

187. Chapman, R. W. *et al.* CXCR2 antagonists for the treatment of pulmonary disease. *Pharmacol. Ther.* **121,** 55–68 (2009).

188. Dyer, M. R. *et al.* Deep vein thrombosis in mice is regulated by platelet HMGB1 through release of neutrophil-extracellular traps and DNA. *Sci. Rep.* **8,** 2–3 (2018).

189. Wolach, O. *et al.* Increased neutrophil extracellular trap formation promotes thrombosis in myeloproliferative neoplasms. *Sci. Transl. Med.* **10,** 1–2 (2018).

190. Brandt, S. *et al.* Polyphosphates form antigenic complexes with platelet factor 4 (PF4) and enhance PF4-binding to bacteria. *Thromb. Haemost.* **114,** 1189–1198 (2015).

191. Neumann, A. *et al.* Novel role of the antimicrobial peptide LL-37 in the protection of neutrophil extracellular Traps against degradation by bacterial nucleases. *J. Innate Immun.* **6,** 860–868 (2014).

192. Leffler, J. *et al.* Neutrophil Extracellular Traps That Are Not Degraded in Systemic Lupus Erythematosus Activate Complement Exacerbating the Disease. *J. Immunol.* **188,** 3522–3531 (2012).

193. Leffler, J. *et al.* Degradation of neutrophil extracellular traps is decreased in patients with antiphospholipid syndrome. *Clin. Exp. Rheumatol.* **32,** (2013).

194. Lewis, H. D. *et al.* Inhibition of PAD4 activity is sufficient to disrupt mouse and human NET formation. *Nat. Chem. Biol.* **11,** 189–191 (2015).

195. Holz, O. *et al.* SCH527123, a novel CXCR2 antagonist, inhibits ozone-induced neutrophilia in healthy subjects. *Eur. Respir. J.* **35,** 564–570 (2010).

196. Levi, M. Recombinant soluble thrombomodulin: Coagulation takes another chance to reduce sepsis mortality. *J. Thromb. Haemost.* **13,** 505–507 (2015).

197. Fiusa, M. M. L., Carvalho-Filho, M. A., Annichino-Bizzacchi, J. M. & De Paula, E.

V. Causes and consequences of coagulation activation in sepsis: An evolutionary medicine perspective. *BMC Med.* **13,** (2015).

198. Jh, F. & Em, C. Cross Talk Pathways Between Coagulation and Inflammation . **118,** 1–2 (2018).

199. Engelmann, B. & Massberg, S. Thrombosis as an intravascular effector of innate immunity. *Nat. Rev. Immunol.* **13,** 34–45 (2013).

200. Allingstrup, M., Wetterslev, J., Fb, R., Am, M. & Afshari, A. Antithrombin III for critically ill patients . 2016–2018 (2018). doi:10.1002/14651858.CD005370.pub3.Full

201. Martí-Carvajal, A. J., Solà, I., Gluud, C., Lathyris, D. & Anand, V. Human recombinant protein C for severe sepsis and septic shock in adult and paediatric patients. *Cochrane Database Syst. Rev.* **3435,** 9–10 (2012).

202. Jaimes, F. *et al.* Unfractioned heparin for treatment of sepsis: A randomized clinical trial (The HETRASE Study). *Crit. Care Med.* **37,** 1185–1196 (2009).

203. Zarychanski, R. *et al.* The efficacy and safety of heparin in patients with sepsis: A systematic review and metaanalysis. *Crit. Care Med.* **43,** 511–518 (2015).

204. Boehme, M. W. *et al.* Release of thrombomodulin from endothelial cells by concerted action of TNF-alpha and neutrophils: in vivo and in vitro studies. *Immunology* **87,** 134–40 (1996).

205. Macgregor, I. R., Perrie, A. M., Donnelly, S. C. & Haslett, C. Modulation of human endothelial thrombomodulin by neutrophils and their release products. *Am. J. Respir. Crit. Care Med.* **155,** 47–52 (1997).

206. Xu, J., Qu, D., Esmon, N. L. & Esmon, C. T. Metalloproteolytic release of endothelial cell protein C receptor. *J. Biol. Chem.* **275,** 6038–6044 (2000).

207. Gu, J. M. *et al.* Endotoxin and thrombin elevate rodent endothelial cell protein C

receptor mRNA levels and increase receptor shedding in vivo. *Blood* **95,** 1687–93 (2000).

208. He, X. *et al.* Anti-human tissue factor antibody ameliorated intestinal ischemia reperfusion-induced acute lung injury in human tissue factor knock-in mice. *PLoS One* **3,** 1–2 (2008).

209. Witkowski, M., Landmesser, U. & Rauch, U. Tissue factor as a link between inflammation and coagulation. *Trends Cardiovasc. Med.* **26,** 297–303 (2016).

210. Vincent, J.-L. *et al.* A Randomized, Double-Blind, Placebo-Controlled, Phase 2b Study to Evaluate the Safety and Efficacy of Recombinant Human Soluble Thrombomodulin, ART-123, in Patients With Sepsis and Suspected Disseminated Intravascular Coagulation*. *Crit. Care Med.* **41,** 2069–2079 (2013).

211. Greineder, C. F., Howard, M. D., Carnemolla, R., Cines, D. B. & Muzykantov, V. R. Advanced drug delivery systems for antithrombotic agents. *Blood* **122,** 1565–1575 (2013).

212. Greineder, C. F. *et al.* Vascular immunotargeting to endothelial determinant ICAM-1 enables optimal partnering of recombinant scFv-Thrombomodulin fusion with endogenous cofactor. *PLoS One* **8,** (2013).

213. Antoniak, S., Witkowski, M., Landmesser, U. & Rauch, U. Editorial Commentary : Tissue factor expression by the endothelium : Coagulation or inflammation ? ☆. **1738,** 3–5 (2018).

214. Witkowski, M. & Rauch, U. Letter to the Editor: Tissue factor of endothelial origin: Just another brick in the wall? *Trends Cardiovasc. Med.* **27,** 155–156 (2017).

215. Drake, T. A., Cheng, J., Chang, A. & Taylor, F. B. Expression of tissue factor, thrombomodulin, and E-selectin in baboons with lethal Escherichia coli sepsis. *Am. J. Pathol.* **142,** 1458–70 (1993).

216. Shaver, C. M. *et al.* Myeloid tissue factor does not modulate lung inflammation or permeability during experimental acute lung injury. *Sci. Rep.* **6,** (2016).

217. Shaver, C. M. *et al.* Regulation of alveolar procoagulant activity and permeability in direct acute lung injury by lung epithelial tissue factor. *Am. J. Respir. Cell Mol. Biol.* **53,** 719–727 (2015).

218. Pawlinski, R. *et al.* Hematopoietic and nonhematopoietic cell tissue factor activates the coagulation cascade in endotoxemic mice. *Blood* **116,** 806–814 (2010).

219. Crikis, S. *et al.* Antiinflammatory and anticoagulant effects of transgenic expression of human thrombomodulin in mice. *Am. J. Transplant.* **10,** 242–250 (2010).

220. Raife, T. J. *et al.* Human thrombomodulin knock-in mice reveal differential effects of human thrombomodulin on thrombosis and atherosclerosis. *Arterioscler. Thromb. Vasc. Biol.* **31,** 2509–2517 (2011).

221. Brinkmann, V., Laube, B., Abu Abed, U., Goosmann, C. & Zychlinsky, A. Neutrophil Extracellular Traps: How to Generate and Visualize Them. *J. Vis. Exp.* (2010). doi:10.3791/1724

222. Colace, T. V., Tormoen, G. W., McCarty, O. J. T. & Diamond, S. L. Microfluidics and Coagulation Biology. *Annu. Rev. Biomed. Eng.* **15,** 283–303 (2013).

223. Smith, C. W. *et al.* Recognition of an endothelial determinant for CD18-dependent human neutrophil adherence and transendothelial migration. *J. Clin. Invest.* **82,** 1746–1756 (1988).

224. Lipowsky, H. Shear Stress in the Circulation. *Flow-Dependent Regul. Vasc. Funct. SE - 2* 28–45 (1995). doi:10.1007/978-1-4614-7527-9_2

225. Clark, S. R. *et al.* Platelet TLR4 activates neutrophil extracellular traps to ensnare

bacteria in septic blood. *Nat. Med.* **13,** 463–469 (2007).

226. Ikezoe, T. *et al.* The fifth epidermal growth factor-like region of thrombomodulin exerts cytoprotective function and prevents SOS in a murine model. *Bone Marrow Transplant.* **52,** 73–79 (2017).

227. Mohri, M., Sugimoto, E., Sata, M. & Asano, T. The inhibitory effect of recombinant human soluble thrombomodulin on initiation and extension of coagulation--a comparison with other anticoagulants. *Thromb. Haemost.* **82,** 1687–93 (1999).

228. Böhmer, R. H., Trinkle, L. S. & Staneck, J. L. Dose effects of LPS on neutrophils-in a whole blood flow cytometric assay of phagocytosis and oxidative burst. *Cytometry* **13,** 525–531 (1992).

229. Butenas, S., Bouchard, B. A., Brummel-Ziedins, K. E., Parhami-Seren, B. & Mann, K. G. Tissue factor activity in whole blood. *Blood* **105,** 2764–2770 (2005).

230. Zhao, X. *et al.* Targeted Inhibition of Activated Protein C Anticoagulant Activity By Monoclonal Antibody HAPC1573 for Treatment of Hemophilia Cookie Notification and Disclosure : 1–7 (2018).

231. Takahashi, H. et al. Protein C levels in disseminated intravascular coagulation and thrombotic thrombocytopenic purpura: its correlation with other coagulation parameters. *Thromb. Haemost.* **54,** 445–449 (1985).

232. Fisher, C. J. & Yan, S. B. Protein C levels as a prognostic indicator of outcome in sepsis and related diseases. *Crit. Care Med.* **28,** S49–S56 (2000).

233. Lb, W., Fang, X. & Ma, M. Protein C and thrombomodulin in human acute lung injury . **285,** (2018).

234. Coll, E., Robles-Carrillo, L., Reyes, E., Francis, J. L. & Amirkhosravi, A. Assessment of protein C anticoagulant pathway by thrombin generation assay in the presence of endothelial cells. *J. Thromb. Haemost.* **11,** 1916–1919 (2013).

235. Salmela, K. *et al.* A randomized multicenter trial of the anti-ICAM-1 monoclonal antibody (enlimomab) for the prevention of acute rejection and delayed onset of graft function in cadaveric renal transplantation: A report of the European Anti-ICAM-1 Renal Transplant Study gr. *Transplantation* **67,** 729–736 (1999).

236. Investigators, E. A. S. T. Use of anti-ICAM-1 therapy in ischemic stroke: results of the Enlimomab Acute Stroke Trial. *Neurology* **57,** 1428–34 (2001).

237. Cosimi, A. B. *et al.* In vivo effects of monoclonal antibody to ICAM-1 (CD54) in nonhuman primates with renal allografts. *J. Immunol.* **144,** 4604–12 (1990).

238. Vuorte, J. *et al.* Anti-ICAM-1 monoclonal antibody R6.5 (Enlimomab) promotes activation of neutrophils in whole blood. *J. Immunol.* **162,** 2353–7 (1999).

239. Zheng, Y. *et al.* In vitro microvessels for the study of angiogenesis and thrombosis. *Proc. Natl. Acad. Sci.* **109,** 9342–9347 (2012).

240. Tsai, M. *et al.* In vitro modeling of the microvascular occlusion and thrombosis that occur in hematologic diseases using microfluidic technology. *J. Clin. Invest.* **122,** 408–418 (2012).

241. Tourovskaia, A., Fauver, M., Kramer, G., Simonson, S. & Neumann, T. Tissue-engineered microenvironment systems for modeling human vasculature. *Exp. Biol. Med.* **239,** 1264–1271 (2014).

242. Ew, E. Organs-on-chips at the frontiers of drug discovery . **14,** 4–5 (2018).

243. Ma, R., Ss, K., Kt, P. & Zheng, Y. Micropatterning and Assembly of 3D Microvessels . 2–3 (2018). doi:10.3791/54457

244. Carnemolla, R. *et al.* Targeting thrombomodulin to circulating red blood cells augments its protective effects in models of endotoxemia and ischemia-reperfusion injury. *FASEB J.* **31,** 761–770 (2017).

245. Ch, V., Dc, P., Db, C., Dl, S. & Vr, M. Delivery of drugs bound to erythrocytes :

new avenues for an old intravascular carrier . **6,** 1–2 (2018).

246. Fuentes, R. E. *et al.* A chimeric platelet-targeted urokinase prodrug selectively blocks new thrombus formation. *J. Clin. Invest.* **126,** 483–494 (2016).

247. Polacheck, W. J., Li, R., Uzel, S. G. M. & Kamm, R. D. Microfluidic platforms for mechanobiology. *Lab Chip* **13,** 2252 (2013).

248. Lupu, C. *et al.* Tissue factor-dependent coagulation is preferentially up-regulated within arterial branching areas in a baboon model of Escherichia coli sepsis. *Am. J. Pathol.* **167,** 1161–1172 (2005).

249. Antoniak, S. & Mackman, N. Letter to Editor response: Endothelial cell tissue factor and coagulation. *Trends Cardiovasc. Med.* **27,** 4–6 (2017).

250. Nickel, K. F., Long, A. T., Fuchs, T. A., Butler, L. M. & Renné, T. Factor XII as a therapeutic target in thromboembolic and inflammatory diseases. *Arterioscler. Thromb. Vasc. Biol.* **37,** 13–20 (2017).

251. Ding, B. Sen *et al.* Anchoring fusion thrombomodulin to the endothelial lumen protects against injury-induced lung thrombosis and inflammation. *Am. J. Respir. Crit. Care Med.* **180,** 247–256 (2009).

252. Greineder, C. F. *et al.* Dual targeting of therapeutics to endothelial cells: Collaborative enhancement of delivery and effect. *FASEB J.* **29,** 3483–3492 (2015).

253. Tosi, M. F. *et al.* Induction of ICAM-1 expression on human airway epithelial cells by inflammatory cytokines: effects on neutrophil-epithelial cell adhesion. *Am. J. Respir. Cell Mol. Biol.* **7,** 214–221 (1992).

254. Stern, D., Nawroth, P., Handley, D. & Kisiel, W. An endothelial cell-dependent pathway of coagulation. *Proc. Natl. Acad. Sci. U. S. A.* **82,** 2523–2527 (1985).

255. Ivanciu, L., Krishnaswamy, S. & Camire, R. M. New insights into the

spatiotemporal localization of prothrombinase in vivo. *Blood* **124,** 1705–1714 (2014).

256. Stearns-Kurosawa, D. J., Kurosawa, S., Mollica, J. S., Ferrell, G. L. & Esmon, C. T. The endothelial cell protein C receptor augments protein C activation by the thrombin-thrombomodulin complex. *Proc. Natl. Acad. Sci. U. S. A.* **93,** 10212–6 (1996).

257. Manco-Johnson, M. J. *et al.* Efficacy and safety of protein C concentrate to treat purpura fulminans and thromboembolic events in severe congenital protein C deficiency. *Thromb. Haemost.* **116,** 58–68 (2016).

258. Gao, L. & Lipowsky Herbert H., H. H. Composition of the endothelial glycocalyx and its relation to its thickness and diffusion of small solutes. *Microvasc. Res.* **80,** 394–401 (2010).

259. Mosnier, L. O., Sinha, R. K., Burnier, L., Bouwens, E. A. & Griffin, J. H. Biased agonism of protease-activated receptor 1 by activated protein C caused by noncanonical cleavage at Arg46. *Blood* **120,** 5237–5246 (2012).

260. Hemostasis, Thrombosis, and Vascular Biology_ The ligand occupancy of endothelial protein C receptor switches the protease-activated receptor 1-dependent signaling specificity of thrombin from a permeability-enhancing to a barrier-protective response .pdf.

261. Riewald, M. & Ruf, W. Protease-activated receptor-1 signaling by activated protein C in cytokine-perturbed endothelial cells is distinct from thrombin signaling. *J. Biol. Chem.* **280,** 19808–19814 (2005).

262. Kowalska, M. A. *et al.* Antibodies associated with heparin-induced thrombocytopenia (HIT) inhibit activated protein C generation: New insights into the prothrombotic nature of HIT. *Blood* **118,** 2882–2888 (2011).

263. Mosnier, L. O., Yang, X. V. & Griffin, J. H. Activated protein C mutant with minimal anticoagulant activity, normal cytoprotective activity, and preservation of thrombin activable fibrinolysis inhibitor-dependent cytoprotective functions. *J. Biol. Chem.* **282,** 33022–33033 (2007).

264. Guo, H. *et al.* Neuroprotective activities of activated protein C mutant with reduced anticoagulant activity. *Eur. J. Neurosci.* **29,** 1119–1130 (2009).

265. Kerschen, E. J. *et al.* Endotoxemia and sepsis mortality reduction by non-anticoagulant–activated protein C. *J. Exp. Med.* **204,** 2439–2448 (2007).

266. F. Gragnano, S. Sperlongano, E. Golia, F. Natale, R. Bianchi, M. Crisci, F. Fimiani, I. Pariggiano, V. Diana, A. Carbone, A. Cesaro, C. Concilio, G. Limongelli, M. Russo, and P. C. The Role of von Willebrand Factor in Vascular Inflammation: From Pathogenesis to Targeted Therapy. *Mediators Inflamm.* **2017,** (2017).

267. Walenga, J. M. *et al.* Vascular damage correlates between heparin-induced thrombocytopenia and the antiphospholipid syndrome. *Clin Appl Thromb Hemost* **5 Suppl 1,** S76-84 (1999).

268. Ostertag, E. M. *et al.* ADAMTS13 autoantibodies cloned from patients with acquired thrombotic thrombocytopenic purpura: 2. Pathogenicity in an animal model. *Transfusion* **56,** 1775–1785 (2016).

269. Mody, N. A., Lomakin, O., Doggett, T. A., Diacovo, T. G. & King, M. R. Mechanics of transient platelet adhesion to von Willebrand factor under flow. *Biophys. J.* **88,** 1432–1443 (2005).

270. Witsch, T. *et al.* Recombinant human ADAMTS13 treatment improves myocardial remodeling and functionality after pressure overload injury in mice. *J. Am. Heart Assoc.* **7,** 1–14 (2018).

271. Cai, Z. *et al.* Atomic description of the immune complex involved in heparin-induced thrombocytopenia. *Nat. Commun.* **6,** 1–10 (2015).

272. Denis, C. *et al.* A mouse model of severe von Willebrand disease: defects in hemostasis and thrombosis. *Proc Natl Acad Sci USA* **95,** 9524–9529 (1998).

273. Martens, C. L. *et al.* Peptides which bind to E-selectin and block neutrophil adhesion. *J. Biol. Chem.* **270,** 21129–21136 (1995).

274. Ataga, K. I. *et al.* Crizanlizumab for the Prevention of Pain Crises in Sickle Cell Disease. *N. Engl. J. Med.* **376,** 429–439 (2017).

275. Zahr, A. *et al.* Endomucin prevents leukocyte-endothelial cell adhesion and has a critical role under resting and inflammatory conditions. *Nat. Commun.* **7,** (2016).

276. Barnado, A., Crofford, L. J. & Oates, J. C. At the Bedside: Neutrophil extracellular traps (NETs) as targets for biomarkers and therapies in autoimmune diseases. *J. Leukoc. Biol.* **99,** 265–278 (2016).

277. Lapponi, M. J. *et al.* Regulation of Neutrophil Extracellular Trap Formation by Anti-Inflammatory Drugs. *J. Pharmacol. Exp. Ther.* **345,** 430–437 (2013).